THE UNIVERSITY OF HULL

EXCIMER LASER MICROMACHINING OF INORGANIC MATERIALS

being a Thesis submitted for the degree of Doctor of Philosophy

by

Philip Henry Key, B.Sc.,M.Sc. (Hull).

November, 1989

AKNOWLEDGEMENTS

The technical assistance and expertise of Brian Tait and Paul Monk of the Opto-eletronics and Lasers Research Group in the Department of Applied Physics is gratefully aknowledged as is the support given by the other members of the technical staff at Hull.

Special thanks are due to my supervisors Professor P.E. Dyer and Dr. R.D. Greenough for their advice and encouragement going back to my time as an undergraduate student. My thanks also go to those material scientists from other institutions whom I have met at conferences and who have given advice.

The financial assistance of H.Tinsley PLC, G.E.C. Hirst and the Science and Engineering Research Council was much appreciated.

Most importantly, my thanks go to my wife, Gill, and daughter, Michelle, in recognition of the support and encouragement they have given and for organising my life even when I did not see the need.

CONTENTS page

0.0.

INTRODUCTION

The processing of materials has emerged over the last few years as an area in which lasers, as a highly controlable source of energy, have found increasing importance. The development of lasers with reliable outputs ranging from the mid-infrared (CO_2 at 10.6 μm) to the deep ultraviolet (ArF at 193 nm) has provided the material scientist with a tool kit capable of rapidly heating solid surfaces to vaporisation temperatures, initiating chemical reactions or inducing structural changes.

On the large scale, infrared lasers are now routinely used in industry for bulk metal processing both in cutting, usually of intricate parts, welding and for surface modification such as heat treatment to achieve a desired surface hardness or for alloying. [1-4].

Much research has been, and continues to be, done in the field of laser processing on a microscopic scale for micro-electronics applications. This interest includes laser etching, deposition and compositional or structural modification of metals, semi-conductors and insulators. Much of the work relates to silicon based technology and the desire to develop techniques for high density device manufacture, in which the number of processing steps and transport of wafers are minimised, ie. in-situ processing [5-9].

Laser interactions with organic materials, and in particular long-chain polymers, have also received a good deal of

attention both because of their use as etch resists and passivation materials in microelectronics processing and because their similarity with biological materials allows the potential for laser surgery to be assessed [10-13].

The work presented here is concerned with the UV-excimer laser ablation of inorganic materials and in particular with processes compatible with pattern generation in a regime intermediate between large scale cutting and sub-micron technologies. This regime of laser processing, involving feature sizes of a few microns, is of interest for small component manufacture for electronic, mechanical or optical applications. The term ablation will be used to describe the removal of material from a surface and is not intended to imply any particular removal mechanism other than it being laser induced.

For good thermal conductors, such as metals, heat flow from the area being processed into the non-irradiated surrounding zone can severely limit the patterning capabilities on this scale. It is desirable, therefore, to operate in a regime of energy input in which high temperature excursions are avoided. Ablation at lower fluences (energy per unit area) than those required for vaporisation of a surface can often be achieved by laser-chemical processing in which surface chemistry plays an important role.

Oxidation or halogenation of metal surfaces in appropriate gaseous environments, for example, can provide a route to relatively low fluence processing. This method is exemplified in this work by systematic studies of the processing of copper, a material chosen because of its wide

spread use. The ablation of some alloys and ceramic materials is also considered, albeit in rather less detail.

Chapter 1 of this thesis presents a brief review of laser ablation mechanisms and strategies for laser patterning reported in the literature. It has been shown in a previous work [14,15] that a variety of metal films on a number of different substrates can be patterned by ablation using a single,UV-excimer laser pulse. This work is reviewed and the limitations of the process discussed to provide a background against which this current work can be set.

In chapter 2 some aspects of the absorption of laser radiation at solid surfaces, from the point of view of the optical properties of materials, are discussed. The re-distribution of energy, as heat, following the absorption of the laser pulse is considered and computer modelled temperature-time profiles for a one-dimensional heat flow in thin conductors are compared with experimental data. Some preliminary results showing the effects of environmental conditions on the multiple pulse, UV-excimer laser irradiation of bulk metals are presented.

Chapter 3 presents an outline of the optics of thin, weakly absorbing films leading to a description of the technique of their thickness measurement using the observed temporal modulation of reflectance due to interference effects. Results of studies of the growth rates of chloride layers as a function of chlorine gas pressure and copper substrate temperature are presented. The diffusion limited growth rate deduced from these measurements is used to predict the effect of these parameters on the laser etch-rate.

Chapter 4 presents the results of studies of the UV-excimer laser etching of polycrystalline copper foils in a chlorine gas environment. The experimental arrangement and methodology are described and data on the influence of laser wavelength, pulse repetition frequency (prf) and ambient gas pressure on the measured etch-rates are presented. UV-visible spectroscopy of the ablated plume was used to determine the major ablated species and, using time-resolved signals, to estimate their velocity. A discussion of these results presents evidence in support of the theory that the etch-rate, at a given fluence, is dependent upon the thickness of the chloride layer addressed by the laser radiation and may be, therefore, governed by the growth kinetics.

The fifth chapter indicates the versatility of UV-excimer lasers for ablation. Etch-rate and qualitative data on the ablation of some alloys and insulator materials are presented.

The generation of patterns by laser ablation is discussed in the penultimate chapter, 6, and both the optical system used and the response of material, with a non-linear dependence of etch-rate, to fluence gradients at the edge of pattern features is considered. Examples of both single pulse ablation of thin films and multi-pulse etching of foils are used to demonstrate that the feature resolution achieved can be better than predicted from consideration of the limits of the optical system alone.

The results of these studies are summarised in chapter 7 and some conclusions regarding the applicability and limitations

of this technique of material patterning by UV-excimer laser ablation are drawn

Each chapter has been divided into sections and, in the interests of textual continuity, the relevant diagrams placed at the end of each section. References appear at the end of each chapter.

0.1

REFERENCES

[1] Koebner,H.
in 'Industrial Applications of Lasers'
ed. H.Koebner
John Wiley & Sons, Chichester, (1984).

[2] Gagliano,F.P. & Zaleckas,V.J.
in 'Lasers in Industry', ed. S.S.Charschan.
Van Nostrand Reinhold, New York, (1972).

[3] Gomersall,A.
'Lasers in Material Processing'
I.F.S./Springer-Verlag, Kempston, (1986).

[4] Ready,J.F.
'Industrial Applications of Lasers'
Academic Press, New York, (1978).

[5] Duly,W.W.
'Laser Processing & Analysis of Materials'
Plenum, New York, (1983).

[6] White,C.W. & Peercy,P.S. (eds.)
'Laser & Electron Beam Processing of Materials'
Academic Press, New York, (1980).

[7] Bäuerle,D. (ed.)
'Laser Processing and Diagnostics'
Springer-Verlag, Berlin, (1984).

[8] Laude,L.D.,Bäuerle,D. & Wautelet,M. (eds.)
'Interfaces Under Laser Irradiation'
Martinus Nijhoff, Dordrecht, (1987).

[9] Ehrlich,D.J. & Nguyen,V.T. (eds.)
'Emerging Technologies for In Situ Processing'
Martinus Nijhoff, Dordrecht, (1988).

[10] Srinivasan,R. & Mayne-Bonton,V.
Appl. Phys. Lett. 41, (1982), 576.

[11] Andrew,J.E.,Dyer,P.E.,Forster,D. & Key,P.H.
Appl. Phys. Lett. 43, (1983), 717.

[12] Dyer,P.E. & Sidhu,J.
J. Appl. Phys. 57, (1985), 1420.

[13] Srinivasan,R.,Dyer,P.E. & Braren,B.
'Far-UV Laser Ablation of Cornea'
I.B.M. Research Report. RC 11620 (1985).

[14] Andrew,J.E.,Dyer,P.E.,Greenough,R.D. & Key,P.H.
Appl. Phys. Lett. 43, (1983), 1076.

[15] Key,P.H.
M.Sc. Thesis,
University of Hull, (1985).

CHAPTER ONE

LASER PROCESSING OF MATERIALS

1.0 Introduction.

1.1 Single Excimer Laser Pulse Patterning of Metal Films.

1.2 Mechanisms and Processes.

1.3 References.

1.0
INTRODUCTION

In the time since the experimental work described in this thesis was completed, a series of monographs by Bäuerle [1], Von Allmen [2] and Boyd [3] have been published which give comprehensive treatments and excellent reviews of the many and varied topics in the subject area of laser-material interactions and processing. In the light of this and the interdisciplinary nature of the use of lasers in material science, full treatment of the theoretical basis of the interactions and phenomena encountered is not attempted in this text. It is hoped that the brief descriptions and included references will suffice to give the flavour of the subject matter in the absence of the recipe.

The single laser pulse patterning of thin metal films, deposited on substrates [4,5] is reviewed in the next section. This technique, using discharge-pumped UV-excimer lasers, is limited in its application to film thicknesses of less than 3 microns. Such film thicknesses represent one of three regimes that can be identified and are distinguised by the optical and thermal properties of the metal.

The first of these regimes is 'optically thin' in which the absorption of photon energy is small and consequently a proportion of the light incident on one face is transmitted to the opposite face. These films are limited in thickness to a few nanometres in the UV, except in the case of silver at 308 nm, and when deposited on a suitably transmitting substrate may be used as attenuators. Since some absorption

does occur, care must be exercised in their use to avoid damage.

In the regime of 'optically thick - thermally thin' films, whilst photon energy is absorbed in a thin surface layer, thermal energy may be transmitted across them in the time scale of the laser pulse length. This regime represents the upper limit of thickness that can be patterned by a single laser pulse.

The final regime is represented by 'thermally thick' films which require time scales longer than the laser pulse length to attain thermal equilibrium between the two faces and thus, over the pulse length, may be considered to be semi-infinite.

It is with this latter regime and, in particular, with the laser patterning of polycrystalline copper foils some 10's of microns thick that the bulk of this thesis is concerned. Some of the mechanisms involved in laser ablation and strategies adopted for inducing and controlling material removal are reviewed in the final section.

1.1

SINGLE EXCIMER LASER PULSE PATTERNING OF METAL FILMS

As early as 1968 patterning of thin metal films on ceramic substrates was achieved by overlapping areas of ablation produced by successive Q-switched ruby laser pulses [6]. Zaleckas and Koo [7] reported the removal of thin copper films without damage to the epoxy substrates using both CO_2 and Nd:YAG lasers. Because of the high reflectivity of metals in the infrared, fluences of about 4 J cm^{-2} were needed to remove 50 nm thick films whereas the fluence requirement using UV-excimer lasers was found to be two orders lower [4,5].

Thin deposited films of copper, nickel, aluminium, gold, silver and chromium have been removed by single UV excimer laser pulse ablation from substrates of polymers, quartz, glass and aluminium [5]. Selective removal to form patterns was achieved by the projection etching technique in which the image of a remote mask is formed at the target plane and the pattern is defined where the clear areas are ablated to leave the opaque regions intact. This patterning technique is dicussed more fully in chapter 6.

For this regime of processing there exists a well defined fluence for pattern formation which is dependent upon film thickness. Below the threshold fluence no material removal is observed, whereas fluences not much greater than the threshold result in disruption of the pattern. At higher fluences substrate damage is often observed.

Calculation of the energy requirements for vaporisation of

the metal, taking into account the optical and thermal properties of the films, predicted a higher fluence for removal than the thresholds measured for each of the metal-substrate combinations investigated. The threshold fluences were observed to be close to those calculated to be required for melting and are typified by the example of Fig.1.1.1 in which the ablation thresholds for nickel films on mylar substrates are shown as a function of film thickness together with the calculated fluences for vaporisation and melting.

For copper, the reflectivities at ArF, KrF & XeCl laser wavelengths are very similar [8] so that at equal fluences approximately equal amounts of energy are absorbed at each of these wavelengths. There is, however, a factor in excess of 1.5 in the photon energy between the shortest (ArF : 193 nm) and longest (XeCl : 308 nm) of these wavelengths. The data show that the fluence requirements are independent of wavelength, Fig.1.1.2, and this would suggest that the removal is via a thermal (pyrolytic) mechanism.

It has been suggested [4] that the removal mechanism is due to a rapid transfer of absorbed energy, as heat, to the film-substrate interface in times of the order of the laser pulse length ($\tau \approx 20$ ns fwhm). The fast temperature rise at the interface leads to de-gassing or decomposition at the substrate surface resulting in the explosive removal of the metal in the liquid phase. This is further evidenced by examination of the ablated material collected on a quartz plate placed in front of the target as shown in Fig.1.1.3. Here it can be seen that the collected fragments

from the film ablation are spherical with diameters ranging from sub-micron up to ≈ 10 μm. The appearance of the fragments is characteristic of material deposited from the liquid phase. Since the film thickness was ≤ 1 μm, the large diameter fragments must have been formed either by the accretion of smaller fragments in the ablated plume or as the result of coherent removal of the film over quite large areas and the subsequent action of surface tension. It can be seen from Fig.1.1.4, which shows incomplete film removal using a fluence just below the threshold, that large area to thickness ratios of the film are involved. It can be evisaged that these areas of metal, if removed and with a little additional energy, could form a deposit of spherical structures.

The time, t, for heat to diffuse a distance, h, and establish local thermal equilibrium is discussed in the next chapter and may approximated by [9]:

$$t = h^2 / 4 D$$

where D is the thermal diffusivity. In the present case, therefore, h(τ) will represent the upper limit of metal film thickness that can be removed with a single laser pulse. For good thermal conductors such as copper h(20ns) ≈ 3 μm and it was confirmed experimentally that films thicker than this could not be patterned.

Thus the single, UV-excimer laser, pulse patterning of deposited metal films is limited to thicknesses determined by the laser pulse length and the thermal diffusivity of the metal and, furthermore, depends upon an explosive mechanism, such as degassing or decomposition, at the film-substrate

interface.

The film-substrate interface clearly plays an important role although the results obtained did not lead to any information regarding the exact nature of the removal mechanism. There was found to be no difference in in the removal theshold fluences between commercial and in-house deposited aluminium films on mylar substrates. Furthermore, no systematic differences were found between these thresholds and those measured for aluminium deposited on glass. In the latter case the glass substrates were prepared prior to deposition in two ways; degreasing with alcohol or by de-gassing for 2 hours at 500 K in vacuum. No removal of copper deposited on clean copper substrates was observed whereas patterning was achieved by ablation of copper films deposited on aluminium having a thin oxide layer at the interface.

An example, typical of this removal and patterning regime, is shown in Fig.1.1.5 in which 80 nm thick aluminium has been removed from the mylar substrate to leave a pair of conductor tracks which are the image of cross-wires in the object plane of the optical system.

A possible application of this patterning technique is in the manufacture of thin film conductor based devices such as inter-digital fingers for surface acoustic wave generation or strain gauges. One type of re-usable strain gauge consists of a thin (< 0.5 μm) gold film on a kapton substrate and this combination of materials would be suitable for single laser pulse conductor pattern generation. The majority of strain gauges manufactured,

however, are of 5 μm thick constantan alloy (50%Cu-50%Ni) with a polyimide film backing. This alloy is used because it has a very small temperature coefficient of resistance and good elastic properties when correctly heat treated. It also has a small value of thermal diffusivity such that $h(20\ ns) \approx 0.7\ \mu m$ and, therefore, cannot be patterned using the single laser ablation pulse technique.

UV-excimer lasers have been constructed with pulse lengths of the order $\tau \approx 1\ \mu s$ (fwhm) but such a device was not available for this work. If high fluences were used, in an attempt to remove the constantan via thermal evaporation, uncontrolled rupture of the metal or polyimide resulted. The use of such high fluences is, even for free-standing foils, undesirable since excess heat conduction in the direction transverse to the metal thickness can result in disruption of small pattern features or annealing in an extensive heat affected zone.

Fig.1.1.1.

SINGLE ArF (193 nm) LASER PULSE ABLATION OF NICKEL FILMS ON MYLAR SUBSTRATES.

Fluence threshold (J cm^{-2}) as a function of film thickness (μm) and calculated fluence requirements for melt and evaporation.

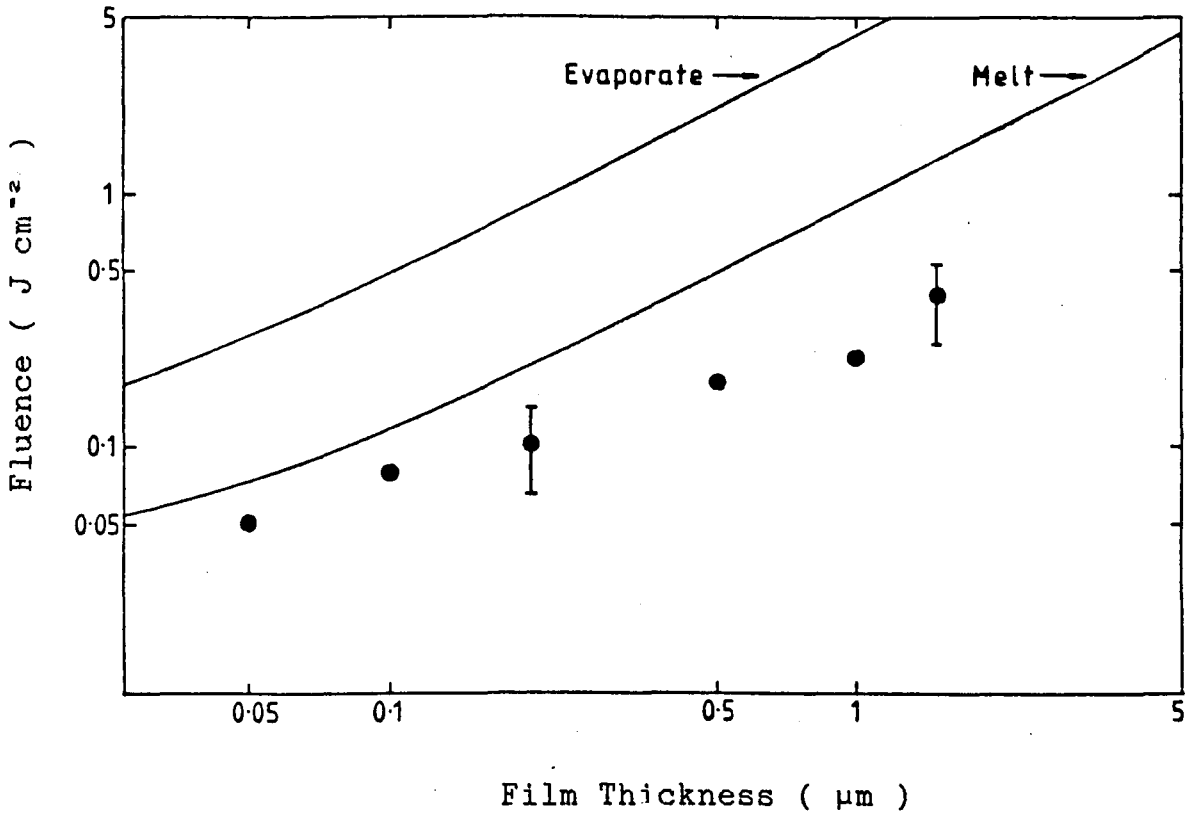

Fig.1.1.2.

SINGLE UV=EXCIMER LASER PULSE ABLATION
OF COPPER FILMS ON MYLAR SUBSTRATES.

Fluence threshold (J cm^{-2}) as a function of film thickness (μm) at ArF (193 nm), KrF (248 nm) and XeCl (308 nm) wavelengths.

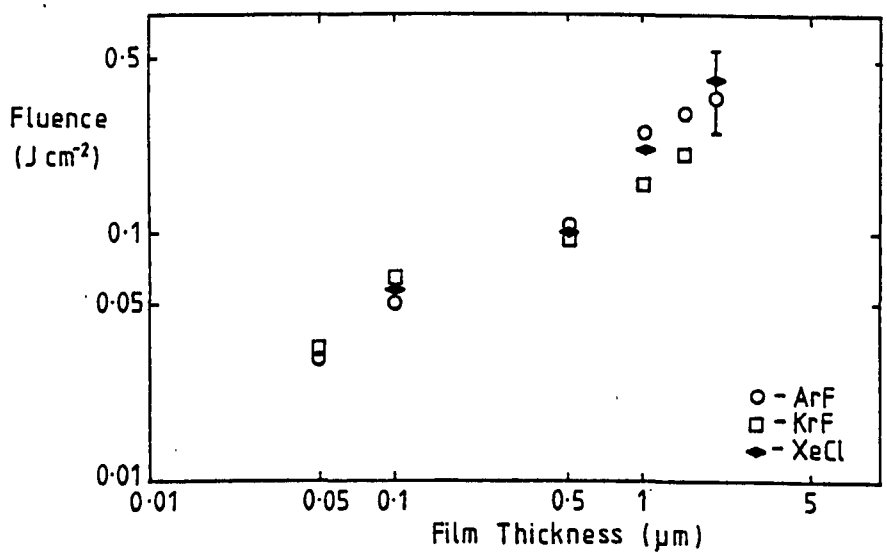

SCANNING ELECTRON MICROGRAPH (SEM)

Debris from XeCl laser ablated Al film, collected on quartz plate placed 1 cm in front of target.

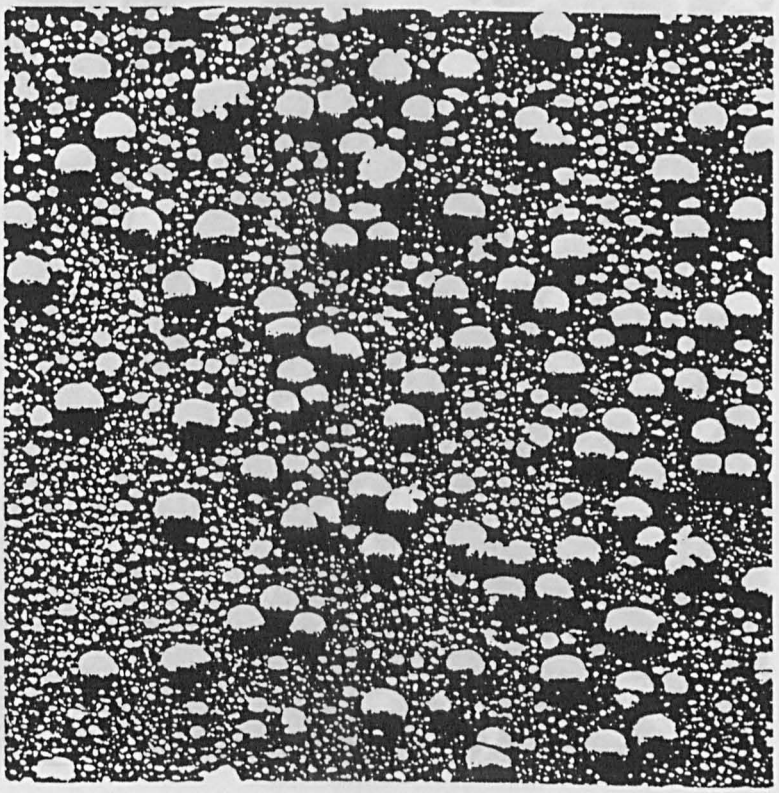

SCANNING ELECTRON MICROGRAPH (SEM)

Incomplete removal of Cr film after single, sub-threshold ArF laser pulse irradiation.

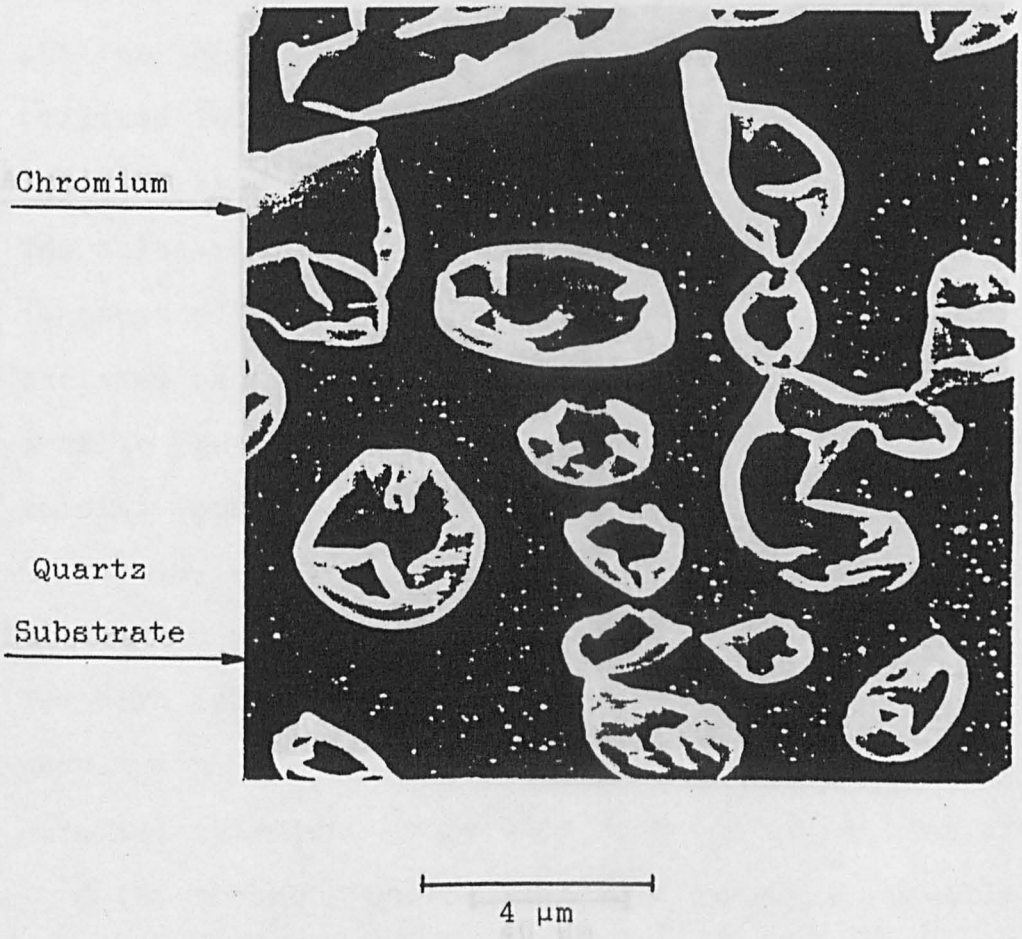

Fig.1.1.5

SCANNING ELECTRON MICROGRAPH (SEM).

Example of single, UV-excimer laser pulse patterning of aluminium film (80 nm thick) on Mylar substrate.

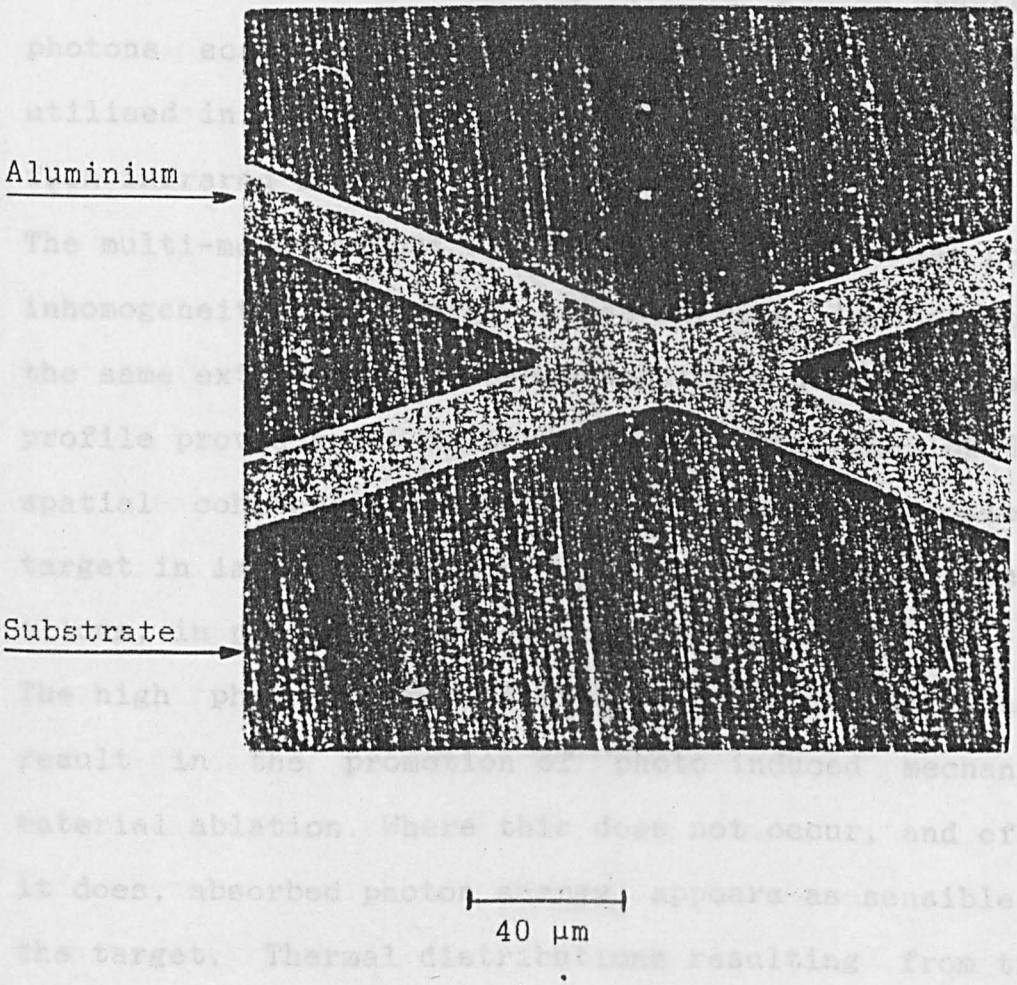

1.2

MECHANISMS AND PROCESSES

The interaction of laser light with solid surfaces starts, necessarily, with the absorption of photons; the optical properties of materials, and in particular metals, are discussed in the next chapter. The relatively low reflectivity of metals and insulators in the UV leads to the efficient coupling of excimer laser energy to the target. Furthermore, since the threshold fluence for plasma formation scales as $1/\lambda^2$ [10] and plasma absorption of photons scales as λ^2, UV radiation is more effectively utilised in interacting directly with the target than that from infrared lasers.

The multi-mode output of UV-excimer lasers does not suffer inhomogeneities of energy cross-section, ie.'hot spots', to the same extent as CO_2 lasers and their quasi 'top-hat' beam profile provides for uniform illumination. The low degree of spatial coherence essentially elliminates speckle at the target in image projection systems and the short wavelength allows, in principle, sub-micron resolution.

The high photon energy (eV's) of UV-excimer lasers can result in the promotion of photo-induced mechanisms of material ablation. Where this does not occur, and often when it does, absorbed photon energy appears as sensible heat in the target. Thermal distributions resulting from transient surface heating by pulsed lasers may be influential in the resolution attainable in pattern generation by ablation and are briefly discussed in the next chapter.

The mechanisms of laser ablation are varied and may depend upon laser power density as well as wavelength and material properties. In general, the exact mechanisms of laser induced material removal are not well understood and in many cases the distinction between photolytic and pyrolytic processes is blurred.

Some laser induced processes may exhibit a strong wavelength dependence such that a small change in wavelength produces a dis-proportionate change in yield. On the other hand, the ablation process may be initiated by the action of a photon and then proceed via a thermal route. In the case of desorption of gas or impurities from a solid surface, the photon induced excitation of the molecule may be sufficient to reduce the binding energy to the surface to a level at which it may be overcome by the thermal lattice energy. The wavelength dependence of desorption rate is usually a complex function of surface coverage and the modification of surface energy levels by the presence of other species. For pure substances the removal of intrinsic species may follow a similar route. Binary compounds may be ablated by lattice energy removal of one component following the photolytic removal of the other. Townsend [11] proposes a number of combinations of mechanisms in which photolytic processes reduce the energy requirements for removal and the momentum for ablation is supplied by the lattice energy.

In a purely thermally driven material removal regime both the reduction in binding energy and the momentum of the ejected particles must come from the sensible heat of the lattice. This implies times and distances over which

thermodynamic quantities, such as thermal conductivity, pertain and the removal process may not be as prompt as that resulting from purely photonic mechanisms.

A distinction must be made between surface and volume evaporation and, although it is assumed that both proceed from the liquid phase, a macroscopic view will allow the former to occur at the solid-vapour interface. The effect of an increase in temperature is to shift the equilibrium vapour pressure to higher values and evaporation depends upon the rate of desorption from the surface exceeding the rate of re-condensation from the vapour. The net rate of material removal, therefore, is governed by the kinetics of the desorption-adsorption mechanism. Volume evaporation requires the nucleation and growth of vapour bubbles within the liquid phase and is normally associated with liquid temperatures higher than those required for surface evaporation, i.e. superheating.

A third mechanism is that of 'hydrodynamical sputtering' in which material may be removed in the liquid phase. Here the formation of surface irregularities leads to the removal of projections as droplets being accelerated away from the surface by the combined effects of the volume change on melting followed by thermal expansion of the liquid. These thermally induced ablation phenomena have been studied in a variety of metals by Kelly and Rothenberg [12].

The removal of material from a metal surface by thermal mechanisms requires the supply of energy with a spatial profile into the bulk that will allow evaporation at the surface. For materials with low thermal diffusivities the

temperature profile into the bulk from the surface will be governed by the optical absorption coefficient. Since any material having a temperature in excess of some critical value, Tc, along the thermal gradient will be evaporated, provided that the removal is not flux limited [12], we can define an incident threshold fluence, F_t, such that the absorbed energy produces the temperature Tc at the surface as shown in Fig.1.2.1. Thus, from Beers law, the removal rate (etch depth per pulse) can be described as a function of incident fluence, F, by :

$$z = \delta \ln(F/F_t)$$

In the case of high thermal diffusivity materials where the temperature profile at some given time has the form shown in Fig.1.2.2, the relationship between removal rate and incident fluence is rather more complicated.

Fig.1.2.3 shows a comparison of the etch rate, as a function of fluence, that is to be expected from the two cases and, here, the curves have been normalised to the same threshold and etch rate at one point. Typical errors in etch-rate measurement due to a 10% uncertainty in fluence are also shown in Fig.1.2.3 and it can be seen that for $F/F_t < 5$ the two cases cannot be distinguished. In the case of the temperature profile governed by thermal diffusion there will exist a maximum depth to which heat can travel in the time scale considered and this represents the maximum removal rate that can be achieved.

In both cases, for F/F_t greater than unity, it is assumed that the surface region can achieve temperatures in excess of Tc before removal and such superheating is known to

occur [12]. However, if evaporation commences as soon as the temperature Tc is reached at the surface two complications to the simple etch rate model arise.

In the first instance the surface temperature may be 'clamped' at Tc due to the heat content of the evaporating layer being removed with the material. In this case the situation is that of continuous evaporation from a surface and the etch rate will be determined by the velocity with which the evaporation surface recedes into the bulk and the time over which the laser power density is sufficiently high. If the energy dissipated per unit area in a time interval Δt is $W \times \Delta t$, and the depth of material removed in this time is Δz, then from simple energy balance :

$$W \times \Delta t = V \times \Delta z$$

where V is the heat required to vapourise unit thickness of material. In the limit :

$$dz/dt = W/V$$

i.e. the limiting velocity of the evaporating boundary is proportional to the power density and, for metals, is approximately 1 m s^{-1} at 1 MW cm^{-2} absorbed power density so that for a 10 ns laser pulse we might expect an average removal depth of 1 micron for 1 J cm^{-2} absorbed. However, where thermal diffusivity is important, losses occur so that the evaporation controlled velocity shown above represents an upper limit to material removal rates. A model which takes losses due to thermal diffusivity into account has been developed by Andrews and Atthey [13].

The second complication is that due to the interaction between the ejected material and the incoming laser pulse

and can occur with any removal mechanism. In this case, if removal starts early in the laser pulse, the expanding plume of ablated material may absorb or scatter incoming photons and effectively block a significant portion of the laser radiation to the surface. The greater the amount of material removed early in the pulse the denser will be the plume and hence the more effective at blocking the beam. Thus the use of short laser pulses may be the most efficient removal strategy. Alternatively if the energy absorbed by the plume is re-radiated onto the surface and this energy contributes to material removal then long laser pulses may be most suitable for evaporation controlled removal.

It is clear from the foregoing discussion that the fluence threshold for removal will depend upon the thermal conditions necessary for evaporation, that is, upon the depth to which the material must be raised to the evaporation temperature. From simple energy balance considerations we can estimate F_t, for metals, to be of the order of 10 J cm^{-2} in the thermal diffusion depth case or, 0.05 J cm^{-2} if the optical absorption depth applies.

Surface damage, characterised by morphological changes or the detection of ablated material, may occur at fluences much lower than those necessary for bulk removal due to the presence of impurities at the surface. Once such contaminants have been removed from the surface and the 'clean' surface is exposed, the fluence required for removal of further material will increase to the true etching value. 'Etching', in this sense therefore, implies the removal of equal amounts of material with sucessive laser pulses.

For copper the threshold value for surface damage is seen from the literature to depend strongly on wavelength and pre-irradiation condition of the surface [14-16]. Thus the modification of the surface composition or the adsorption of contaminant species prior to irradiation can dramatically reduce the fluence requirements for ablation. This point is emphasised in the next chapter where preliminary results of the UV-excimer laser etching of bulk samples of metals are presented.

Laser induced or initiated chemical etching of materials in gaseous environments fall broadly into three categories; in the first the laser energy is instrumental in enhancing an exsiting etching process. In this case the reaction between the gas and surface is to produce a volatile compound at the ambient temperature and the role of the laser energy is to increase the reaction rate by raising the surface temperature. Such processing is of little value in practice since the etching is not arrested when the laser is off.

In the second category, the activation energy for the process is supplied by the laser. The mechanism involved may be the photolysis of the gas to produce reactive radicals in the vicinity of the surface or the photo-initiation of a surface reaction. In the former case, the illumination may be either parallel or normal to the surface. The products of the reaction may be volatile or may be removed by the influence of the laser pulse.

The final category is one in which the laser is used to remove non-volatile products of chemisorbed species at the surface. In this case the surface-gas compound forms in the

absence of laser irradiation (dark reaction) and the laser is able to remove the compound at fluences lower than would be required for ablation of the pure surface material. The dark reaction may be self limiting, as in the oxidation of aluminium, or, as will be shown to be the case in the chlorination of copper, continue via diffusion of reactants through the product layer.

Before reviewing some of the strategies reported in the literature concerning the laser-chemical etching of materials it is, perhaps, worth noting that laser induced surface chemistry, without material removal, is also of use. The growth of oxide layers on metals and semiconductors to form insulating layers or to act as etch resists has recieved particular attention. In the case of SiO_2 layers on Si, both CW [17] and pulsed [18] lasers have been sucessfully employed. The results of studies of the oxidation of copper in air using Ar^+ and Kr^+ lasers [19,20] indicated a purely thermal mechanism. In contrast, the oxidation of Niobium using a XeCl laser [21] was reported to give higher yields and better composition than when using a CO_2 laser [22]. Studies of Nd:YAG laser induced oxidation of Chromium showed the effects of laser pulse duration on patterning resolution [23,24].

Not suprisingly, a good deal of effort has been put into investigations of laser-chemical etching of semiconductors. This arises because of the desire to go to smaller feature sizes, which may be limited by the anisotropy of conventional wet etching techniques, and because of the problems of radiation and impact damage found with x-ray,

E-beam and ion beam etching.

A linear increase in the etch yield of Si in SF_6 gas with CO_2 laser pulse energy was observed by Chuang [25]. A strong wavelength dependence was found in comparing the P(22) and R(20) lines of the laser and it was concluded that the excitation of the SF_6 by the laser was a necessary step in the etching process, the thermal excitation of the substrate not contributing to the chemical reaction. Furthermore, the importance of the laser field at the interface was shown by the yield increasing by two orders of magnitude when the laser beam was normal to the surface over that with parallel illumination.

These studies were extended to the use of Ar^+ lasers [26] and high resolution etching of single and poly-crystalline Si was achieved using the Ar^+ laser and gas phase Cl_2 and HCl [27]. It was found that a higher incident power was required with HCl and etch rates were found to depend on crystallographic orientation with low laser power (< 5 W).

UV-excimer laser etching of single-crystal Si in Cl_2 by a group at Toshiba [28] found that n-type Si is etched spontaneously by photo-dissociated Cl radicals whilst p-type Si etching proceeds only at the irradiated surface. In both cases the etch rate depends upon crystal orientation. The same group have also shown that similar results may be obtained using a non-laser UV source [29].

Mechanistic studies [30], using time-of-flight mass spectroscopy measurements, of desorbed species from UV-excimer laser etching of Si in Cl_2 gas as a function of pressure lead to the conclusion that the main desorption

process is that of evaporation. In contrast Kullmer and Bäuerle [31] distinguish between a low fluence (<0.1 J cm^{-2}) non-thermal regime and a high fluence (>0.44 J cm^{-2}) regime involving surface melting and thermally activated etching using pulsed KrF lasers.

The photolysis of methyl-halides (CH_3Br or CF_3I), using a frequency doubled Ar^+ laser (257.2 nm), has been used to produce localised photo-etching of GaAs and InP with etch-rates $> 10^4$ times that of the dark reaction [32]. Ar^+ at 514.5 nm was used with CCl_4, Cl_2 and $SiCl_4$ gases to etch fine lines in GaAs [33].

UV-excimer laser (193 nm) etching of single-crystal GaAs in CF_3Br, CH_3Br, CF_3Cl and CH_3Cl required a heated substrate to aid removal of the gas-surface products [34]. A comparison of normal incidence and parallel illumination at this wavelength showed that the laser-surface interaction is an important aspect of the etching of GaAs in HBr [35]. With the KrF laser, Koren and Hurst found that efficient etching of GaAs in a Cl_2 environment was possible, whereas in O_3 a thick oxide layer was formed [36]. The etching of GaAs in aqueous solutions has also been shown to be enhanced by laser illumination [37-39].

Mono-crystalline diamond and diamond-like films of hard carbon have been etched using an ArF laser [40]. Cl_2, NO_2 and NH_3 gasses at pressures up to 1000 torr were used to optimise the process.

Relatively little work has been done on the laser-chemical etching of metals since the thickness of deposited films used in micro-electronics applications can be readily

processed using the single UV-excimer laser pulse technique described earlier.

Ar^+ laser etching of Al films in aqueous solutions has shown laser enhancement of etch rates of the order of 3.5 and produces clean, debris-free results [41]. The main etching mechanism for Al films in Cl_2 gas and under XeCl laser irradiation was found to be the ablation of aluminium chloride layers formed between laser pulses [42,43]. The chlorination reaction and frequency-doubled (532 nm) Nd:YAG laser stimulated desorption from Ag film surfaces has been studied in some detail by Sesselmann & Chuang [44].

Etching of thin (2 μm) films of copper in low pressure ($\approx 5x10^{-6}$ torr) Cl_2 and using a UV-excimer laser has been studied by Sesselmann et al. [45] who deduce that the desorption is not a simple evaporation process.

Tungsten foils some 150 μm thick have been etched in air using an Ar^+ laser [46] and here it is reported that the mechanism is via the rapid oxidation of W to WO_3 which volatalises readily. The ArF laser photolysis of NF_3 to produce F atoms has been employed in the etching of thin Mo and Ti films on SiO_2 substrates [47].

The main work presented here, in chapters 3 & 4, is concerned with the UV-excimer laser etching of copper foils in a relatively high pressure chlorine environment and therefore represents a regime of processing not previously investigated.

Fig.1.2. 1.

TEMPERATURE DISTRIBUTION MODEL

Temperature profile for optical absorption type distribution.

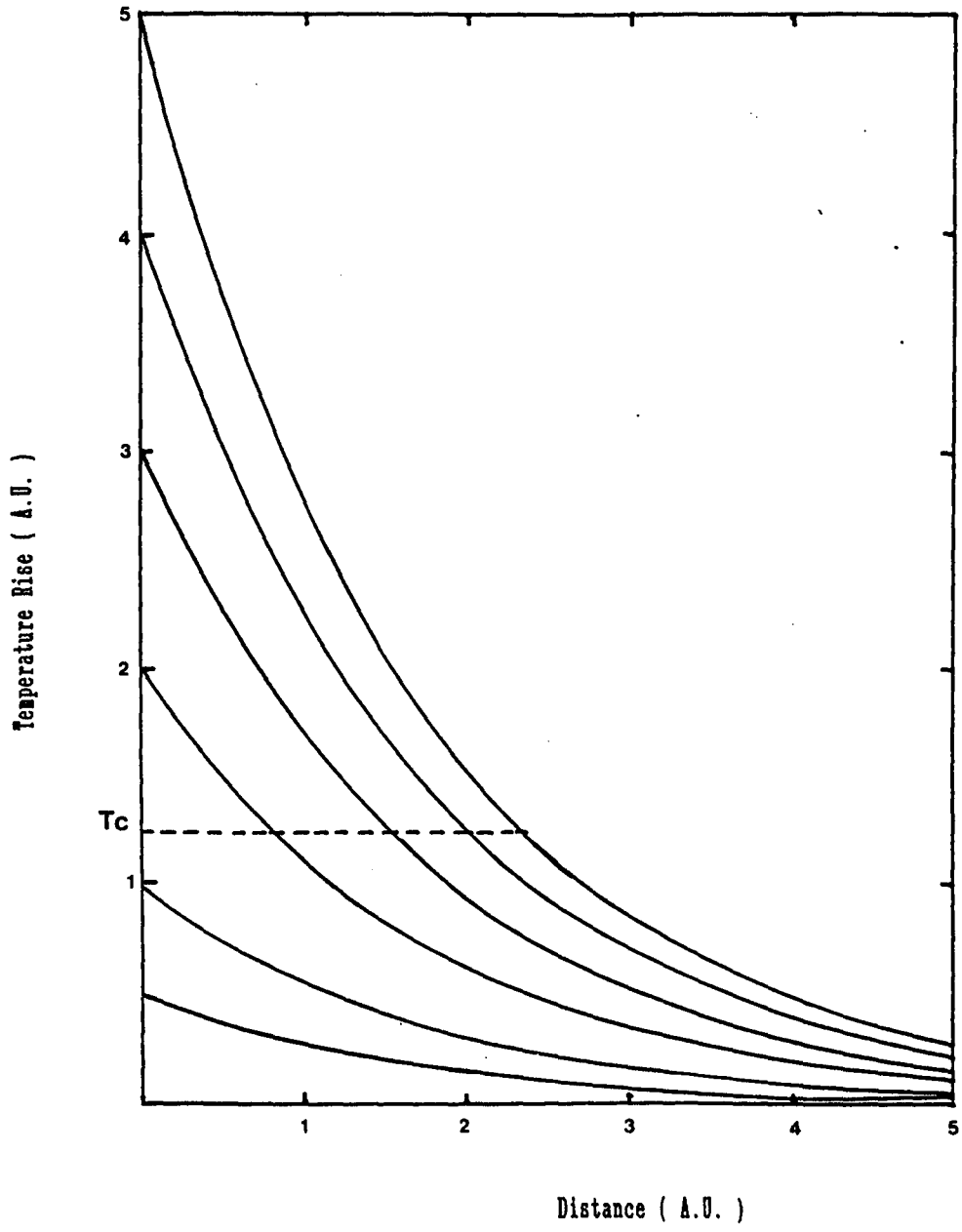

Fig.1.2. 2.

TEMPERATURE DISTRIBUTION MODEL

Temperature profile for high thermal diffusivity type distribution.

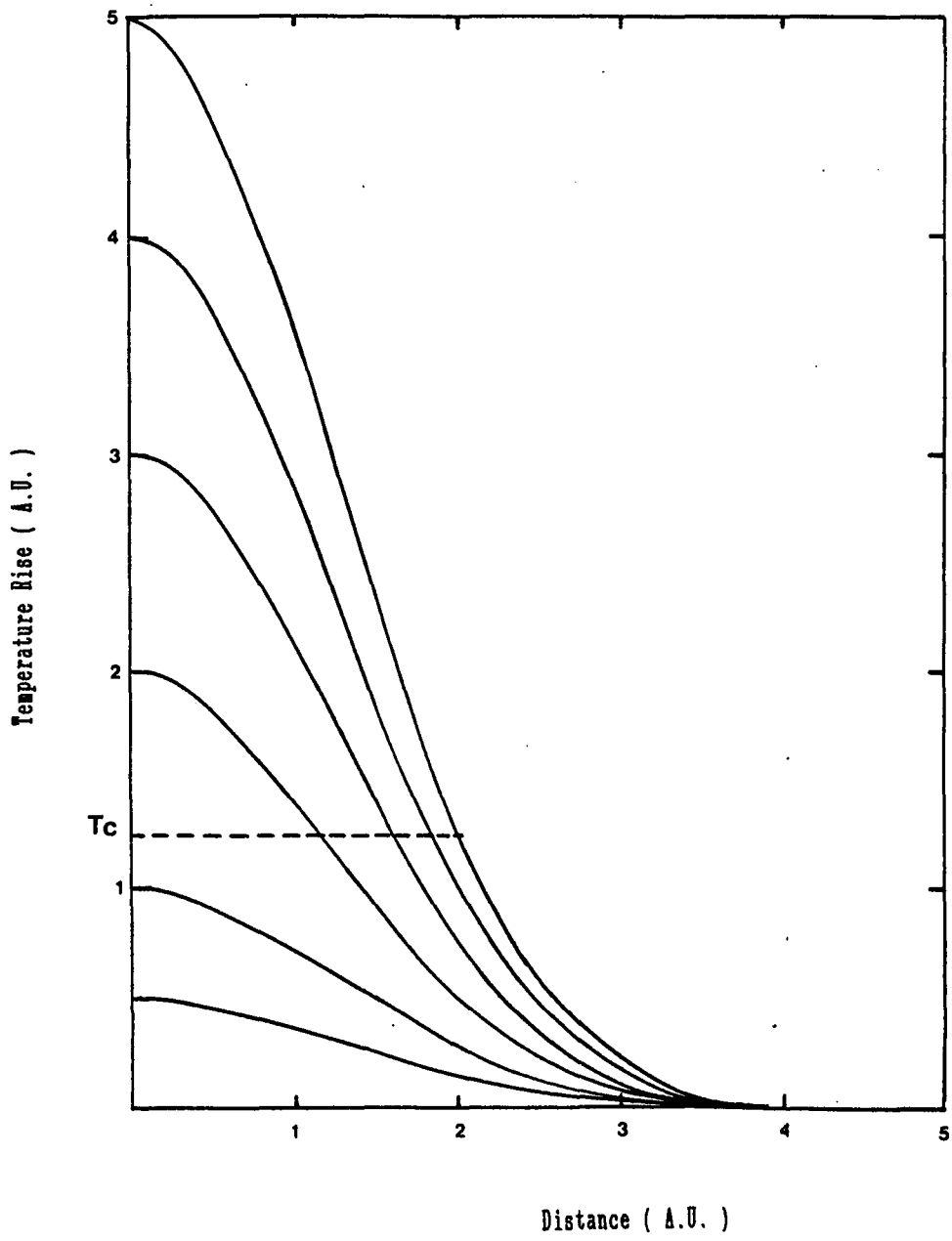

Fig.1.2.3.

OPTICAL & THERMAL MODEL ETCH RATES

Etch yield as a function of fluence showing similarity of curves for optical and thermal distributions of absorbed fluence for F/Ft < 5.

ΔY errors due to 10% error in F.

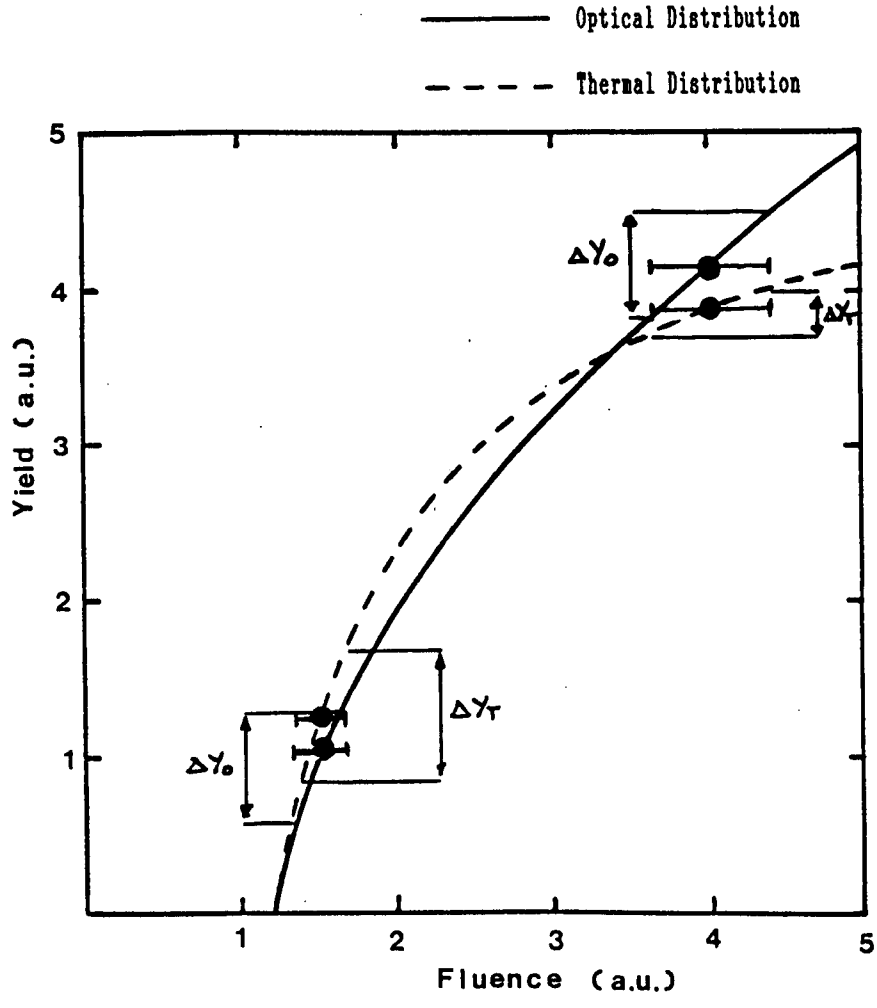

1.3.

REFERENCES

[1] Bäuerle,D.
'Chemical Processing with Lasers'
Springer-Verlag, Berlin, (1986).

[2] Von Allmen,M.
'Laser Beam Interactions with Materials'
Springer-Verlag, Berlin, (1987).

[3] Boyd,I.W.
'Laser Processing of Thin Films & Microstructures'
Springer-Verlag, Berlin, (1987).

[4] Andrew,J.E.,Dyer,P.E.,Greenough,R.D. & Key,P.H.
Appl. Phys. Lett. 43, (1983), 1076.

[5] Key,P.H.
M.Sc. Thesis, University of Hull, (1985).

[6] Cohen,M.I.,Unger,B.A. & Milkosky,J.F.
Bell System Tech. J., 47, (1968), 385.

[7] Zaleckas,V.J. & Koo,J.C.
Appl. Phys. Lett. 31, (1977), 615.

[8] Weaver,J.H.,Krafka,C., Lynch,D.W. & Koch,E.E.
'Optical Properties of Metals', 2 Vols.
Fachinformationszentrum, (1981).

[9] Ready,J.F.
'Effects of High-Power Laser Radiation'
Academic Press, New York, (1971).

[10] Boni,A.A. & Meskan,D.A.
Optics Comm. 14, (1975), 115

[11] Townsend,P.D.

Surf. Sci. 90, (1979), 256.

[12] Kelly,R. & Rothenberg,J.E.

Nucl. Instr. & Meth. B7/8, (1985), 755.

[13] Andrews,J.G. & Atthey,D.R.

'Mathematical Modelling', eds. Andrews & McLone.

Butterworths, London, (1976).

[14] Ageev,V.P., Garbunov,A.A., et al.

Sov. J. Kvant. Elektron., 13, (1983), 954.

[15] Hussla,I. & Viswanathan,R.

Surf. Sci. 145, (1984), L488.

[16] Ursu.I.,Apostol,I. et al.

J. Phys. D., Appl. Phys., 17, (1984), 709.

[17] Boyd,I.W. & Wilson,J.I.B.

Appl. Phys. Lett. 41, (1982), 162.

[18] Orlowski,T.E. & Richter,H.

Appl. Phys. Lett. 45, (1984), 241.

[19] Andrew,R.

J. Appl. Phys. B, 41, (1986), 205.

[20] Andrew,R., Baufay,L.,Pigeolet,A. & Wautelet,M.

Mat. Res. Soc. Symp. Proc. 17, (1983), 283.

[21] Marks,R.F. & Pollak,R.A.

J. Chem. Phys. 81, (1984), 1019.

[22] Marks,R.F.,Pollak,R.A.,Avouris,P.,Lin,C.T.,Thefaire,Y.

J. Chem. Phys. 78, (1983), 4270.

[23] Metev,S.M.,Savtchenko,S.K. et al.

IEEE J. Quant. Electron. QE14, (1981), 2004.

[24] Gerassimov,R.B.,Metev,S.M. & Savtchenko,S.K.

J. Phys. D, Appl. Phys. 17, (1984), 1671.

[25] Chuang,T.J.

J. Chem. Phys. 72, (1980) 6303.

[26] Chuang.T.J.

IBM J. Res. & Develop. 26, (1982), 145

[27] Ehrlich,D.J.,Osgood,R.M. & Deutsch,T.F.

Appl. Phys. Lett. 33, (1981), 1018.

[28] Arikado,T.,Sekine,M.,Okano,H. & Horike,Y.

Mat. Res. Soc. Symp. Proc. 29, (1984), 167.

[29] Okano,H.,Horike,Y. & Sekine,M.

Jap. J. Appl. Phys. 24, (1985), 68.

[30] Baller,T.,Oostra,D.J.,de Vries,A.E. & van Veen,G.N.A.

J. Appl. Phys. 60, (1986), 2321.

[31] Kullmer,R. & Bäuerle,D.

Appl. Phys. A, 43, (1987), 227.

[32] Ehrlich,D.J.,Osgood,R.M. & Deutsch,T.F.

Appl. Phys. Lett. 36, (1980), 689.

[33] Takai,M,Tsuchimoto,J.,Nakai,H.,Gamo,K.,& Nambas,K.

Jap. J. Appl. Phys. 23, (1984), L852.

[34] Brewer,P.D.,Halle,S. & Osgood,R.M.

Mat. Res. Soc. Symp. Proc. 29, (1984), 179.

[35] Brewer,P.D.,McClure,D. & Osgood,R.M.

Appl. Phys. Lett. 47, (1985), 310.

[36] Koren,G. & Hurst,J.E.

Appl. Phys. A. 45, (1988), 301.

[37] Osgood,R.M.,Sanchez-Rubio,A.,Ehrlich,D.J. & Doneu,V.

Appl. Phys. Lett. 40, (1982), 391.

[38] Podlesnik,D.V.,Gilgen,H.H. & Osgood,R.M.

Appl. Phys. Lett. 43, (1983), 1083.

[39] Podlesnik,D.V.,Gilgen,H.H. & Osgood,R.M.
Appl. Phys. Lett. 45, (1984), 563.

[40] Rothschild,M.,Arnone,C. & Ehrlich,D.J.
J. Vac. Sci. Technol. B. 4, (1986), 310.

[41] Tsao,J.Y. & Ehrlich,D.J.
Appl. Phys. Lett. 43, (1983), 146.

[42] Koren,G.,Ho,F. & Ritsko,J.J.
Appl. Phys. Lett. 46, (1985), 1006

[43] Koren,G.,Ho,F. & Ritsko,J.J.
J. Appl. Phys. A. 40, (1986),13.

[44] Sesselmann,W. & Chuang,T.J.
Surf. Sci. 162, (1985),1007.

[45] Sesselmann,W.,Marinero,E.E. & Chuang,T.J.
J. Appl. Phys. A. 41, (1986), 209.

[46] Koren,G.
J. Appl. Phys. A. 40, (1986), 215.

[47] Loper,G.L. & Tabat,M.D.
Appl. Phys. Lett. 46, (1985), 654.

CHAPTER TWO

MULTIPULSE ETCHING OF MATERIALS

2.0
INTRODUCTION

It was seen in the last chapter that the absorption of laser radiation at a solid surface can lead to the removal of material. The strategy adopted for etching will depend upon the properties of the material and the choice of a suitable laser. The modification of the surface composition by a chemical step during the process can dramatically change the optical and thermal properties of the target and allow etching to proceed at fluences much lower than required for simple evaporation of the solid.

The proportion of incident energy that is absorbed by the target and the depth to which that absorption occurs are effectively defined by the optical constants of the material. An outline of the optical properties of materials is given in the next section. Some of the effects of optical properties on the ablation process are discussed.

In the second section the thermalisation of the absorbed photon energy and the distribution of heat by thermal conduction, in particular over the time-scale of the laser pulse, is discussed. Some measurements of thermal transients in thin metal foils are compared with computed results from a one-dimensional heat transfer model. The measurement of the thermal diffusivity of the layer formed by the chlorination of copper is described.

Preliminary results of UV-excimer laser etching of metals and the effects of surface contamination by environmental gases are presented in the final section.

2.1
OPTICAL PROPERTIES

The optical properties of a material are described by the constants n and k which are in fact only constant for any given wavelength at a fixed temperature. The constants are generally combined in the form :

$$N = n - jk$$

where N is the so called 'complex refractive index'. This is, of course, a misnomer since the term 'refractive index' refers specifically to the ratio of two velocities which, therefore, must be a real number.

The wave equation, derived from Maxwells equations, can be shown [1] to have a solution which describes the variation, in time and space, of the electric or magnetic field vectors, U, of a plane, monochromatic wave of frequency, w, in a medium as:

$$U = Uo \exp[-j(wt-nqz)] \exp[-kqz]$$

where q=w/c, the wavevector in free-space, and z represents the position in the direction of propagation for the one-dimensional case.

Thus n represents the ratio of phase velocity in the medium to that in free-space and k represents the attenuation of the amplitude such that the field vector, U, is damped by a fraction exp[-2πk] per free-space wavelength, λ.

At the air-surface interface, N may be substituted into the usual Fresnel expressions so that the normal incidence amplitude reflection coefficient, r, may be written as:

$$r = (1-n+jk) / (1+n-jk)$$

The reflectance, R, of power, at the surface is found by multiplying the expression for r by its compex conjugate and hence:

$$R = [(1-n)^2 + k^2] / [(1+n)^2 + k^2]$$

In the pulsed laser case it is more usual to consider the energy and, unless the product kz is small enough to allow transmission, the energy is absorbed such that :

$$Ea = Ei\ (1-R)$$

with Ei and Ea representing the incident and absorbed energies respectively. The absorption occurs over a distance characterised by:

$$\delta = \lambda / 4\pi k$$

where δ is the distance into the medium at which the energy has fallen to 1/e of its value at the surface. Thus 98% of the energy has been absorbed at a distance of 4δ.

The values of n and k can vary considerably with wavelength [2]. For metals in the IR region of the spectrum k is much greater than n, typical values being $n \approx 1$, $k \approx 10$ so that k is dominant and R approaches unity; hence the use of metal for mirrors. In the visible, with the exception of some 'coloured' metals, the ratio $k/n \approx 2.5$ and R is still quite large. In the UV region n and k tend to be approximately equal and in the range 1.5 - 2.0 so that, for normal incidence, $R \approx 0.4$ and δ is typically $\approx$ 10nm. The reflectivities, as a function of wavelength, of some common metals are shown in Fig.2.1.1.

It is interesting to note that for copper in the UV, shown in Fig.2.1.2, there is a local minimum in R at 280 nm and a local maximum at 220 nm and that at the three excimer

wavelengths of 308 nm (XeCl), 248 nm (KrF) and 193 nm (ArF) the reflectivity is approximately constant at 0.35.

It may be appropriate to consider whether this fact might be exploited towards determining the mechanisms of laser induced processes. We will not specify the process, which may be etching, deposition, diffusion or annealing etc., but refer to the quantifiable end result as the yield. Since the reflectivity is the same in each case then equal energies will be absorbed for a given fluence but the number of photons involved will be different.

In a purely pyrolytic process we might expect the yield to depend only on the total energy absorbed, for equal pulse lengths, and hence be independent of wavelength. If the process depends on the number of photons absorbed (photolytic), and is independent of their energy, then there should be an increase in yield with increasing wavelength. However the absorption depth is wavelength dependent and if the process requires a given photon density then this will mitigate against the longer wavelength. This factor may also be important for the pyrolytic case; however for metals, the thermal energy distribution may not be too dependent upon the initial optical absorption depth.

Where processes require a minimum photon energy there may be a marked difference in yield between the long and short wavelength cases. This does not, however, take account of multiphoton absorption processes the probability of which, for either coherent or stepwise excitation, is known to be higher for short, intense laser pulses and is diminishingly small at low irradiance levels.

Direct evidence of the processing mechanism is, therefore, difficult to obtain from a simple comparison of yields; it is, however, possible to obtain evidence of photonic enhancement in some processes [3].

UV absorption processes in solids involve the interaction of photons with electrons and both macroscopic and microscopic theories of the electronic transitions associated with absorption over a wide range of optical frequencies in metals, semiconductors and insulators are discussed by Abeles [4] and Hodgson [5].

Electron transitions associated with photon absorption may, generally, be considered to occur within partially filled energy bands (intraband transitions) and between energy bands (interband transitions). In many materials the intraband transitions allow absorption of radiation down to zero frequency whereas interband transitions have specific minimum energy requirements; the contributions of interband and intraband transitions are additive in the absorption spectrum. Thus at long wavelengths the absorption, though often small, is dominated by intraband transitions and exhibits a continuum of the absorption spectrum, the optical constants vary little with wavelength.

As the wavelength decreases interband transitions become more important and structure in the curves of optical constants as a function of wavelength is observed. We might thus expect to find greater sensitivity of the optical constants in the UV to perturbations in the band structure due to defects, impurities, or in the case of compounds, changes in composition.

The optical constants of CuO and Cu_2O exhibit this behaviour as shown in Fig.2.1.3 (reproduced from the work of Karlsson et al [6]). A phenomenon similar to this will be seen to be important in chapters 4 and 5 where measurements using a visible wavelength to monitor the growth of a chloride layer on copper are found to be little affected by the stoichiometry of the compound whereas changes in the optical properties in the UV are found to influence ablation rates.

Fig.2.1.1.

NORMAL INCIDENCE REFLECTIVITY OF SELECTED METALS AS A FUNCTION OF WAVELENGTH

Calculated from data in [2]

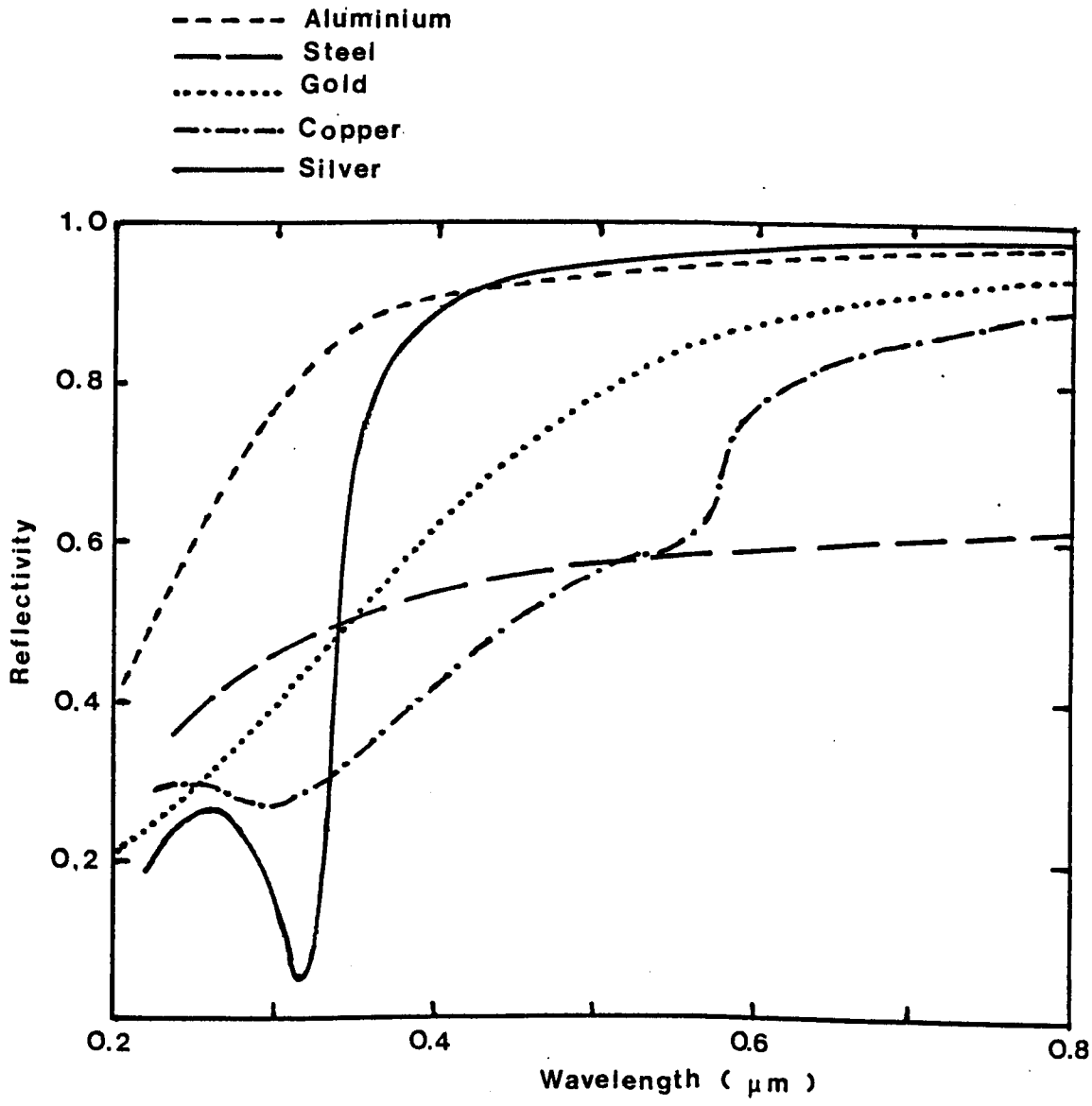

Fig.2.1.2.

REFLECTIVITY OF COPPER AS A FUNCTION
OF WAVELENGTH IN UV-EXCIMER REGION.

Calculated from data in [2]

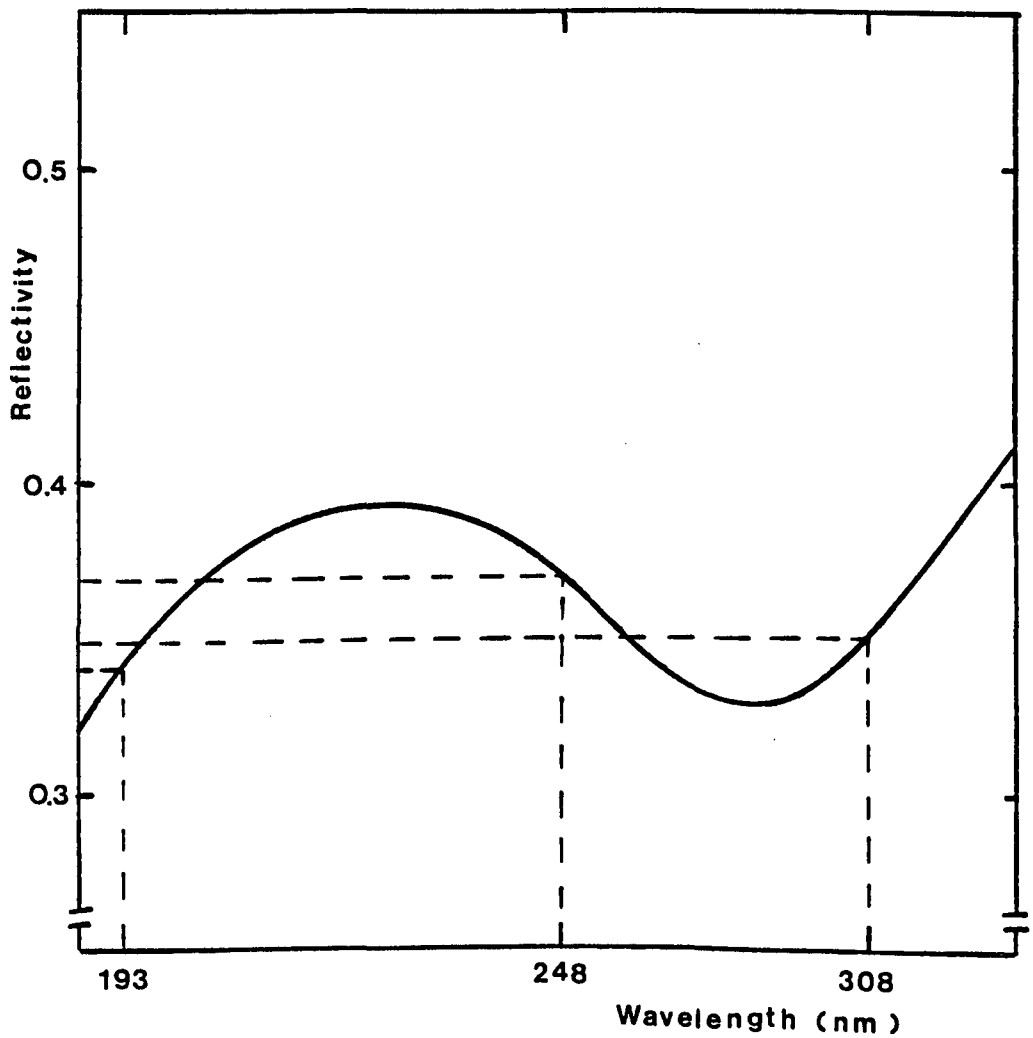

Fig.2.1.3.

THE OPTICAL CONSTANTS (n and k) of
COPPER OXIDES AS A FUNCTION OF WAVELENGTH

From Karlsson et. al. [5]

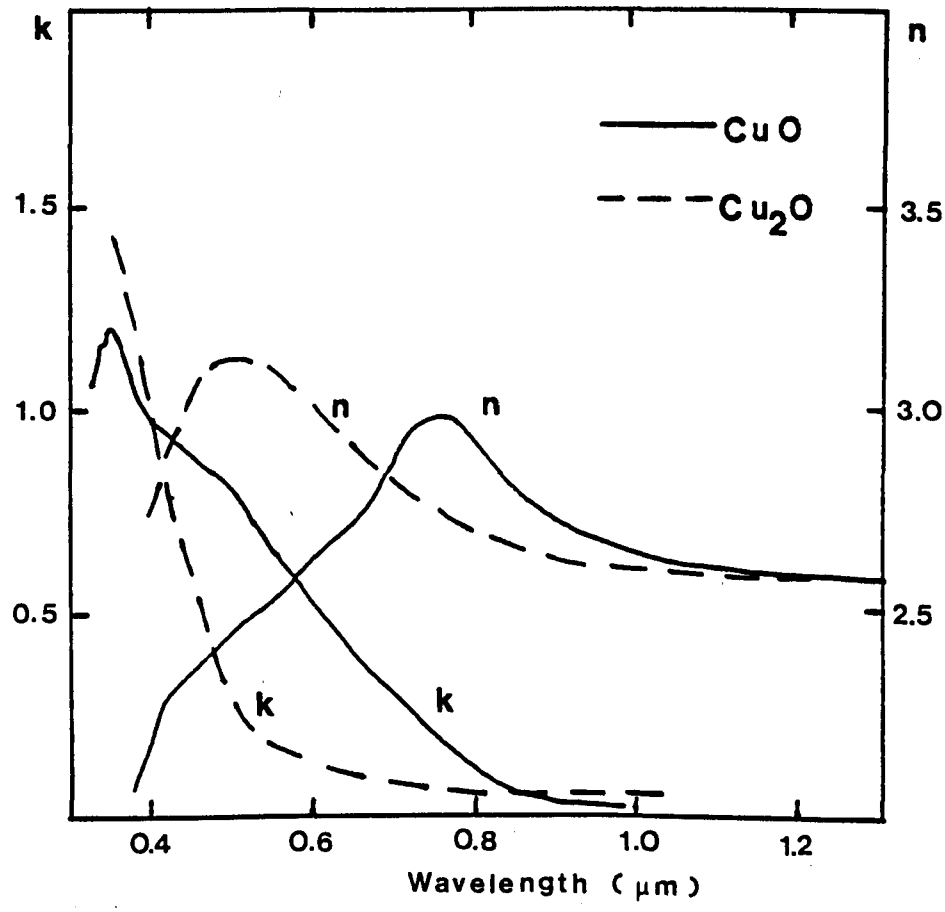

2.2
THERMAL CONSIDERATIONS

The excitation of electrons by the absorption of photon energy may lead directly to the removal of material as was seen in the last chapter. In the absence of any such mechanism, the excitation energy of the electron is transferred, via scattering processes, to ultimately appear as sensible heat in the lattice. Temperature rises can be large and rapid under pulsed laser irradiation conditions and result in thermally driven material removal. Whatever the ablative mechanism, photolytic or pyrolytic, it is unlikely for all of the absorbed energy to go into the material being removed and the excess is left to be dissipated by heat diffusion from the irradiated zone.

Heating, at rates lower than required for material removal, can have undesirable effects on the surrounding material and result in the perturbation of patterning capabilities, heat treatment or dopant diffusion. In this section some of the time scales and distances involved in the thermalisation of photon energy and the heat distribution resulting from thermal transport within the solid are discussed.

The characteristic time over which electrons transfer energy through collisions is called the relaxation time, t_r, and is given [7] by :

$$t_r = m\sigma / Ne^2$$

where m, N and e are the effective electron mass, electron density and charge respectively and σ is the conductivity.

The thermal diffusivity, D, of a material is the ratio of

thermal conductivity to its thermal mass :

$$D = K / C$$

where C is the heat capacity (specific heat x density).

Since thermal transport occurs over a finite time, thermal gradients may exist in a solid for significant periods. The thermal diffusion length, h, is given for a one-dimensioal geometry by [8]:

$$h = \sqrt{4Dt}$$

representing a 'thermal horizon' as the distance over which heat diffuses in time, t. Consequently t represents the time taken for a thin film, of thickness h and heated on one face, to approach thermal equilibrium.

Substituting the typical value of $t_r \approx 10^{-14}$ s for t we find that, for a good conductor with $D \approx 10^{-4}$ m^2 s^{-1}, $h \approx 2$ nm which is approximately an order of magnitude smaller than the UV absorption depth, δ. Thus the temperature excursion of an irradiated metal should have an 'instantaneous' spatial profile following that of the photon absorption i.e. falling exponentially into the material. The laser pulse, however, is of a finite duration so that photons are delivered to the target over a time $\tau \approx 10$ ns (f.w.h.m) for a typical discharge pumped excimer laser. Over this time scale the heat diffusion is of the order of 2 microns, two orders of magnitude greater than δ.

Calculations of the surface temperature during the laser pulse are further complicated by the temperature dependencies of both the optical and thermal properties of the target. The increase in the optical absorption of metals at elevated temperatures induced by UV laser pulses has been

examined in a previous work [9]. The relationship between the optical constants and temperature has been enumerated by Ujihara [10] for the intraband absorption region and the measurement of changes in IR laser reflectivity has been reported in the literature [11,12].

A number of schemes have been devised which give analytical or numerical solutions to the laser heating problem for both pulsed and cw irradiation [8,13-16]

For thin samples and the one-dimensional case, which is applicable when the dimensions of the irradiated area are much greater than the thickness, the thermal distribution in time and space following the laser pulse may be readily evaluated. The purpose of the scheme presented here is to allow experimental determination of the thermal properties of irradiated material and to evaluate the extent to which temperature excursions outside of the irradiated zone will effect the spatial resolution of thermally induced patterning processes.

The temperature, T, at any position, h, and time, t, in the material can be found from a suitable solution to the heat conduction equation [17] :

$$\partial^2 T/\partial h^2 - 1/D \; T/\partial t = -Q(t)/K$$

where Q(t) is the source function.

Assuming that the deposited laser energy corresponds to a heat source of thickness, g, being either the optical absorption depth or heat diffusion depth at the end of the laser pulse, and is much smaller than the thickness of the sample, H, then the initial conditions are :

$$T\,(h,0) = 0 \qquad \text{for } h > g$$

and $T(h,0) = F / Cg$ for $h < g$

where F is the absorbed laser fluence.

The subsequent temperature distribution is shown by Carslaw and Jaeger [17] to be described by a solution to the heat conduction equation of the form:

$$T(h,t) = F/CH \{ 1+2 \sum_{n=1}^{\infty} \text{Cos} [(n\pi h/H) \text{Sin}(n\pi g/H)/(n\pi g/H)] \text{Exp}[-n^2\pi^2 Dt/H^2]\}$$

assuming no other heat losses and applying the initial conditions given above.

An example of T plotted as a function of time for a typical metal is shown in Fig.2.2.1. The summation converges rapidly and thus for small values of n (10 say) and g/H we can make the approximation Sin (A) ≈ A and write :

$$T(h,t) = F/CH \{ 1+2 \sum_{n=1}^{n=10} \text{Cos} (n\pi h/H) \text{Exp}[-n^2\pi^2 Dt/H^2] \}$$

and at the rear face of the sample, where h=H, the equation reduces to :

$$T(H,t) = F/CH \{ 1+2 \sum_{n=1}^{n=10} (-1)^n \text{Exp}[-n^2\pi^2 Dt/H^2] \}$$

Experiments were performed to monitor the rear face temperature excursions of thin metal foils under XeCl (308 nm, 10 ns) laser irradiation. In the case of a 50 μm thick copper sample we expect the rear face to reach its maximum temperature after approximately 5 μs. In practice this is a rather short time scale over which to measure temperature rises by usual thermocouple techniques. The

smallest commercially available thermocouples have weld bead junctions some 50 μm diameter and the rise time is, at best, two orders of magnitude greater than required. The experimental technique adopted was to make the sample foil one half of the thermocouple junction and to complete the circuit with a fine wire of dissimilar metal in contact on the rear face in the centre of the irradiated zone as shown in Fig.2.2.2. Transverse heat flow could also be monitored with this arrangement by translating the laser beam with respect to the position of the junction.

Oscilloscope triggering was achieved by means of a fast photodiode picking up reflected laser light from the surface of the target and a typical trace is shown in Fig.2.2.3. It can be seen that the shape and time scale of the measured thermal excursion are consistent with those predicted by the model for a 25 μm thick copper foil and shown in Fig.2.2.4. Parker et al. [18] have suggested that rear face temperature measurements may be used to determine the thermal diffusivity of thin samples and that the method more satisfactorily matches the actual and theoretical boundary conditions than the conventional insulated rod technique.

Calibration of the thermocouple is rendered unnecessary by normalising the temperature-time curve to the maximum temperature, Tm, of the rear face :

$$X = T / Tm$$

and, by making the substitution $W = \pi^2 Dt / H^2$ we can write:

$$X = 1+2 \sum_{n=1}^{n=10} (-1)^n \, Exp[-n^2 W]$$

Fig.2.2.5 shows the normalised temperature plotted as a function of W. It can be seen that when X=0.5, W=1.38 and therefore by measuring the time, t´, at which the temperature reaches half of its maximum value and from the known thickness of the sample the thermal diffusivity can be calculated as:

$$D = 1.38\ H^2 / \pi^2\ t'$$

Using this technique the thermal diffusivity of CuCl, grown as a 1.3 μm thick layer on the surface of the copper by the method described in chapter 3, was measured. The signal trace is shown in Fig.2.2.6 from which the thermal diffusivity is calculated to be $\approx 7.5 \times 10^{-6}\ m^2\ s^{-1}$.

The transverse heat flow in foil targets was also measured and, for time scales greater than the time required for thermal equilibrium to be established across the thickness of the target, the one-dimensional heat flow model was found to be applicable. The transverse temperature distribution at the end of each laser pulse, which effectively defines the heat removal from the irradiated zone, is an important consideration in high pulse repetition frequency processes. Cumulative heating leading to high average temperatures in the irradiated zone and for significant distances in the transverse direction may limit pattern edge resolution. Typical thermocouple signals, showing the development of the quasi-steady state or background temperature, are shown for a number of prf conditions in Fig.2.2.7. The average temperature as a function of laser power density at the target is shown in Fig.2.2.8.

Fig.2.2.1.

TEMPERATURE-TIME PROFILE IN COPPER FOIL

Temperature at various distances from transiently heated surface of 10 μm thick foil as a function of time. 1-D heat flow.

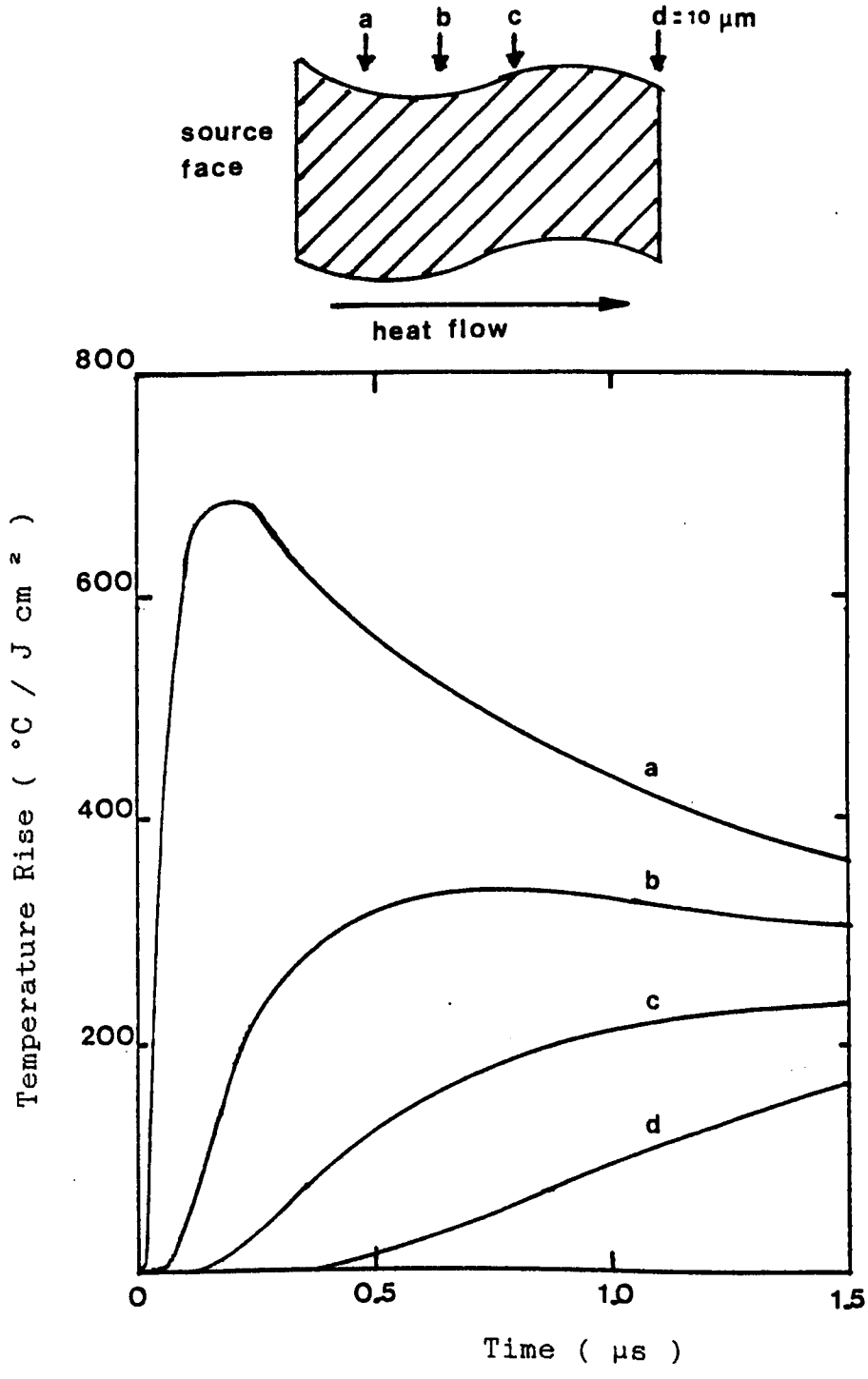

Fig.2.2.2.

FLASH THERMAL DIFFUSIVITY MEASUREMENT

Experimental arrangement.

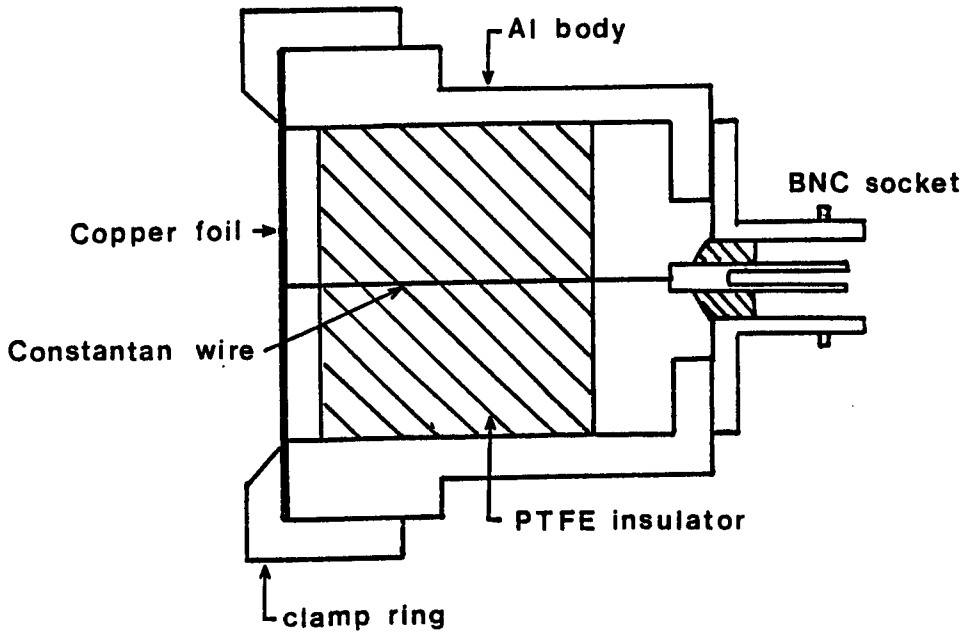

Fig.2.2.3.

TEMPERATURE OF REAR OF COPPER FOIL

Measured Temperature as a function of Time following 15 ns XeCl laser irradiation. Oxide free, 25 μm thick copper foil.

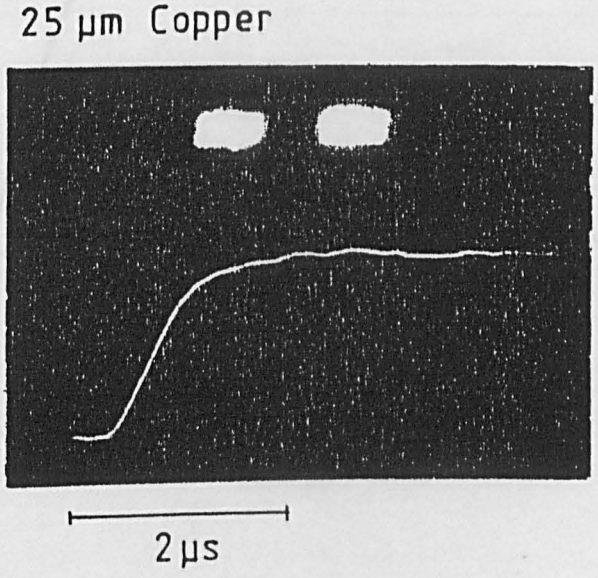

Fig.2.2.4.

MODEL TEMPERATURE OF REAR OF COPPER FOIL

Calculated temperature as a function of
Time following irradiation of front face.
One-dimensional heat flow calculation.

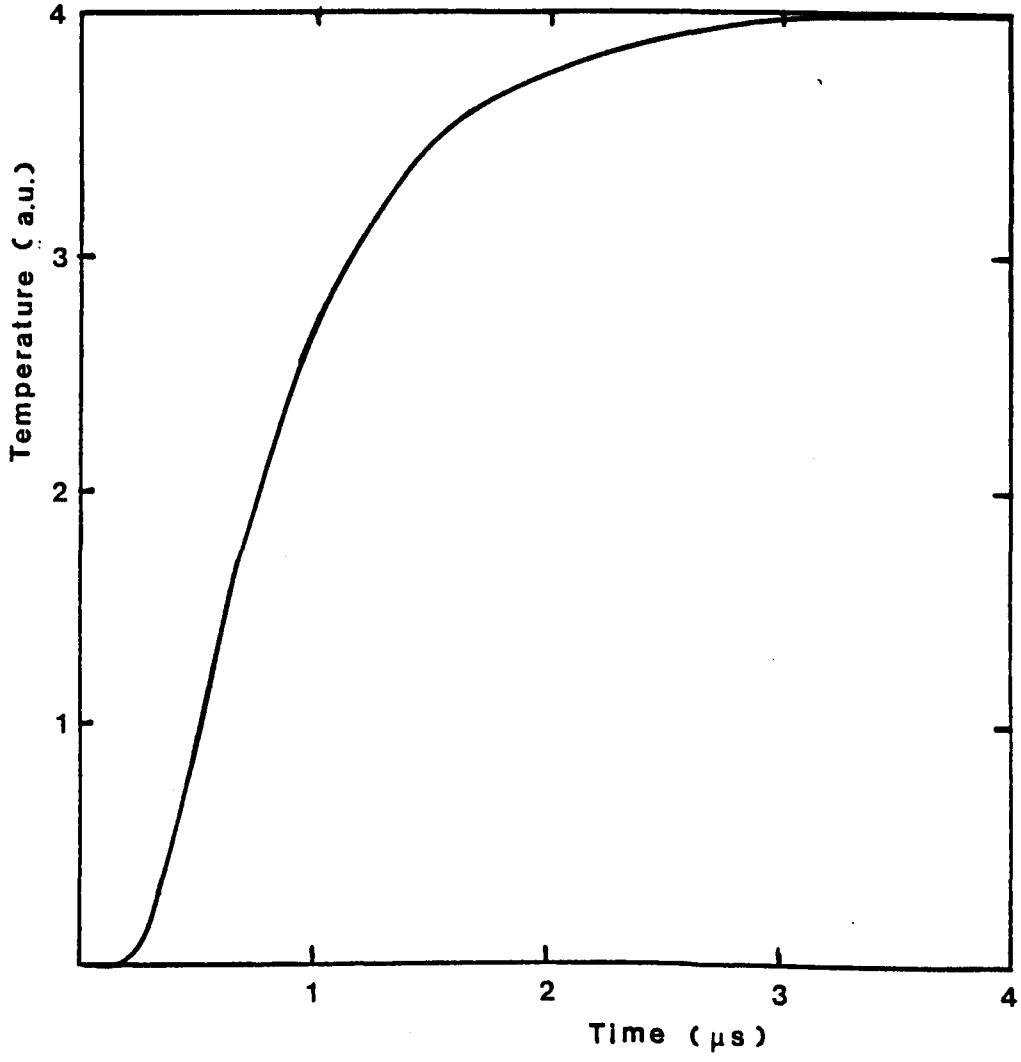

Fig.2.2.5.

NORMALISED TEMPERATURE RISE CURVE

Dimensionless rear face temperature rise parameter, X.

Dimensionless time parameter, W.

$X = T / Tm$

$W = \pi^2 Dt / H^2$

$W = 1.38$ at $X = 0.5$

$W = 4.00$ at $X \approx 0.95$

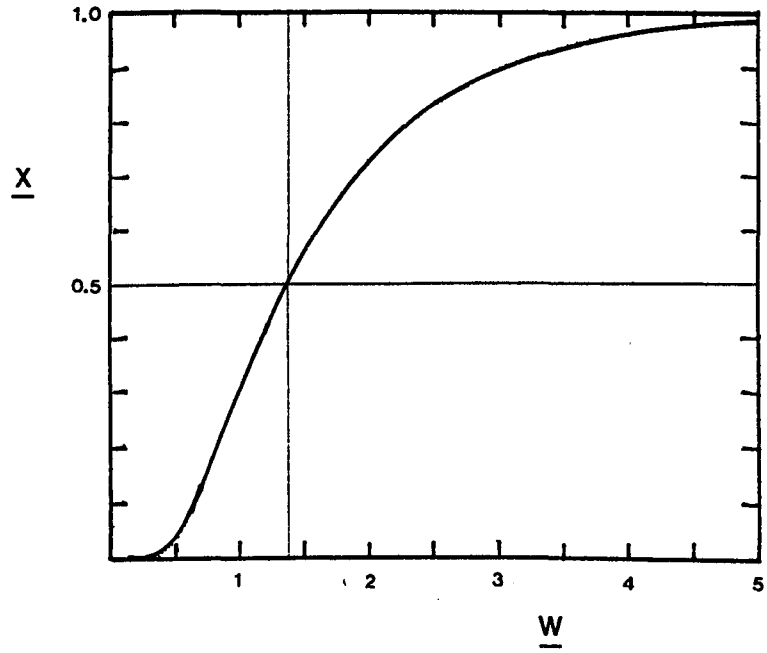

Fig.2.2.6.

TEMPERATURE AT REAR OF COPPER FOIL

Measured Temperature as a function of Time following 15 ns XeCl laser irradiation of 1.3 μm thick CuCl layer on 25 μm Copper.

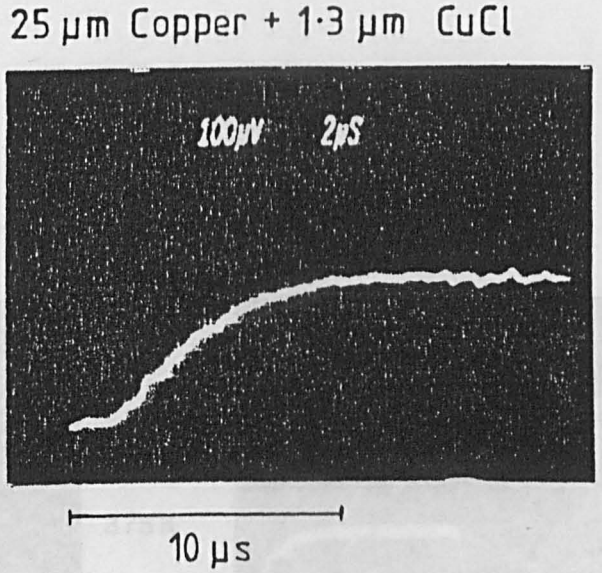

Fig.2.2.7.

TEMPERATURE OF REAR OF SILVER FOIL

50 μm foil: Measured 'steady-state' temperature as a function of laser prf.

1 Hz

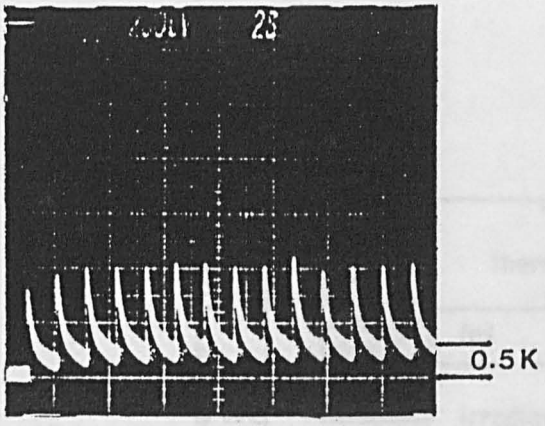

5 Hz

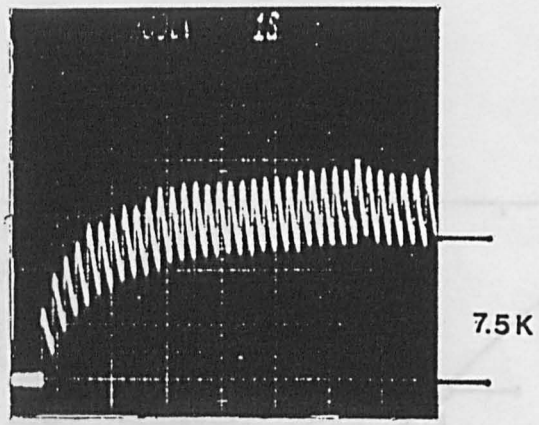

100 Hz

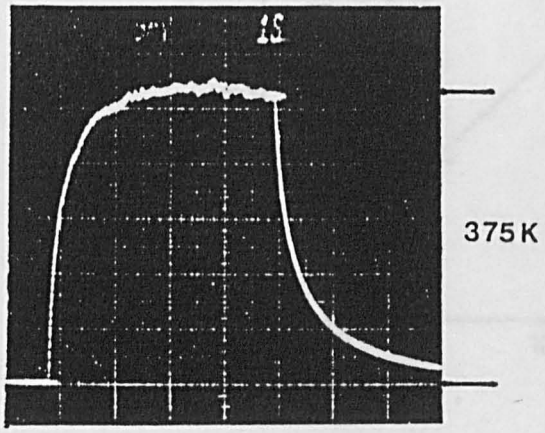

500 Hz

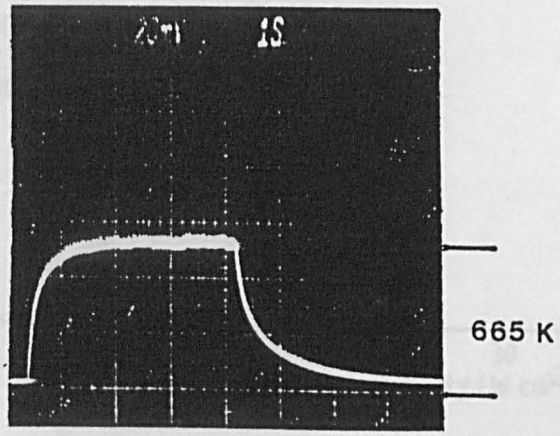

Fig.2.2.8.

TEMPERATURE OF REAR OF NICKEL FOIL

50 μm foil: Measured 'steady-state' temperature as a function of laser average power density.

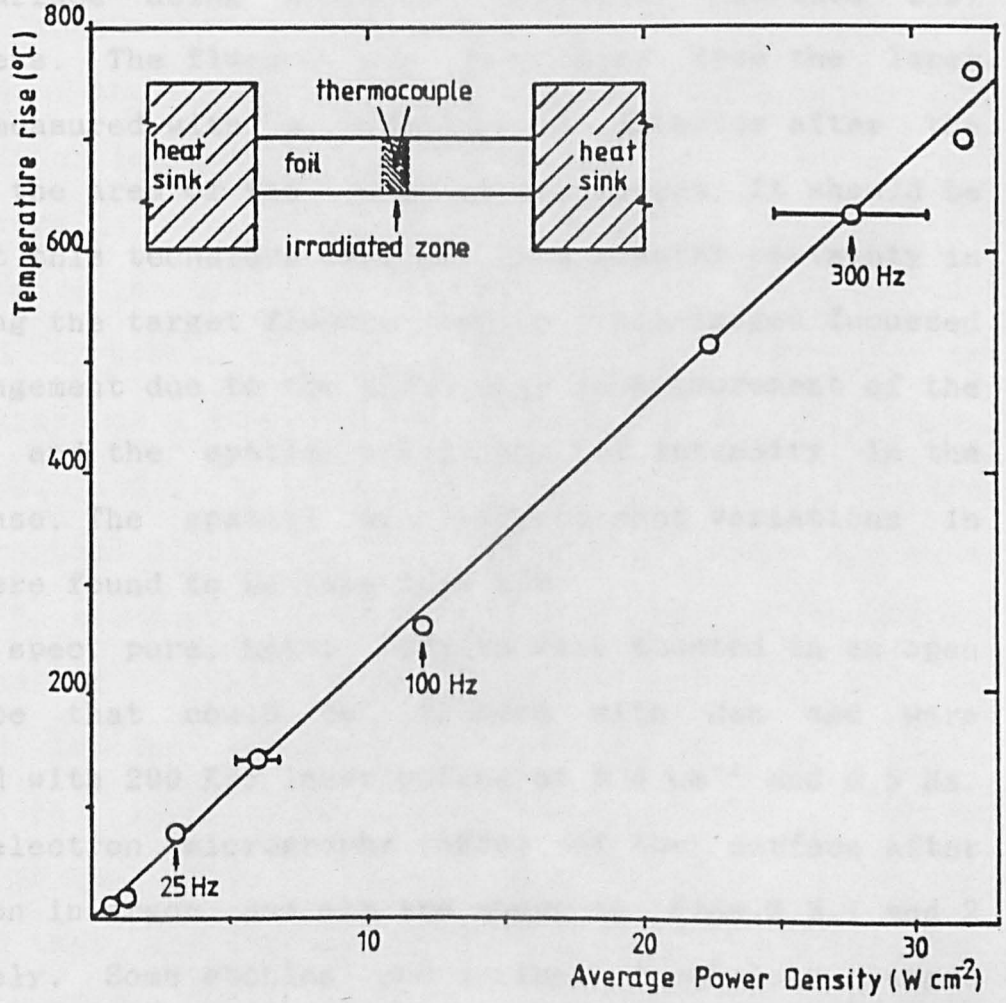

2.3
EXCIMER LASER ETCHING OF METALS

Bulk metal samples of Copper, Nickel and Constantan (50% Cu-50% Ni) were irradiated under different environmental conditions in order to assess the effects of surface contamination.

The image of a simple mask placed in the beam path to select a region of uniform fluence was projected onto the metal target surface using a single, numerical aperture f/8, quartz lens. The fluence was calculated from the laser energy, measured with a pyroelectric detector after the lens, and the area of the image at the target. It should be noted that this technique results in a greater certainty in determining the target fluence than in a non-imaged focussed beam arrangement due to the difficulty in measurement of the spot size and the spatial variations of intensity in the latter case. The spatial and shot-to-shot variations in fluence were found to be less than 10%.

The bulk, spec. pure, metal targets were mounted in an open ended tube that could be flooded with gas and were irradiated with 200 KrF laser pulses at 5 J cm^{-2} and 0.5 Hz. Scanning electron micrographs (SEMs) of the surface after irradiation in argon and air are shown in Figs.2.3.1 and 2 respectively. Some etching and surface morphology changes were observed in both cases, but the most marked difference between the two sets of results was the formation in air of a distinct surface layer, clearly seen at the edges of the irradiated zone in Fig.2.3.3.

The surface layers are thought to be oxides since their heat of formation ($-\Delta H \approx 10$ kJ mol) is an energetically more favourable process than nitridation ($-\Delta H \approx -4$ kJ mol). An evacuable cell was constructed to more exactly control the environmental conditions during irradiation. SEMs of 50 μm thick copper foils irradiated with 4500 XeCl laser pulses at 1 J cm^{-2} and 1 Hz in a vacuum of 0.01 torr, in air at 1 Atm and in oxygen at 25 torr are shown in Fig.2.3.4. It can be seen that under reduced pressure conditions little material has been removed and that the pattern of non-irradiated diagonal lines are poorly defined. In contrast the definition of the pattern produced by irradiation in air and oxygen is much improved and, clearly, much more material has been removed.

The etch-rate at 193 nm was measured for copper foils irradiated at 0.5 Hz in a vacuum of $\approx 10^{-4}$ torr and in 25 torr oxygen as a function of fluence and these are shown in Figs.2.3.5 and 6. It can be seen that there is a decrease in the threshold fluence in the presence of oxygen and that at 1 J cm^{-2} the etch-rate is almost an order of magnitude greater than in the vacuum case. The improved etch rate is attributed to the formation of readily ablated surface oxides in the inter-pulse period. Although the mechanism involved in the oxide ablation is not known, it can be speculated that the thermal diffusivity will be lower than that of the parent metal and may be effectivly isolated from it thus suffering less heat loss and allowing higher temperatures per unit fluence to be developed in the oxide.

The micro machining of metals by means of UV-laser assisted,

or initiated, surface chemical reactions may involve complex and subtle processes both in the formation of surface layers of compounds of the metal and environmental gas and in their removal. Chlorine gas is known to react with many metals at room temperature leading to the formation of surface chloride layers. The etch-rate of copper in 2.5 torr chlorine as a function of ArF laser fluence at 1 Hz is shown in Fig.2.3.7. Here the form of the etch-rate curve is very different from the previous two cases and significant removal rates can be achieved at fluences of less than 1 J cm^{-2}.

Detailed studies of the UV-excimer laser etching of polycrystalline copper foils by the ablation of surface layers formed in chlorine gas environments are presented in the next two chapters.

Fig.2.3.1.

SCANNING ELECTRON MICROGRAPH

Surface of bulk Constantan after
200 KrF laser pulses at 5 J cm^{-2}, 0.5 Hz.
Argon ambient.

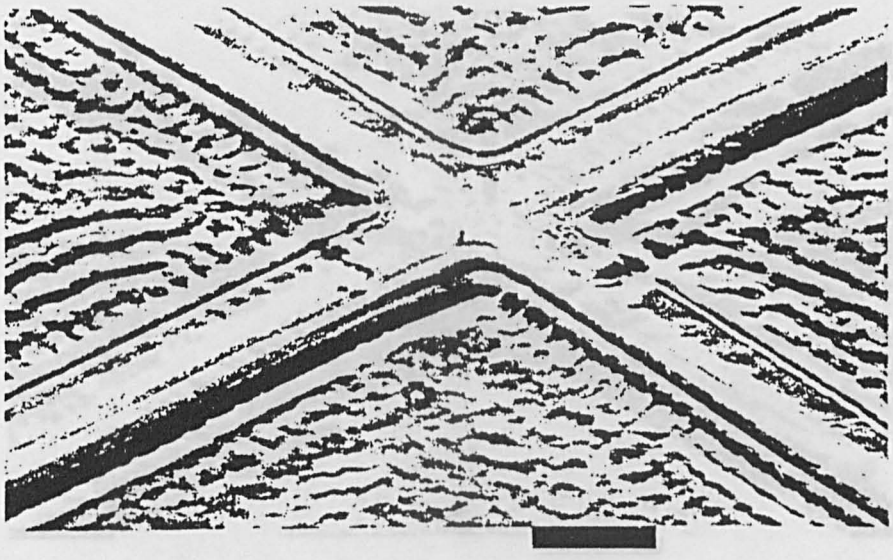

Fig.2.3.2.

SCANNING ELECTRON MICROGRAPH

Surface of bulk Constantan after
200 KrF laser pulses at 5 J cm $^{-2}$, 0.5 Hz.
Air ambient.

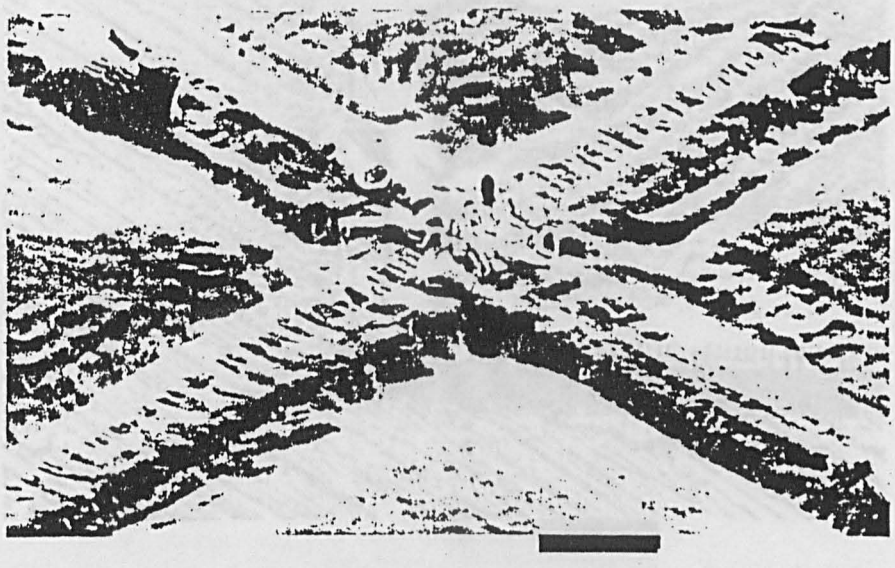

Fig.2.3.3.

SCANNING ELECTRON MICROGRAPH

Surface of bulk Constantan after

200 KrF laser pulses at 5 J cm $^{-2}$, 0.5 Hz.

Air ambient.

Showing detail of surface layer.

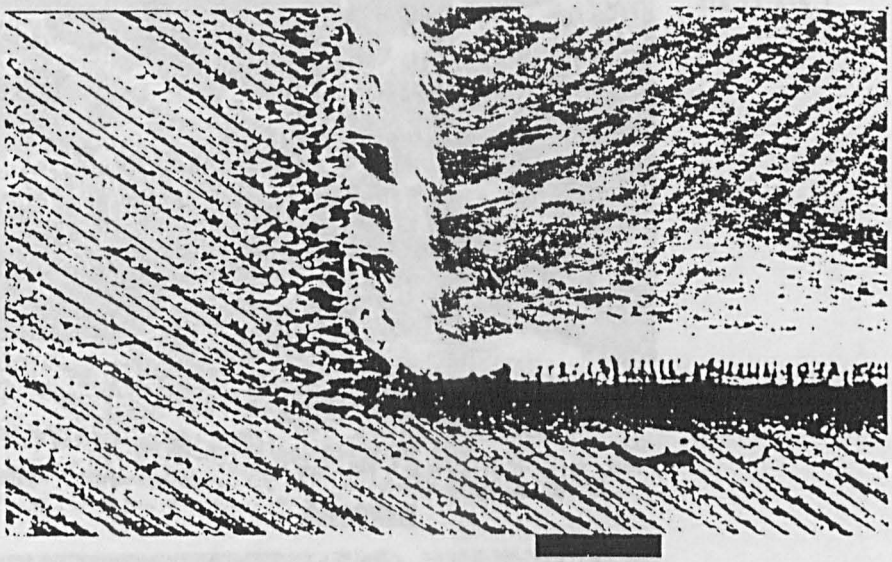

Fig.2.3.4.

S.E.M's. OF XeCl-LASER IRRADIATED COPPER

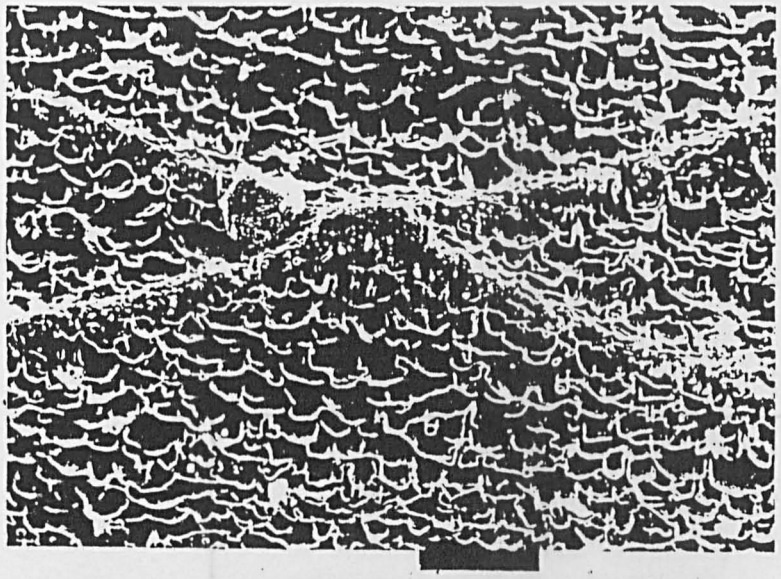

VACUUM (0.01 torr)

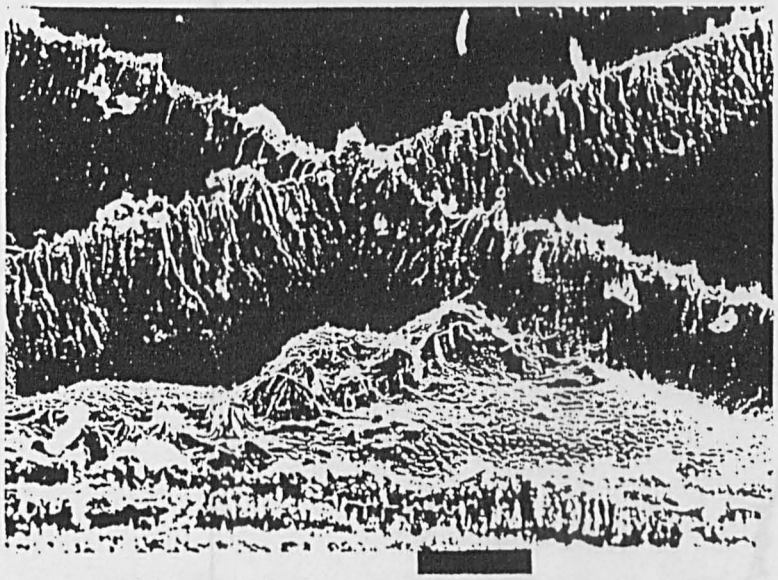

AIR (1 Atm.)

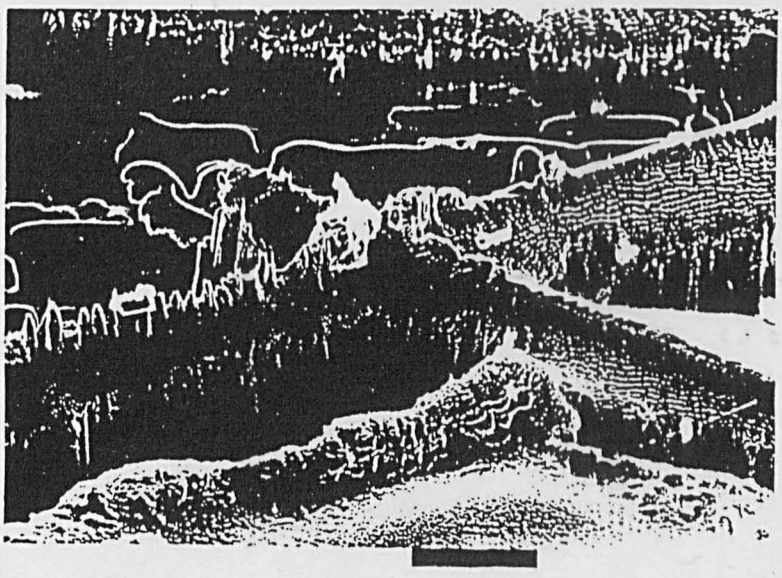

OXYGEN (25 torr)

Fig.2.3.5.

ArF-LASER ETCH-RATE OF COPPER

Etch-depth per pulse as a function

Fluence at 0.5 Hz in Vacuum.

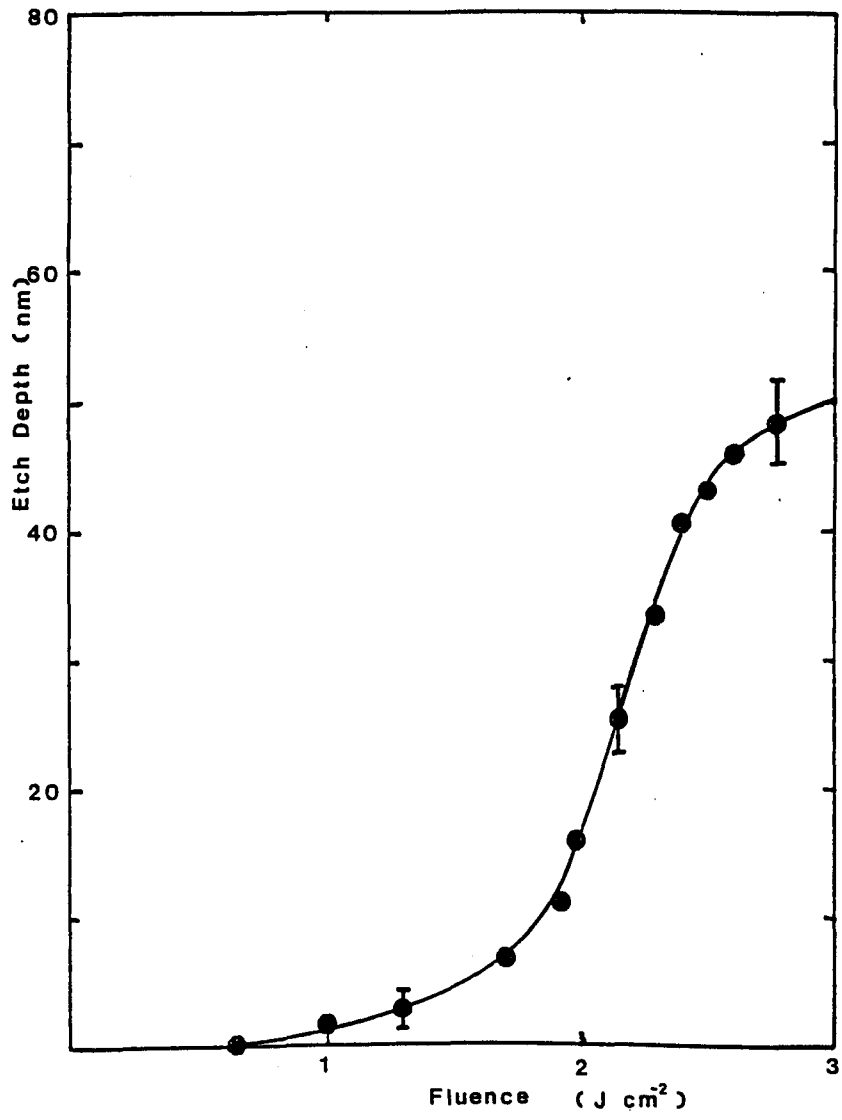

Fig.2.3.6.

ArF-LASER ETCH-RATE OF COPPER

Etch-depth per pulse as a function

Fluence at 0.5 Hz in Oxygen.

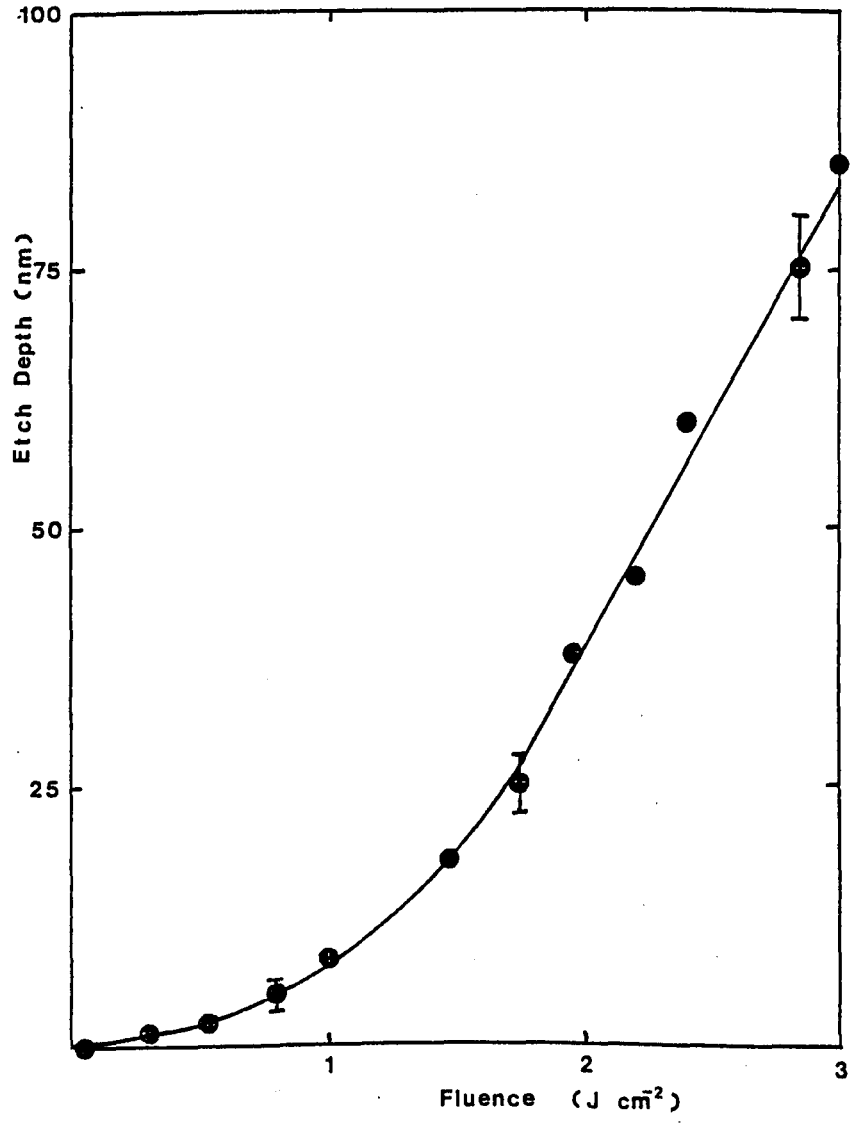

Fig.2.3.7.

ArF-LASER ETCH-RATE OF COPPER

Etch-depth per pulse as a function

Fluence at 1.0 Hz in Chlorine.

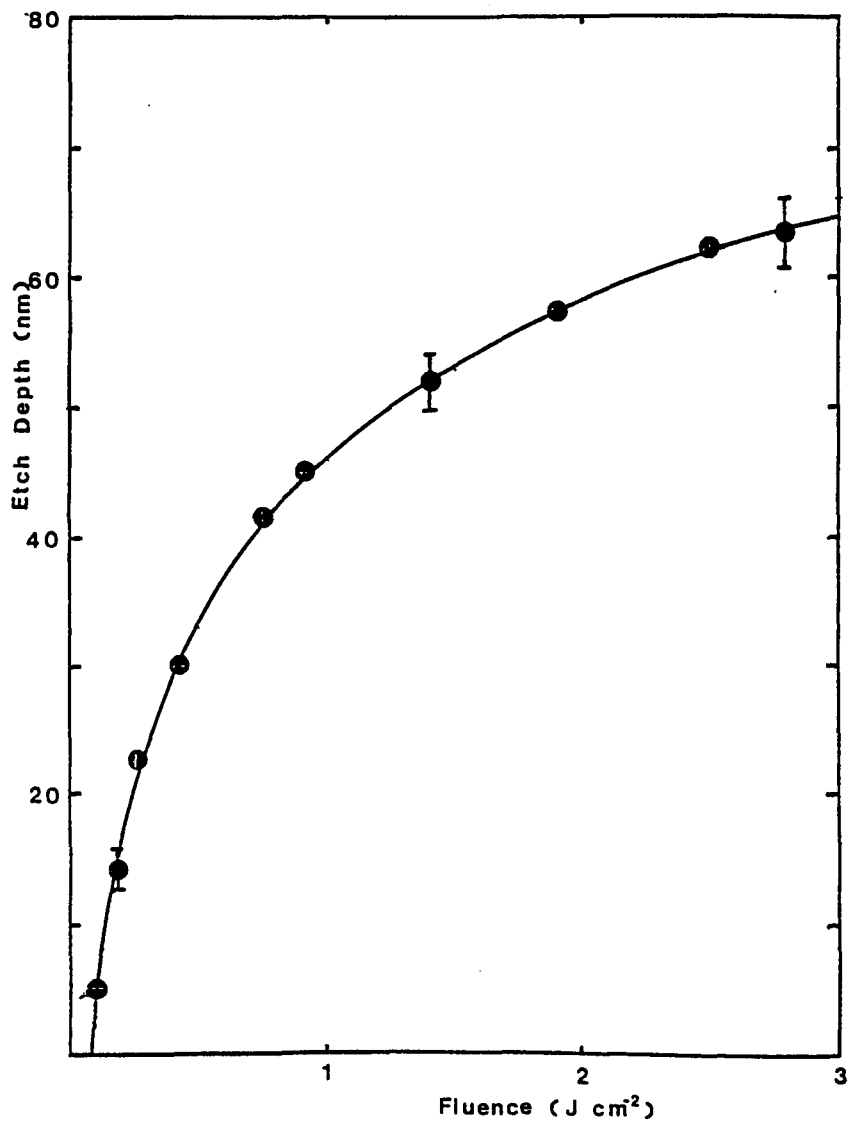

2.4

REFERENCES

[1] Ziman,J.M.
'Principles of the Theory of Solids'
Cambridge U.P.,Cambridge, (1964).

[2] Weaver,J.H.,Krafka,C.,Lynch,D.W. and Koch,E.E.
'Optical Properties of Metals', 2 Vols.
Fachinformationszentrum, (1981).

[3] Boyd,I.W. and Micheli,F.
Electron Lett. 23, (1987), 298.

[4] Abelès,F.
'Optical Properties of Solids'
North-Holland, Amsterdam, (1972).

[5] Hodgson,J.N.
'Optical Absorption and Dispersion in Solids'
Chapman and Hall, London, (1970).

[6] Karlsson,B.,Ribbing,C.G.,Roos,A.,Vakanen,E.,Karlsson,T
Physica Scripta, 45, (1982), 826.

[7] Drude,P.
Ann. Phys. 1, (1900), 566.

[8] Ready,J.F.
'Effects of High-Power Laser Radiation'
Academic Press, New York, (1971).

[9] Key,P.H.
M.Sc. Thesis
University of Hull, (1985).

[10] Ujihara,K.

J. Appl. Phys. 43, (1972), 2376.

[11] Von Allmen,M.,Blaser,P.,Affolter,K.,Sturmer,E.

IEEE. J. Quantum Electron. QE14, (1978), 85.

[12] Bonch-Bruevich,A.M.,Imas,Y.A. et al.

Sov. Phys. Tech. Phys. 13, (1968), 640.

[13] La Rocca,A.V.

5th G.C.L. Symp. Conf. Ser.72.

Inst. Phys., Oxford, (1984).

[14] Popawe,R.,Beyer,E.,Herziger,G.

5th G.C.L. Symp. Conf. Ser.72.

Inst. Phys., Oxford, (1984).

[15] Dona dalle Rose,L.F.

J. de Phys. 44C5, (1983), 469.

[16] Lax,M.

J. Appl. Phys. 48, (1977), 3919.

[17] Carslaw,H.S. and Jaeger,J.C.

'Conduction of Heat in Solids', 2nd Edition.

O.U.P. Oxford, (1959).

[18] Parker,W.,Jenkins,R.J., Butler,C.P.,Abbot,G.L.

J. Appl. Phys. 32, (1961), 1679.

CHAPTER THREE

THE CHLORINATION OF COPPER SURFACES

3.0
INTRODUCTION

In the last chapter it was demonstrated that the laser etching of metals can be greatly enhanced by a suitable choice of environmental conditions and proceeding via a laser induced or laser assisted chemical etching mechanism. It was shown that, in the case of copper, the presence of chlorine gas not only increased the etch rate dramatically but also reduced the threshold fluence at which measurable material removal commenced.

In this chapter studies of the exposure of copper to chlorine gas and the dark reaction resulting in the formation of low ablation threshold chloride layers are discussed with a view to a quantitative understanding of the contributions of the environmental parameters leading to optimisation of the etching process.

In the first section some general comments concerning the metal-gas interface precede a summary of some of the main points of relevant work reported in the literature.

The second section introduces the principles of the optical technique of interferometry for the measurement of thin film thickness and its application to the real-time measurement of the growth-rate of surface layers. The applicability of the technique to this work is demonstrated by the comparison of the results of computer modelling with a typical experimental result.

The results of studies of the growth of chloride layers using this technique are presented in the penultimate

section. The evolution of the surface layers in time as a function of chlorine gas pressure and copper substrate temperature are shown.

The concluding section presents a summary of the observed chlorination of copper and predicts the influence of the environmental conditions on the etch-rate.

3.1.

THE METAL-GAS INTERFACE : COPPER-CHLORINE

The science of surfaces is a large and, with the advent of sophisticated surface analysis instrumentation, growing area of study. The excellent texts by Tompkins [1] and Roberts and McKee [2] give comprehensive surveys of the subject of chemisorption on metals from both a theoretical and experimental perspective and, since the interest here is in the macroscopic effects, a detailed treatment would be inappropriate in this work. Some basic ideas are presented, however, as an introduction to results found in the literature that are of specific interest.

The surface atoms of a crystalline solid, not being subject to the equilibrium of forces experienced by atoms in the bulk, exert attractive forces normal to the surface plane and thus present favourable energy conditions for the concentration of gas molecules at the interface to exceed that of the gas phase (adsorption). The efficiency with which colliding gaseous adsorbate molecules are captured is measured by the condensation coefficient which, for clean metal surfaces, approaches unity. Adsorbed gas molecules may form chemical bonds with adsorbent atoms (chemisorption) and the ratio of the rate of capture into the chemisorbed state to the rate of collision is the sticking probability. The sticking probability is generally lower than the condensation coefficient since the collision of an incoming gas molecule with a chemisorbed adspecies may involve energy exchanges resulting in a gas molecule being returned to the

gaseous state. Thus the sticking coefficient may decrease with increasing surface coverage as the number of non-occupied lattice sites reduces. When the gas molecule is diatomic a dissociative step necessary for chemisorption may occur before or after the initial adsorption step. Dissociative chemisorption may be self driven via excess surface energy or externally initiated by the supply of thermal or photon energy.

If the chemical bonding process is able, by some mechanism, to continue into the absorbent species lattice a three dimensional compound may be formed. The development of a surface compound with thickness in excess of one monolayer depends upon the ability of adsorbate or adsorbent species to move across the compound and allow further reactions to take place. The ease with which atoms may move through a crystal lattice will depend upon the relative dimensions of the diffusing species and the lattice parameter or, if by way of vacancies, the defect density.

In the case of interstitial diffusion, surface layers may form most rapidly on planes with the smallest atom density, or low co-ordination number, whilst the converse may be true for a substitutional mechanism. Thus for single crystals there may be a marked anisotropy in the rate of formation of surface layers as seen in the oxidation of copper [3], Fig 3.1.1.

Polycrystaline materials may exhibit variations in surface layer thickness due to the differential reaction rates of the the various planes of the crystallites. However, this anisotropy of reaction rate may be short ranged since it is

unlikely that good substrate to surface layer lattice matching will occur on a polycrystaline substrate. Reconstruction of the layer may occur to produce some preferred orientation of the surface plane.

A measure of the total exposure of a surface to a gas is the pressure-time product, the units of which are the Langmuir, L, where 1 L = 10^{-6} torr sec.

The exposure of a clean copper surface to chlorine gas results in rapid chemisorption and, when the surface is saturated, the formation of a chloride surface layer. Studies of sub-monolayer chemisorption on the single crystal Cu(111) and Cu(100) surfaces [4-8] have shown that the adsorption and resulting surface structures are similar and that the copper surface becomes saturated at exposures as low as 1 L. Extensive studies in the exposure range 10^{2} to 10^{9} L have been reported by Sesselmann and Chuang [9], in which rather thicker layers were formed. Their experiments were carried out on Cu films, up to 5 microns thick, deposited on quartz or ceramic substrates and which were predominantly (111) oriented. The results show that the diffusion of Cu through the chloride layer is the most likely principal mechanism for the continued reaction and layer growth.

Their experiments, with combinations of exposure time and pressure, revealed that the chloride layer is not stoichiometric CuCl but rather Cu_xCl with $x \geq 1$ for the initial stages of formation and particularly with pressures below 10^{-3} torr. However, at higher pressures x tends to unity although, since Cu must diffuse through the layer for

the reaction to continue, the stoichiometric composition can never be fully realised. Whilst the results give insight into the composition and growth mechanism of chloride growth there is little useful information to be found concerning the kinetics of the process that will allow the growth rate to be evaluated. The data indicate that the pressure-time product is an inadequate parameter with which to define the chloride thickness since a given thickness may be achieved by many different exposure conditions and upon which the composition may depend.

Data is therefore needed to allow the thickness to be expressed as a function of time with pressure, and possibly temperature, as variable parameters. Some clue to the shape of the growth curve may be gained by the supposition that halogenation of metals is analogous to the oxidation process [9].

The oxidation of metals has been of interest for many years and particularly on a macroscopic scale involving engineering materials. More recently the controlled formation of oxides up to a few microns thick and on a variety of materials has attracted attention because of their use as semi-conducting and insulating layers in micro-electronics applications [10-12].

Whilst the growth rates and temperature of processing vary greatly with the parent material and the species of oxide required, many oxidation processes have been found to follow a parabolic rate law often with a diffusion dependence indicated by thickness being a function of $\sqrt{t}$ [13-15].

Measurements of the growth of chloride layers on polycrystalline copper are described in the next two sections. Preliminary experiments gave some qualitative properties of the chloride.

Under white light illumination the copper surface underwent a sequence of colour changes on initial exposure to the chlorine. As the layer increased in thickness the surface took on the appearance of a semi-transparent crystalline material. When subjected to a bending force large flakes of the chloride became detatched revealing the bright copper surface. The flakes were thought to be highly crystalline since they tended to fracture in specific directions with relatively long straight edges. The chloride was found to be insoluble in water but soluble in ammonia solution; however when exposed to water for one hour the chloride became green-blue in colour.

Based on the assumption that the growth is essentially one-dimensional and from considerations of the relative molecular weights and densities, the thickness of the chloride layer is calculated to be 3.45 times the thickness of copper parent metal consumed.

OXIDATION OF COPPER

Kinetics of oxidation of copper in relation to crystal orientation.
1 Atm. oxygen at 250°C. [Ref. 3]

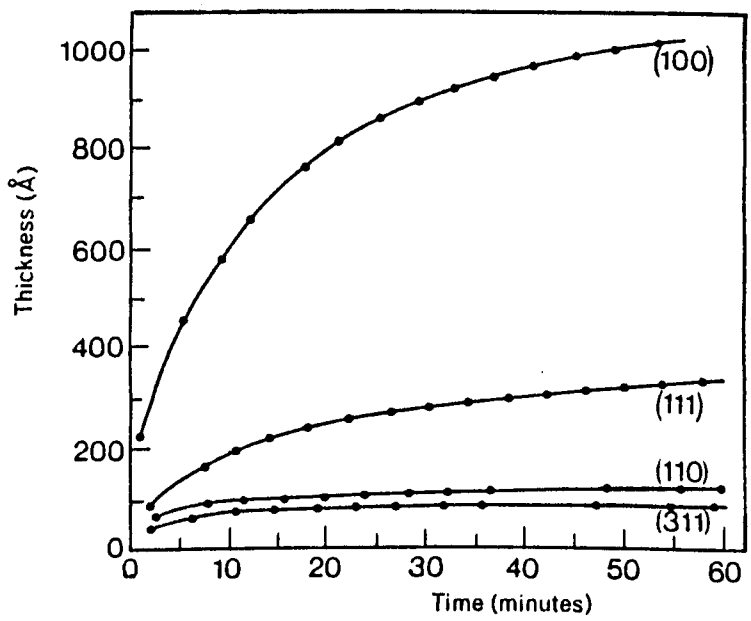

3.2

INTERFEROMETRIC MEASUREMENT OF THE GROWTH OF THIN CHLORIDE FILMS ON COPPER IN A CHLORINE GAS ENVIRONMENT.

The phenomenon of optical interference arising from the division of wave amplitude due to reflection and refraction at the interfaces of thin transparent films has been known since the observation of colours of liquid layers illuminated by white light was explained by Isaac Newton in the 17th century. In 1890, P. Drude applied the equations of reflection coefficients, derived by Fresnel some 80 years earlier, to the problem of reflections from thin film covered surfaces. Because of the number and complexity of calculations involved, however, it was not until the advent of high speed digital computers that the deduction of optical properties from reflection measurements became a practical proposition.

Using the nomenclature for wave optics given in section 2.1, the normal incidence Fresnel coefficient for the ratio of reflected to incident amplitudes (r = Er/Ei) at the interface between two absorbing media, **a** and **b**, may be written as;

$$r = \Gamma \exp[j\phi] = N_a - N_b / N_a + N_b$$

where $N_a = n_a - jk_a$ and $N_b = n_b - jk_b$

so that, explicitly;

$$r = \frac{n_a^2 - n_b^2 + k_a^2 - k_b^2 + 2j(n_a k_b - n_b k_a)}{(n_a + n_b)^2 + (k_a + k_b)^2}$$

The reflectance of intensity, R, is given by;

$$R = (Re.r)^2 + (Im.r)^2$$

and the change in phase, ϕ, on reflection by:

$$\phi = \arctan [(Im.r)/(Re.r)]$$

In the case of an absorbing film on an absorbing substrate, we must consider the reflection and phase change at the air-film interface, the transmission and attenuation in the film and the reflection and phase change at the film-substrate interface. If the attenuation of the film is not too great, the re-emergent wave will combine with that reflected from the film and the resultant amplitude will be dependent upon their phase relationship and attenuation in the film. The explicit expression for the reflected amplitude from an absorbing film on an absorbing substrate in terms of the real and imaginary parts of the complex refractive indices, phase relationship and attenuation is extremely complicated. Fortunately the problem may be approached in a stepwise manner and lends itself to digital computation [16].

The importance of contributions to the reflected amplitude from multiple reflections within the film may be assessed by considering a model situation, shown schematically in Fig.3.2.1. From this model the ratio of total reflected to incident amplitude can be seen to be;

$$\Gamma = Er/Ei = r + (1-r)^2A^2 + (1-r)^2A\, r + (1-r)^2A\, r^2 + \ldots$$

or

$$\Gamma = r + (1-r)^2 \sum_{i=1}^{\infty} A^{2i}\, r^{(i-1)}$$

where it is assumed that r(air-film) = r(film-air) and the substrate is a 100% reflector. In this case the attenuation

in the film and phase changes on reflection are given by;

$$A = \exp[-\alpha H] \exp[jknH]$$

each additional reflection, therefore, makes a contribution of; $\Delta\Gamma = \Gamma^{i} - \Gamma^{i-1} = (1-r)^2 r^{(i-1)} A^{2i}$

If all the emergent components, r^{i}, are in phase with the reflection, r, from the film surface, ie. exp[knH] = 1, then the reflection coefficient, Γ, will be a maximum; its value depending only on r and the number of internal reflections for any film thickness, H, and attenuation, α.

Examples of plots of Γ as a function of r for different values of i, the number of emerging components, and attenuation coefficient, αH, are shown in Fig.3.2.2. It can be seen that for $\alpha H \geq 0.1$, values of i = 1 or 2 are sufficient to achieve a reasonable degree of accuracy in calculating Γ. Furthermore, this requirement will be reduced for substrates having $r < 1.0$. In practical terms, the inclusion of only two internal reflections is necessary for film thickness $H \geq 0.15\lambda$ with k = 0.1.

The effective phase differences arise because of the additive effects of the phase changes on reflection and that due to the optical path difference between reflected waves r and r^{i}. The phase shifts from reflection at the film, ϕ_f, and substrate, ϕ_s, are dependant only on the refractive indices of the media bounding the interfaces and may therefore be summed algebraicaly as ϕ.

The phase shift due to optical path length, however, will vary with film thickness and thus a change in the metrical thickness of the film will result in a modulation of the observed reflected intensity.

A maximum in total reflected intensity occurs when the film thickness is such that the optical path length produces zero phase shift with respect to the reflection from the film surface, that is , when the optical path length is an even number of half wavelengths.

viz:

$$2\pi/\lambda.(2nH) + \phi = 2\pi m$$

where m is an integer. As the film thickness is increased the reflected intensity decreases until a minimum is reached when the path difference is an odd number of half wavelengths. The next maximum occurs when the zero phase shift condition is again satisfied, ie.:

$$2\pi/\lambda.(2n(H+\Delta H)) + \phi = 2\pi(m+1)$$

Thus maxima are observed in the reflected intensity each time the film thickness increases by an amount ΔH:

$$\Delta H = \lambda/2n$$

This is seen in Fig.3.2.3, in which the reflectance, R, of a film-substrate combination is shown as a function of film thickness. The computational procedure used follows the considerations of reflection and transmission coefficients, phase relationships and attenuation outlined above and is based upon an analysis by Heavens [16].

Thus the growth of surface layers on a substrate may be monitored by recording the reflected intensity of a probe beam as a function of time (time-resolved interferometry) and, by comparing this with theoretical calculations, the evolution of the thickness deduced.

The probe beam must, of course, be monochromatic and the choice of wavelength depends upon the optical properties of

the film and substrate combination under consideration. In the case of CuCl films on Cu substrates the He-Ne laser at 0.63 μm is an ideal candidate since copper is a near perfect reflector at this wavelength and the refractive index and absorption coefficient of CuCl [17] are such that six maxima should be resolved as modelled in Fig 3.2.4. It is interesting to note that R(0)=0.9, smaller than found for pure copper in the literature (R = 0.92 [18]), since the model assumes an infinitesimal initial layer.

The experimental arrangement is shown in Fig 3.2.5; it was necessary to use the probe beam at near normal incidence so as to eliminate polarisation effects and to simplify the reflectivity calculations. The presence of the quartz window and gas in the cell were found to make no significant difference to the reflected signals from a dummy target consisting of a back coated glass mirror.

The signal from the fast photodiode detector was recorded by use of a chart recorder or digital storage system. A narrow band pass filter, centred at 632.8 nm, was placed directly in front of the detector to eliminate extraneous light.

The area of the probe beam was approximately 0.5 mm^2 and although some diffuse reflections due to the surface imperfections of the target samples were observed, the specular reflections were seen to dominate. All of the light reflected from the target surface was collected by a large aperture lens and care was taken to ensure that any light reflected from the cell window was removed by spatial filtering.

The samples used were of the same material as those used in

the etching experiments and were cleaned prior to use by either washing in 20% v/v nitric acid, heating to ≥ 500 K in a hydrogen atmosphere or by several high fluence laser pulses in a vacuum of < 10^{-4} torr. There were no significant differences in the results obtained from samples prepared by any one of these methods.

A typical trace of the reflected intensity during the exposure of copper to chlorine is shown in Fig.3.2.6 and it can be seen to be of the same general form as the modelled reflectance of Fig.3.2.4.

The growth curve of the surface compound may be constructed by plotting the spatial periodicity of the reflectivity maxima and minima as a function of their temporal periodicity. Taking the spatial periodicity of the maxima (and minima) to be constant at $\lambda/2n$ the temporal evolution of the film thickness is as shown in Fig 3.2.7. The same data, plotted with film thickness against $\sqrt{t}$, reveals, in Fig 3.2.8, the data to be a good fit to a straight line, for all but the inital stages, and this would suggest a diffusion limited process.

The deduction that the growth-rate slows with thickness, consistent with a diffusion limited regime, is valid only if the spatial periodicity of the reflected signal maxima is constant. This will not be the case, however, if n is a function of film thickness due to the non-stoichiometry of the layer as discussed in the last section [9]. It is worth considering the possibility that the experimentally observed variation in temporal periodicity of the reflection maxima is due to effects other than a temporal variation in the

chloride layer growth.

Consideration is given to the case in which concentration gradients of the constituents of the film exist such that the lattice layers closest to the substrate are rich in substrate atoms and, as the layer thickness increases, the outer layers become more like the stoichiometric compound. In the case of the copper substrate in chlorine gas, we might expect the composition of the chloride layer to vary from CuCl at the surface to Cu_xCl ($x \geq 1$) at the interface. We might also expect the concentration gradient to decrease with increasing film thickness and it may only extend over a limited number of layers. The optical properties of the layers with $x \geq 1$ may be expected to be intermediate between those of the substrate and stoichiometric compound.

The Fresnel expressions for reflection coefficients assume that the media are homogeneous with sharp, well defined interfaces. The modelling of reflectivity for media with inhomogeneity of optical properties, therefore, poses a problem.Vasicek [19] has shown that an inhomogeneous layer may be considered as a series of homogeneous sub-layers with optical constants intermediate between those of the front and back surfaces. His results of calculated reflectivity are found to rapidly converge as the number of sub-layers considered is increased, however, with only two sub-layers the error can be less than 5%.

Thus, here, we use a two sub-layer model to simulate the reflectivity curves that might be expected for a number of CuCl-Cu_xCl-Cu configurations and to look in

particular for variations in the spatial periodicity of maxima and minima as well as the general form of the signal. The optical constants for Cu_xCl layers have been chosen to be intermediate between the published values for CuCl [17] and Cu [18], however, it must be remembered that n and k are not independent variables and as n decreases, leading to a smaller value of ΔH, k increases and thus greater attenuation occurs.

In the first example we consider the case of a non-stoichiometric layer with composition varying continuously from CuCl at the gas-solid interface to Cu at the substrate. Using a two sub-layer model and taking values of n and k for the sub-layers to be intermediate between those for CuCl and Cu the resultant reflectivity as a function of total layer thickness is shown in Fig.3.2.9. It can be seen that there is no modulation of the reflectivity and suggests that the continuously varying film model does not pertain.

Fig.3.2.10 shows the calculated reflectivity for two cases as above but with the values of n and k chosen to be more CuCl like and, hence, less absorbing. Whilst, in this case, some modulation of reflectivity is observed there is still no correlation with the measured results of Fig.3.2.6.

The case in which the stoichiometry of the layer is such that the Cu concentration gradient is non-linear is given in Fig.3.2.11. Here the thickness of the outer layer is 5 times that of the inner layer. A higher degree of modulation is observed in the case when the values of n and k are biased towards those for CuCl, Fig.3.2.11(ii).

Taking this a stage further in Fig.3.2.12, we consider a stoichiometric CuCl layer and an intermediate layer of Cu_xCl at two values of thickness ratio. Again there is little correlation with the measured results, although the larger thickness ratio, ie thinner intermediate layer, gives a better form to the curve.

Finally, in Fig.3.2.13, we consider a stoichiometric CuCl layer growth with a narrow transition layer of Cu_xCl next to the Cu substrate. Clearly the two curves shown are more like the experimentally obtained curve, particularly when the transition layer is not too dissimilar from the CuCl in its optical properties.

These examples represent a sample of many such reflectivity simulations using the two sub-layer model, none of which showed any variation in periodicity of the maxima as a function of layer thickness. There is no evidence to suggest that the observed variations in temporal periodicity of the reflectivity maxima (and minima) are due to other than variations in growth-rate of the layer. Whilst a variation in stoichiometry across the layer may exist this does not appear to have a significant effect on the optical properties at the probe beam wavelength.

A further check was made on the validity of the deduction that the chloride growth-rate is diffusion limited by monitoring the gas consumption during chlorination. An example of the chlorine pressure variation during the exposure of a copper sample together with the simultaneous reflected probe beam signal is shown in Fig.3.2.14. In this case the pressure was found to fall at a slightly lower rate

than expected from a $\sqrt{t}$ dependence and this is due to the pressure dependence of chloride growth rate shown in the next section.

A little practice at metering the chlorine gas input to the cell allowed the chloride growth to be controlled by arresting the chlorination process at a selected thickness. Using this method a number of samples were prepared and the chloride selectively laser ablated back to the copper substrate. Metrical thickness measurements of the step height were made using a scanning electron microscope and compared with the thickness from the reflectivity measurements. The measured thickness is shown as a function of the product of observed maxima order and half wavelength in Fig.3.2.16. Since the metrical thickness, H, wavelength, λ, and maxima order, m, are related by $H = m\lambda/2n$ the real part of the refractive index, n, can be obtained from the gradient. The value of $n = 2.0 \mp 0.2$, found by this method compares well with those for stoichiometric CuCl reported in the literature; 1.96 [20], 1.97 [21] and 1.95 [22]. An error of 10% in n, resulting in a similar error in H, is acceptable since the modulation of the reflectivity is not a pure sinusoidal form and hence interpolation between maxima is a matter of judgement. Furthermore, the pressure and temperature effects on growth rate, shown in the next section, are used as an indicator of the conditions pertaining during the laser ablation process and do not depend upon knowing the chloride layer thickness to a high degree of accuracy.

Fig.3.2.1.

FILM-SUBSTRATE REFLECTIVITY MODEL

Schematic diagram of multiple internal reflections and resultant waves for absorbing film on absorbing substrate.

Ei - Incident field amplitude.

r - Reflection at air-film interafce.

a - Attenuation .

Er - Total reflected field amplitude.

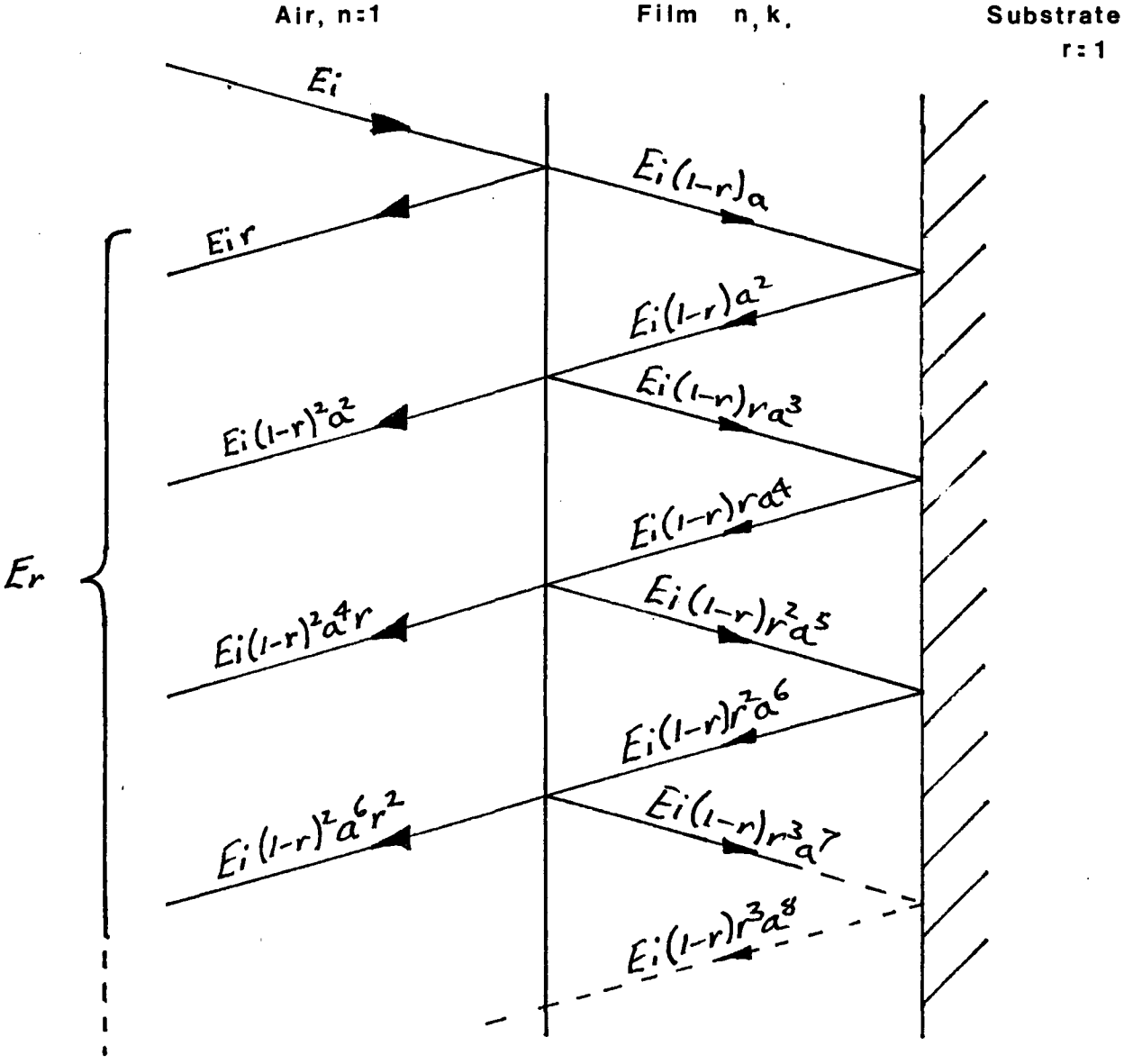

Fig.3.2.2.

FILM-SUBSTRATE REFLECTIVITY MODEL

Reflectivity, Γ, as a function of reflection coefficient, r, of film thickness, H, attenuation index, α. Increasing contributions from component waves, i = 1 to 5.

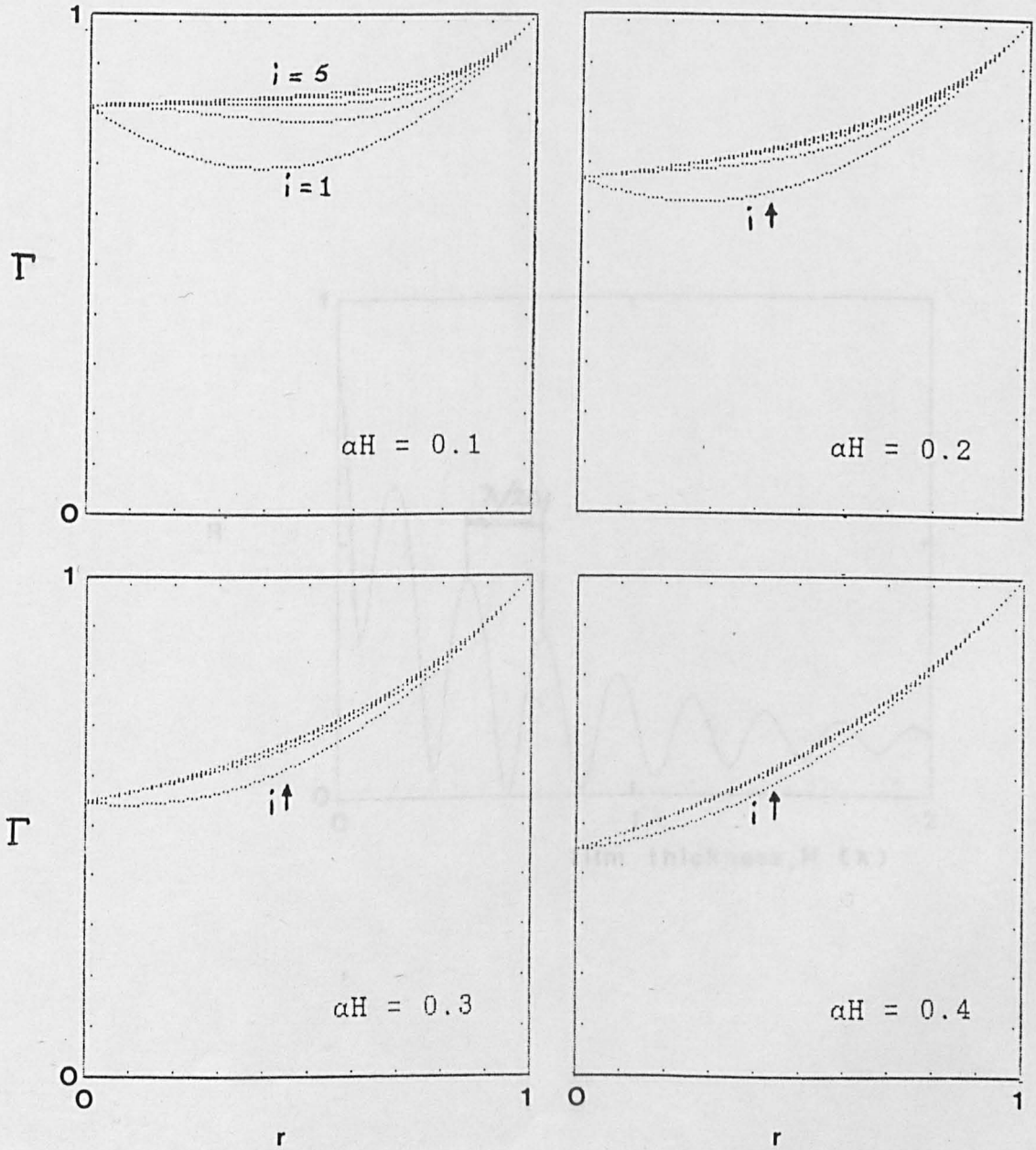

Fig.3.2.3.

FILM-SUBSTRATE REFLECTIVITY MODEL

Computed Reflectance, R, as a function of film thickness, H, (wavelengths).

Film; $n_f = 2.00$, $k_f = 0.125$.

Substrate; $n_s = 0.25$, $k_s = 2.500$.

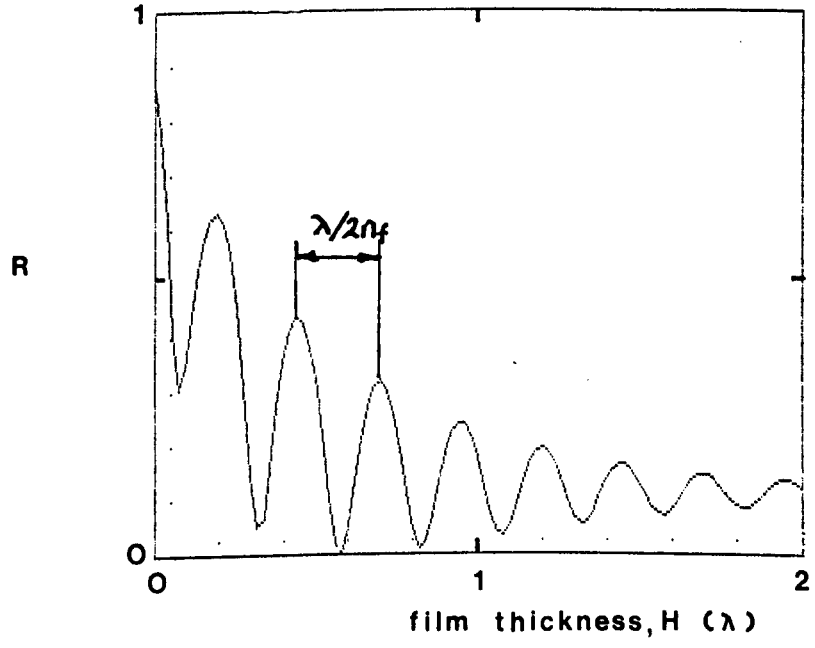

Fig.3.2.4.

FILM-SUBSTRATE REFLECTIVITY MODEL

Computed Reflectance, R, of CuCl film on Cu sbstrate as a function of film thickness, H, at 0.63 μm wavelength.

CuCl; n = 1.95, k = 0.20.

Cu; n = 0.27, k = 3.25.

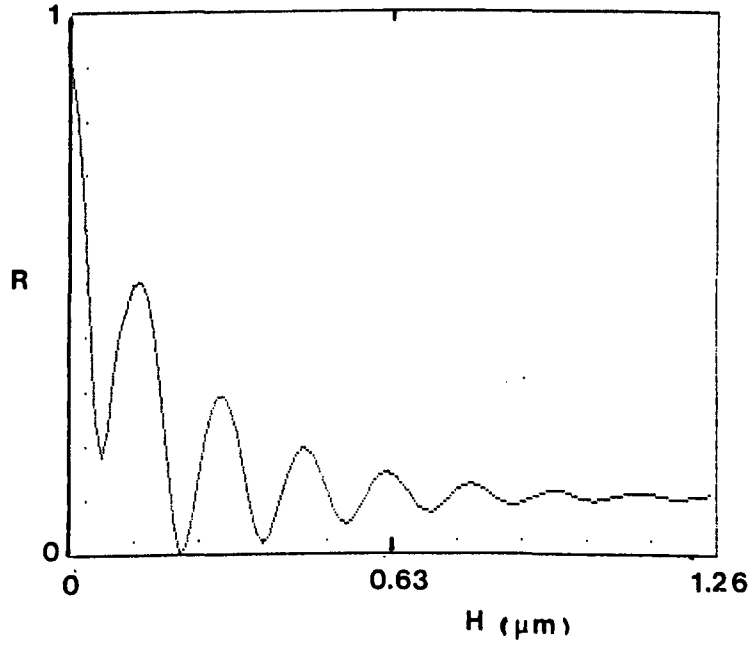

Fig.3.2.5.

TIME-RESOLVED REFLECTIVITY MEASUREMENT

Experimental Arrangement.

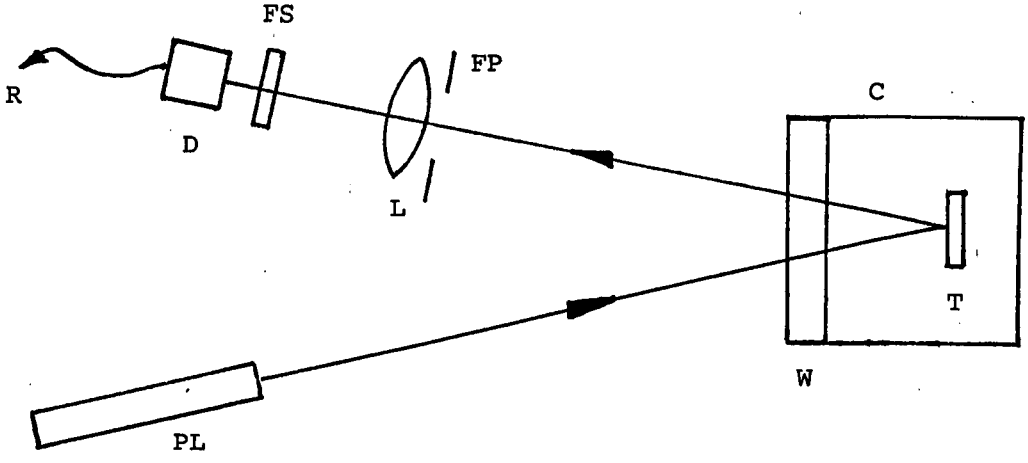

PL : He-Ne Laser.
T : Film-Substrate.
C : Evacuable Cell.
W : Quartz Window.
FP : Spatial Filter.
FS : Spectral Filter.
L : Lens.
D : Detector.
R : Digitiser / Recorder.

Fig.3.2.6.

TIME-RESOLVED REFLECTIVITY MEASUREMENT

Digitised signal (200 samples s^{-1}) of reflected He-Ne laser intensity as a function of exposure time of Cu to Cl
Pressure ≈ 5 torr, Temperature ≈ 25°C.

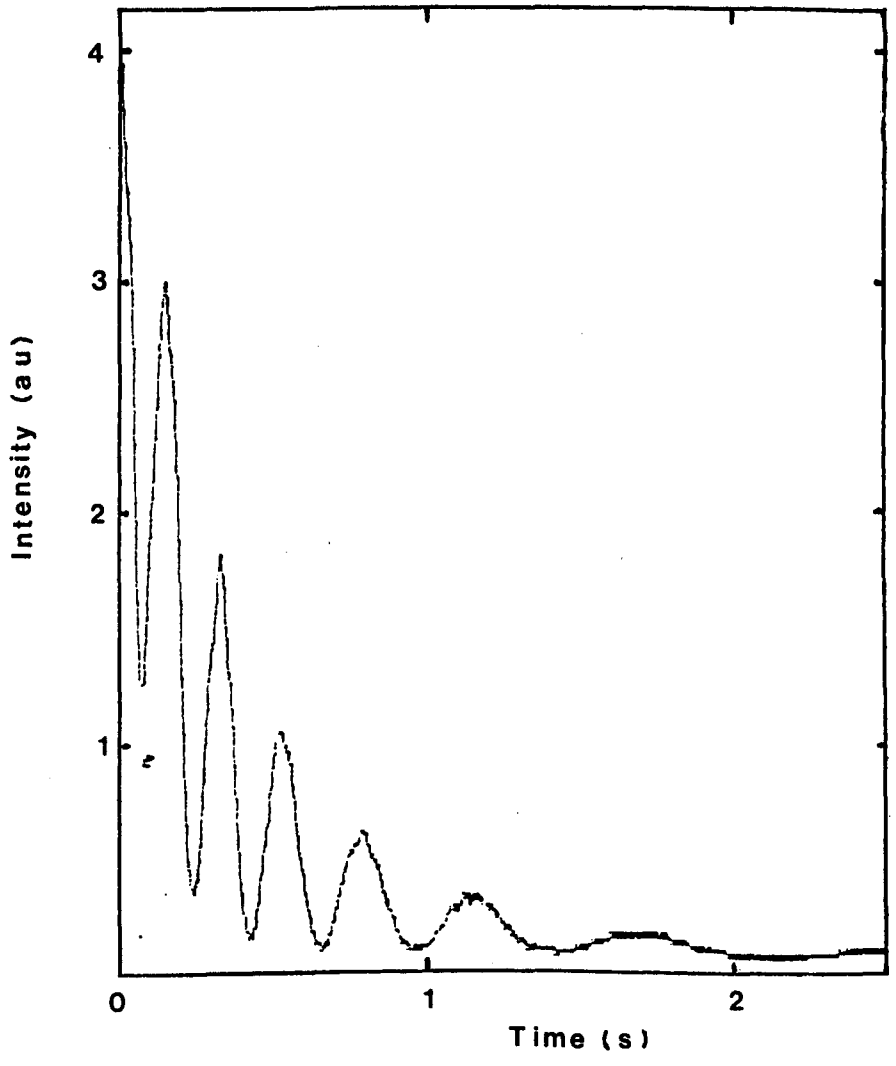

Fig.3.2.7.

GROWTH OF CHLORIDE LAYER ON COPPER

Chloride growth curve constructed from reflectivity maxima and minima order, m, as a function of time, t.

$m = 2nH/\lambda$

● - maxima.

■ - minima.

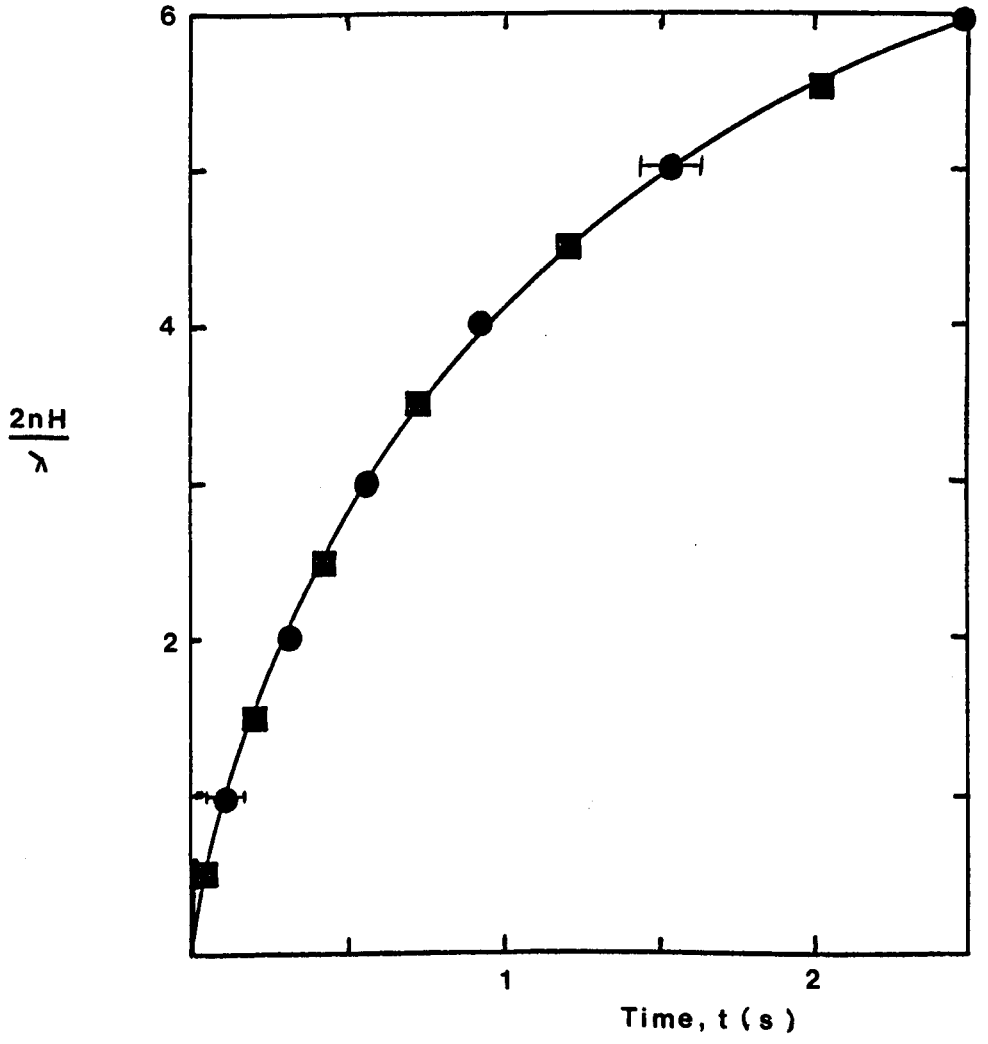

Fig.3.2.8.

GROWTH OF CHLORIDE LAYER ON COPPER

Chloride growth curve constructed from reflectivity maxima and minima order,m, as a function of root time,t.

$m = 2nH/\lambda$

● - maxima.

■ - minima.

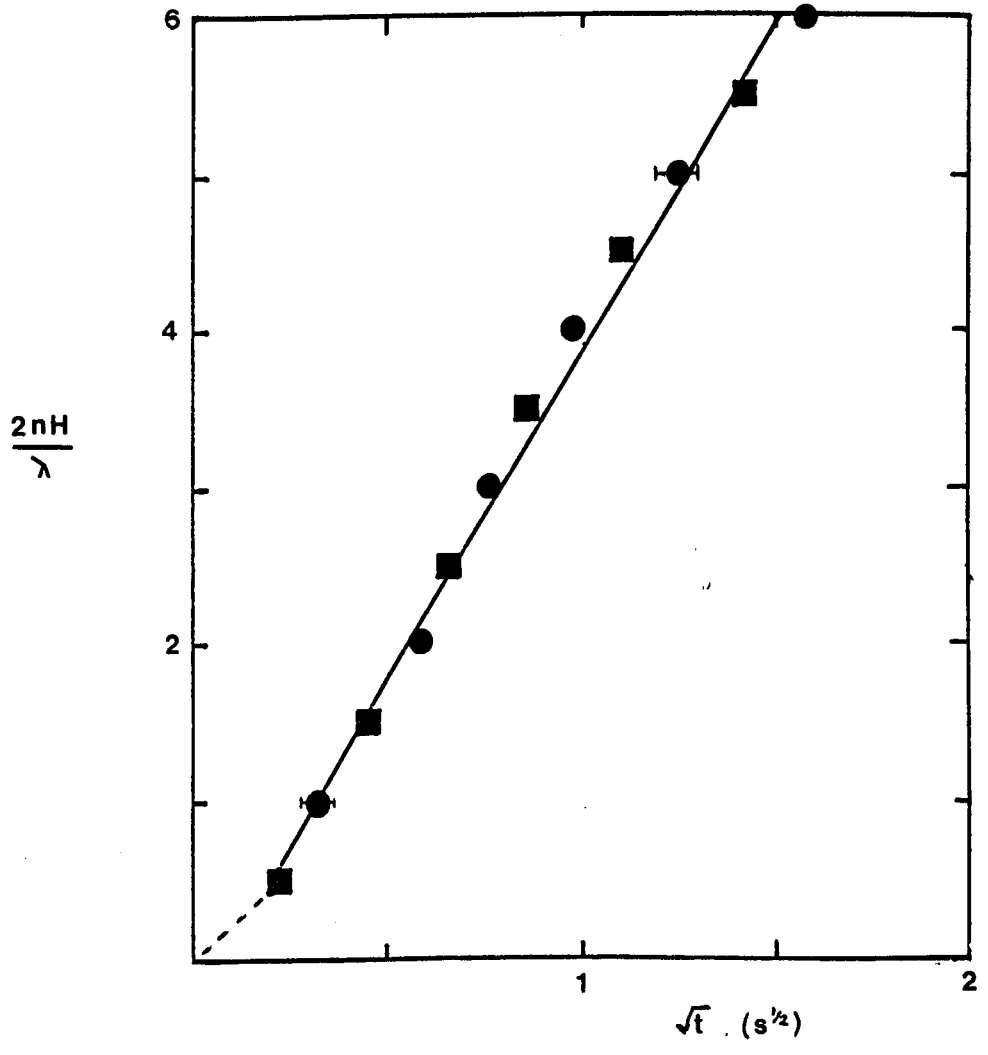

Fig.3.2.9.

TWO SUB-LAYER REFLECTIVITY MODEL

Reflectivity, R, vs. total thickness, H.

a; n=1.75, k=1.29 (Cu_xCl)

b; n=1.01, k=2.38 (Cu_xCl)

c; n=0.27, k=3.25 (Cu)

H = Ha + Hb, Ha/Hb = 1.0

Wavelength, λ= 0.63 μm.

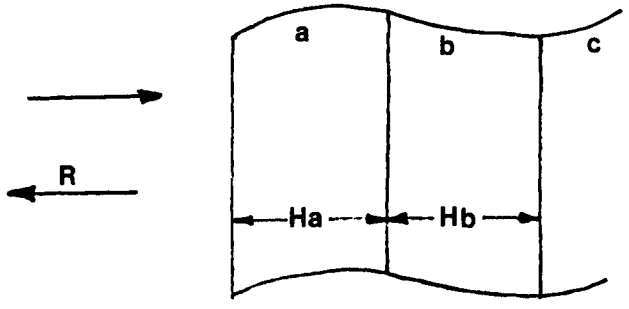

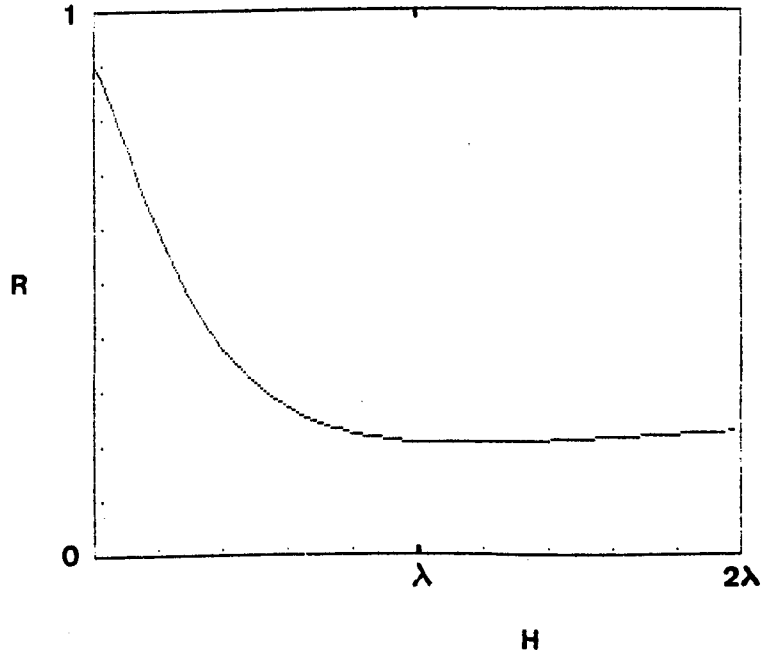

Fig.3.2.10.

TWO SUB-LAYER REFLECTIVITY MODEL

Reflectivity, R, vs total thickness, H.

(i) a; n=1.75, k=0.55, b; n=1.53, k=0.95

(ii) a; n=1.85, k=0.35, b; n=1.75, k=0.55

(i) α (ii) c; n=0.27, k=3.25 (Cu)

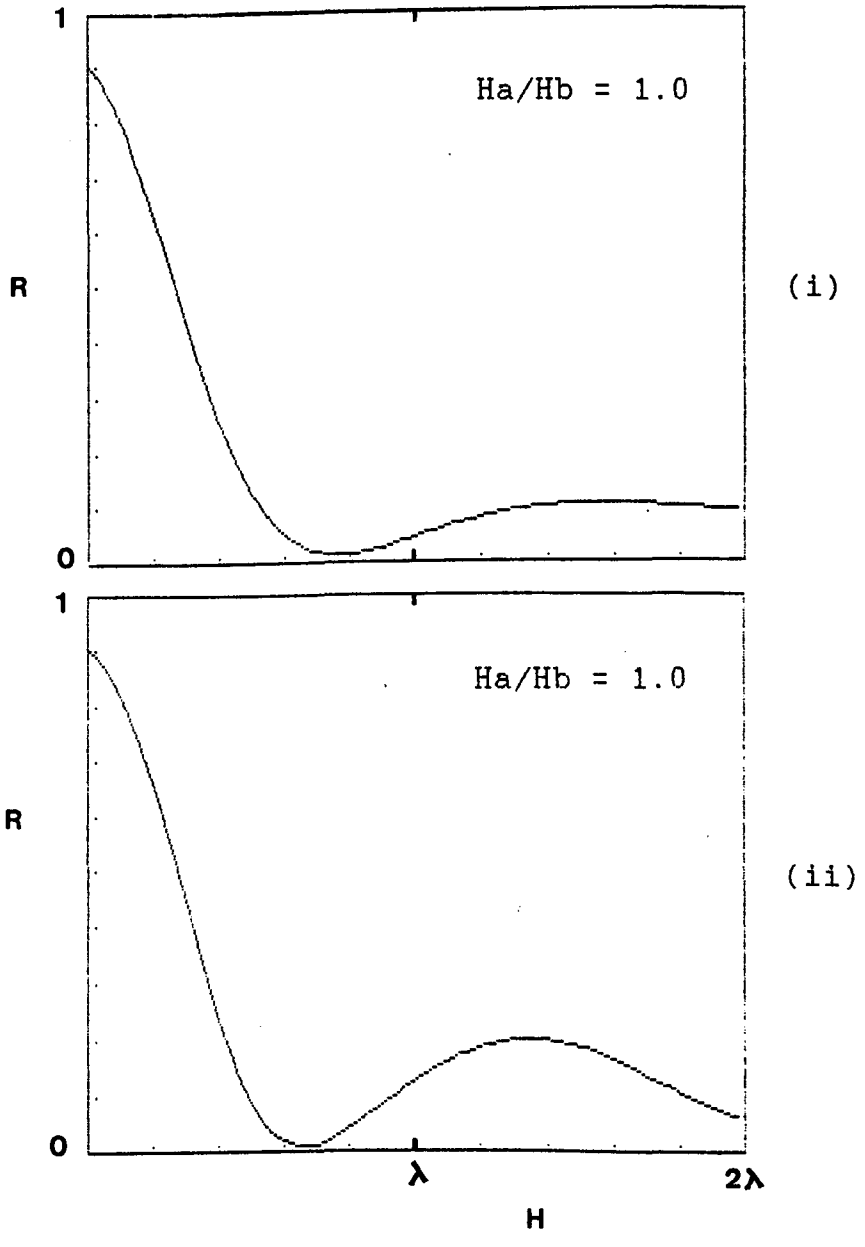

Fig.3.2.11.

TWO SUB-LAYER REFLECTIVITY MODEL

Reflectivity, R, vs total thickness, H.

(i) a; n=1.75, k=0.55, b; n=1.53, k=0.95

(ii) a; n=1.85, k=0.35, b; n=1.75, k=0.55

(i) α (ii) c; n=0.27, k=3.25 (Cu)

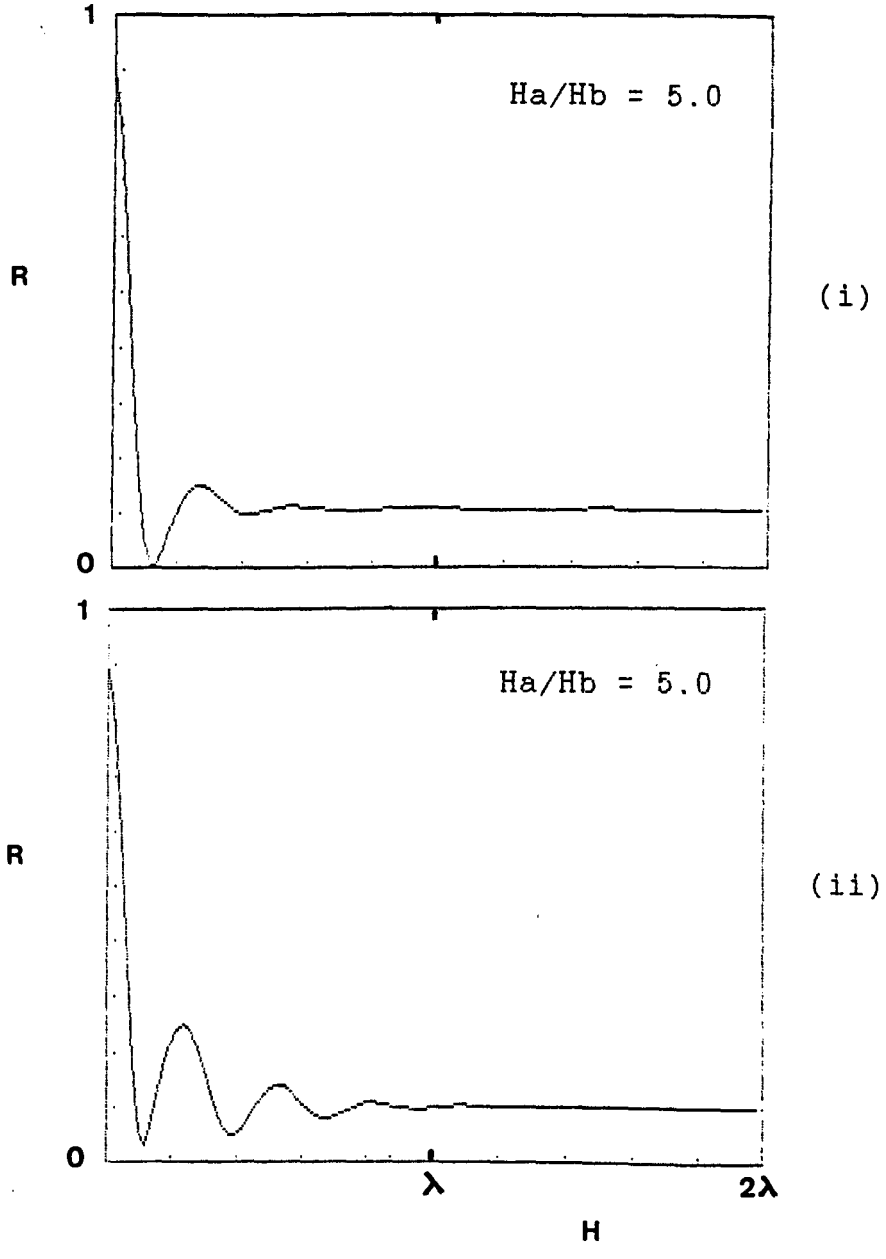

Fig.3.2.12.

TWO SUB-LAYER REFLECTIVITY MODEL

Reflectivity, R, vs total thickness, H.

a; n=1.95, k=0.20 (CuCl)

b; n=1.53, k=0.95 (Cu_xCl)

c; n=0.27, k=3.25 (Cu)

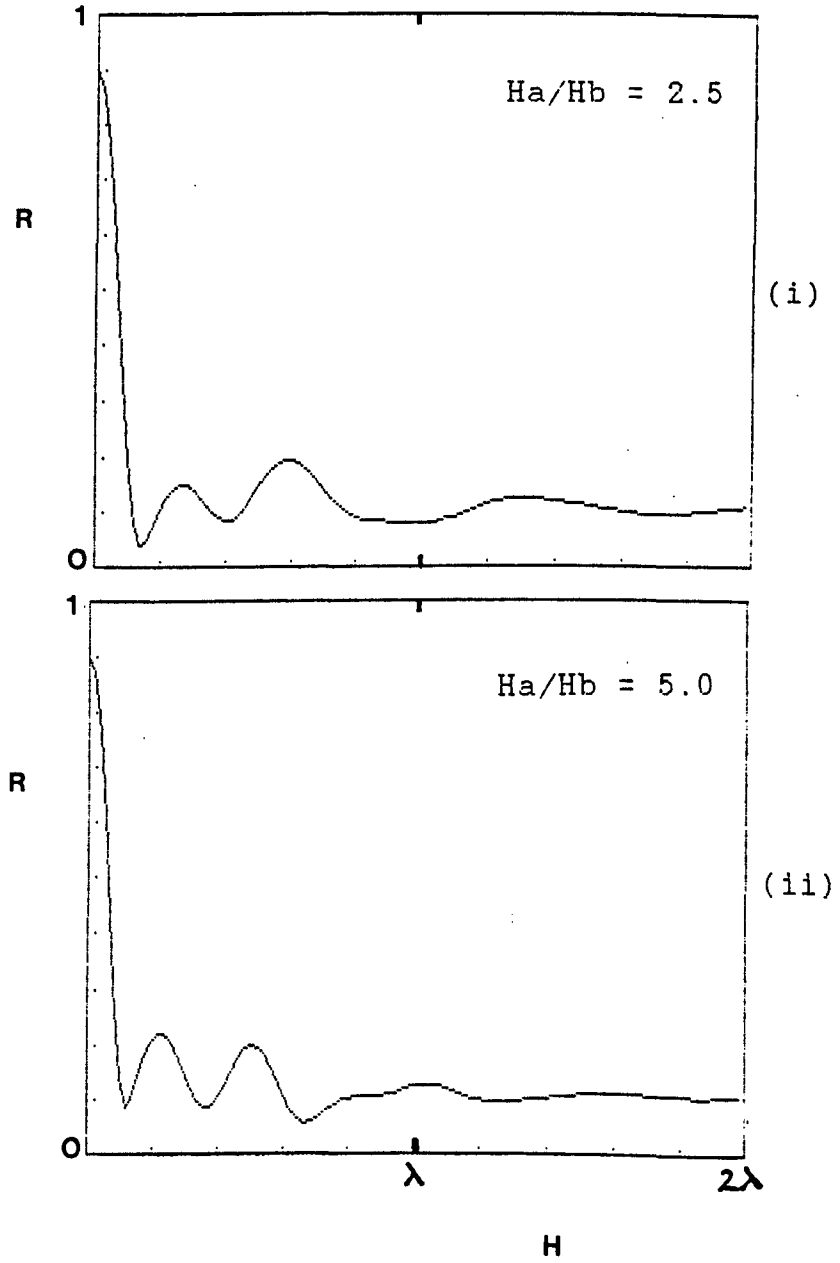

Fig.3.2.13.

TWO SUB-LAYER REFLECTIVITY MODEL

Reflectivity, R, vs total thickness, H.

a; n=1.95, k=0.20 (CuCl)

b (i); n=1.53, k=0.95 (Cu Cl)

b(ii); n=1.75, k=0.55 (Cu Cl)

c; n=0.27, k=3.25 (Cu)

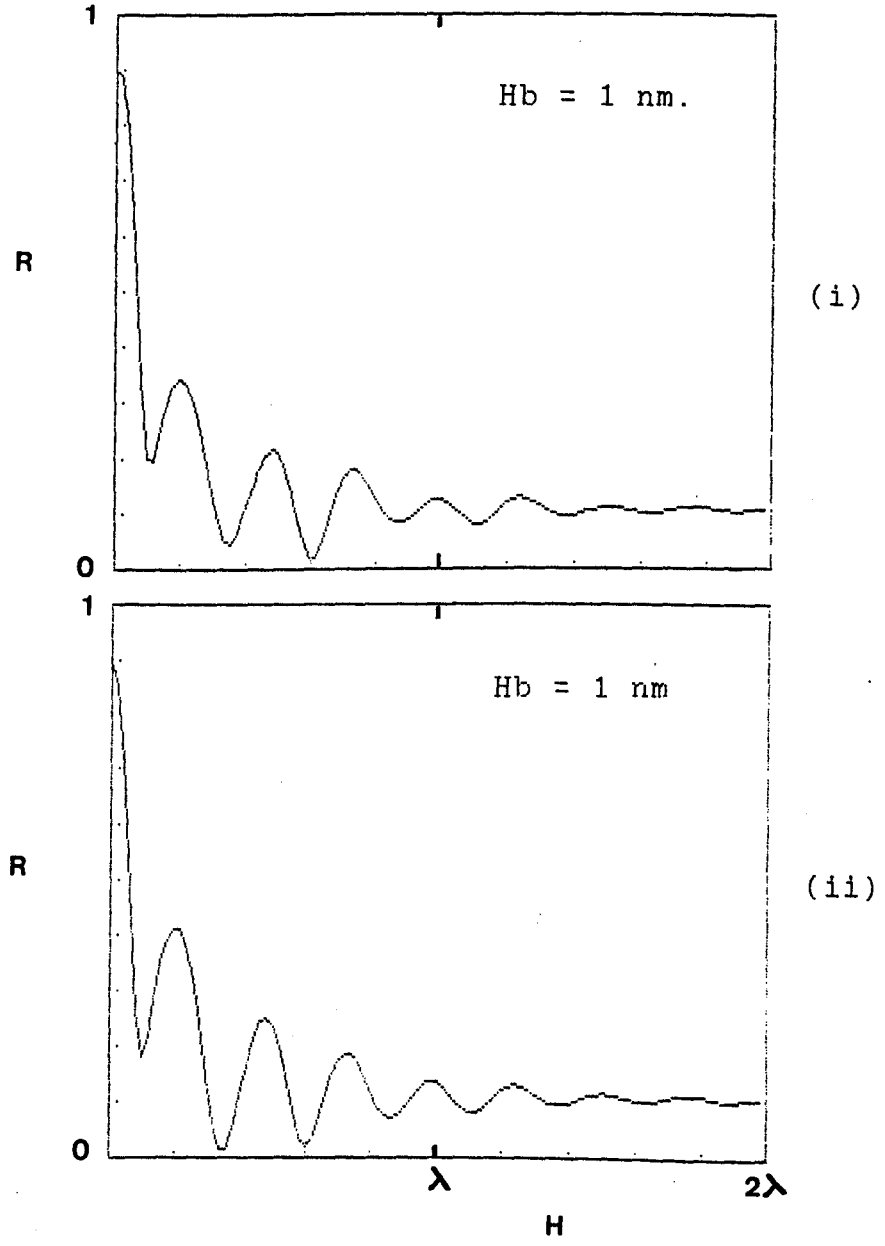

Fig.3.2.14.

CHLORINATION OF COPPER

Reflected intensity of probe beam and monitored chlorine gas pressure in cell as a function of time.

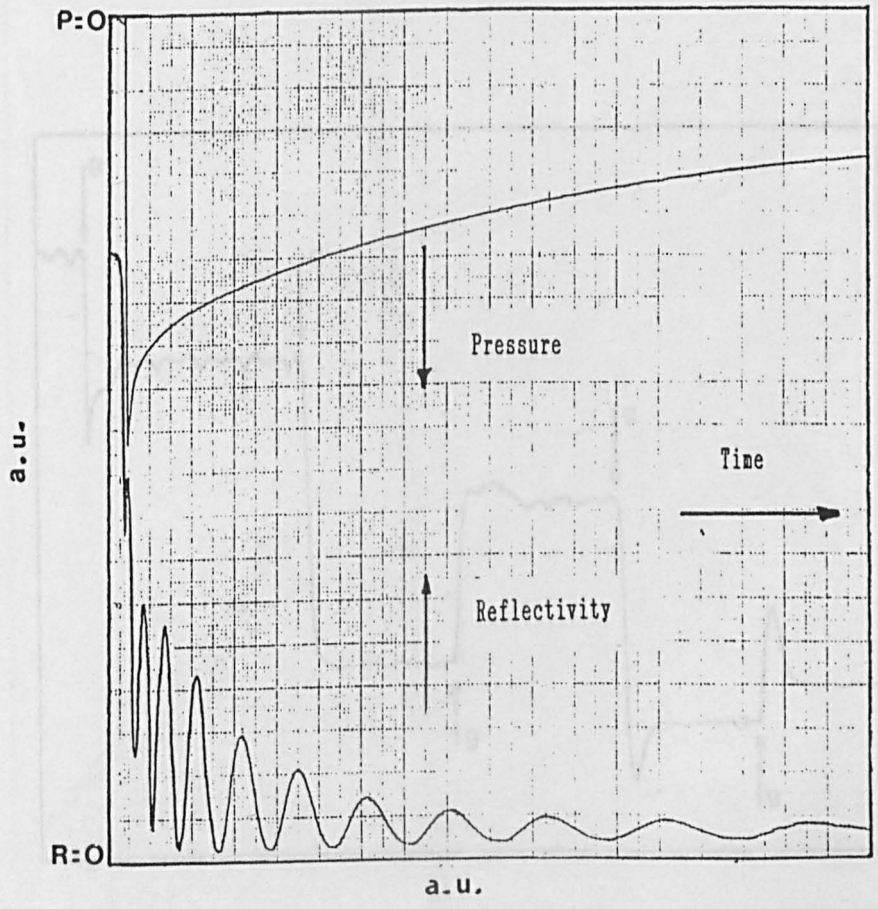

Fig.3.2.15.

CONTROLLED GROWTH OF CHLORIDE LAYER

Reflected Intensity of probe beam during controlled injection of chlorine gas into cell.

g - gas injection point.

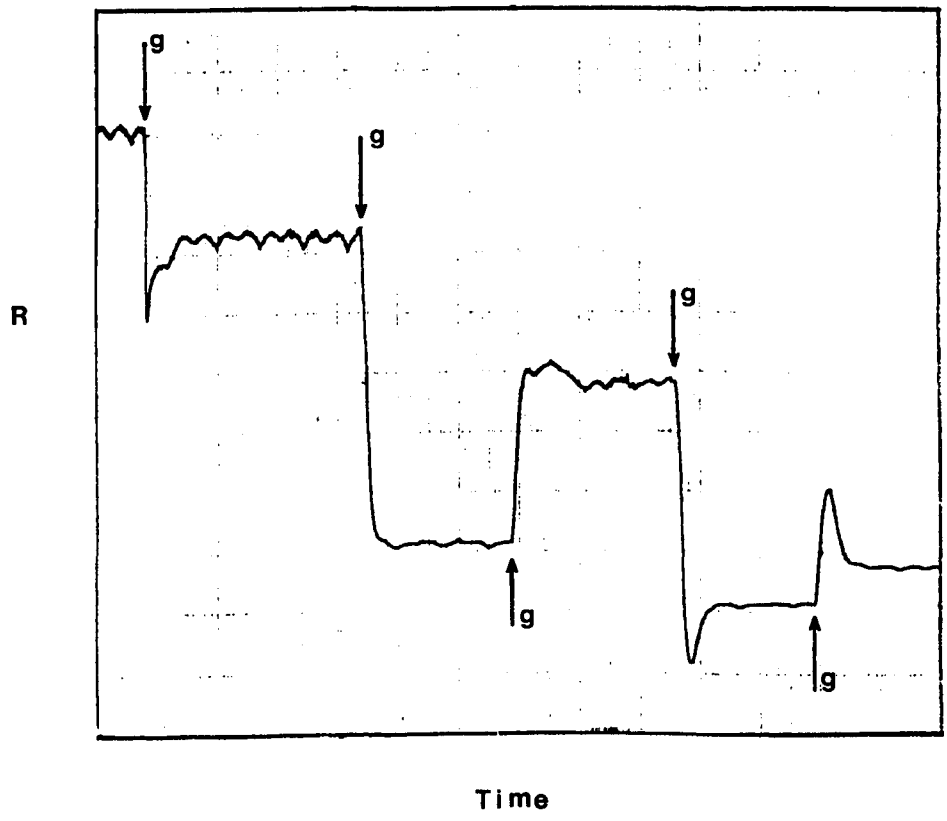

Fig.3.2.16.

DETERMINATION OF REFRACTIVE INDEX, n.

Measured metrical thickness of chloride layers as a function of product of maxima number, m, and half wavelengths, $\lambda/2$.

Gradient $1/n = 2H/m\lambda$

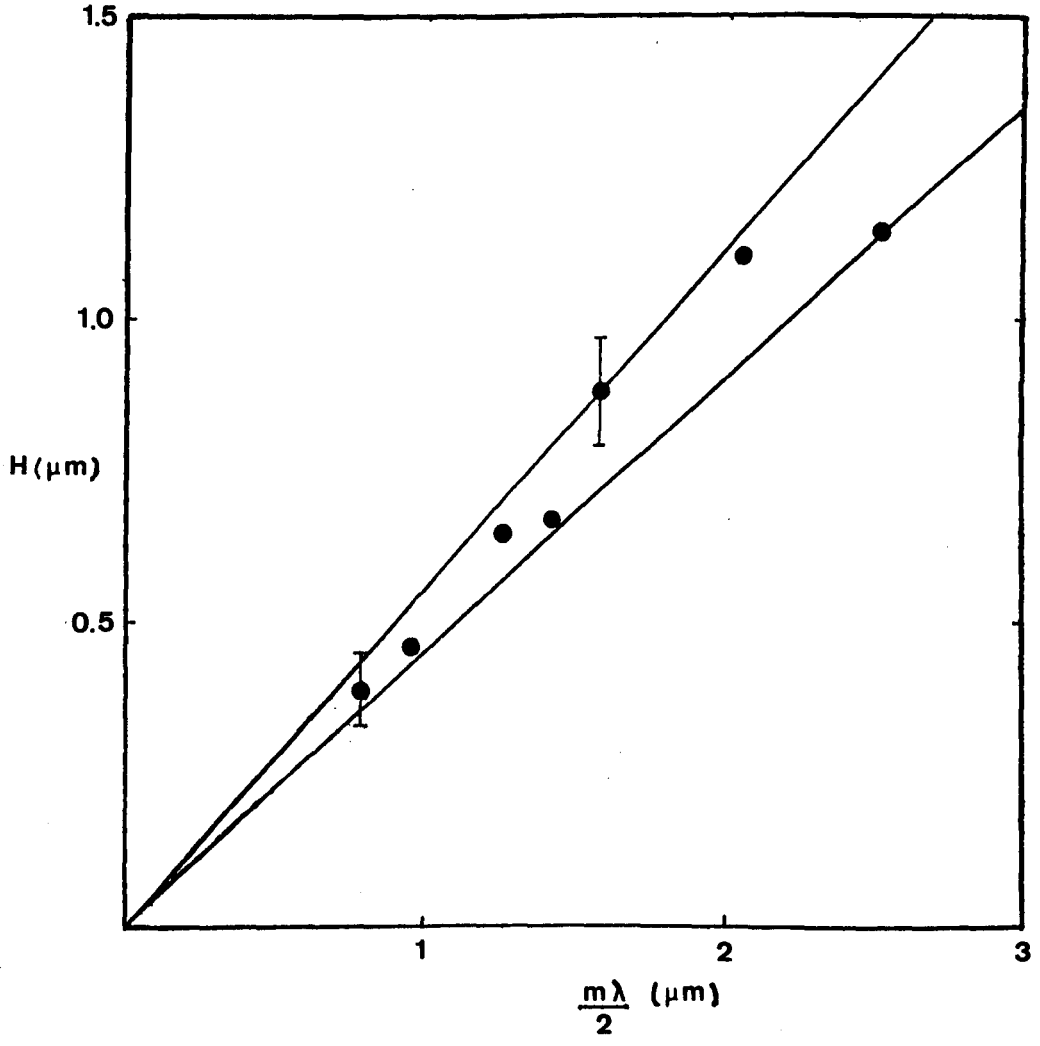

3.3. RESULTS AND OBSERVATIONS

In this section the results of chloride growth-rate measurements, using the time-resolved interferometry technique, are presented. The chlorination of copper samples under a variety of chlorine pressure and copper substrate temperature conditions are presented.

In order to maintain conditions of constant pressure during the chloride growth it is necessary to ensure that the substrate area is comparatively small so that the amount of chlorine consumed is a small proportion of the total gas introduced into the cell. The latter strategy was employed to investigate the chloride growth rate as a function of pressure. Preliminary experiments carried out in the absence of a target substrate indicated that the gas consumption by the fabric of the cell was negligible in the pressure range investigated (0.05-25 torr) and of the order of 0.5 lusec (litre/mtorr/sec).

The 'instantaneous' exposure of copper samples to known chlorine gas pressures was achieved by means of a metering tube gas inlet to the cell. With the cell evacuated to base pressure of 10^{-6} torr the metering tube, having a volume of 1/100 of the total system, was filled to the required proportionate pressure and sealed from the gas line. The gas was introduced into the cell via a large bore 1/4 turn ball valve.

The chloride growth curves, i.e. thickness as a function of time, for foils exposed to 0.1,0.5,1.0,2.5,& 5.0 torr of

chorine at room temperature are shown in Fig.3.3.1. Some data points, corresponding to thicknesses that are multiples of $\lambda/4n$, have been omitted in the interests of clarity and the curve represents the best line drawn through all data points. The growth-rate, dH/dt, can be seen to increase with pressure and decrease with time.

Diffusion controlled behaviour of the gas is indicated by the fit of the data at each pressure to a straight line when H is plotted against $\sqrt{t}$ as shown in Fig 3.3.2. The line, however, does not pass through the origin and this initial growth up to approximately 50 nm is assumed, because of the difficulty of resolving the growth rate in this regime, to be linear with time. It should be noted that even at the lowest pressure studied the time to grow a 50nm film is less than 0.2 sec.

From the data an expression for the chloride thickness, H, with exposure parameters of pressure, p, and time, t, is assumed to be of the form :

$$H(p,t) = Ho(p) + B(p)\sqrt{(t - to)} \qquad (i)$$

Where Ho(p) is the thickness at time to, below which :

$$H(p,t) = A(p)t \quad \{ H < Ho,\ t < to \} \qquad (ii)$$

A(p) and B(p) are pressure dependent rate constants.

In order to evaluate A(p) and B(p) the gradient of the growth curve for the relevant regime is required. The gradients, $dH/d\sqrt{t}$, taken from Fig 3.3.2 are plotted as a function of pressure in fig 3.3.3, and the logarithmic plot of fig 3.3.4 yields :

$$B(p) = 0.415\ p^{0.3}$$

Similarly, for t<to, Fig.3.3.5 gives:

$$A(p) = 0.65\ p^{0.4}$$

Using these values together with equations (i) and (ii) model calculations for the growth curves with p=5.0 torr and p=0.1 torr are compared with the experimental results in Fig 3.3.6.

The temperature dependence of the chloride growth rate was investigated by controlling the copper substrate temperature during exposure to the gas. For temperatures above ambient the substrates were mounted on an electrically heated block of large thermal mass while for low temperatures the heater was replaced by a heat pipe which passed to the outside of the cell and the end of which could be immersed in a cold bath. The temperature of the sample was monitored by a fine wire, fast-response thermocouple sandwiched between the sample and block.

Growth curves for copper substrates exposed to 5 torr of chlorine gas in the temperature range of 5 to 100 °C are shown in Fig.3.3.7 from which it can be seen that there is an increase in growth rate with temperature. Diffusion controlled growth, indicated by a linear plot of H against $\sqrt{t}$, is less marked at high temperatures as illustrated by Fig 3.3.8 and the transition from linear to parabolic growth occurs at increasing thickness as the temperature is increased. The relationships dH/dt and dH/d$\sqrt{t}$ as a function of temperature for the early and later stages of the chloride layer development are shown in Figs.3.3.9 & 10 respectively.

The activation energy, Ea, for a chemical reaction is often derived from an Arrhenius-type rate expression:

$$Rate = C \exp [-Ea/RT]$$

where the pre-exponential factor, C, may be a function of temperature, T(K), and R is the gas constant (8.314J/K/mol). If the reaction rate is taken to be synonymous with the initial growth-rate, dH/dt, of the chloride layer, then a plot of ln(dH/dt) against 1/T should yield the activation energy from the gradient. Fig 3.3.11 shows that Ea varies from ~40 kJ mol^{-1} at low temperature to ~10 kJ mol^{-1} at the higher temperatures. These values are consistent with those expected for gas-surface reactions [1,2] but should be treated with some caution since the polycrystalline, engineering grade, copper and relatively high chlorine gas pressure used are not conducive to the discipline of well defined surface chemistry studies.

X-ray diffraction scans were obtained of four chloride layers prepared under conditions with P=0.5 & 5.0 torr and T = 15 & 75 °C, an example of which is shown in Fig.3.3.12. In each case the peak corresponding to the (111) plane of CuCl predominated by an order of magnitude over that of the next highest peak at (220), and no peaks corresponding to $CuCl_2$ were found. These results, when compared with standard x-ray diffraction patterns (JCPDS powder diffraction file No 6-344), suggest that the chloride layer forms with a preferred orientation which is independent of pressure and temperature.

Fig.3.3.1.

CHLORIDE GROWTH-RATE : PRESSURE

Chloride layer thickness as a function of exposure of copper to chlorine.
a: 5 torr, b: 2.5 torr, c: 1.0 torr
d: 0.5 torr, e: 0.1 torr.

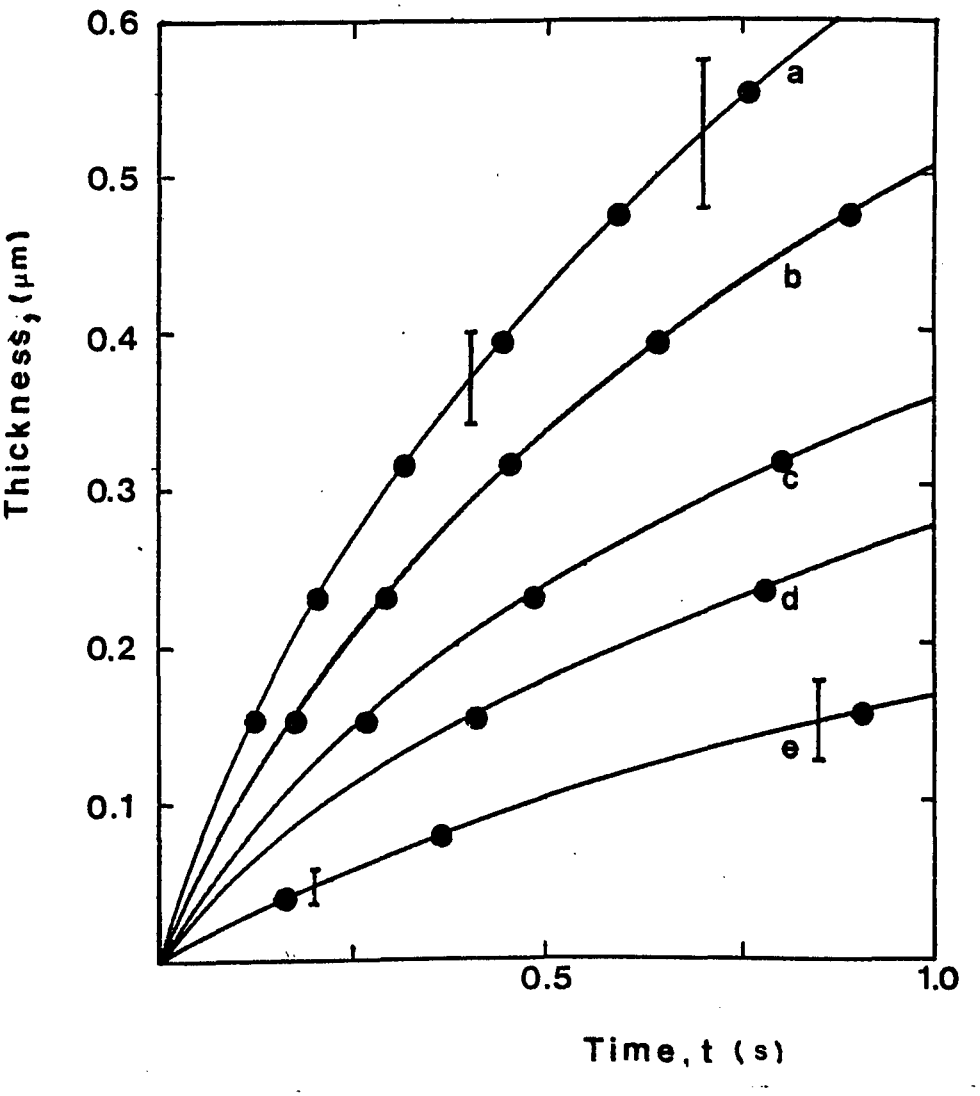

Fig.3.3.2.

CHLORIDE GROWTH-RATE : PRESSURE

Chloride layer thickness as a function of sqr. root of exposure time.
a: 5 torr, b: 2.5 torr, c: 1.0 torr
d: 0.5 torr, e: 0.1 torr.

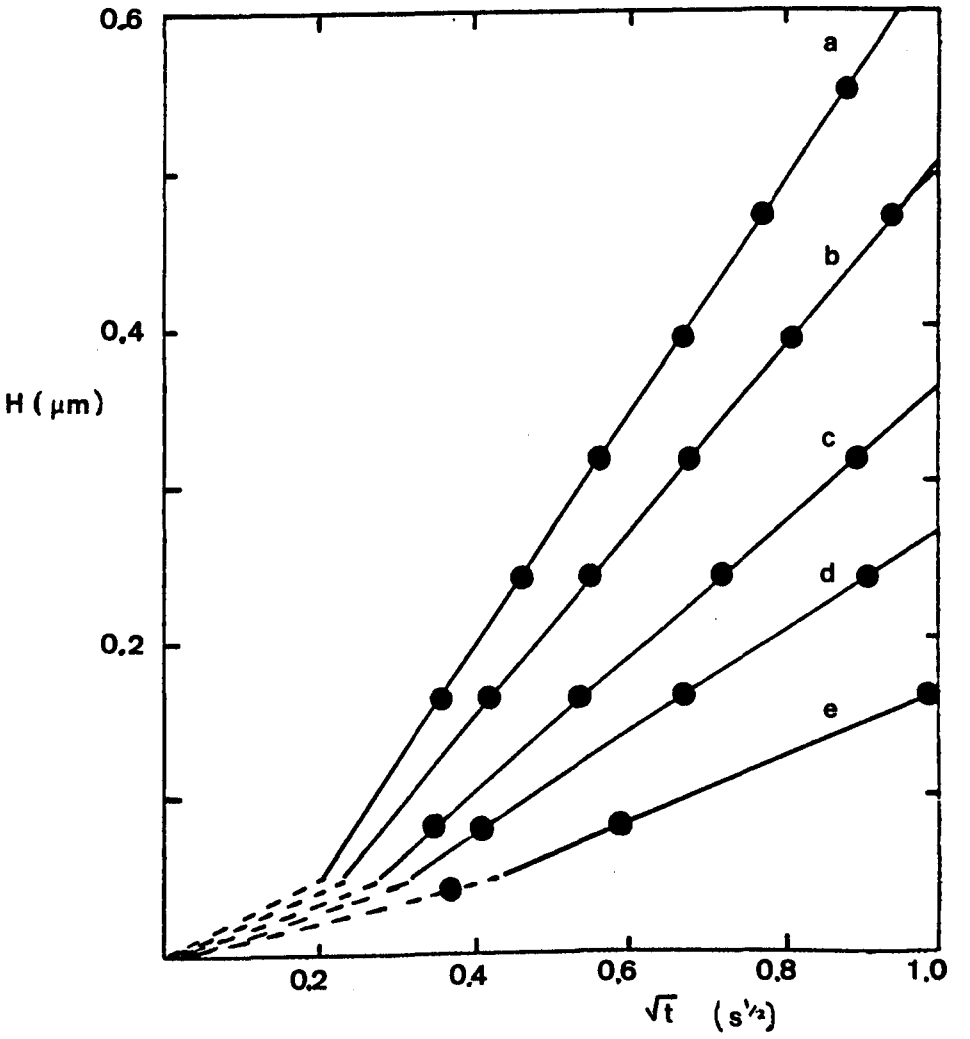

Fig.3.3.3.

CHLORIDE GROWTH-RATE : PRESSURE

Pressure dependence of growth-rate,

$dH/d\sqrt{t}$, (diffusion limited regime).

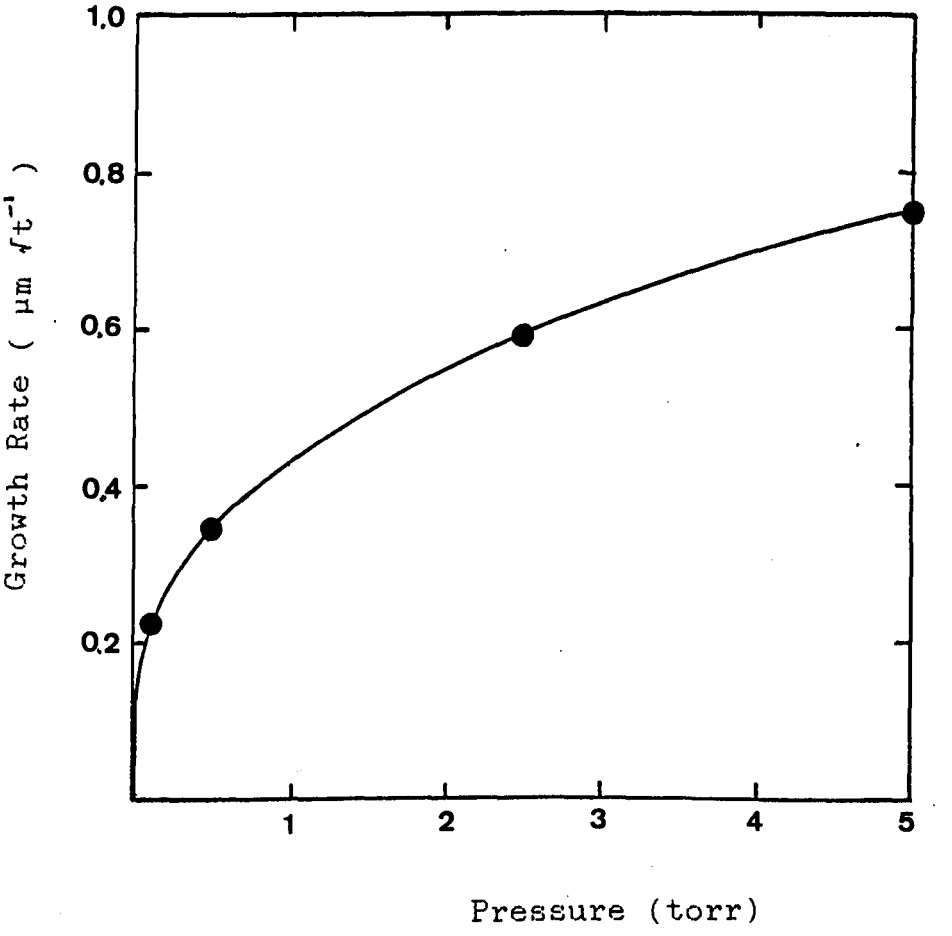

Fig.3.3.4.

CHLORIDE GROWTH-RATE : PRESSURE

Pressure dependence of growth-rate,
dH/d√t, (diffusion limited regime).
log.-log. plot.

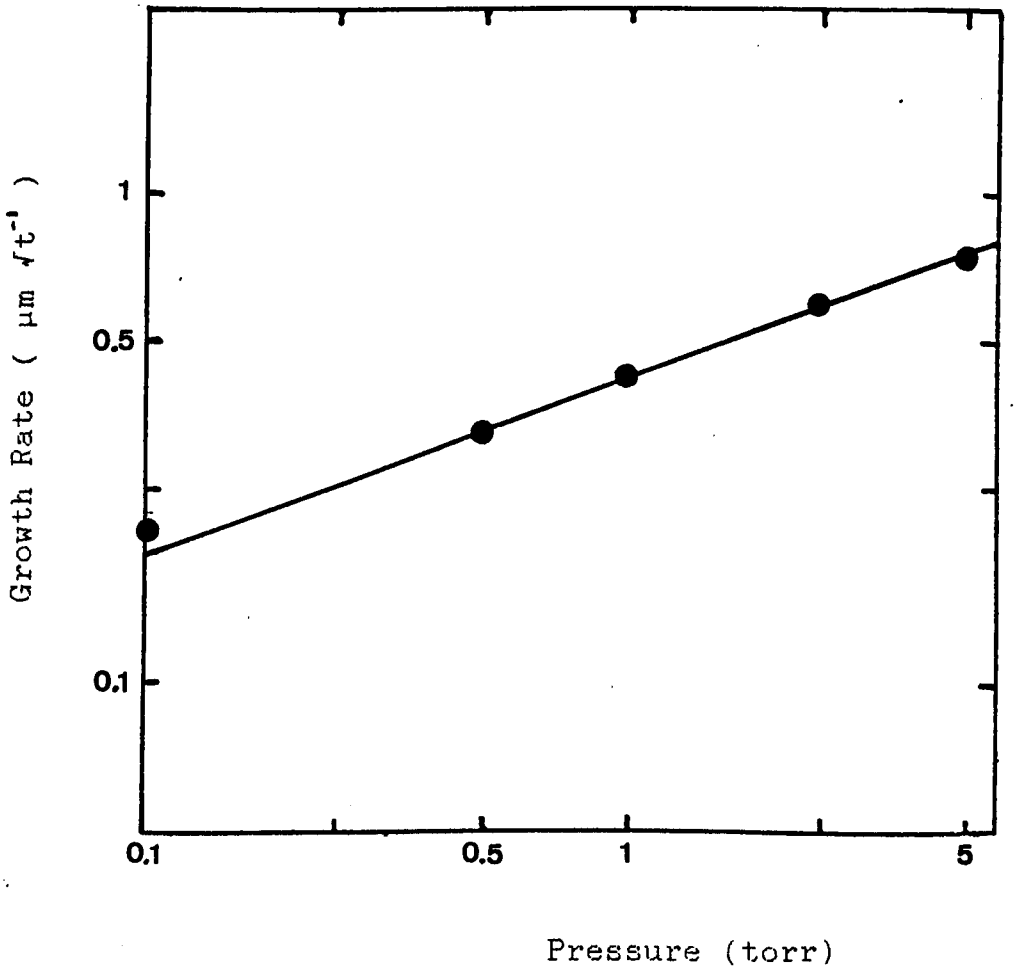

Fig.3.3.5.

CHLORIDE GROWTH-RATE : PRESSURE

Pressure dependence of growth-rate,
dH/dt, (linear growth regime).
log.- log. plot.

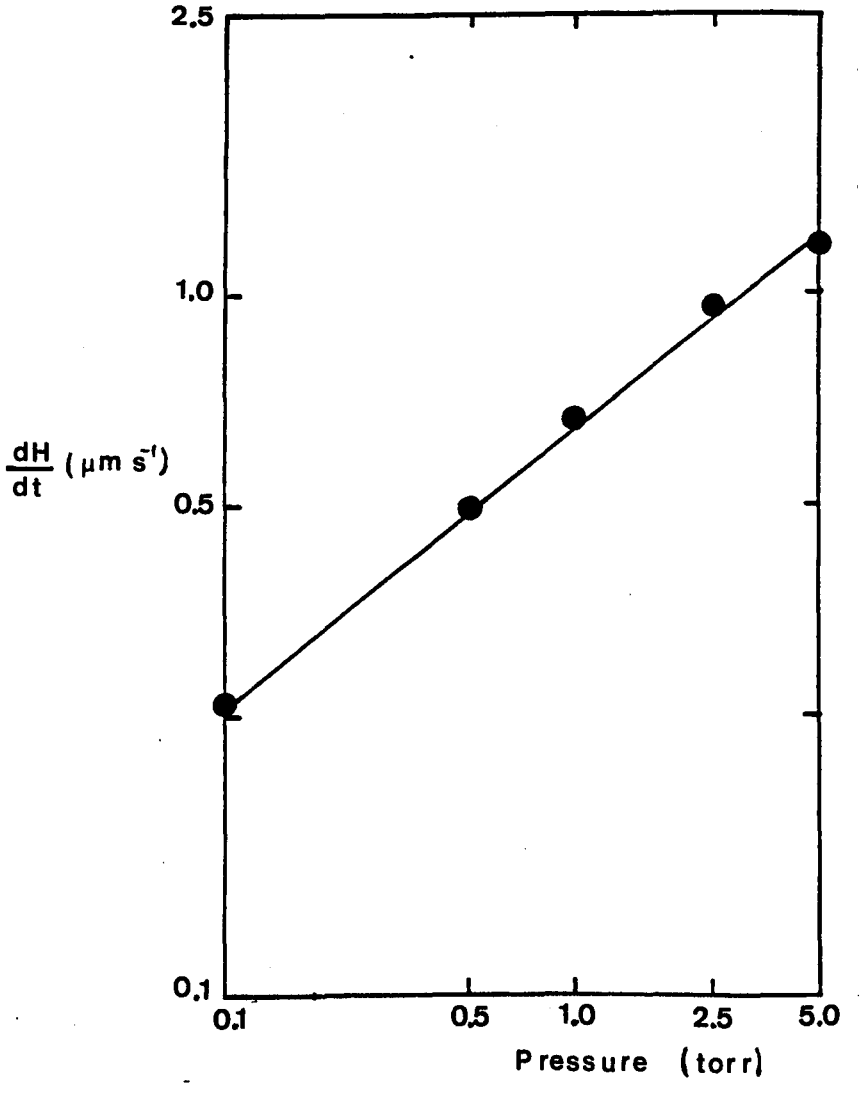

CHLORIDE GROWTH-RATE : PRESSURE

Comparison of model growth-rate
with experimental data.

——: $H = Ho(p) + B(p)(\sqrt{t}-\sqrt{to})$

● : Experimental.

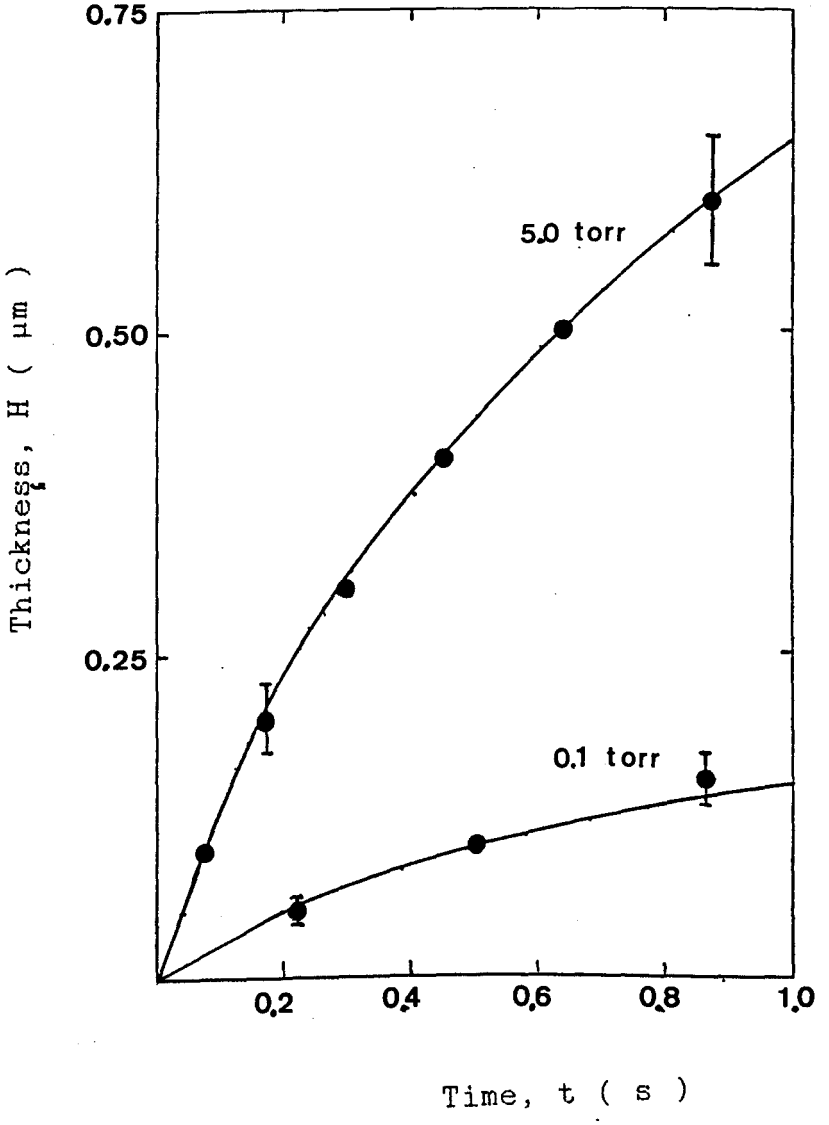

CHLORIDE GROWTH-RATE : TEMPERATURE

Chloride layer thickness as a function of exposure time to 5 torr chlorine.

a: 5 °C, b: 10 °C, c: 25 °C

d: 50 °C, e: 75 °C, f: 100 °C

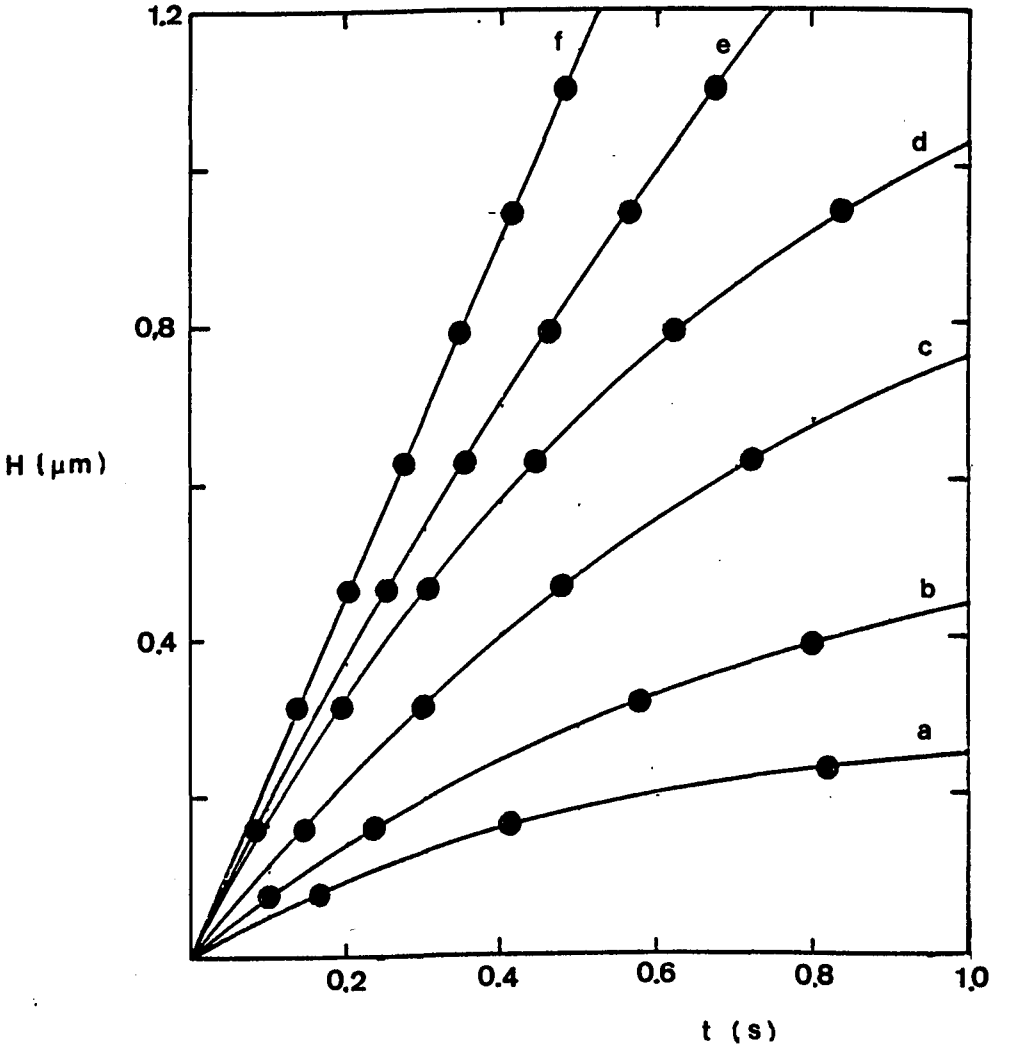

Fig.3.3.8.

CHLORIDE GROWTH-RATE : TEMPERATURE

Chloride layer thickness as a function of sqr. root exposure time (5 torr chlorine).
a: 5 °C, b: 10 °C, c: 25 °C
d: 50 °C, e: 75 °C, f: 100 °C

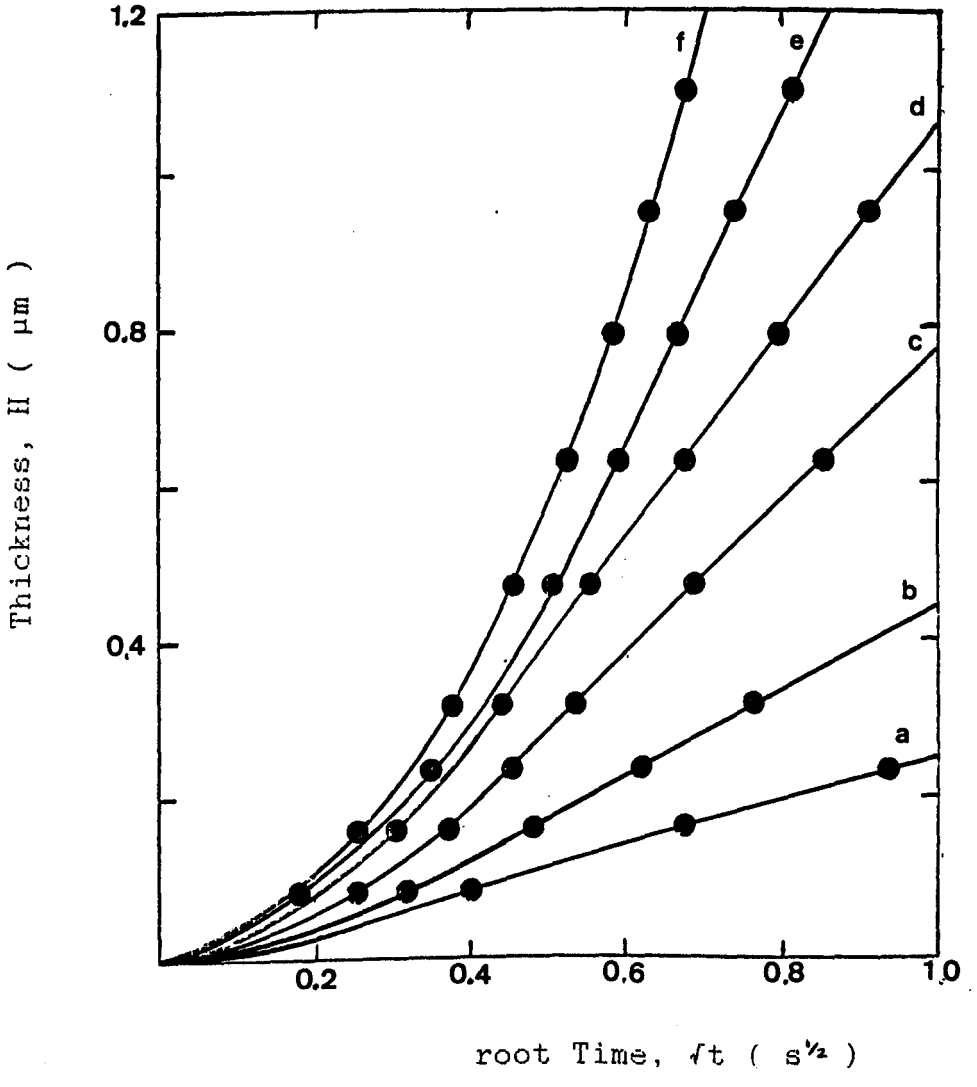

Fig.3.3.9.

CHLORIDE GROWTH-RATE : TEMPERATURE

Temperature dependence of growth-rate.

log.-log. plot (linear growth regime).

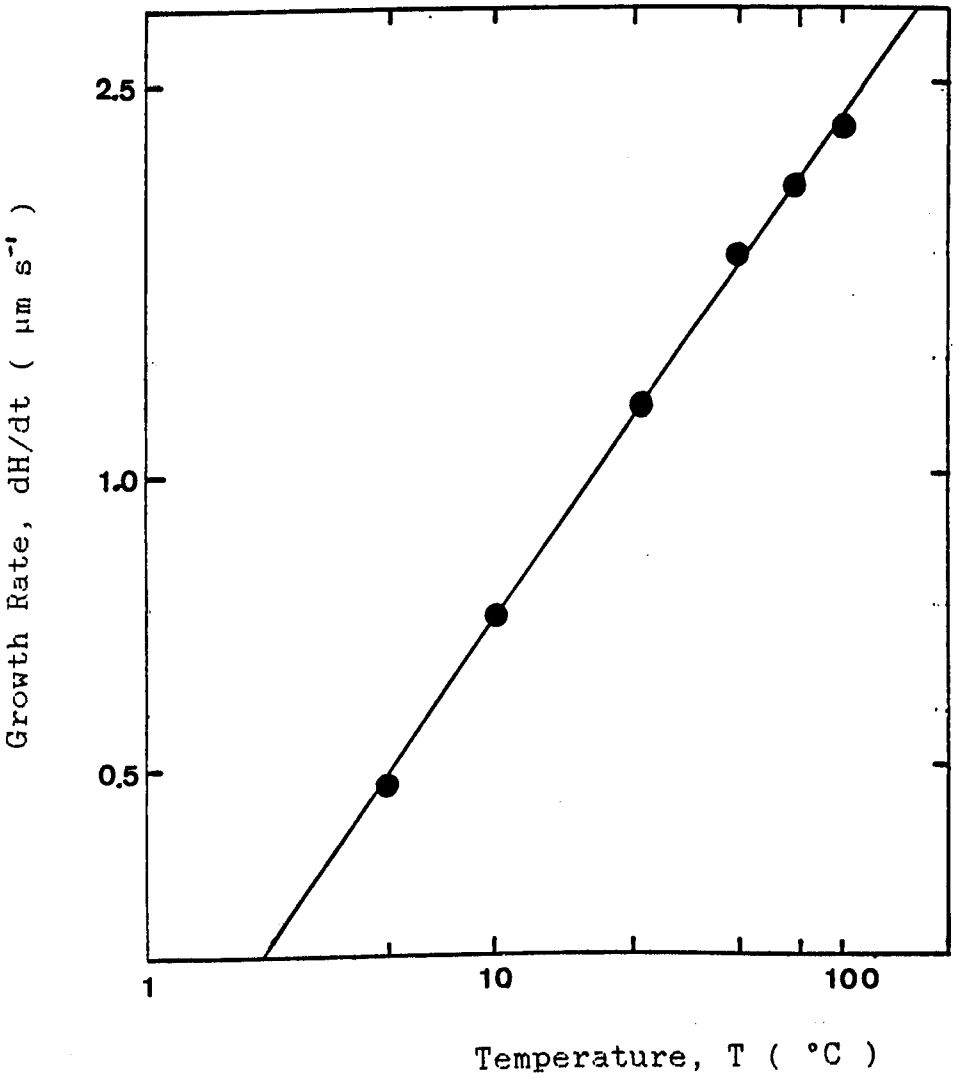

Fig.3.3.10.

CHLORIDE GROWTH-RATE : TEMPERATURE

Temperature dependence of growth-rate.

dH/d√t vs. T (diffusion limited regime).

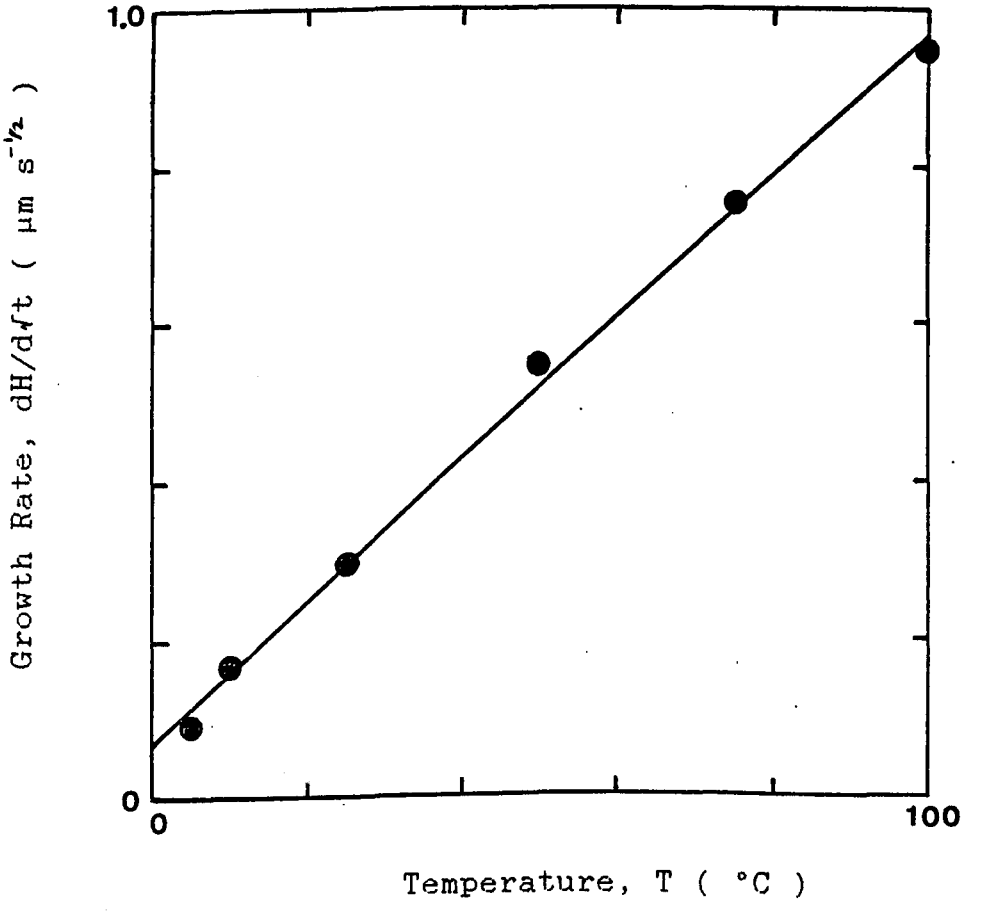

Fig.3.3.11.

CHLORIDE GROWTH-RATE : TEMPERATURE

Arrhenius plot: ln(dH/dt) vs. 1/T.

Initial growth regime.

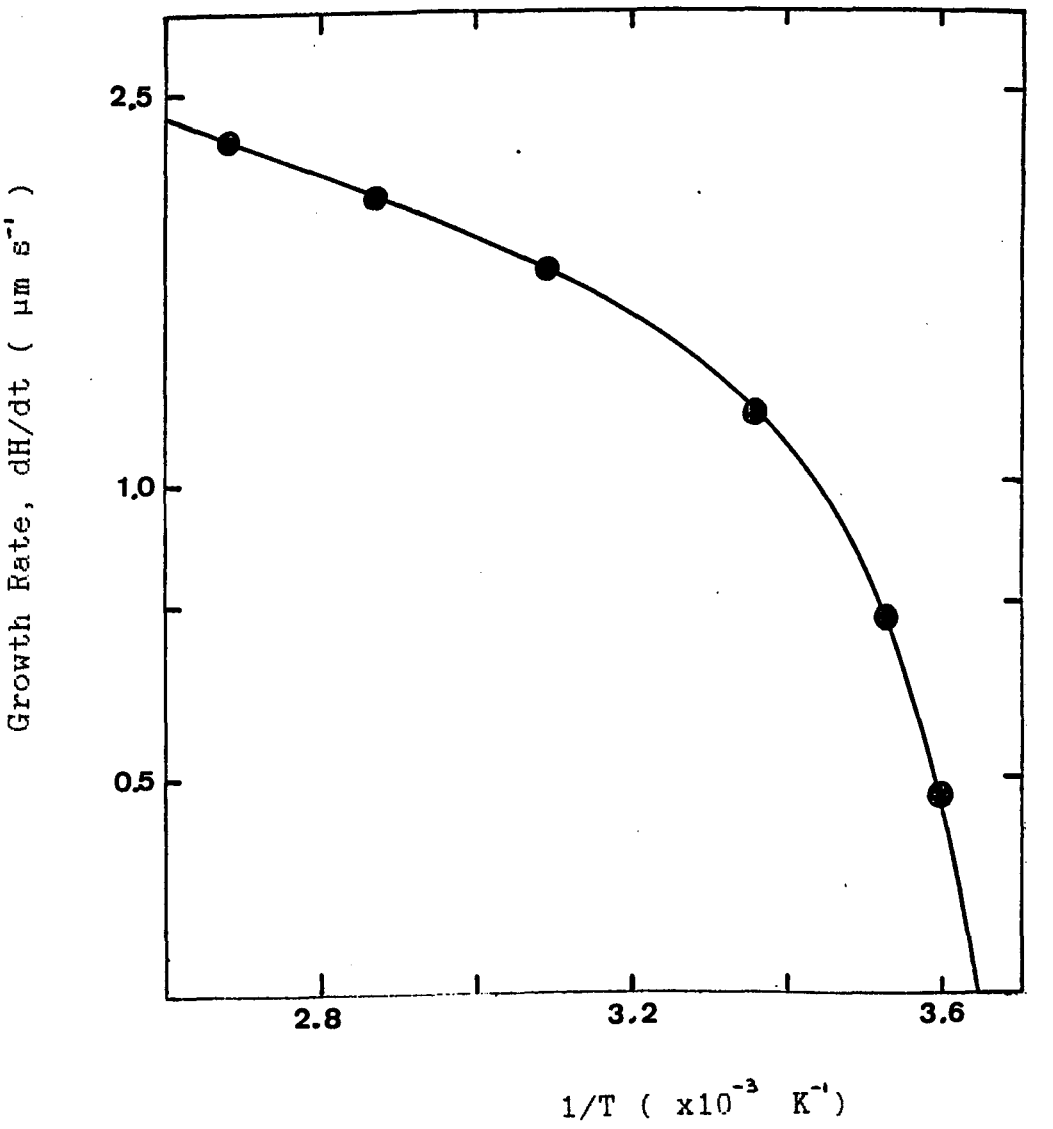

Fig.3.3.12.

. CHLORIDE GROWTH : X-RAY DIFFRACTION

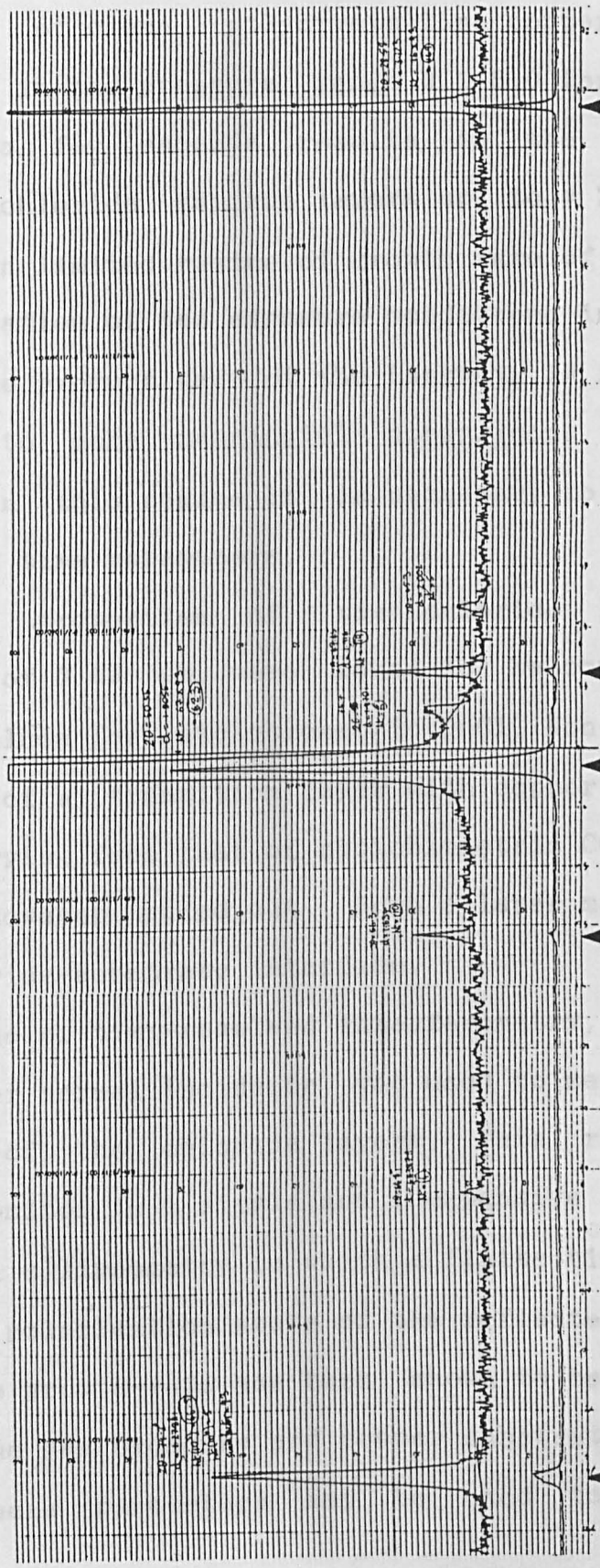

3.4. CONCLUSIONS

The exposure of clean, polycrystalline copper surfaces to chlorine gas in the pressure range 0.1-5.0 torr for periods of up to a few seconds results in the formation of substantial chloride surface layers up to ≈ 2 μm thick. In the diffusion limited regime of growth rate of these layers, the specification of the exposure conditions in terms of the pressure-time product unit of the Langmuir is inappropriate. In order to make meaningful comparisons of exposure conditions in this regime it is necessary to specify both pressure and time parameters.

The optical properties of the chloride layers, at a wavelength of 0.63 μm, were found to be consistent with published values for stoichiometric CuCl. Non-stoichiometry in the form of a transition layer with copper concentration gradient varying from that of stoichiometric CuCl to that of Cu is not, however, ruled out. Such a layer may exist close to the chloride-substrate interface.

The technique of time-resolved interferometry, using a He-Ne laser at near normal incidence, was used to measure the rate of growth of the chloride layers. This real-time film thickness monitor is a simple and inexpensive alternative to conventional ellipsometry in which a finite time is required to scan the polarisation state of the reflected beam.

The chloride growth-rate has been shown to be a function of both chlorine gas pressure and copper substrate temperature. Both of these parameters may be used to control the

growth-rate and the former may be an important factor in the control of the laser-chemical etching process.

The growth of a chloride layer represents a conversion and, hence, a proportional consumption of the copper substrate. Thus the maximum laser etch-rate of the metal can be expected to be limited by the rate at which the chloride layer forms between ablating laser pulses. The laser induced etch-rate will be some function, therefore, of ambient chlorine gas pressure and laser prf as well as the incident laser fluence.

A saturation of the ablation rate will be expected to occur when the fluence is high enough to remove all of the chloride formed in the interpulse period, This is unlikely to appear as a flat plateau on the etch-rate vs. fluence curve, however, since energy in excess of that required for ablation will lead to transient heating of the substrate. With higher substrate temperatures the chloride growth rate is enhanced resulting in a shift of ablation rate saturation to higher thickness values.

In the next chapter studies of UV-excimer laser ablation of copper in a chlorine environment are described.

3.5.

REFERENCES

[1] Tompkins,F.C.
'Chemisorption of Gases on Metals'
Academic Press, London, (1978).

[2] Roberts,M.W. & McKee,C.S.
'Chemistry of the Gas-Metal Interface'
Clarendon Press, Oxford, (1978).

[3] Oudar,J.
'Physics and Chemistry of Surfaces'
Blackie, London, (1975).

[4] Goddard,P.J. and Lambert, R.M.
Surf. Sci. 67, (1977), 180.

[5] Westphal,D. and Goldmann, A.
Surf. Sci. 131, (1983), 92 & 113.

[6] Delamare,F. and Rhead, G.E.
Surf. Sci. 28, (1971), 267.

[7] Citrin,P.H., Hamman,D.R., Mattheiss,L.F. & Rowe,J.E.
Phys. Rev. Lett. 49, (1982), 445.

[8] Winters,H.F.
J. Vac. Sci. Technol. A3, (1985), 786.

[9] Sesselmann,W. and Chuang,T.J.
Surf. Sci. 176, (1986), 32 & 67.

[10] Andrew,R.
Appl. Phys. B 41, (1986), 205.

[11] Baufay,L.,Houle,F.A. & Wilson,R.J.
I.B.M. Research Report RJH.5338 (1986).

[12] Boyd,I.W.

'Laser Processing of Thin Films and Microstructures ' Ch.4 (166 References.) Springer-Verlag, Berlin, (1987).

[13] Cabrera,N. and Mott,N.F.

Rep. Prog. Phys. 12, (1948/9), 163.

[14] Deal,B.E. and Grove,A.S.

J. Appl. Phys. 36, (1965), 3770.

[15] Lewis,E.A. and Irene,E.A.

J. Vac. Sci. Technol. A4, (1986), 916.

[16] Heavens,O.S.

'Optical Properties of Thin Solid Films' Butterworth, London, (1955).

[17] Milek,J.T. and Newberger,M.

'Linear Electrooptic Modular Materials' Handbook of Electronic Materials Vol 8 I.F.I./Plenum, New York. (1972).

[18] Weaver,J.H.,Krafka,C.,Lynch,D.W. and Koch,E.E.

'Optical Properties of Metals' 2 Vols. Fachinformationszentrum, (1981).

[19] Vasicek,A.

'Optics of Thin Films' North-Holland, Amsterdam, (1960)

[20] Jerphagnon, J. et al.

Comptes. Rendus. B. 265, (1967), 1032

[21] Feldman,A. & Horowitz,D.

J. Opt. Soc. America, 59, (1969), 1406.

[22] Kaifu,Y. & Komatso,T

J. Soc. Phys. Japan, 25, (1968), 644.

CHAPTER FOUR

THE EXCIMER LASER ETCHING OF COPPER IN CHLORINE

4.0 INTRODUCTION

It was seen, in the last chapter, that the thickness of the chloride layer formed on copper in a chlorine gas environment is dependent, at constant temperature, upon the gas pressure and time of exposure. These two parameters, together with the incident laser fluence , are thus expected to be important in determining the net etch rate of copper per laser pulse. Since the thickness is not a linear function of the pressure-time product the use of the single parameter 'exposure' would, in this case, not be justifiable as a means of reducing the number of variables.

The etch rates, expressed as depth of material removed per laser pulse, of free-standing, polycrystalline copper foils have been measured under a variety of conditions, albeit non exhaustive, in order to evaluate the contributions of laser fluence, pulse-repetition-frequency (prf), wavelength, and the chlorine gas pressure.

Spectroscopic examination of the UV-visible emission from the luminous plume of ablated material has been carried out to identify the principal species involved. Spatial and time resolved signals were used to calculate the velocity of the ablated particles.

In the first section the experimental arrangement is described and the methodology discussed. The results of studies of the etch rate of copper as a function of laser fluence at different laser wavelengths, chlorine gas pressures and laser prf are presented in the next three

sections. The emission spectra of the ablated material in the UV-visible region together with the ablation velocity of the copper species are shown in section five. The final section consists of a discussion of these results in the light of which a semi-quantitative model of the etching process is presented and compared with real-time thickness monitor laser probe signals obtained during the ablation process.

4.1.

EXPERIMENTAL PROCEDURE

An evacuable chamber in which the environmental conditions of the target could be controlled was constructed of aluminium, a material chosen because of its low cost, excellent machineability and the stable oxide layer which prevents the reaction of the dry chlorine gas with the parent metal. Other internal parts such as target holders and clamps were made of aluminium, nickel plated brass or PTFE as appropriate. It should be noted that 316 grade stainless steel was avoided because of its rather strong reaction with chlorine.

A 75 mm diameter UV grade Suprasil window, having a transmission cut-off at approximately 180 nm, was sealed to the front of the cell with a 'Viton' o-ring as was the back plate and Suprasil side windows. The large front window served to admit the laser radiation normal to the target surface as well as facilitate observation of the target via a stereo microscope and give access for the He-Ne laser interferometry probe beam, Fig.4.1.1.

The target position within the cell could be translated in the direction of the laser beam propogation by micrometer adjustment and the whole cell position could be similarly aligned in the two directions orthogonal to this.

The excimer laser ouput beam fluence profiles were measured in the electrode-electrode direction and at right angles to this using a 'Delta Developments' linear array detector. Typical profiles are shown in Fig.4.1.2. A rectangular

aperture was employed to select an area of uniform energy distribution from the beam and the resultant beam profile, immediately after the aperture, is shown in Fig.4.1.3.

A de-magnified image (M ≈ 0.1) of the mask was projected onto the target by means of a single 'Suprasil' lens with NA = 0.125. The optical system and its use in pattern generation by projection etching is discussed more fully in chapter 6. It should be noted, however, that it is only on image planes within the depth of focus of the optical system that the laser energy distribution at the target can be considered, in the absence of aberrations, to have the same uniformity as measured at the mask plane. It is for this reason that the fluence was varied by the use of attenuators, placed in the beam path before the aperture, rather than by the de-focusing of the image to vary the beam dimensions. Furthermore, in a focussed image system, greater confidence can be placed in determining the laser beam dimensions at the target in order to calculate the target plane fluence.

The laser energy was measured at a position after the target plane, so as to account for window and lens losses, with a pyroelectric detector calibrated against a N.P.L. calibrated device and the beam area measured from ablated holes in a low threshold polymer material ('Mylar').

Alignment of the optical system was achieved by the use of a 'Mylar' sheet target which was exposed to a fluence just above threshold where the etch rate exhibits maximum sensitivity to changes in fluence. Adjustment of the transverse position of the optical components was then

made to minimise inhomogeneities in the etch rate over the irradiated area.

In order to monitor shot-to-shot variations in laser energy over the often long period of the experiments, a small section of the unused portion of the beam was intercepted at the mask plane and directed onto a sensitive pyroelectric detector which was cross calibrated against that used for target energy measurements.

The cell was evacuable to a base pressure of $\approx 10^{-6}$ torr and the chlorine (research grade: 99.96%) gas pressure was monitored with a 'Furness' capacitance manometer the maximum resolution of which was 0.005 torr. To avoid the ingress of water vapour the cell was flooded with dry Argon when opened for sample replacement.

The etch rates were calculated from the number of laser pulses required to etch right through 25 micron thick copper foils (99.9% purity), the progressive etching and the end point being observed by means of the stereo microscope. To check the validity of this approach the number of laser pulses to etch through foils of different thicknesses was measured and is shown in Fig.4.1.4. The linear relationship between pulse number and foil thickness serves to illustrate that the use of a 25 μm thick foil minimises any 'end effects' of the first and last few pulses on the average etch rate and that small variations in foil thickness do not contribute significant errors to the data.

Each experimental point presented in the following results is the average of at least five measurements made on different samples and the error bars represent the standard

deviation of the data. The data were found to be highly reproducible even when using foils of 'engineering' grade copper, provided, as it will be seen, that the environmental and laser conditions were carefully controlled.

The copper foils were used 'as received', i.e. with a native oxide layer thought to be approximately 5 nm thick, being degreased in alcohol and dried before mounting in the cell. The sample mounting was such that the area of foil irradiated was unsupported at the rear.

The luminous plume accompanying the laser ablation was examined spectroscopically in the UV-Visible region with a 300 mm 'Bentham' monochromator (1 nm resolution) and EMI 9813QB photo-multiplier tube. The arrangement, shown in Fig.4.1.1, allowed the plume to be observed at normal incidence to its mean expansion direction and provided either integrated spectra or time resolved (≈ 3 ns rise time) measurements of selected spectral features.

A portion of the plume was imaged onto the entrance slit of the monochromator at a magnification of unity so that the spatial resolution along the target normal was equal to the slit width (≈ 50 μm). Translation of the target and laser focussing lens with respect to the monochromator slit allowed discrete sections of the plume to be examined.

For time-resolved work the photomultiplier output was terminated in 50 Ω and amplified by a Tektroninix 7A15A plug-in. This enabled the time of arrival of luminous species, selected by the monochromator grating, to be measured at the point of observation; By measuring the arrival time at increasing distances along the target normal

the expansion velocity of the species could be deduced.

Emission spectra of the ablated products in the 180-620 nm range were obtained by means of an integrating amplifier with variable input C R time set to an appropriate value for the laser prf and grating scan rate used. The drive for the chart recorder was controlled by a signal from the grating stepper motor and the system calibrated against known spectral line sources.

The monochromator was also used to investigate any possible absorption by the chlorine gas in the range of laser wavelengths of interest. A comparison of emission spectra of a deuterium lamp viewed through the cell under vacuum and with 5 torr chlorine is shown in Fig.4.1.5. It can be seen that for the ArF (193 nm) and KrF (248 nm) lasers, chlorine is essentially transparent whereas the XeCl (308 nm) line lies close to the maximum absorption. The absorption spectrum deduced from this measurement is shown in Fig.4.1.6 for a pressure-path length product of 275 torr cm. A series of chlorine attenuated deuterium lamp spectra, using different path lengths and pressures, together with transmission measurements using the XeCl laser were obtained to determine the absorption coefficient at 308 nm. The data are shown in Figs.4.1.7 & 8 and, as there is little difference between the small signal and laser (1 J cm^{-2}) data, it appears that the value of 5.7±0.4 $torr^{-1}cm^{-1}$ obtained for the absorption coefficient of chlorine is independent of fluence in this regime.

Fig.4.1.1

EXPERIMENTAL ARRANGEMENT

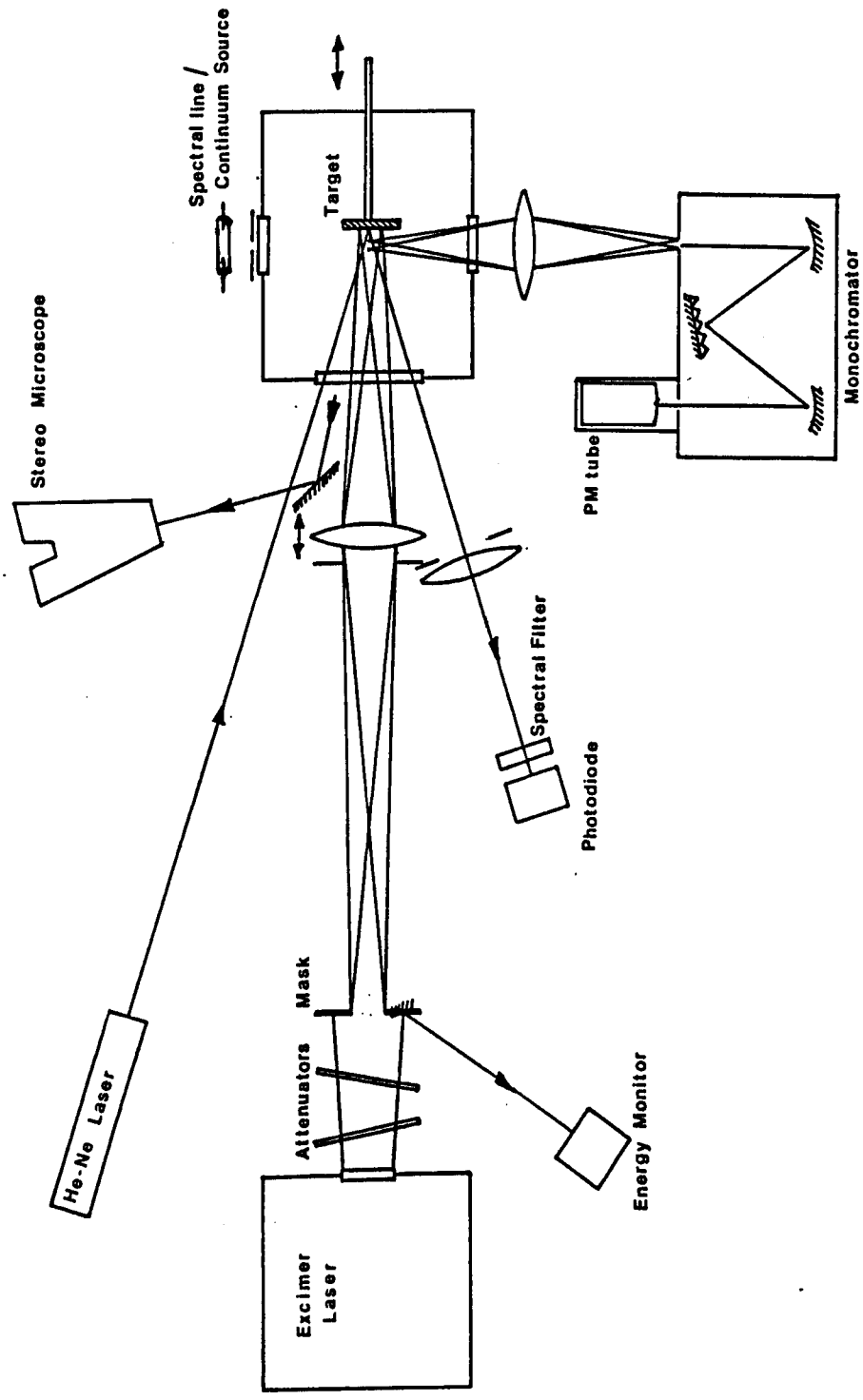

UV-EXCIMER LASER OUTPUT

Beam energy distribution measured
with linear array detector.

A : electrode-electrode.

B : preioniser-preioniser.

A

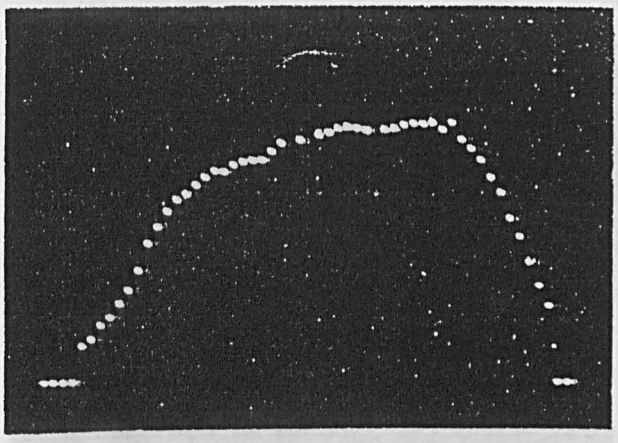

B

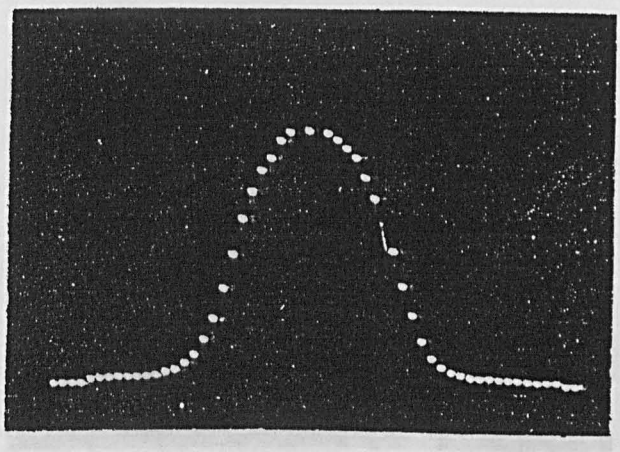

UV-EXCIMER LASER OUTPUT: APERTURED BEAM

Beam energy distribution measured
with linear array detector.

A : electrode-electrode.

B : preioniser-preioniser.

A

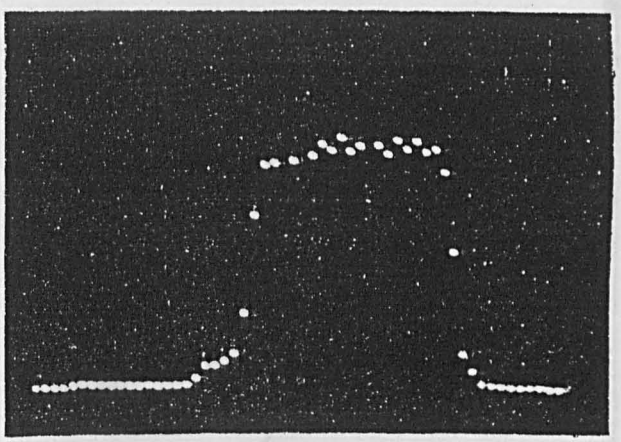

B

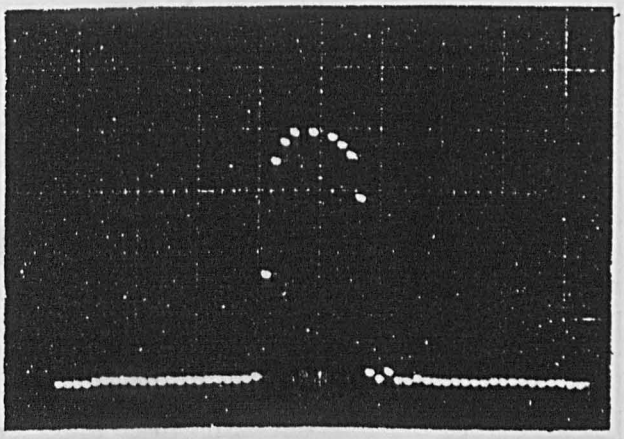

Fig.4.1.4

ETCHING OF COPPER IN CHLORINE

Linear relationship between pulse number and foil thickness for laser etching of through holes.

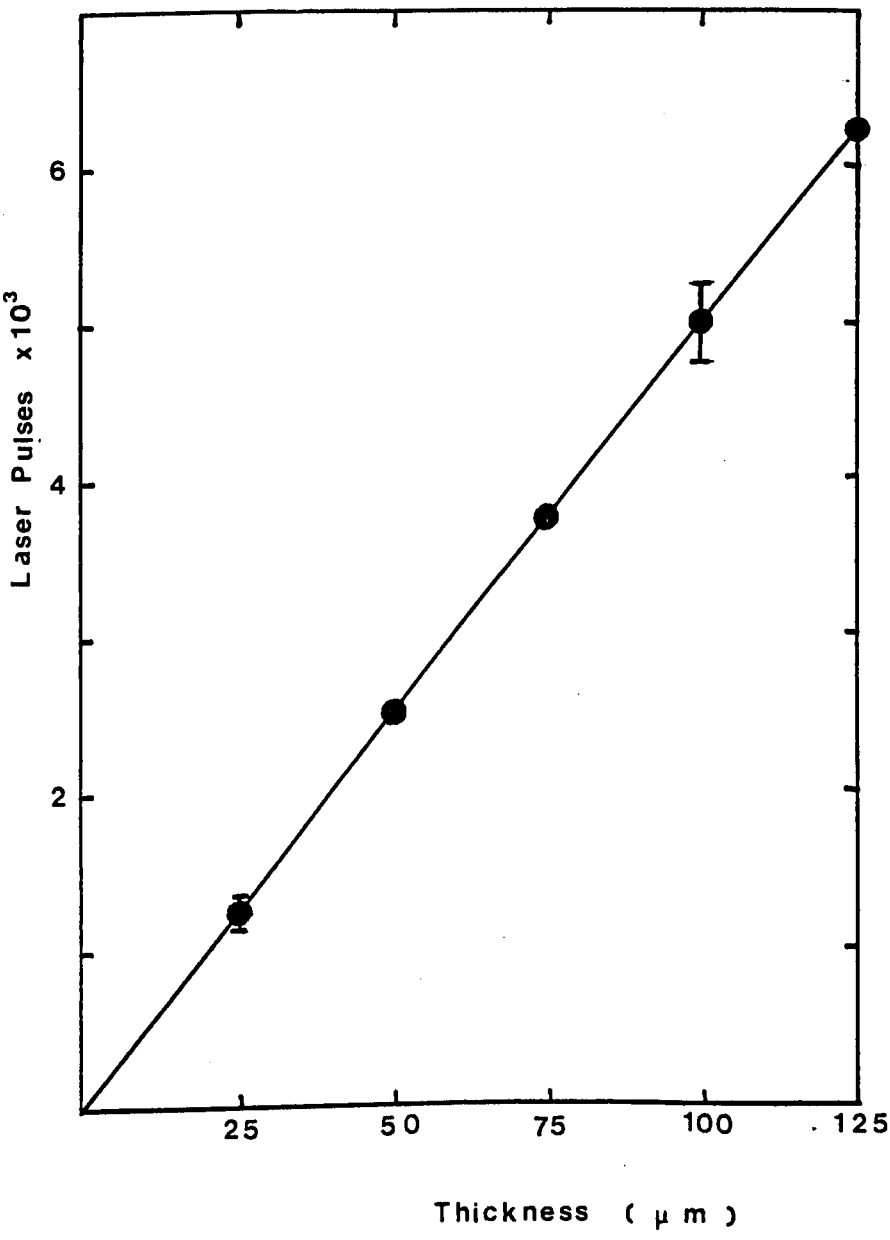

Fig.4.1.5.

OPTICAL ABSORPTION BY CHLORINE GAS

Emission spectra of deuterium lamp viewed through;

(i) Vacuum , P = 0.

(ii) Chlorine, P = 5 torr.

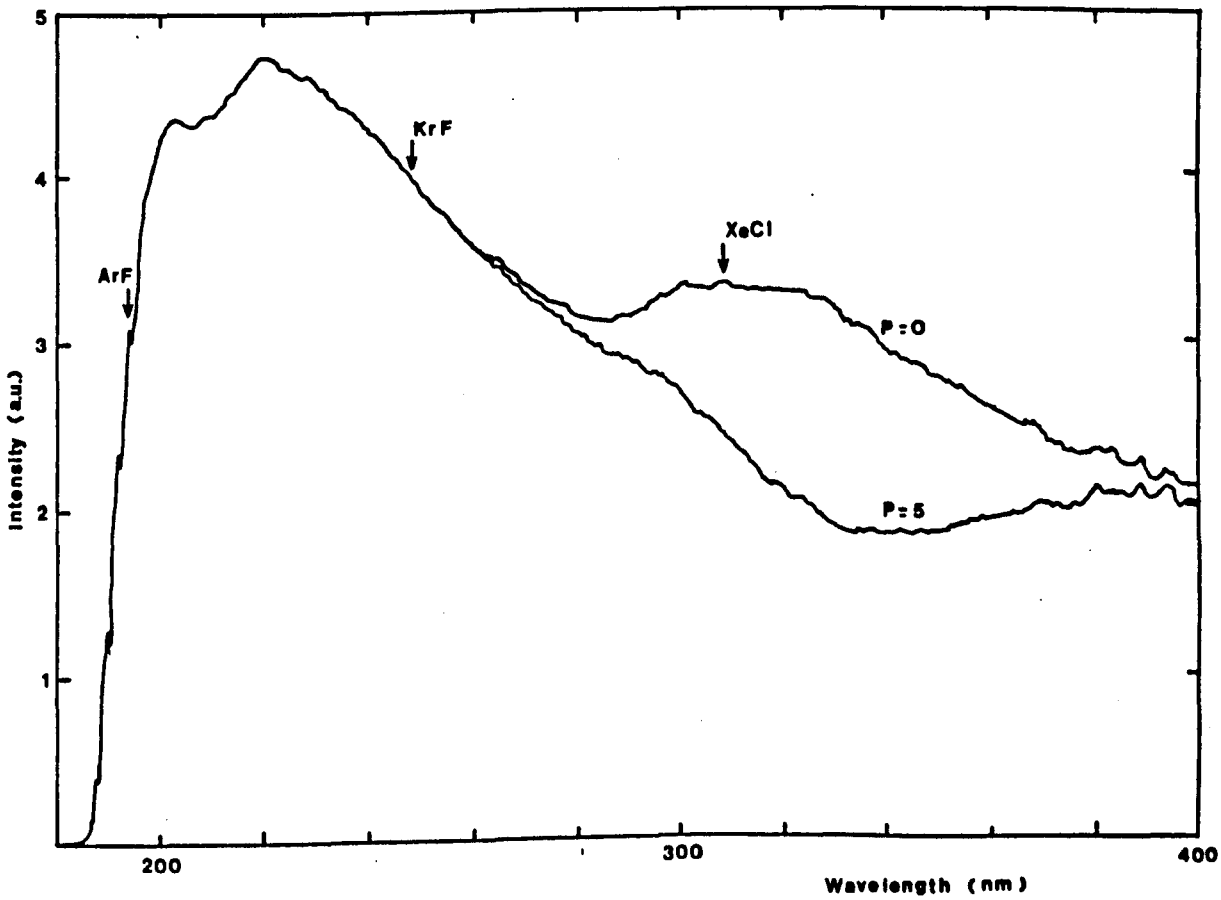

Fig.4.1.6

OPTICAL ABSORPTION SPECTRUM: CHLORINE

Absorption of chlorine at 250-450 nm

pressure-path length product: 275 torr cm.

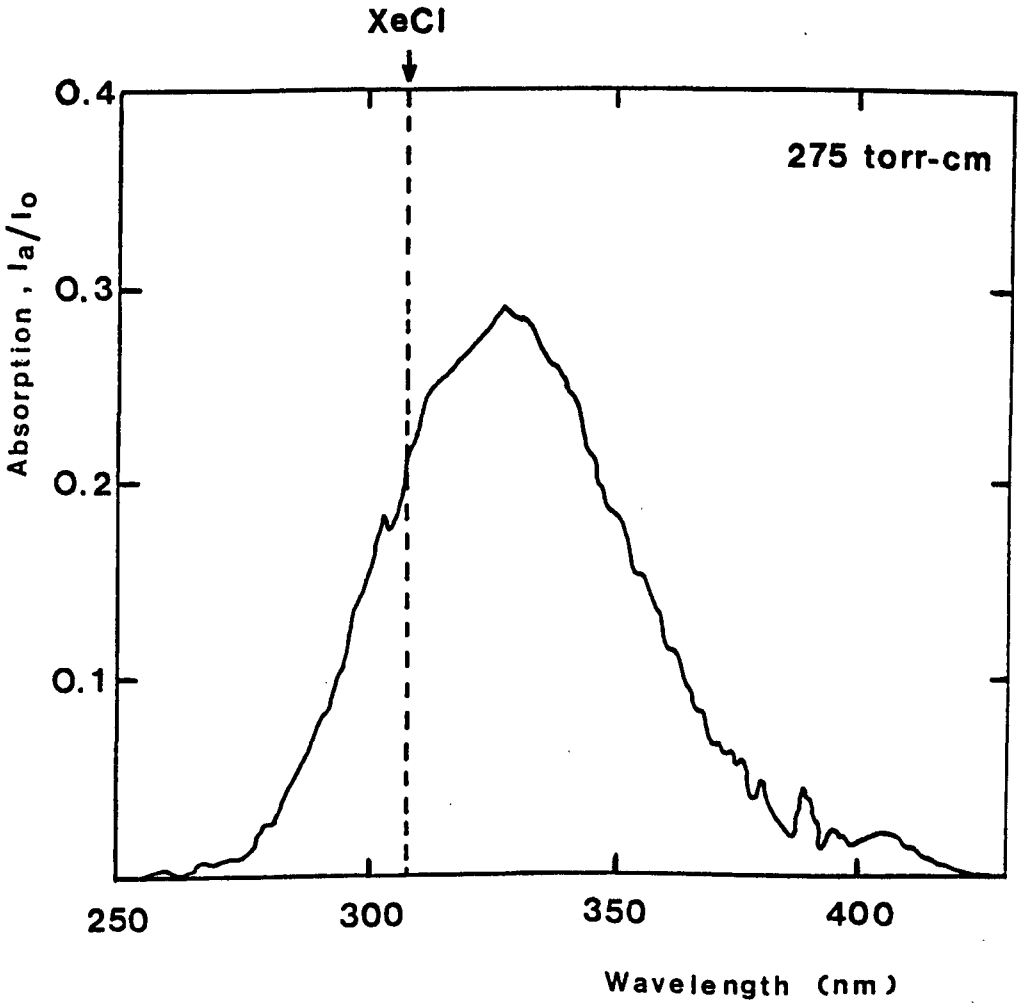

Fig.4.1.7.

OPTICAL ABSORPTION OF CHLORINE: 308 nm.

Transmission of 308 nm radiation by chlorine gas.

□ - deuterium lamp.

● - XeCl laser.

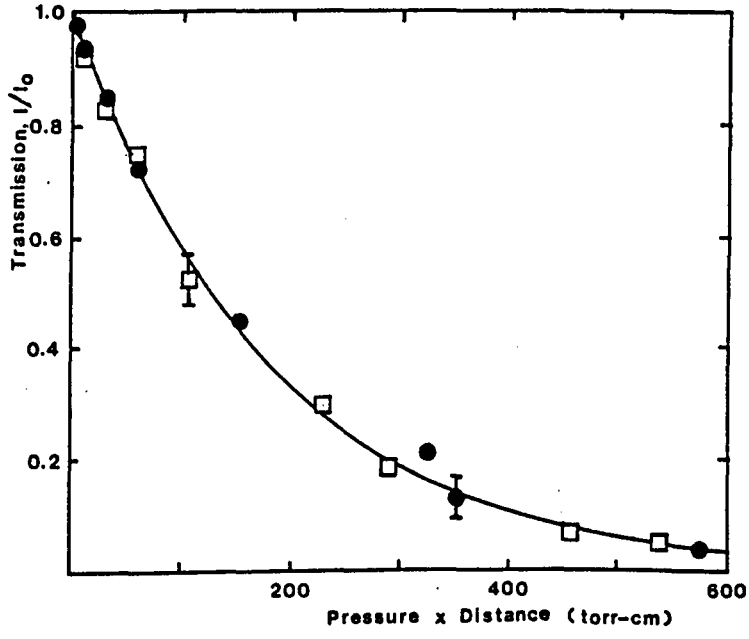

Fig.4.1.8.

OPTICAL ABSORPTION OF CHLORINE: 308 nm.

Transmission of 308 nm radiation by chlorine gas.

□ - deuterium lamp.

● - XeCl laser.

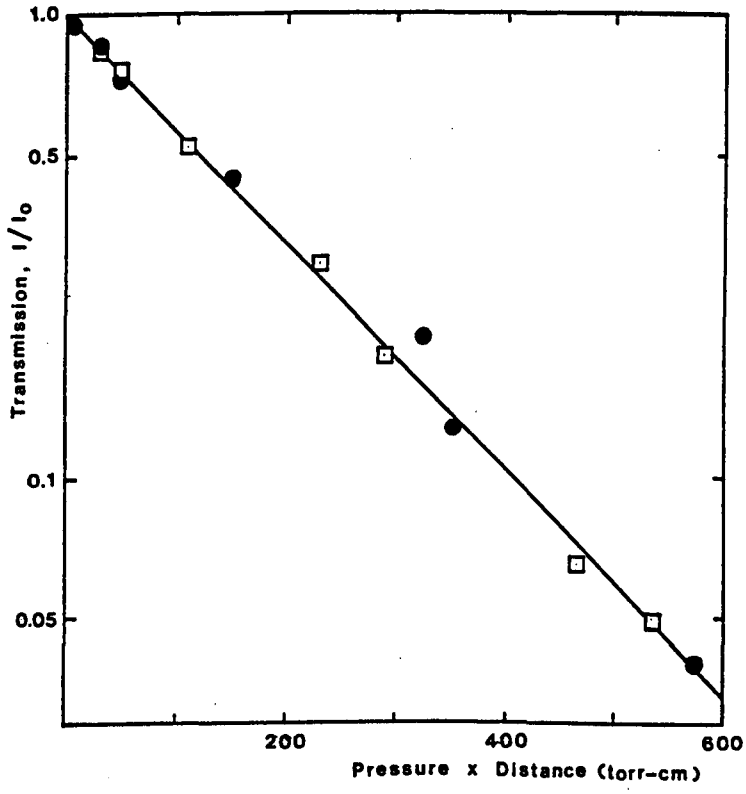

4.2

ETCH RATES - WAVELENGTH

Because of its potential use as an electrooptic modulator material [1] the optical properties of CuCl have been extensively studied in the visible and IR (0.4-50 microns) regions of the spectrum [2-7]. Little quantitative work has been done, however, in the UV region of interest here with the notable exception of the absorption studies of Cardona [8]. The high (photon) energy absorption spectrum of CuCl films is reproduced from [8] in Fig.4.2.1 and upon which the excimer laser wavelengths are indicated.

From these data the absorption coefficients, α, and the deduced optical absorption indices, k, (imaginary part of the complex refractive index) are presented in Table 1.

TABLE 1

Wavelength (nm)	α ($x10^5 cm^{-1}$)	k
193	4.0	0.61
248	1.8	0.36
308	1.0	0.25

Data for the real part, n, of the refractive index in the UV were not found in the literature; however, the two Cauchy type expressions for the visible-IR from [4] and [9] show reasonably good agreement when extrapolated to 150 nm as shown in Fig.4.2.2. Using these values of n and k, the reflectivities of CuCl films on Cu substrates as a function of film thickness were calculated for the three excimer wavelengths, as described previously, and are presented in Fig.4.2.3.

The data reveal that with chloride thicknesses greater than 500 nm, which were seen in the last chapter to occur less than one second after exposure to 2.5 torr chlorine, the laser 'sees' the chloride layer only and no perturbation of the absorbed energy distribution due to interference effects from reflections at the chloride-copper interface occurs.

The etch-rate of copper in 2.5 torr chlorine as a function of fluence ≤ 1 J cm^{-2} is shown for the XeCl laser at 1 Hz in Fig.4.2.4. The same data are seen to be a good fit to a linear dependence of etch-rate on ln(fluence) in Fig.4.2.5.

The corresponding etch-rate data using the ArF and KrF lasers are shown in Fig.4.2.6 and the similarity of behaviour at all three wavelengths is illustrated in Fig.4.2.7 where the data are plotted on common axes and the best fit line drawn.

Whilst the reflectivities at these wavelengths shown in Fig.4.2.3 are approximately equal, and therefore equal energies absorbed at equal fluences, the differing optical absorption indices would suggest that significant differences in etch thresholds and etch-rates might be expected; the 308 nm radiation being absorbed over a depth four times greater than that for the 193 nm radiation.

The observed independence of etch-rate on wavelength indicates that a simple model that assumes the etch-rate is governed by a Beer-Lambert type distribution of energy absorption in the target is inappropriate in this case. Such a model takes no explicit cogniscence of the rate of delivery of energy to the target which can lead, when energy redistribution mechanisms in the target are rapid, to

effective energy absorption over distances appreciably greater than the optical extinction length. The closeness of fit of the data to a linear dependence of etch-rate on the logarithm of fluence does not exclude the possibility of energy re-distribution as discussed in chapter 2.

The temporal profiles of the three lasers used are shown in Fig.4.2.8 and it may be seen that the pulse lengths (fwhm) of the ArF and KrF lasers are approximately equal and 2-3 times that of the XeCl laser.

The actual distribution of energy deposited in the target during the period of the laser pulse is unknown due to the difficulty in modelling the thermal re-distribution from the optical absorption zone for a time-varying irradiance and temperature-dependent optical and thermal properties of the material. Had the temporal profiles of the three lasers been identical it may have been possible to make a positive assessment of the effect of wavelength on the etch rate. Alternatively the availiability of different pulse lengths for a particular wavelength would have given further insight. It is interesting to note, however, that the sums of optical absorption depth and thermal diffusion length during the laser pulse for each of the three lasers used fall within $\pm$ 30% of a value of 0.1 μm and this may go some way towards explaining the similarity of the experimental etch-rate curves.

The remaining etch rate studies were carried out using the XeCl laser since this has long gas life times with reliable output.

Fig.4.2.1.

OPTICAL ABSORPTION OF COPPER CHLORIDE

Absorption coefficient of CuCl as a function of UV wavelength, from [8].

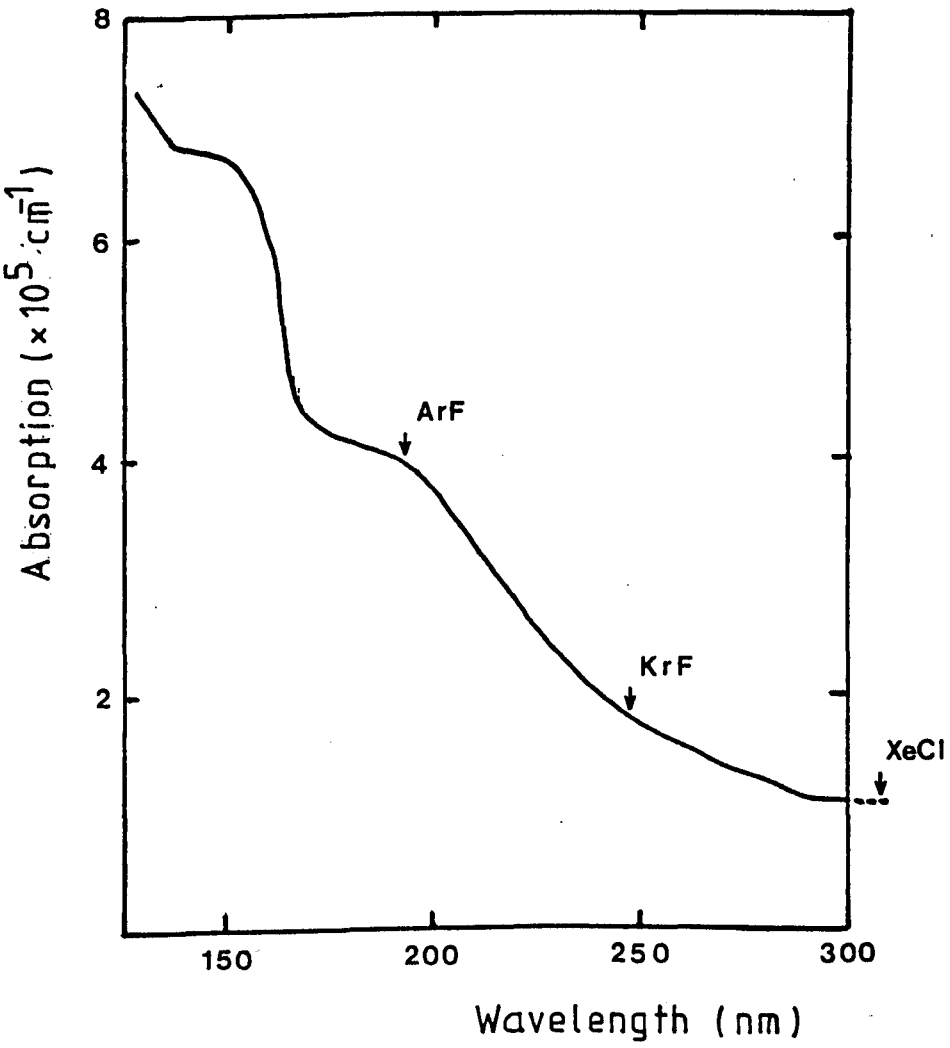

Fig.4.2.2.

REFRACTIVE INDEX OF COPPER CHLORIDE

Real part, n, of complex refractive index of CuCl. Calculated from [4,9]

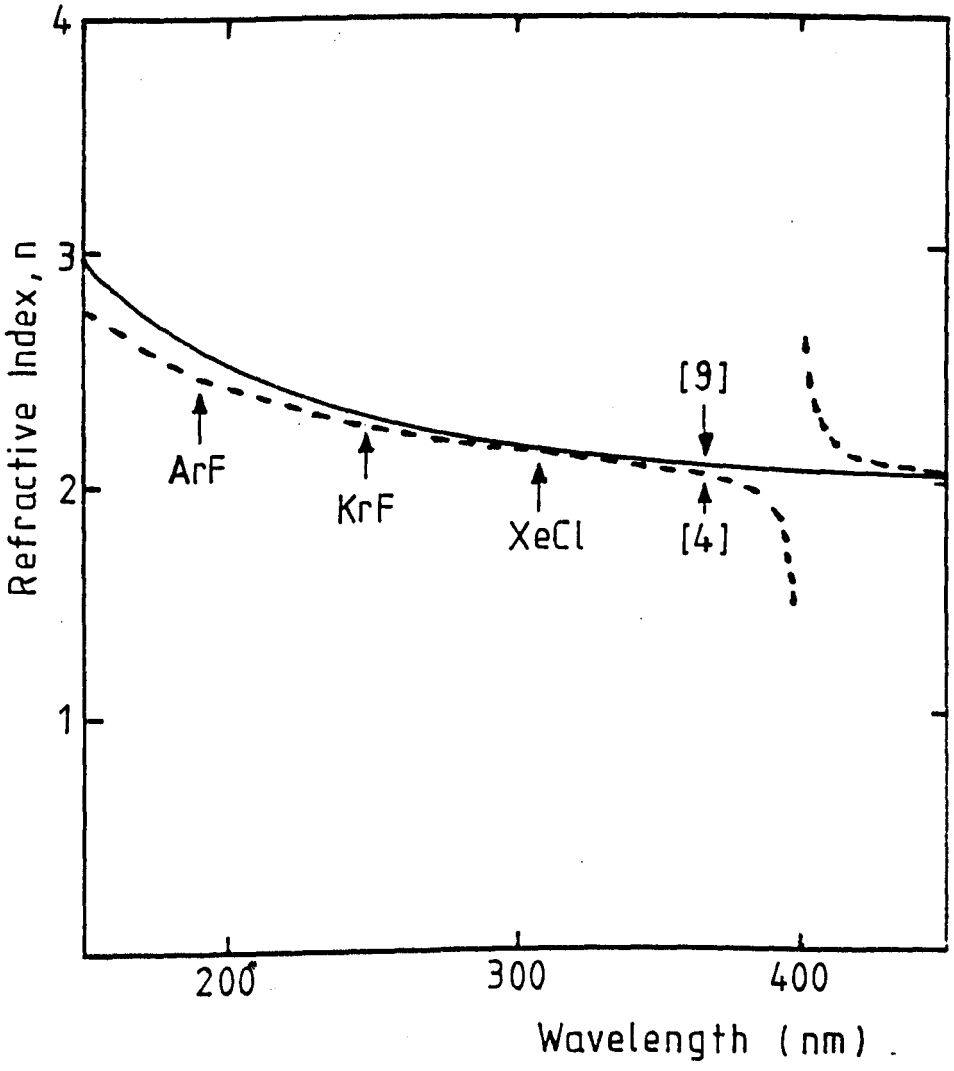

Fig.4.2.3.

REFLECTIVITY OF CuCl FILMS ON COPPER

Calculated reflectivity as a function of chloride film thickness.

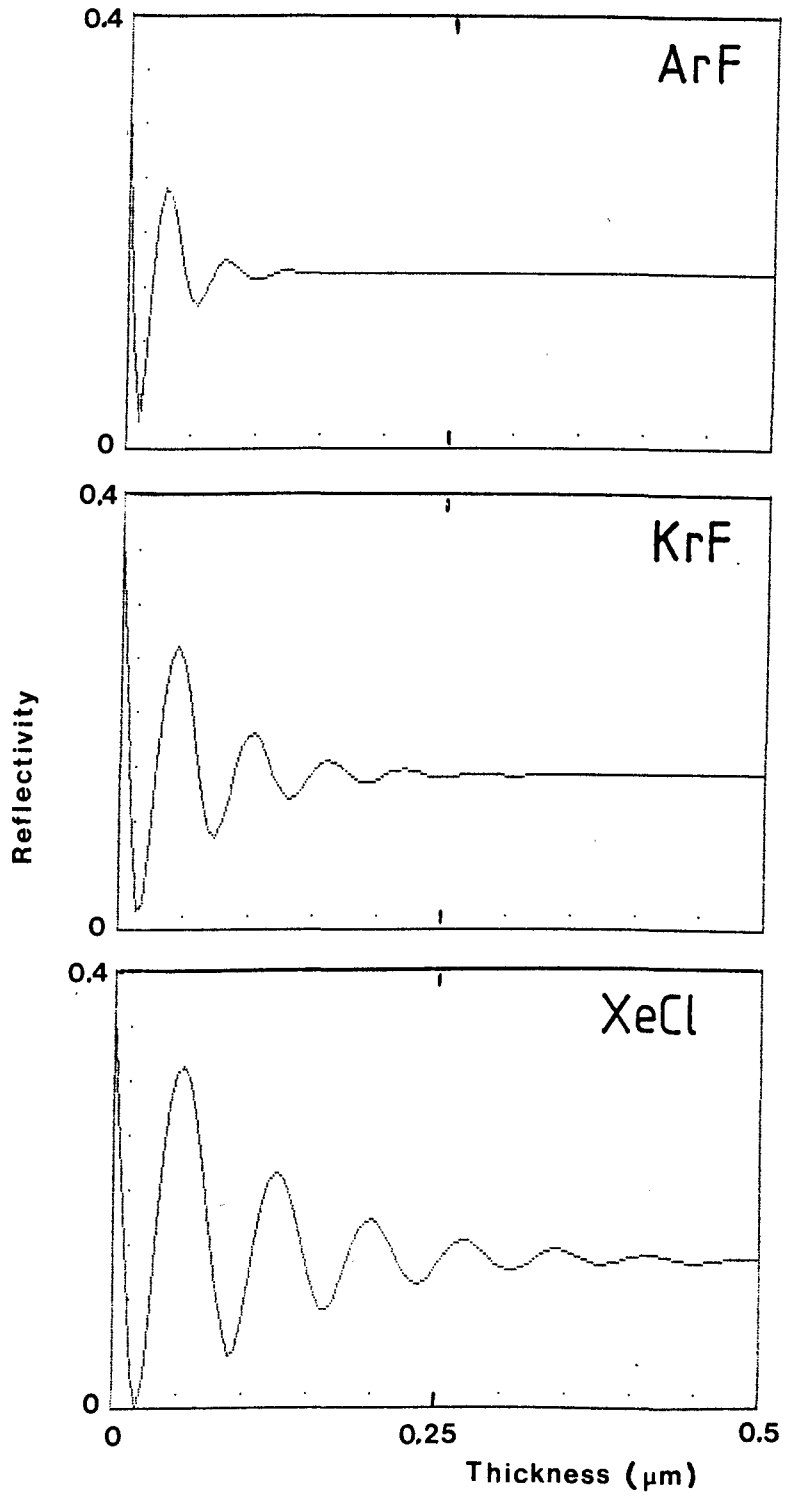

Fig.4.2.4.

ETCH-RATE OF COPPER IN CHLORINE

Etch-rate per pulse as a function of fluence for 308 nm laser at 1 Hz. Gas pressure; 2.5 torr.

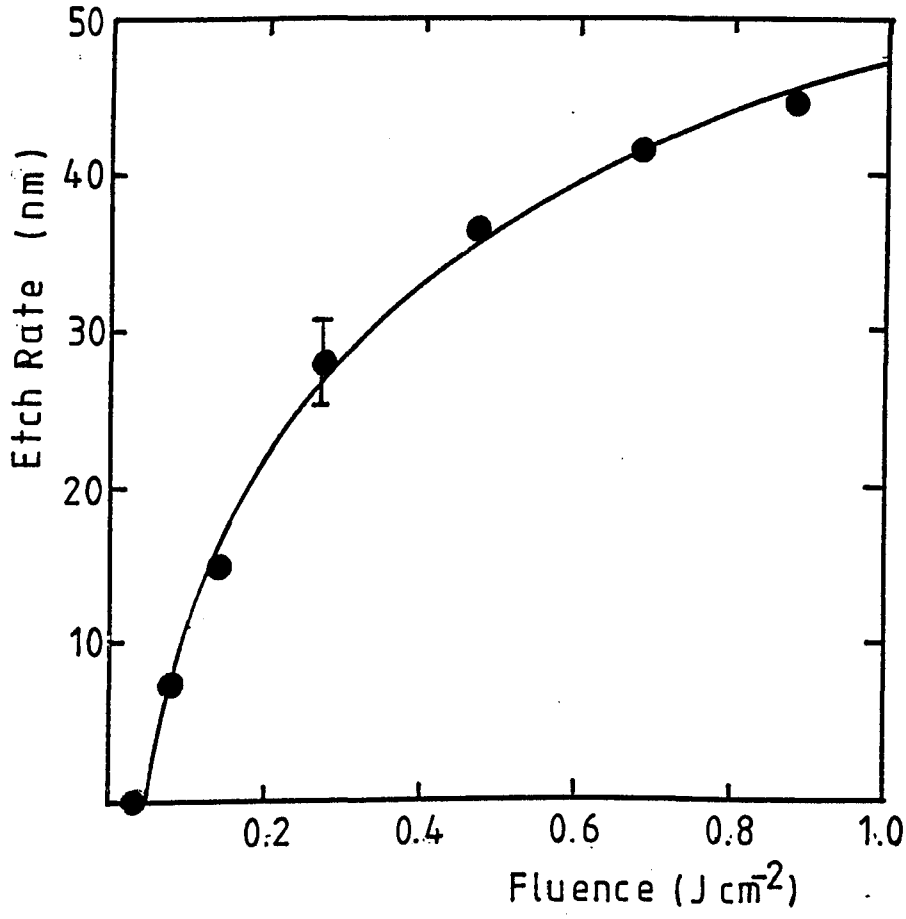

Fig.4.2.5.

ETCH-RATE OF COPPER IN CHLORINE

Etch-rate per pulse as a function of fluence for 308 nm laser at 1 Hz. Gas pressure; 2.5 torr.

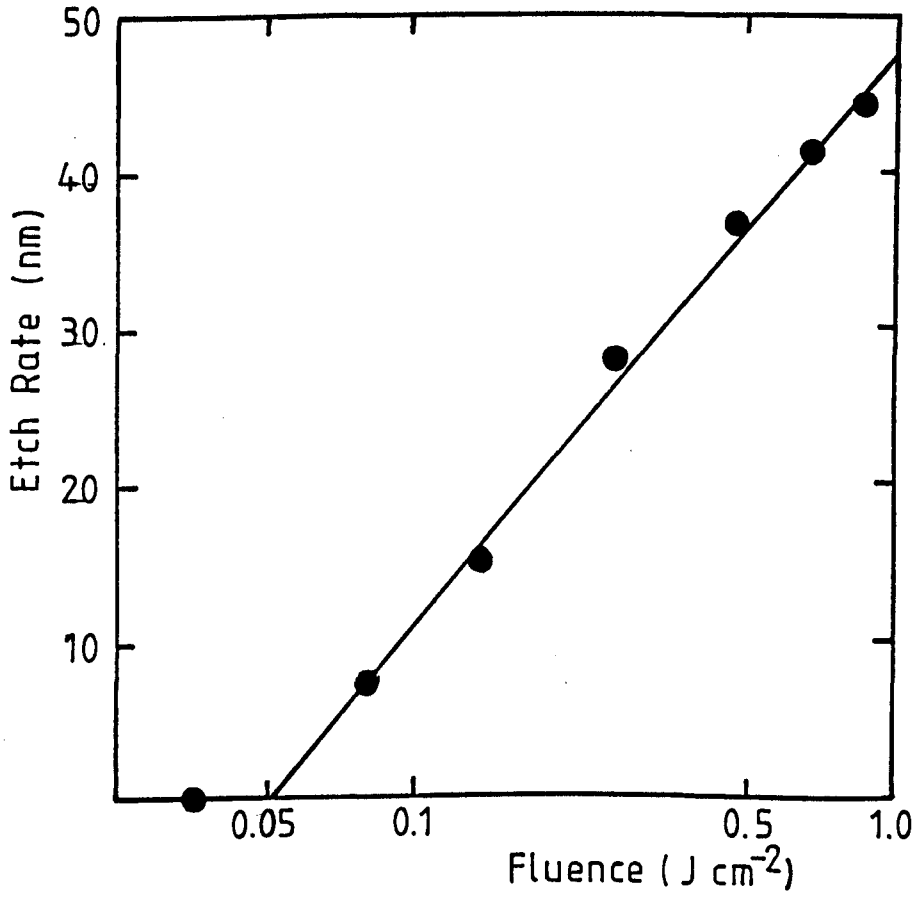

Fig.4.2.6.

ETCH-RATE OF COPPER IN CHLORINE

Etch-rate per pulse as a function

laser fluence at 1 Hz.

Gas pressure; 2.5 torr.

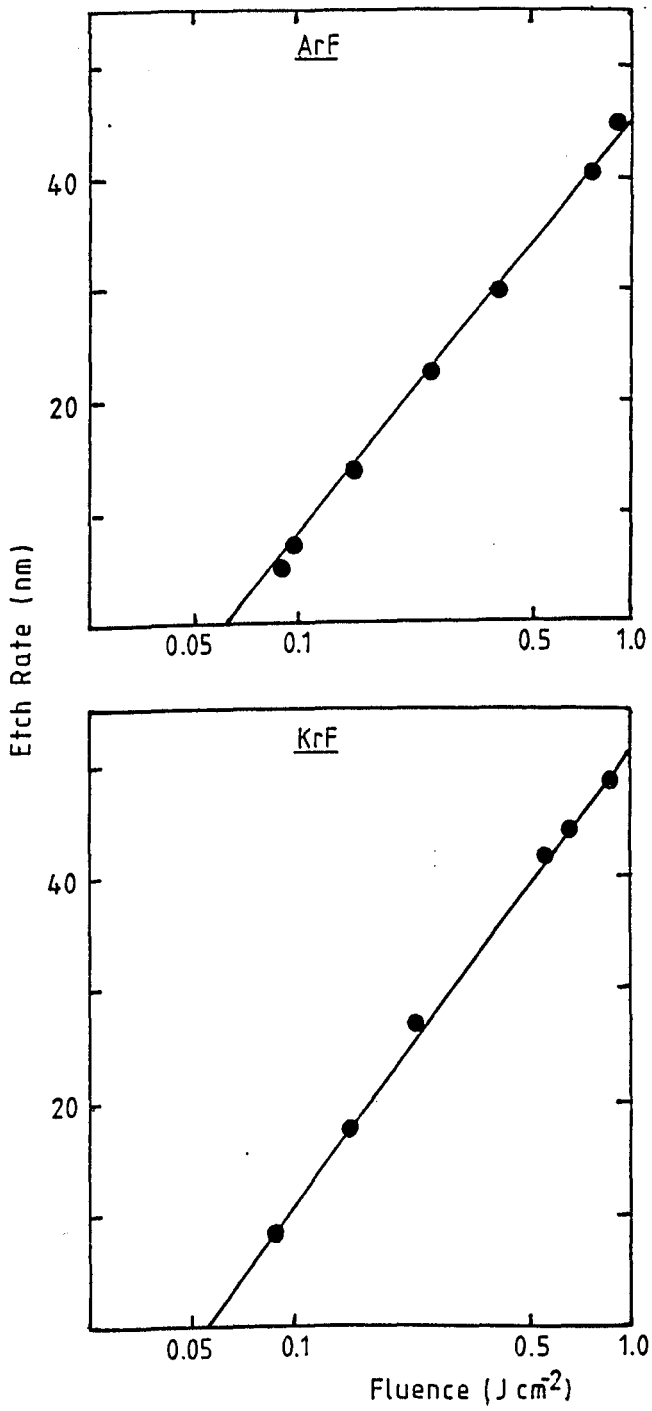

Fig.4.2.7.

ETCH-RATE OF COPPER IN CHLORINE

Etch-rate per pulse as a function
of UV-excimer laser fluence at 1 Hz.
Gas pressure; 2.5 torr.

♦ ArF
■ KrF
● XeCl

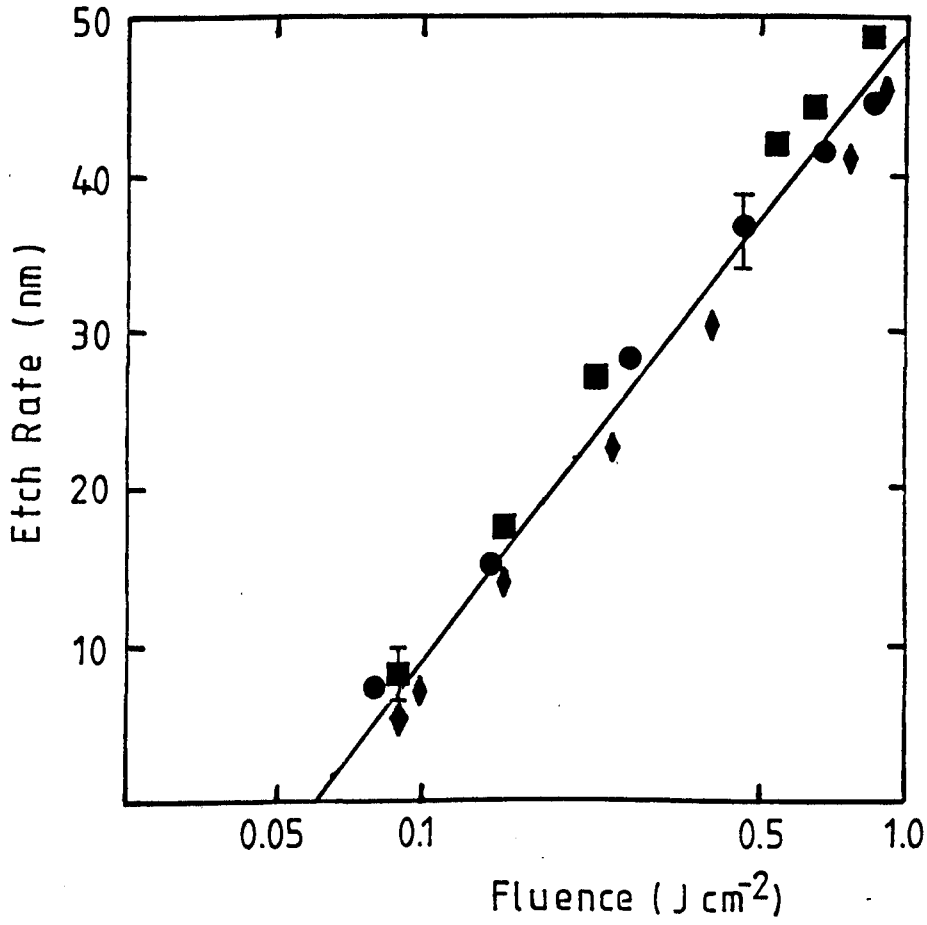

UV-EXCIMER LASER PULSE SHAPES

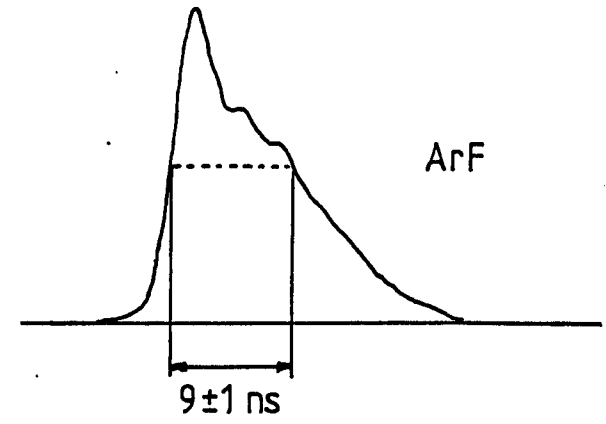

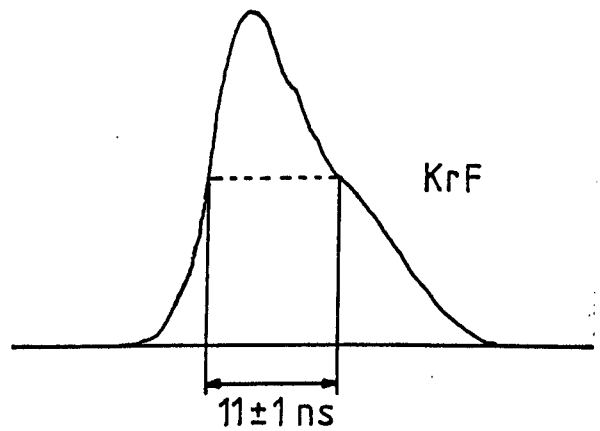

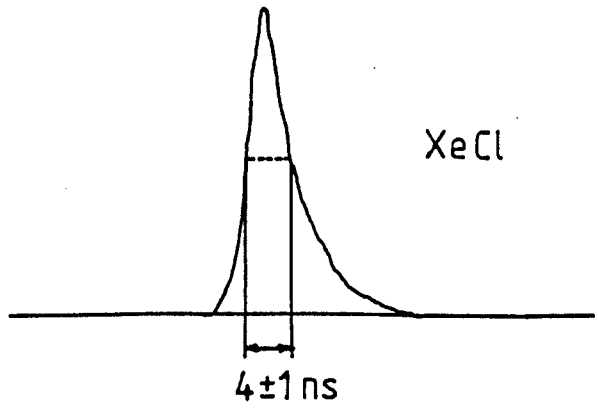

4.3

ETCH RATES - PULSE REPETITION FREQUENCY

The results presented in the last section showed that etching of copper in 2.5 torr chlorine gas at rates approaching 50 nm per pulse can be achieved with XeCl laser fluences ≤ 1 J cm^{-2}. The copper is removed as a copper-chlorine compound and, assuming this to be stoichiometric CuCl, represents chloride removal rates of up to 0.17 $\mu m\ s^{-1}$ at 1 Hz prf.

These equivalent etch-rate data, together with the appropriate chloride growth curve from chapter 3, allow a simple model of the laser etching of copper, via a sequence of steps of growth and ablation of the chloride layer, to be developed. Such a model is described in this section and used to predict the influence of prf on the temporal etch-rate (depth removed per unit time). A comparison with measured etch-rates at increasing prf reveals that the model, in its simplest form, is inadequate and reasons for this are postulated.

At a mid range fluence value of 0.5 J cm^{-2} the copper etch-rate, from Fig 4.2,4, is 36 nm which represents a chloride etch-rate of 0.125 $\mu m\ s^{-1}$ at 1 Hz. The growth-rate curve of chapter 3, Fig.3.3.1, showed that the chloride thickness after 1 s exposure at this pressure is 0.5 μm thus leaving 0.375 μm of chloride immediately after the first laser pulse. This chloride layer continues to increase in thickness, albeit at a slower rate, until the second laser pulse removes a further 0.125 μm. This sequence of growth

and removal continues as illustrated in Fig 4.3.1 from which it can be seen that the residual thickness of chloride addressed by each laser pulse tends to a constant value.

It is clear that this quasi steady-state thickness is achieved when the etch rate of chloride is identically equal to its growth in the interpulse period. The chloride growth rate, found by differentiating the growth curve, and plotted as a function of chloride thickness is shown in Fig.4.3.2. It can be seen that the quasi-equilibrium thickness is approximately 1 μm in this case and is reached after only a few laser pulses, as was seen in Fig 4.3.1.

At a fixed prf the quasi-equilibrium thickness will be inversely proportional to the etch rate and, for a given etch rate, will decrease with increasing prf. The minimum thickness case occurs when the etch rate is such as to remove all of the chloride formed in the initial exposure period and thus represents a chloride growth limited regime of removal.

From this model, therefore, we expect the temporal etch rate to increase linearly with prf upto the growth limited value at which it will be effectively "clamped". The limiting prf will decrease with increasing fluence; although we may allow the possibility that pulse energy in excess of that required to remove all of the chloride may be deposited into the copper and, by raising its temperature, cause an increase in chloride growth rate.

The measured temporal etch rates of copper, using 0.5 J cm^{-2} XeCl laser pulses and in 2.5 torr chlorine, as a function of laser prf are shown in Fig.4.3.3 together with a curve

representing the results expected from the above model. It is immediately clear that these data are at variance with the simple model.

A more complete picture of the behaviour of the temporal etch rate with prf, over the fluence range up to 1 J cm^{-2}, is shown in Fig.4.3.4 from which it can be seen that, except at fluences close to threshold, the amount of material removed per unit time is not linearly proportional to the prf. These results indicate that there is a decrease in the average etch rate per pulse with increasing prf and this is shown in Figs.4.3.5 & 6. Reason for this apparently anomalous behaviour may be found in considering the possible differences in the optical properties of the different chloride layer thicknesses that are addressed by the laser pulse at different prfs.

When the thickness of the chloride layer is greater than the optical absorption length, $\delta = \lambda/2\pi k$, then the laser 'sees' only the chloride and the reflectivity of the bulk will apply. When the thickness of the chloride layer is $\leq \delta/2$, a modulation of reflectivity, and hence absorption, with the thickness addressed by the laser will occur. Intermediate between these two cases is the situation in which the absorption profile is perturbed due to reflections at the substrate, but no change in reflectivity from that of the bulk, or semi-infinite, value is observed.

In all of these cases the reflectivity and absorption may change during the ablation pulse due to temperature effects and the changing layer thickness. An additional complication arises from the possible non-stoichiometry of the layer

which may lead to a graded increase in optical absorption coefficient with depth and result in a rather more complex absorption profile than the form of an exponential decay usually assumed.

The etch rate is plotted as a function of ln(fluence) in Fig.4.3.7 and a linear fit made to the data in the upper half of the fluence range. The gradients of these curves give the effective optical absorption length for each prf and, taking the reciprocal values for the stoichiometric CuCl equivalent, the resultant effective absorption coefficients are shown as a function of prf in Fig.4.3.8. It can be seen that the data show a monotonic increase with prf and that, even at 1 Hz, the absorption coefficient is higher than the small signal value reported by Cardona [8].

Fig.4.3.1.

CHLORIDE GROWTH AND ABLATION MODEL

Comparison of growth curve with growth and ablation simulation

Copper in 2.5 torr Cl_2, 0.5 J cm^{-2}

XeCl at 2 Hz. 0.125 μm per pulse.

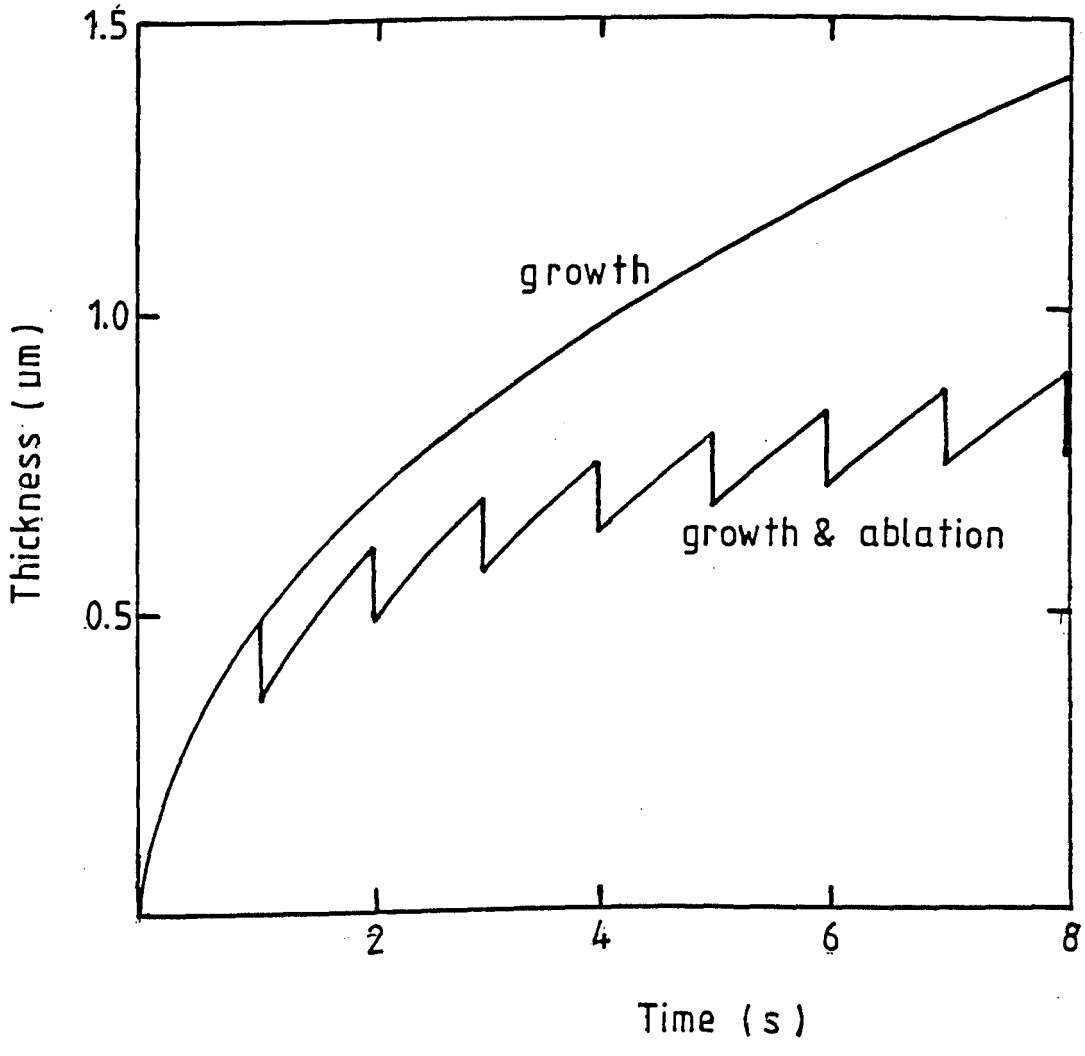

Fig.4.3.2.

CHLORIDE LAYER GROWTH RATE

Growth rate, dH/dt, of Chloride as a function of layer thickness.

2.5 torr Cl_2.

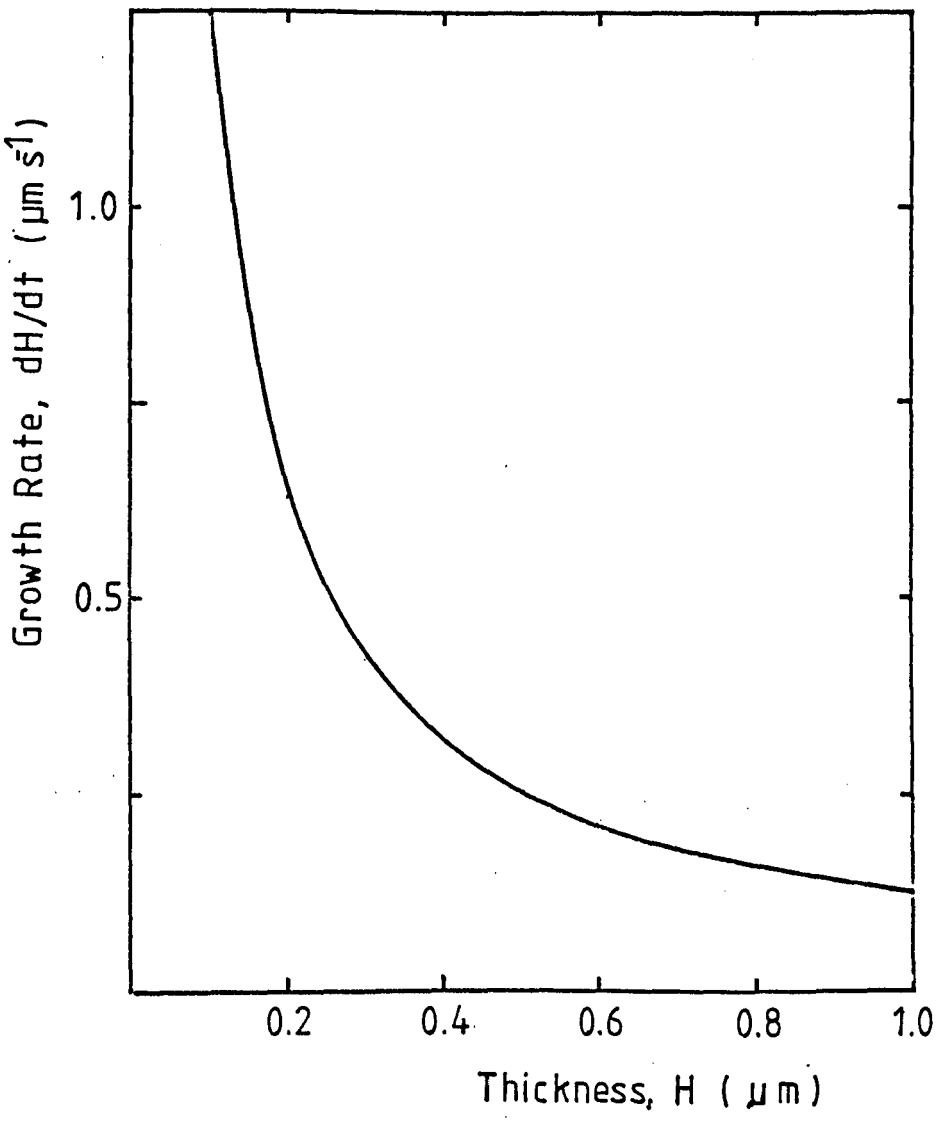

TEMPORAL ETCH-RATE OF CU IN Cl_2

Etch-rate of Cu in 2.5 torr Cl_2 at

0.5 J cm^{-2} XeCl as a function of prf.

- - - - Predicted from dH/dt & 1 Hz data.

—●— Measured

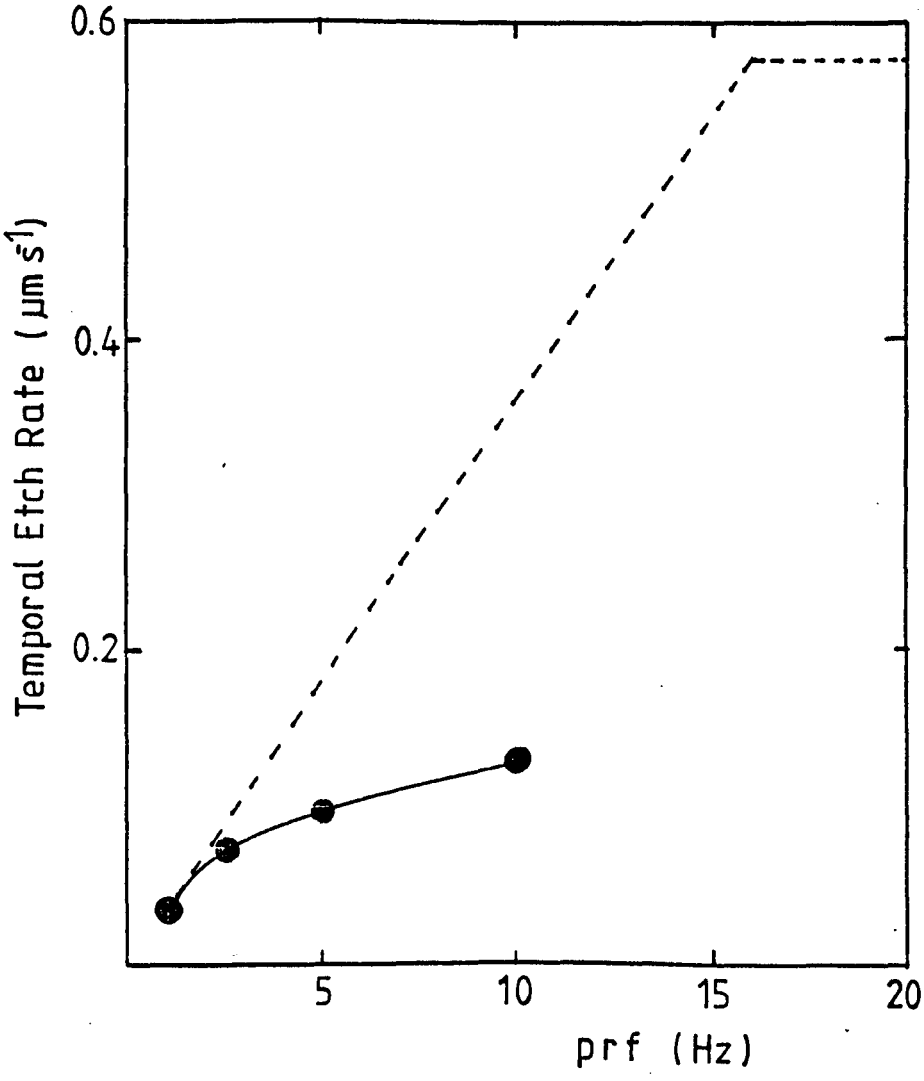

Fig.4.3.4.

TEMPORAL ETCH-RATE of Cu in Cl_2

Etch-rate as a function of fluence
and laser prf. 2.5 torr Cl_2.

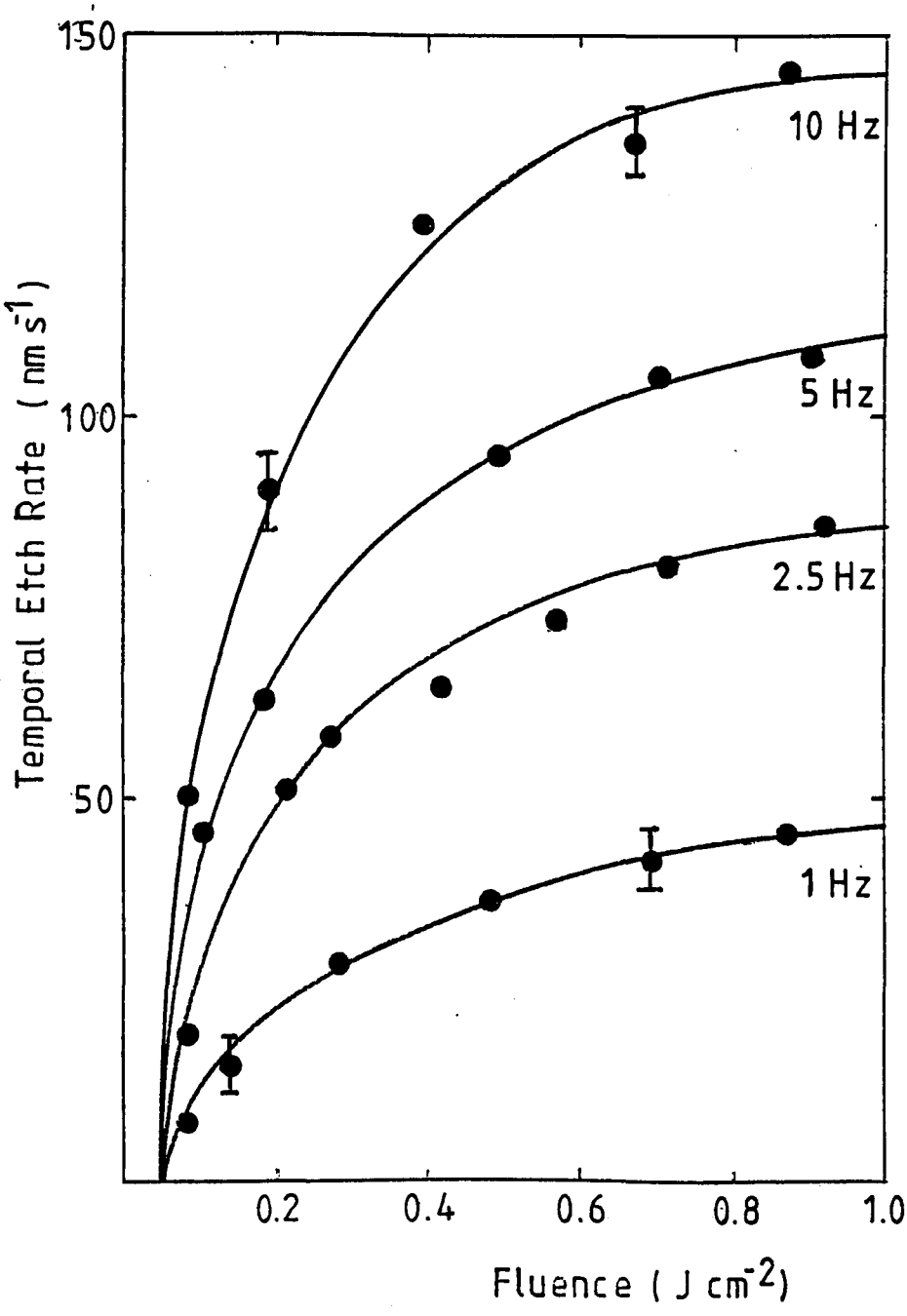

Fig.4.3.5.

ETCH-RATE OF COPPER IN CHLORINE

Etch-rate per pulse as a function of fluence and prf. 2.5 torr Cl_2.

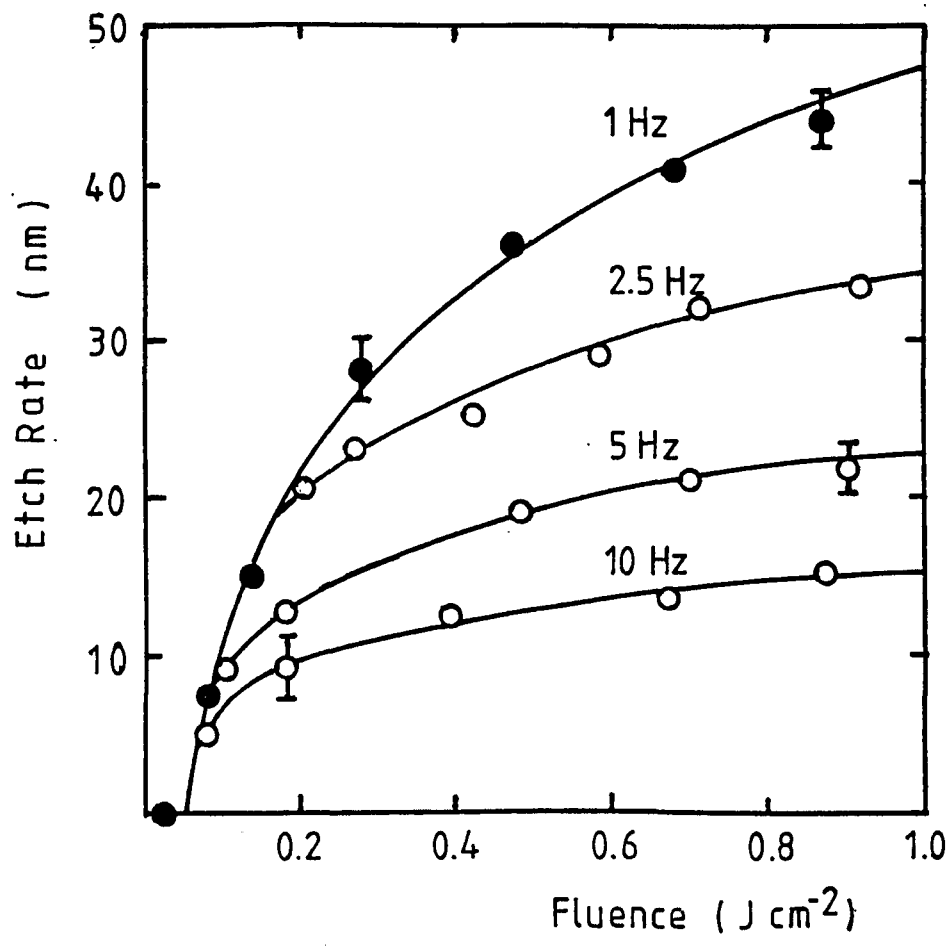

Fig.4.3.6.

ETCH-RATE OF COPPER IN CHLORINE

Etch-rate in 2.5 torr chlorine as a function of prf at various fluences.

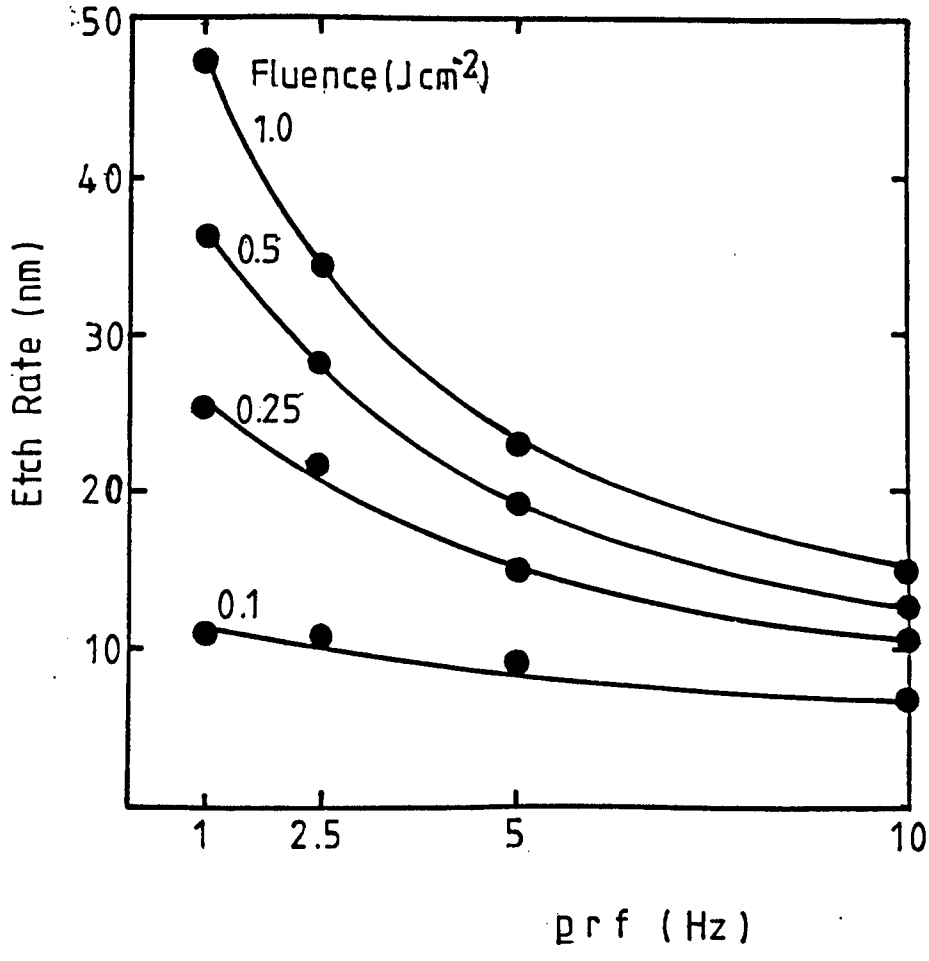

Fig.4.3.7.

ETCH-RATE OF COPPER IN CHLORINE

Etch-rate in 2.5 torr Cl_2 as a function of fluence and prf.

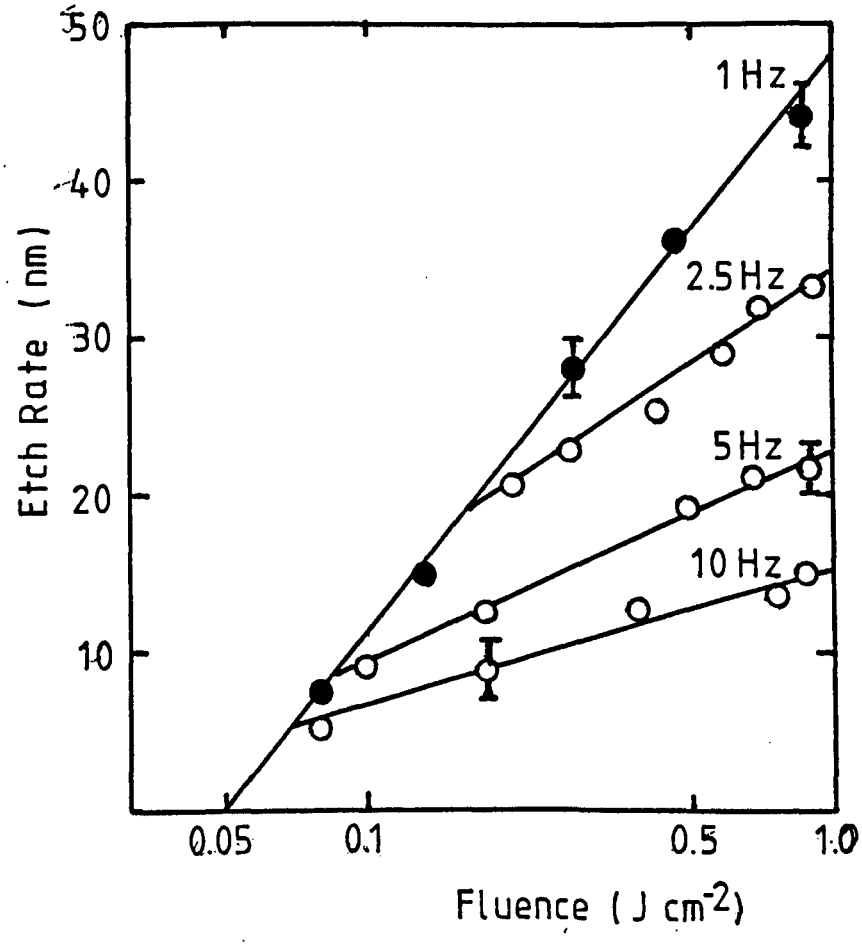

Fig.4.3.8.

EFFECTIVE ABSORPTION COEFFICIENT

Absorption coefficient of CuCl layer deduced from etch-rate data as a function of laser prf. 2.5 torr Cl_2.

■-small signal value from [8].

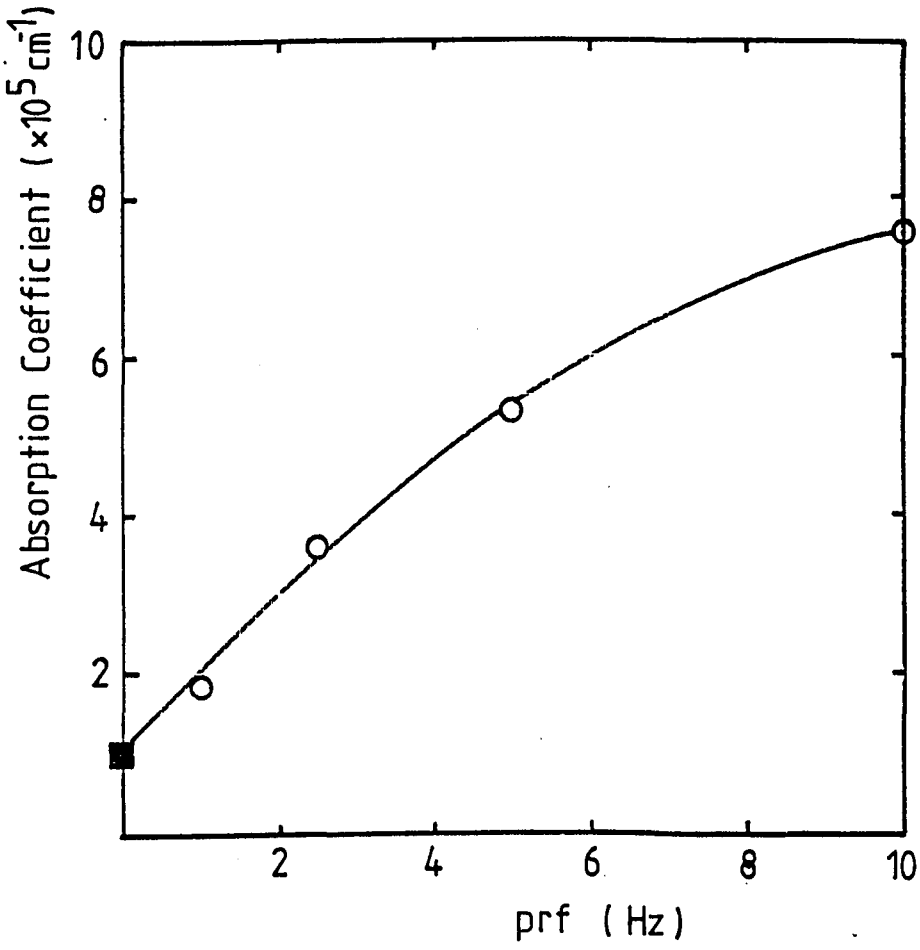

4.4.

ETCH RATES - CHLORINE GAS PRESSURE

In the last section it was argued that, at a given fluence, the etch rate per pulse can vary with prf since the optical properties of the chloride layer addressed by the laser are some function of the thickness that can develop in the inter-pulse period.

A decrease in chlorine gas pressure, resulting in a lower growth rate as seen in chapter 3, should, if the etch rate is chloride thickness controlled, have the same effect as increasing the prf; ie should result in a reduction in etch rate. In order to investigate this, studies of the etch rate of copper in chlorine at various ambient pressures and with a fixed prf were carried out and are reported in this section.

A prf of 5 Hz was chosen for these studies since the results of section 4.3 indicate that the growth rate limitation imposed by a 0.2 s interpulse period, even at 2.5 torr chlorine pressure, produces a significant reduction in etch rate and thus lies in the regime of interest. Furthermore the total time to etch through a 25 μm thick copper foil is not too long (approximately 15 mins at 5 nm/pulse).

The 5 Hz, 2.5 torr data are shown for reference in Fig.4.4.1 and the deviation from the 1 Hz data is evident from Fig.4.4.2.

The chloride thickness after 0.2 s initial exposure of the copper to 2.5 torr chlorine is, from the chapter 3 results, 0.325 μm whereas it is only 0.125 μm at 0.5 torr. This is

seen, from Fig.4.4.3, to result in a further reduction in etch rate at fluences in excess of $2xF_t$ where F_t, the threshold fluence of 0.05 J cm^{-2}, was not observed to vary either with decrease in pressure or increase in prf. The trend of the pressure dependence of etch rate is seen more fully in the data presented in Fig.4.4.4 where the etch rates, as a function of fluence at 5 Hz, are shown for chlorine pressures in the 0.05 to 2.5 torr range. The gradient of the linear fit to the etch rate data plotted against ln(fluence) in the $4xF_t$ to $20xF_t$ range, and shown in Fig.4.4.5, give approximate values for the apparent absorption depth of the laser radiation.

Absolute numerical values for these absorption depths would be inappropriate since they are based on the etch rate of copper whilst the copper is removed as part of the, evidently non-stoichiometric, chloride layer. By normalising the data to the 2.5 torr results, as in Fig.4.4.6, the trend of smaller absorption lengths, and hence larger optical absorption coefficients, with decreasing pressure can be observed. This behaviour is consistent with the ideas postulated in the previous section in that a thinner quasi-equilibrium layer, produced by either a reduction in pressure or an increase in prf, results in a reduction in the etch rate/pulse efficiency. It might be reasonable to expect, therefore, an increse in etch rate for a given fluence at chlorine pressures above 2.5 torr.

The results obtained with an order of magnitude increase in chlorine pressure, ie 25 torr, are shown in Fig.4.4.7. It can be seen that the etch-rate has, in fact, decreased with

increased pressure and the trend of the pressure dependence of etch-rate is illustrated in Fig.4.4.8 for 1 J cm^{-2} pulses at 5 Hz.

The etch rates over a range of fluences, as a function of ln(pressure), are shown in Fig.4.4.9 from which it can be seen that the maximum etch rate occurs with approximately 2.5 torr and with a small shift towards lower pressure at low fluence. This, together with the increase in threshold fluence seen in the 25 torr data of Fig.4.4.7, leads to the deduction that the decline in etch rate is a result of the dissipation of the incident energy by absorption in the ambient chlorine gas and a concomitant reduction in the effective fluence at the target. To confirm this, the absorption loss at pressures up to 50 torr were calculated from the known absorption coefficient of chlorine and the path length. The incident fluence on the cell was increased proportionally so as to produce a constant fluence at the target. A comparison of etch rates with a constant fluence of 0.5 J cm^{-2} at (a) the cell and (b) the target is shown in Fig.4.4.10. The data show that chlorine absorption reduces the effective fluence at the target as expected, the additional energy being deposited into the chlorine. A red glow along the laser path in the gas is observed which increases in intensity with increasing pressure and fluence, although this excitation of the gas does not appear to influence the etch-rate.

The etch-rate as a function of pressure and prf for a fluence of 0.25 J cm^{-2} is presented in Fig.4.4.11 and it can be seen that the pressure at which the maximum etch-rate

occurs increases with increasing prf.

Finally an experiment to determine the effect of external pressure was carried out. The etch-rate in a partial pressure of 5 torr chlorine with an argon buffer up to 1.6 atmospheres is shown in Fig.4.4.12. Here it can be seen that the etch rate decreases linearly with increasing buffer gas pressure. This effect is thought to be due to the external pressure shifting the competing ablation and reabsorption equilibrium processes to higher temperatures, ie. flux limited evaporation. There may also be a contribution due to re-deposition of ablated fragments following collisions with the high pressure ambient gas species. Weight is added to this argument by the observation of an increase in the amount of debris surrounding the ablation zone, a phenomenon similar to that observed in the laser ablation of polymers [10].

Fig.4.4.1.

ETCH-RATE OF COPPER IN CHLORINE

Etch-rate of Cu in 2.5 torr Cl_2
as a function of fluence at 5 Hz.

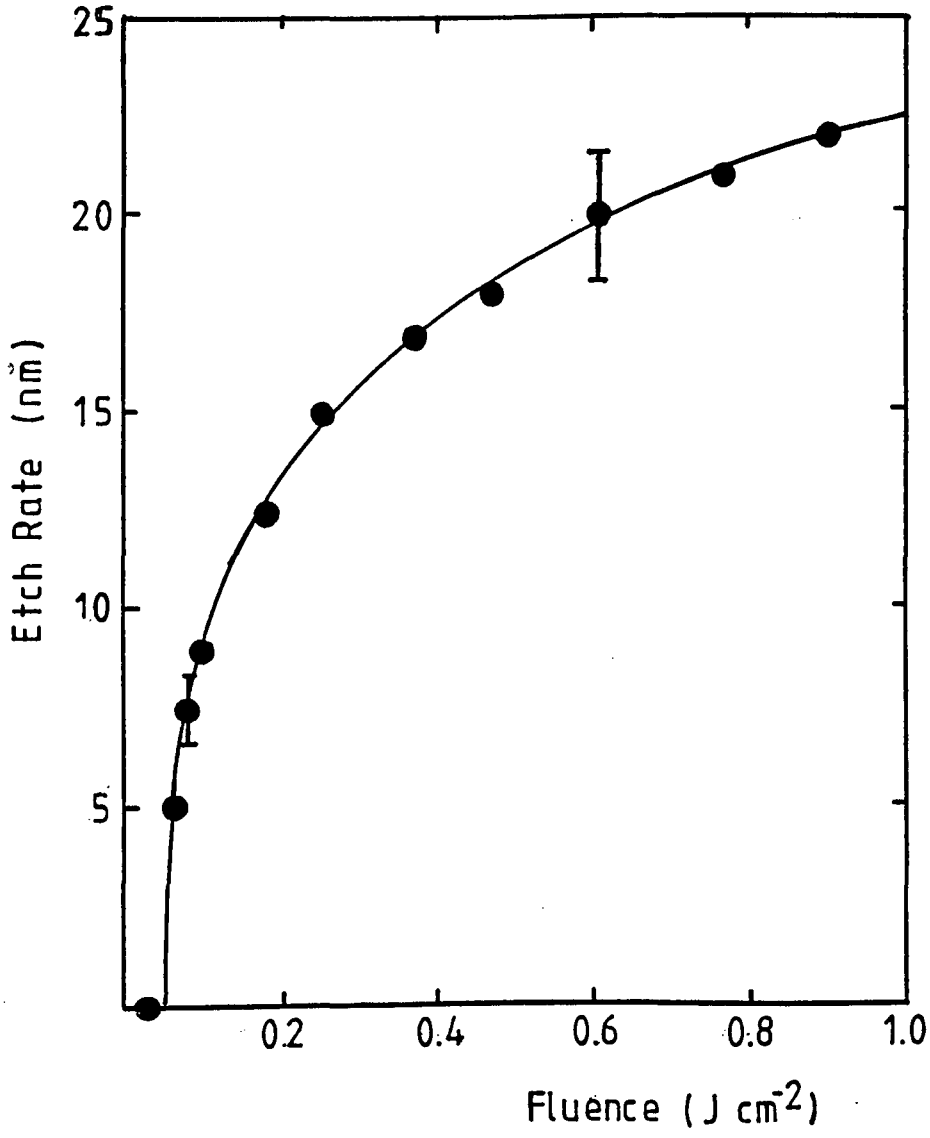

Fig.4.4.2.

ETCH-RATE of Cu in 2.5 torr Cl_2

---- 1 Hz data.

—— 5 Hz.

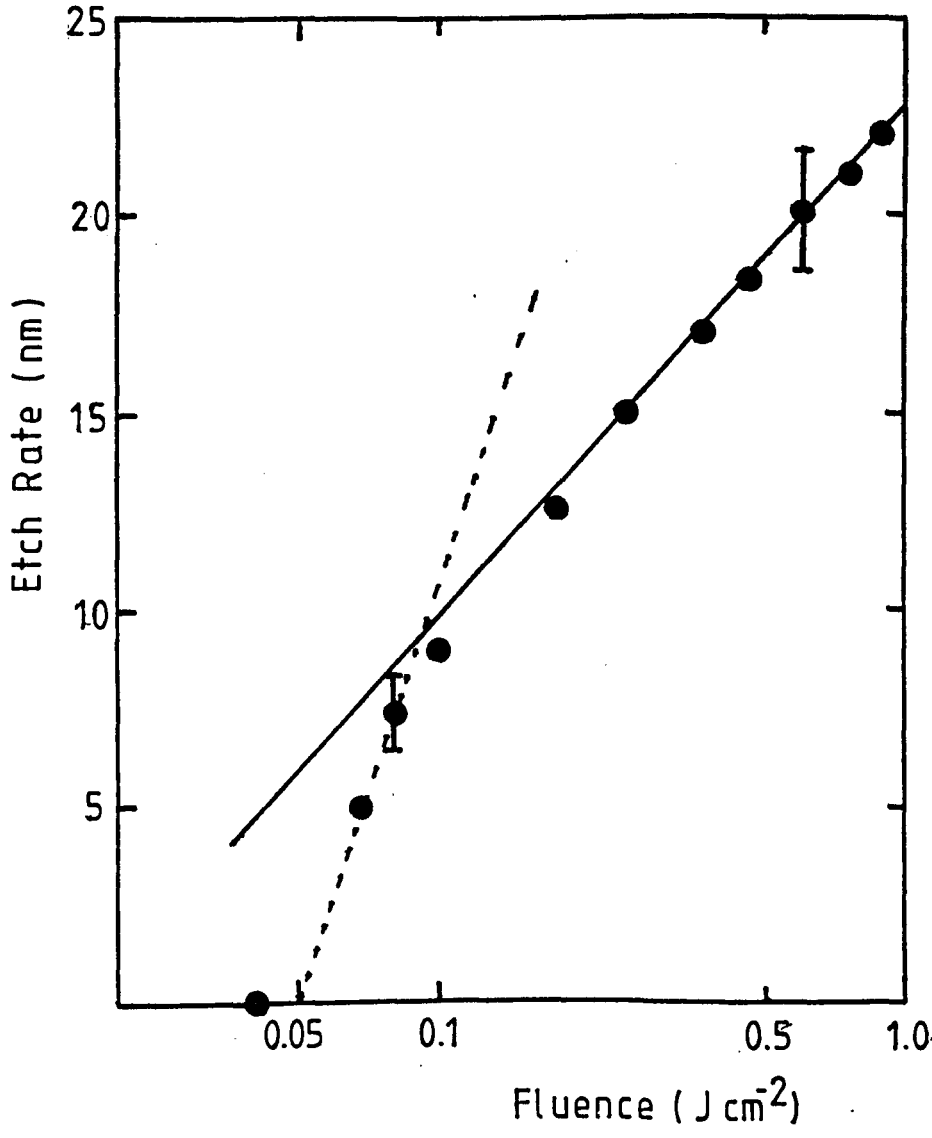

Fig.4.4.3.

ETCH-RATE OF CU IN Cl_2 at 5 Hz.

- - - - 2.5 torr.

——— 0.5 torr.

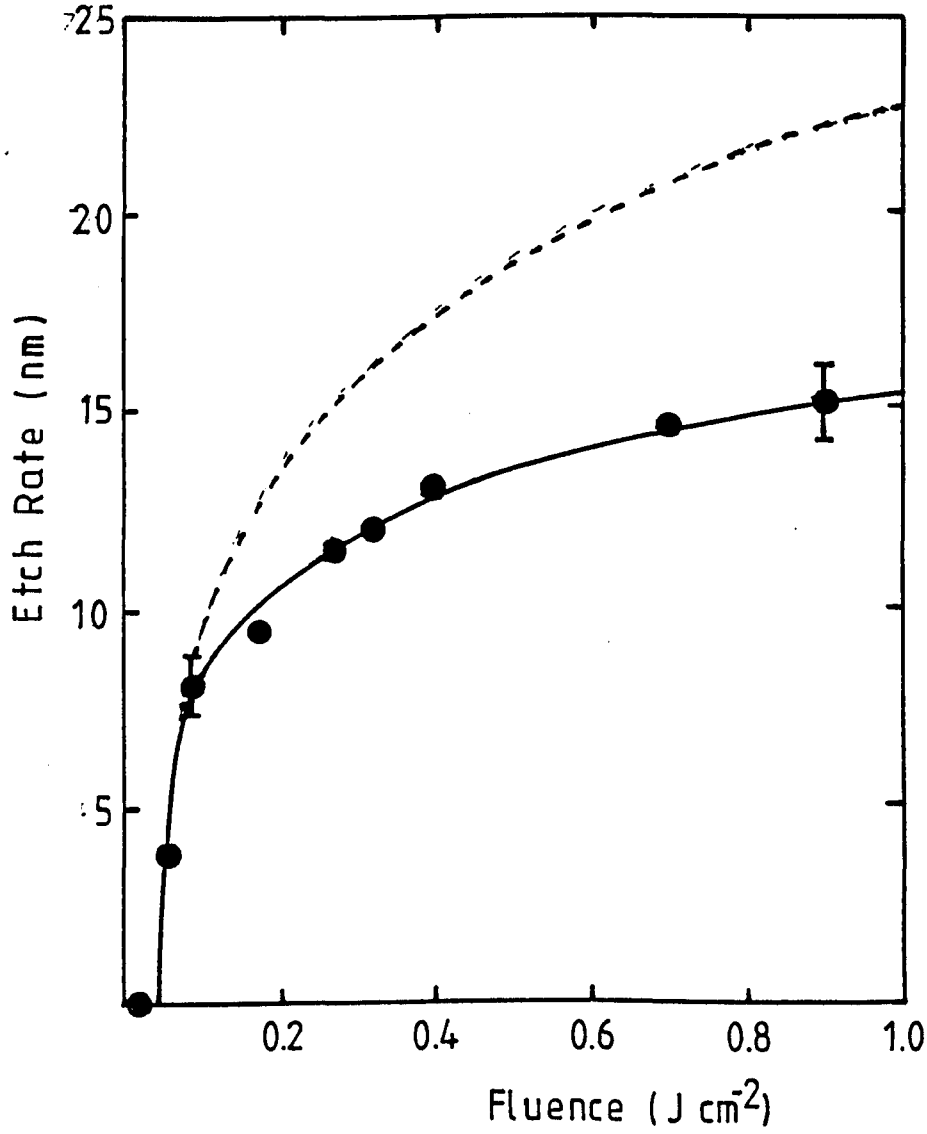

Fig.4.4.4.

ETCH-RATE of Cu in Cl_2, XeCl Laser

Etch-rate as a function of fluence and Cl_2 pressure at 5 Hz.

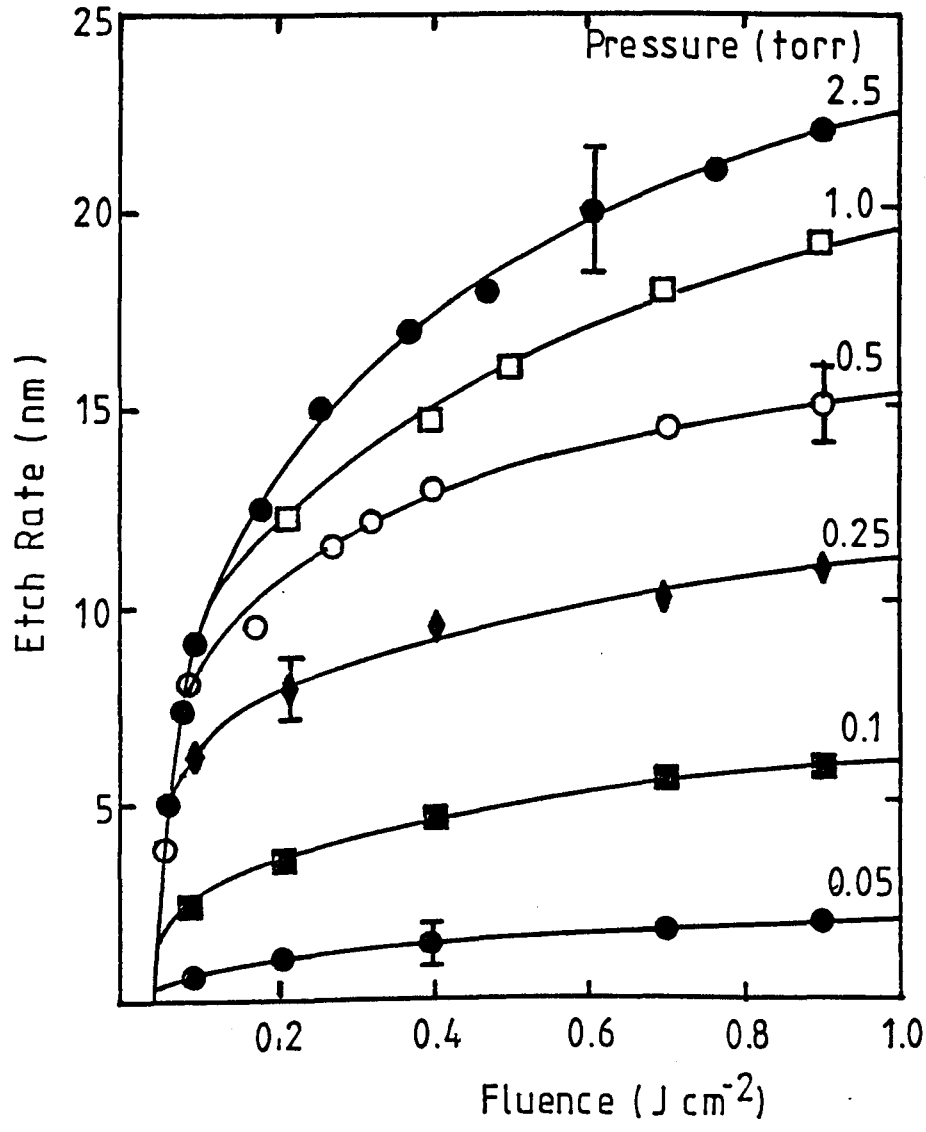

Fig.4.4.5.

ETCH-RATE OF COPPER IN CHLORINE

Etch-rate per pulse as a function of fluence, F $\geq$ 4xFt, and pressure.

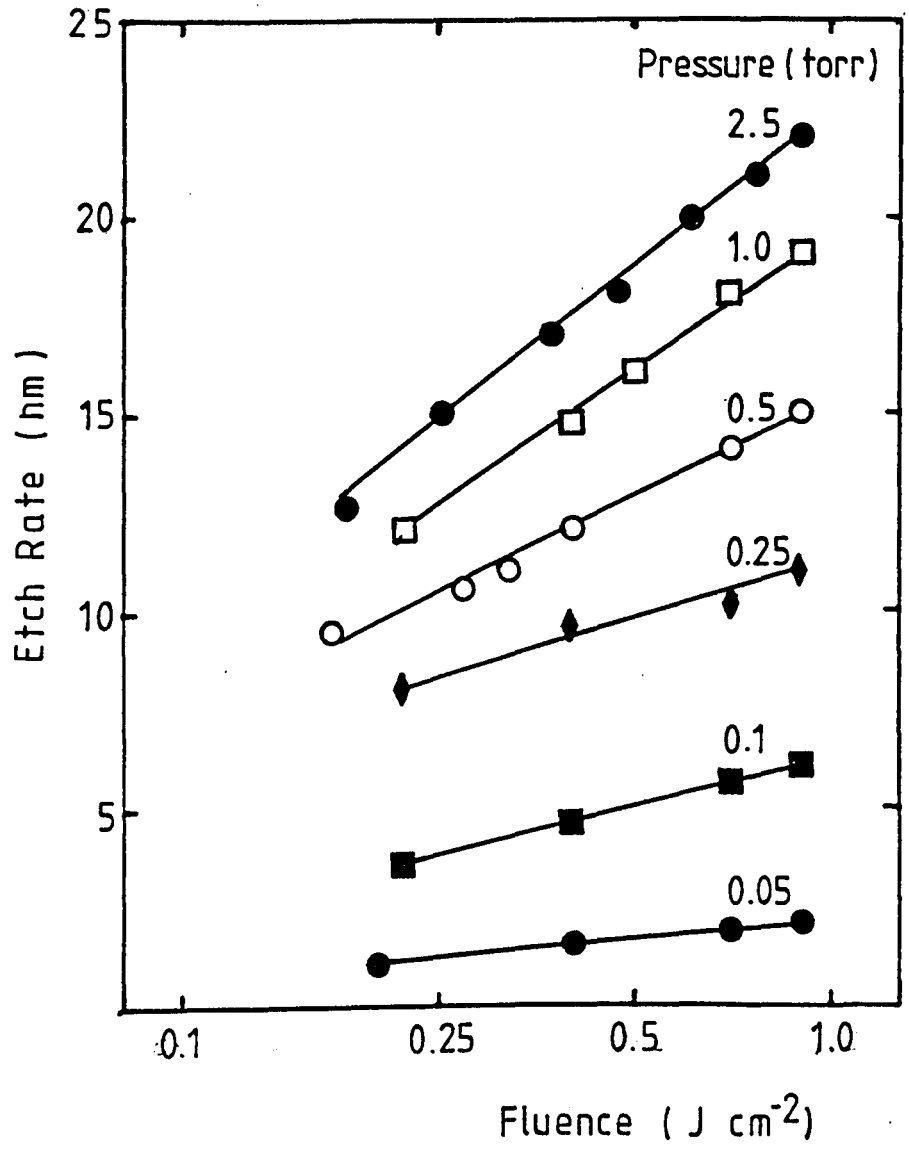

Fig.4.4.6.

RELATIVE ABSORPTION LENGTH vs PRESSURE

CuCl equivalent absorption length for XeCl laser at 5 Hz as function of pressure.

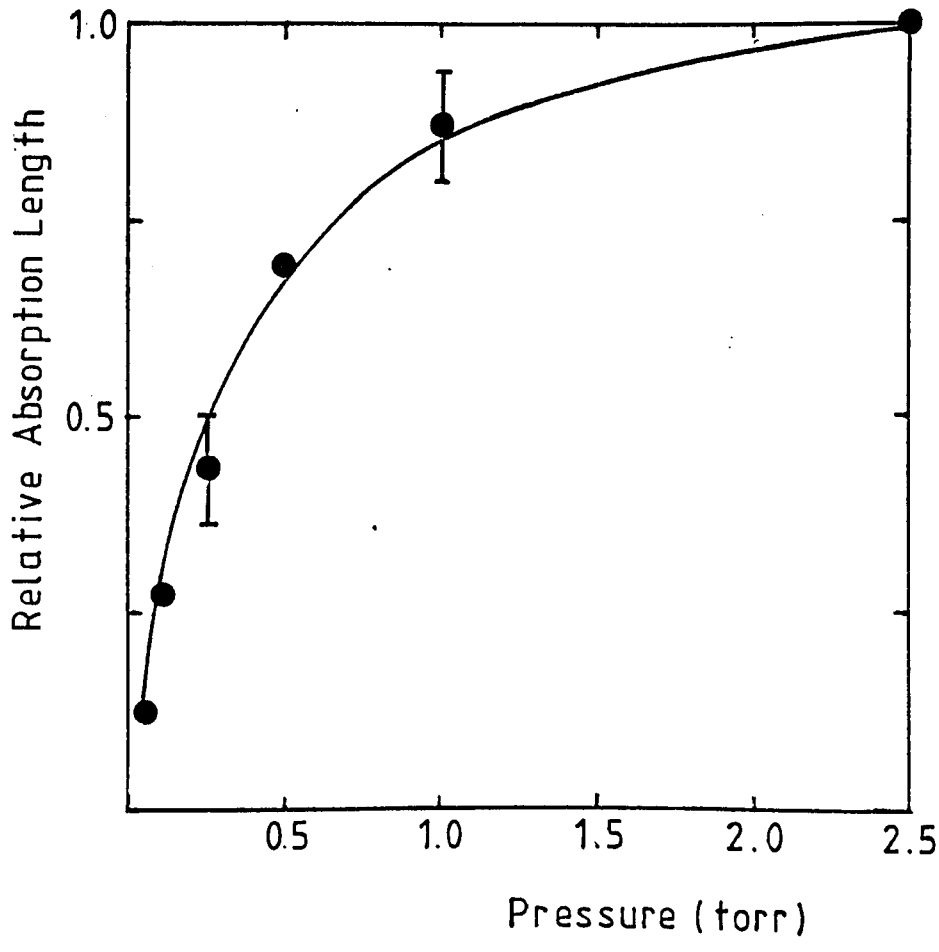

Fig.4.4.7.

ETCH-RATE OF COPPER IN CHLORINE

Etch-rate as a function of fluence

5 Hz, XeCl.

---- 2.5 torr.

——— 25 torr.

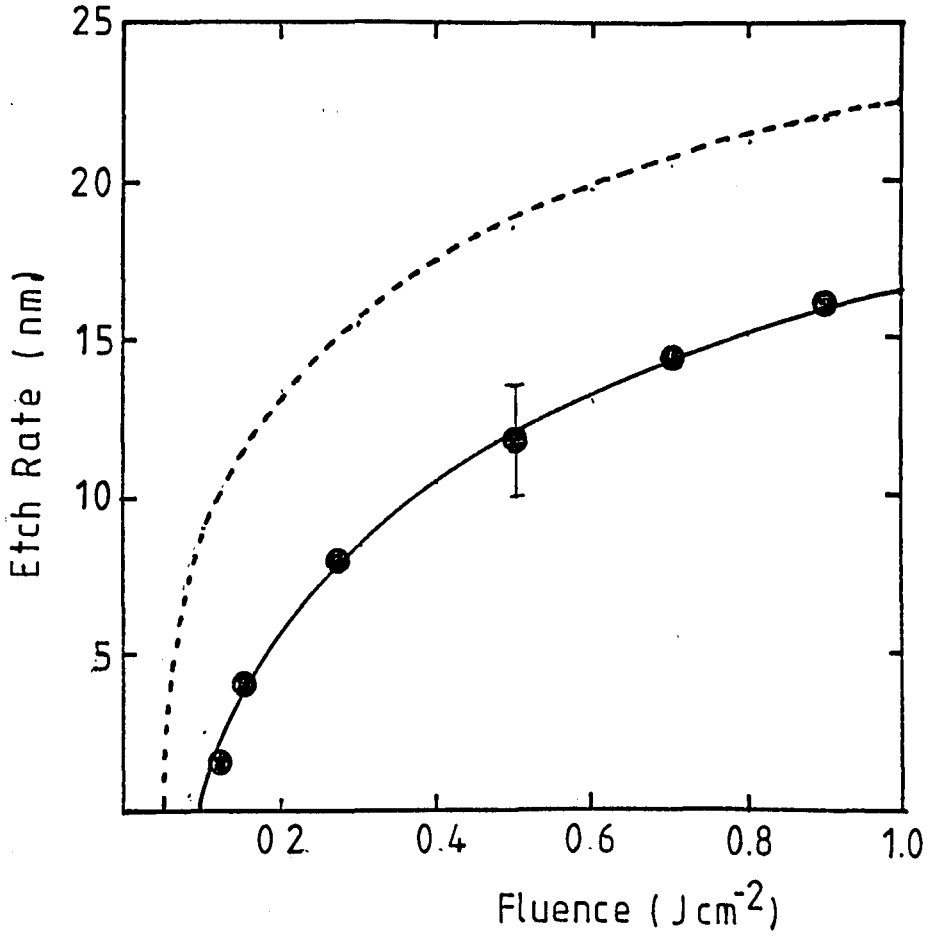

Fig.4.4.8.

ETCH-RATE OF COPPER IN CHLORINE

Etch-rate as a function of pressure,

1 J cm^{-2} XeCl at 5 Hz.

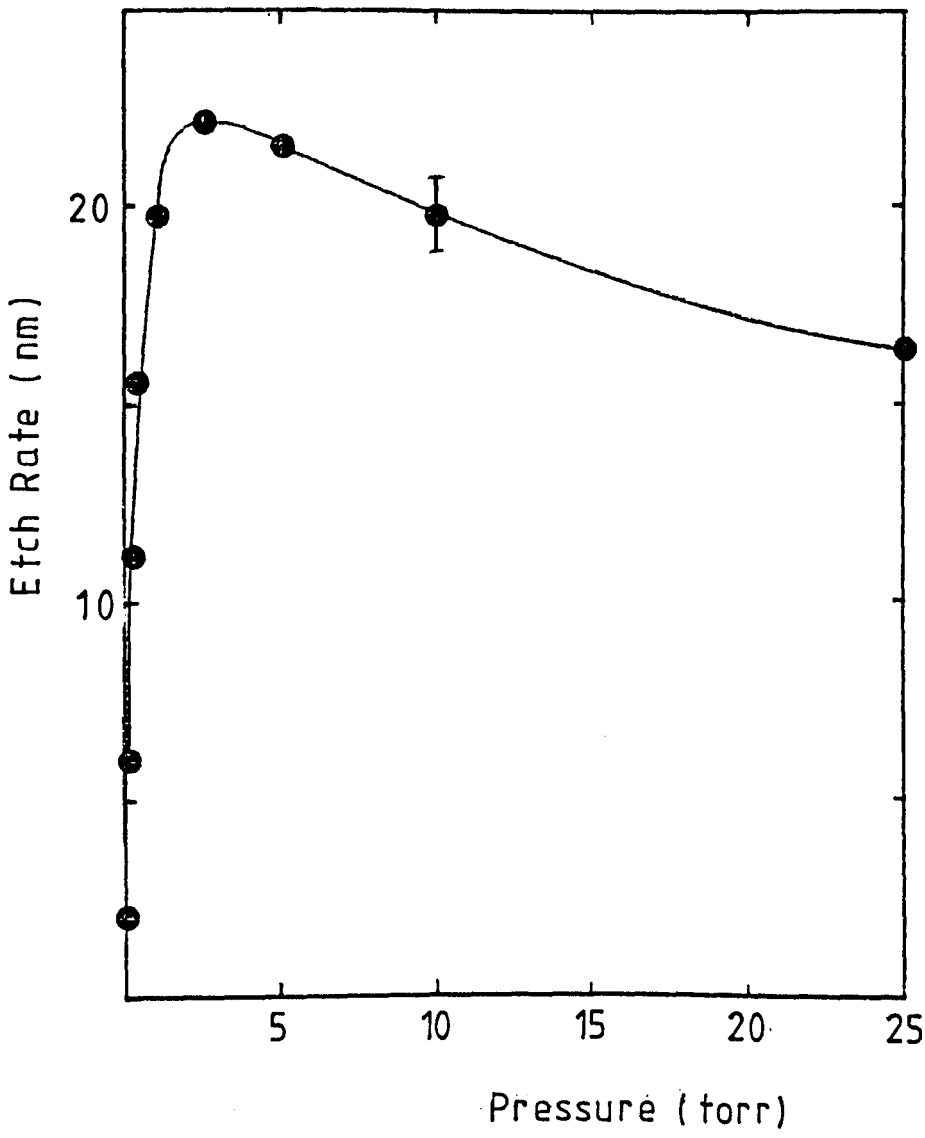

Fig.4.4.9.

ETCH-RATE OF COPPER IN CHLORINE

Etch-rate as a function of pressure
at various fluences.

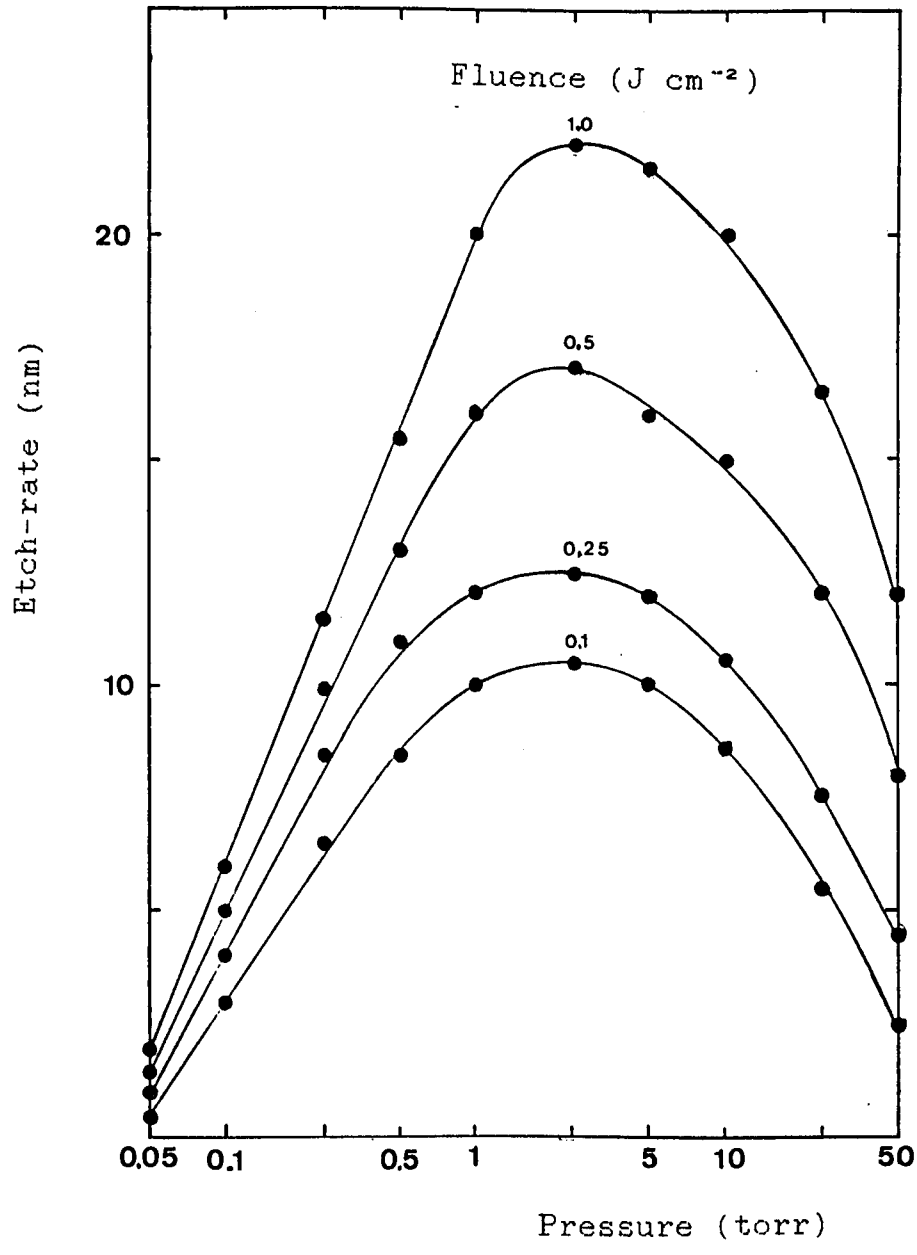

Fig.4.4.10.

ETCH-RATE of Cu at 0.5 J cm $^{-2}$

● constant fluence on cell

□ constant fluence on target

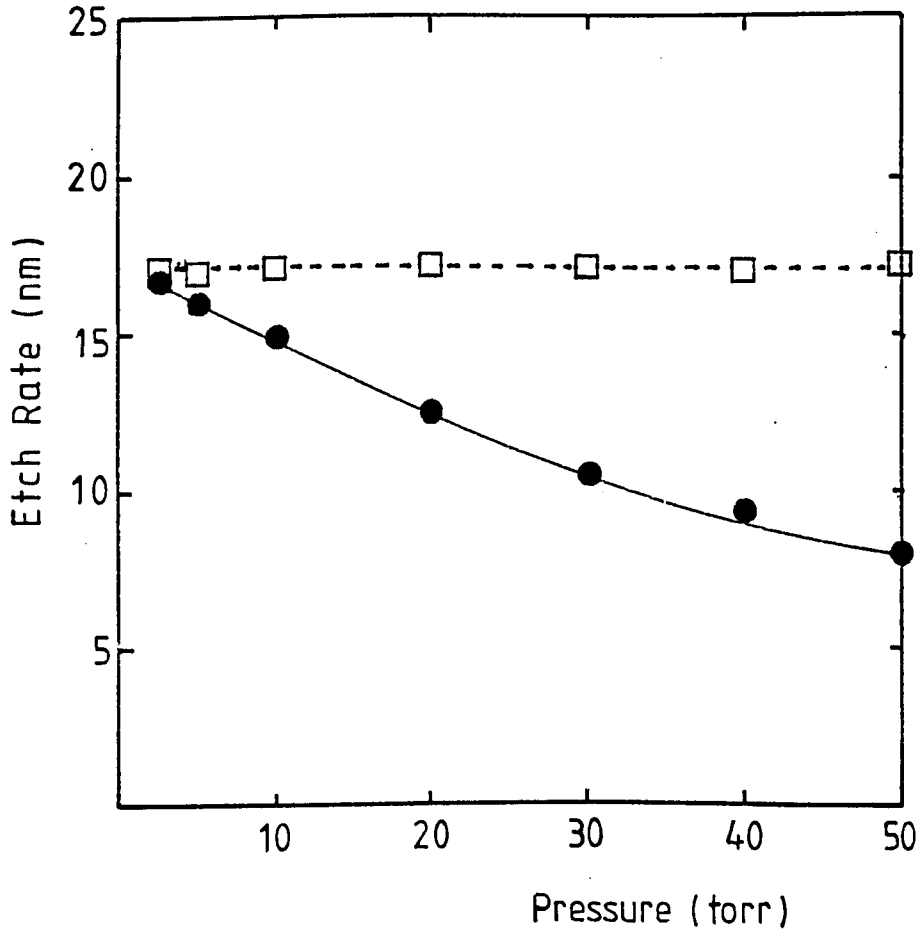

Fig.4.4.11.

ETCH-RATE OF CU IN Cl at 0.25 J cm^{-2}.

Etch-rate as a function of pressure and laser prf.

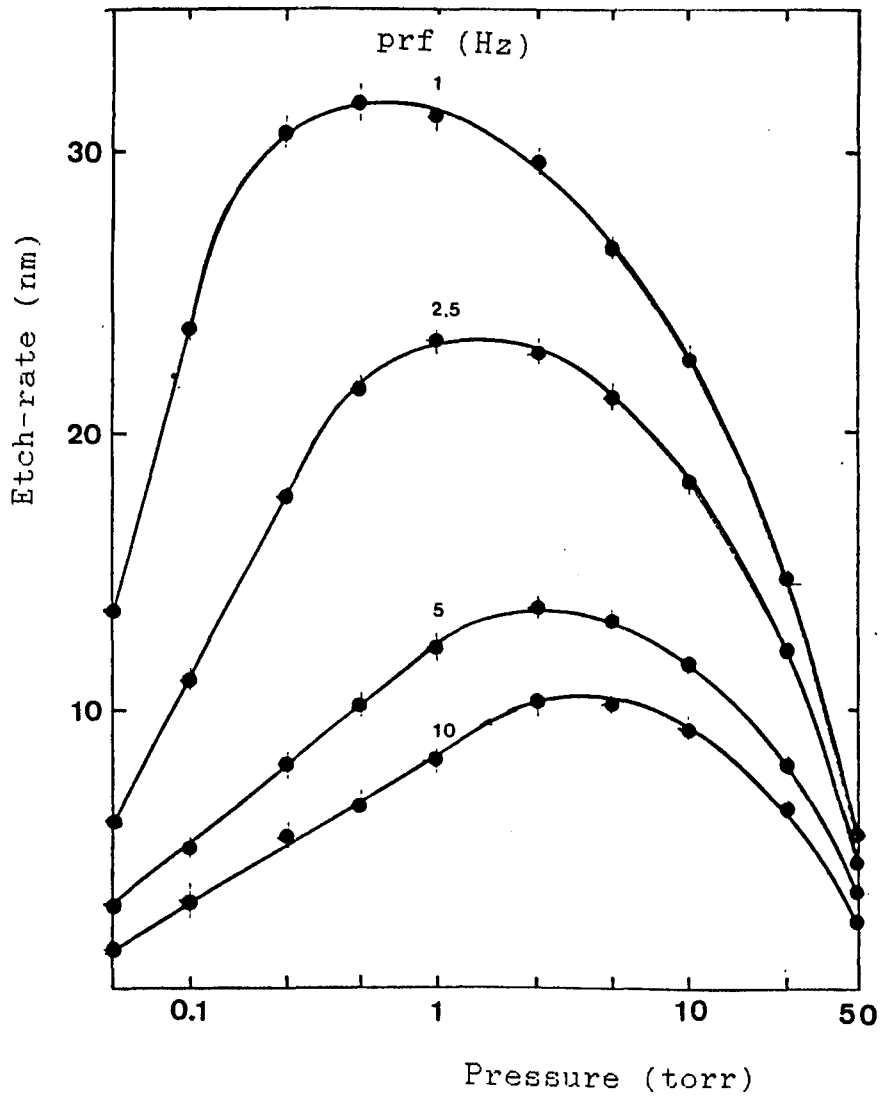

Fig.4.4.12.

ETCH-RATE of Cu in 5 torr Cl

Etch-rate as a function of total pressure, argon buffer gas.

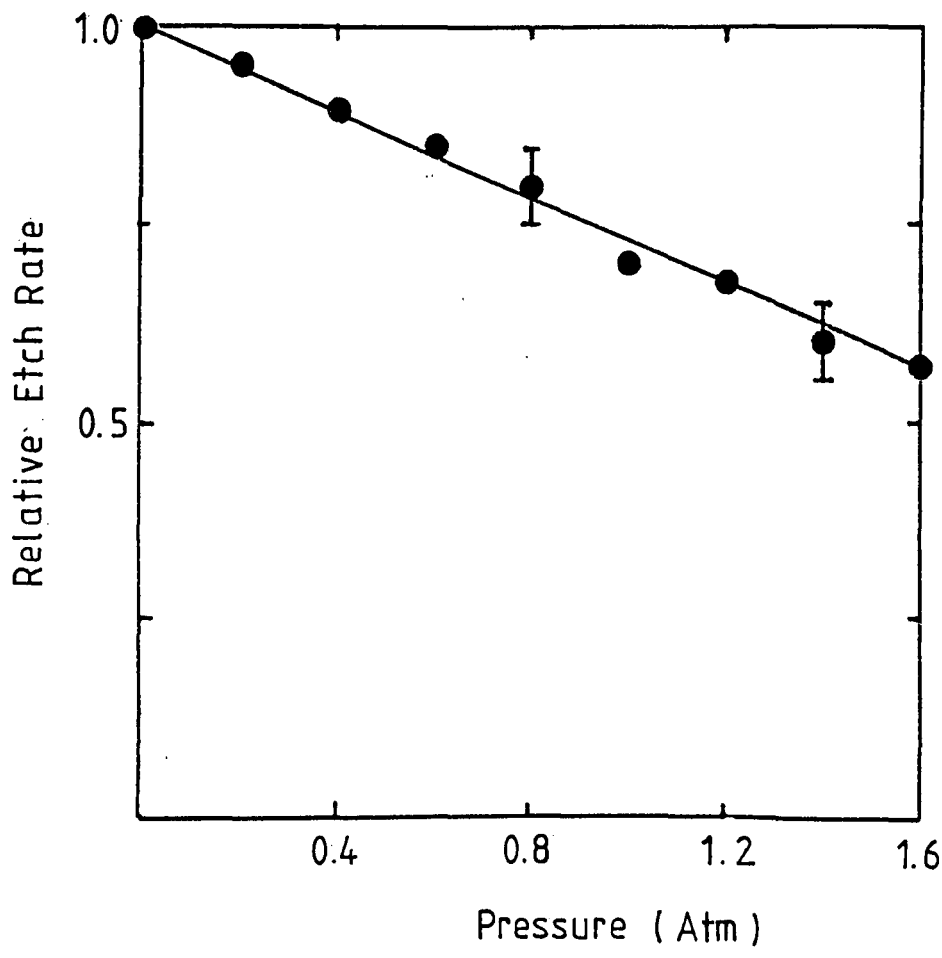

4.5.
UV-VISIBLE SPECTROSCOPY

The excimer laser ablation of copper in chlorine gas is accompanied by a bright visible plume having the blue-green colour that is characteristic of copper compounds. The plume consists of ionic and neutral products from the ablated surface in excited states with some contribution arising from collisions among the ejected species themselves and with the ambient gas molecules.

The plume was observed to expand from the target surface with an included angle of approximately 30° and with its mean direction, which was independent of the incident angle of the laser radiation, normal to the target surface. The dimension of the plume along the target normal was observed to have some dependence on both the fluence and the ambient pressure.

As described earlier, a section of the plume was imaged onto the entrance slit of the monochromator and the emitting species of the plume were observed as they traveled past a "window" equal (with unity magnification) to the width of the slit (50-100 μm). The relative positions of the monochromator and target were arranged so that the spectra were obtained from the plume at approximately 1.0 mm from the target surface along the target normal.

An example of the emission spectrum of the ablation plume is shown in Fig.4.5.1 and the principal lines, identified from standard spectral tables [11-13] are indicated. The spectrum is similar to those found by Rothenberg [14] for laser

ablated CuCl in the 400-520 nm range. This spectrum is representative of the many obtained in this study in that, apart from signal amplitude variations attributable to variations in etch rates, no differences were observed in spectra for a variety of conditions of fluence (0.1-1.0 J cm^{-2}), laser prf (1-10 Hz) or ambient chlorine gas pressure (0.1-5.0 torr). Furthermore, no additional lines were seen when the ambient chlorine pressure was buffered to 10 torr with Argon.

The spectra contained only relatively weak components attributable to emissions from the chlorine gas excited directly by the incoming radiation. In a separate experiment, with the copper target removed from the chamber, the chlorine was found to emit mainly in the red ($\geq$ 600nm) with the exception of some weak lines and continua in the 450-500 nm region.

The emission spectra reveal that Cu, CuCl & Cl are present in the ablated plume although no additional information regarding the form in which these species are desorbed from the surface can be deduced. It was found that CuCl is deposited on the interior of the cell but this does not preclude the possibility of the chloride being dissociatively removed from the target and the free copper subsequently recombining with the ambient gas. The presence of the sharp Cu atomic lines at 510.5, 515.3 & 521.8 nm, which are clearly distinguishable in the spectra, supports the view of a dissociative desorption mechanism.

Quantitative information about the desorbing species and their relative yields may best be obtained from time of

flight mass spectra but this diagnostic was not available.

Some interesting information may be obtained from the time resolved signals with the monochomator tuned to specific spectral features. Typical signals from the strong, 323 nm, copper line emission are reproduced in Fig.4.5.2 for "window" (50 μm) distances of 0 and 2.5 mm from the target surface. These curves represent the average of 5 recorded pulses at each position and the error bars indicate the range of values. The zero time was determined by triggering the oscilloscope on which the pulses were recorded using a fast (≈1 ns rise-time) vacuum photodiode viewing the reflected laser radiation from the target. The distance origin was obtained by just eclipsing the monochromator input axis with the target and then moving the target surface back by an amount equal to the slit width. The electrical rise time of the photomultiplier-oscilloscope system was 3 ns and the transit time of the photomultiplier tube 11 ns; however, these are both small in comparison to the time scale of the spectral emission (≈1 μs) and their effect on the recorded signals can be neglected.

The point in time at which the signal starts to rise, representing the arrival of the first luminous species within the field of view, is difficult to determine. It is, therefore, convenient to define various points on the curves, as shown in Fig.4.5.3, corresponding to the first arrival t(0), 10% amplitude position t(10) or peak height t(100) to enable comparisons to be made between pulses from different positions in the plume.

The distance-time plot for the best estimates of t(0), t(10)

& t(100) for distances up to 2.5 mm from the target are shown in Fig.4.5.4. The times, t(0), representing the best estimates of the earliest times of arrival of luminous species and corresponding to those having the highest velocity, lie on a straight line yielding a constant velocity of $6.6\pm0.7\times10^{5}$ cm s^{-1}. It is interesting to note that the line joining these points does not pass through the origin, within the experimental error. When account is taken of the instrumental delay time (≈15 ns) this suggests that there is an "incubation" time of approximately 30 ns before the material removal from the surface appears as luminous species. The early portion of the t(10) curve confirms the gradient of the t(0) curve.

The shape of the time resolved intensity curves is seen to change with increasing distance from the target in that the delay between the t(0) point and the peak intensity t(100) is seen to increase. The peak intensity occurs on a time scale two orders of magnitude greater than the laser pulse length and the t(100)-distance curve suggests that the velocity of the particles contributing to this part of the pulse is decreasing with distance from the origin. The gradient of this curve as a function of distance is shown in Fig.4.5.5 which indicates that the velocity decreases linearly with distance. This is presumably because of deceleration as the products push the ambient gas ahead of the plume.

The amplitude of the peak intensity as a function of distance up to 1 cm from the target is shown in Fig.4.5.6 from which it can be seen that the signal decreases sharply

over this distance.

The transit time across the 50 micron slit width is of the order of 10 ns for the most rapid particles and 50 ns for those at peak intensity. As the time-scale of the emissions observed is much longer than this, the signal can be taken as reflecting the time-scale of removal of material from the target and the velocity distribution of the ablated particles.

Fig.4.5.1.

EMISSION SPECTRUM OF XeCl LASER ABLATED COPPER IN A CHLORINE ENVIRONMENT.

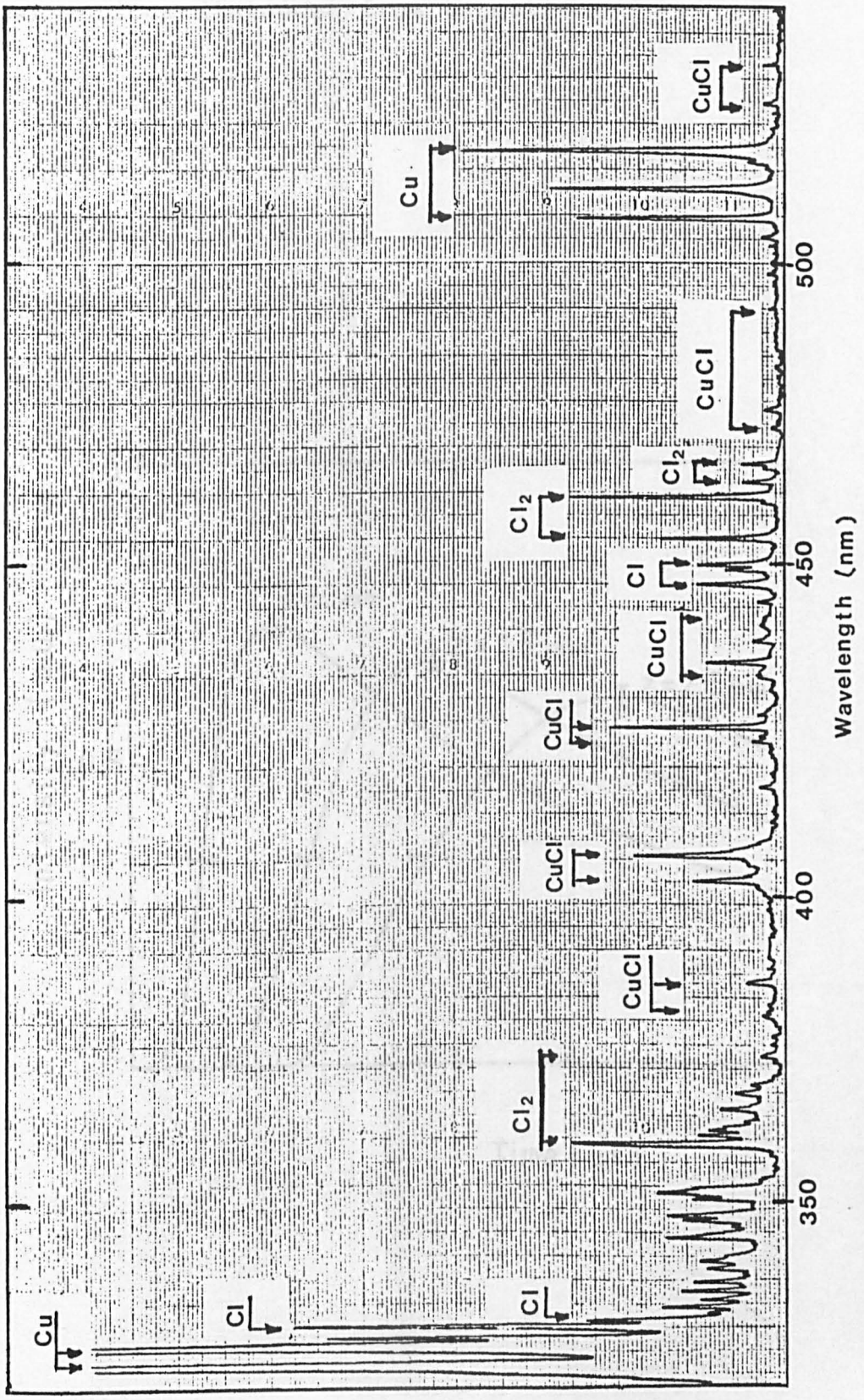

Fig.4.5.2.

EMISSION LINE PULSE SHAPES

Time-resolved emission for Cu

at various distances from target.

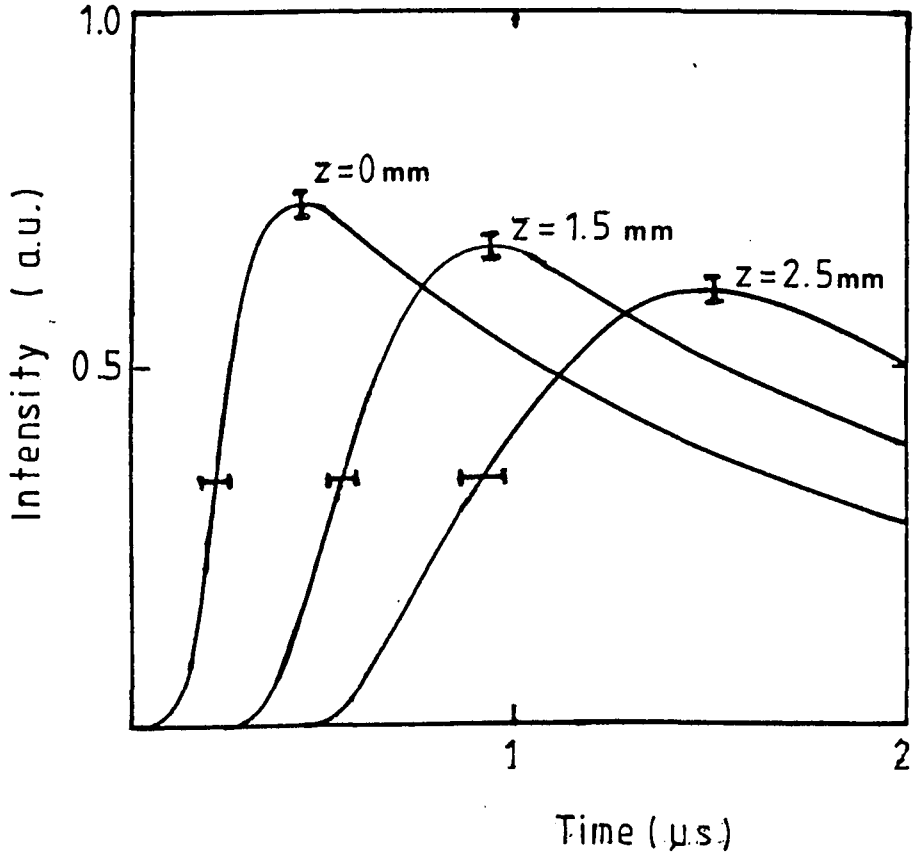

Fig.4.5.3.

EMISSION LINE PULSE SHAPE

Typical pulse shape showing

definition of t(0),t(10) & t(100).

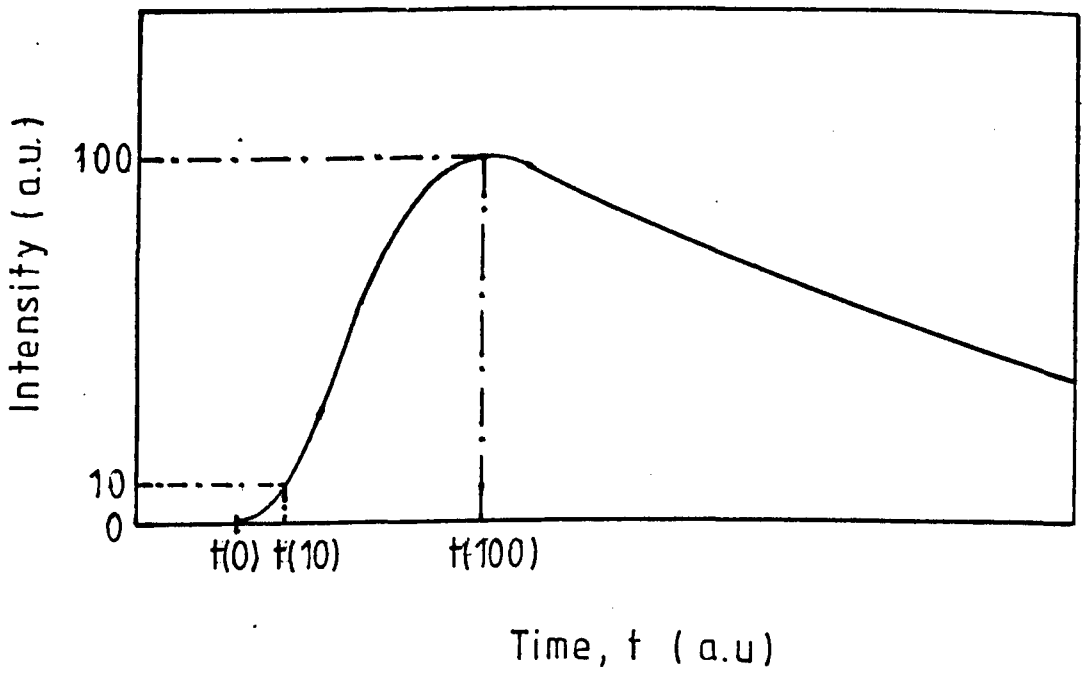

Fig.4.5.4.

DISTANCE-TIME PLOT FROM PULSE SHAPES

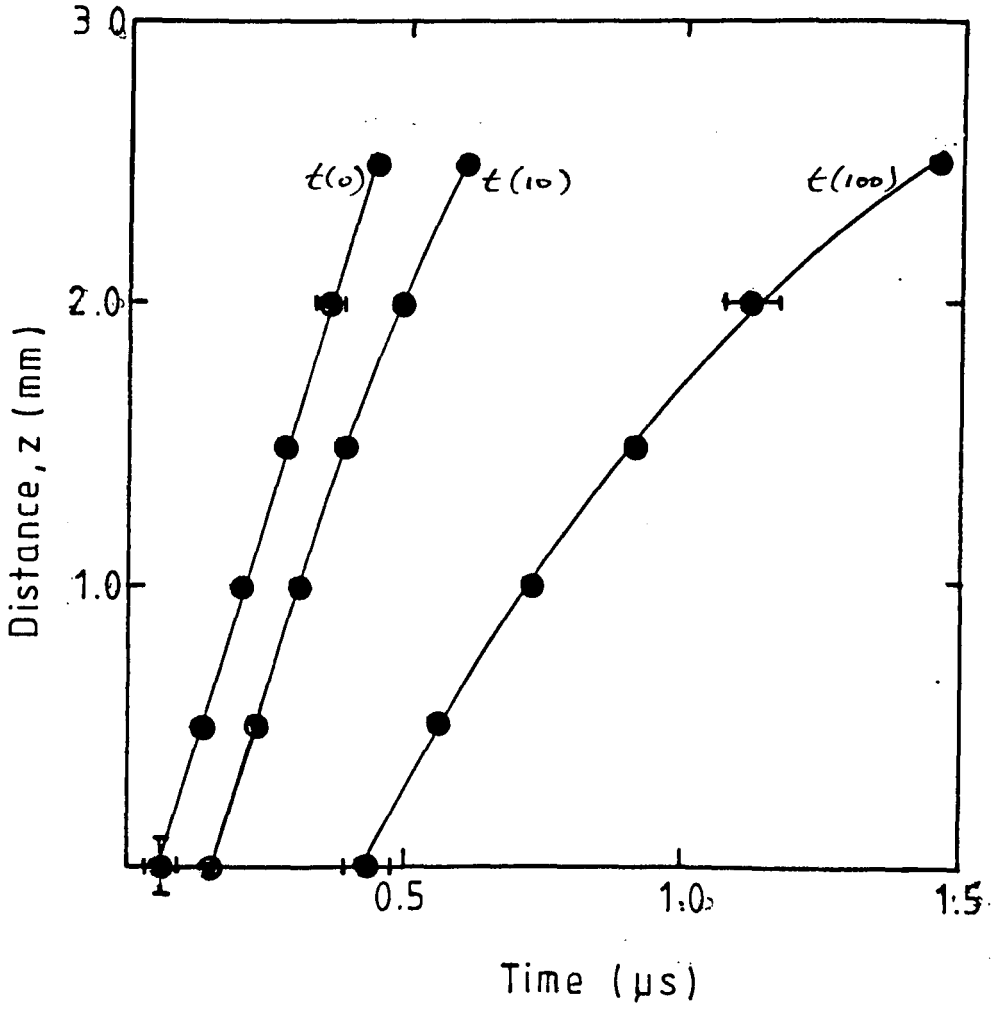

VELOCITY OF Cu SPECIES vs DISTANCE

Velocity of Cu from t(100) peak of emission as a function of distance from target.

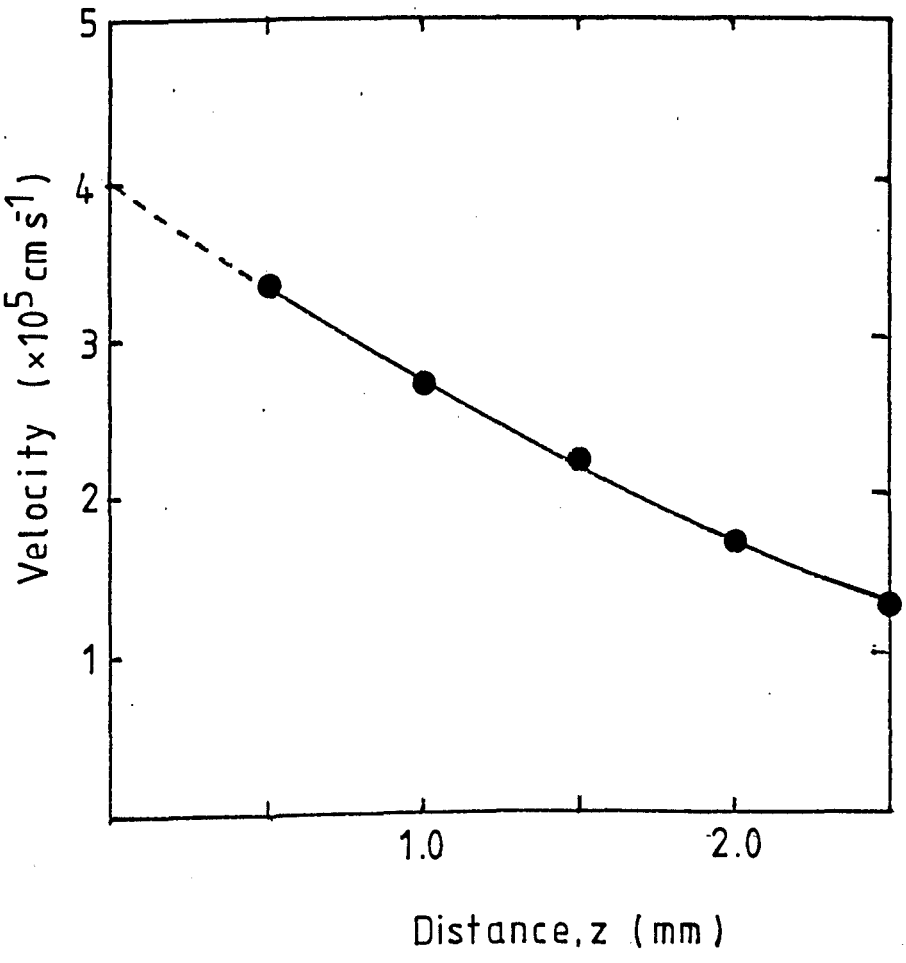

Fig.4.5.6.

RATIO OF EMISSION INTENSITIES

Peak emission intensity as a function of distance from target.

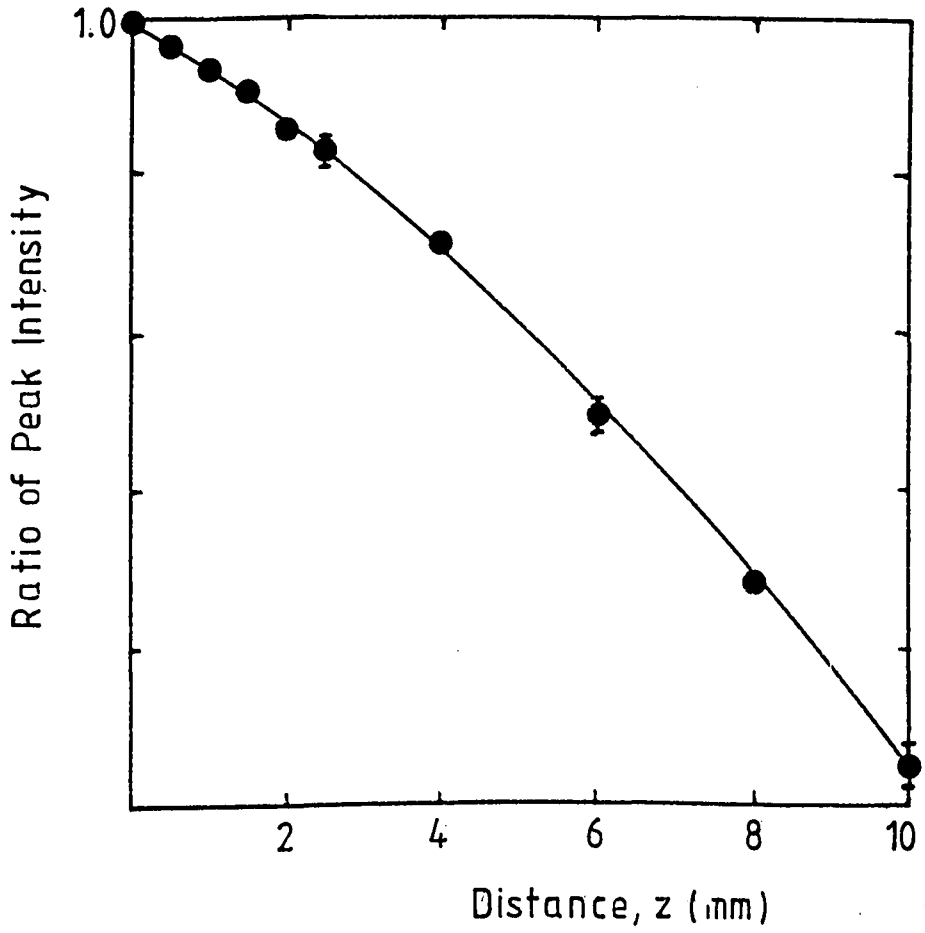

4.6. DISCUSSION

The results of the UV-excimer laser etch-rate studies on copper in a chlorine gas environment reveal that the process is not readily described by a simple function in terms of the parameters of laser fluence, pulse repetition frequency and gas pressure.

The data suggests that three regimes may be distinguished:

(i) The low exposure regime: Here conditions of low pressure and high prf yield chloride layers thin enough to be completely removed by a single laser pulse of high enough fluence. Analogous to the single pulse removal of thin metal films [15], the etch rate is largely independent of fluence above the threshold value for a given chloride thickness. This regime was not examined quantitively because of the difficulty in controlling the pressure at low values ($\leq$ 0.01 torr) for the rather long period required to etch right through 25 μm foils at the rate of a few nanometers per pulse. However, optical microscopic examination of the target during processing at approximately 0.005 torr and 1 Hz allowed observation of a bright metallic copper surface at the instant of ablation followed by a sequence of surface colour changes indicating the re-growth of the thin chloride layer before the next ablation step.

(ii) The intermediate exposure regime: For the range $\approx$ 0.05 to 2.5 torr-s, which covers the bulk of the data presented and discussed in this chapter, the etch-rate is regulated by the chloride growth rate.

(iii) The high exposure regime: This, to some extent, is limited by chloride growth and is further complicated by significant laser energy absorption in the chlorine ambient. In addition re-deposition of ablated material due to near target collisions with ambient gas molecules and the external pressure depression of the chloride vapour pressure add further complexity.

There are, of course, transitional regions between these regimes and a strict delineation is difficult. Between (i) and (ii), for instance, occurs the situation in which growth enhancement of the chloride may occur due to an increase in substrate temperature induced by the absorption of laser energy in excess of that required for ablation and thus constitutes a thermal self regulatory removal regime.

The intermediate regime (ii) is of particular interest since the etch-rate dependence on chloride thickness reflects the non-stoichiometric properties of the layer. The higher copper concentration gradient, postulated for thinner films, implies that the optical absorption depth is reduced but that the thermal diffusivity is increased. Both of these factors will contribute to a higher fluence being required to produce a given removal rate.

It was postulated in section 4.3 that, at a given etch-rate in this regime, there would exist a quasi-equilibrium thickness of chloride reached and maintained when the etch-rate per pulse is balanced by the chloride growth in the interpulse period. It was shown in chapter 3 that the chloride growth may be described by:

$$H(p,t) = H(p,t_0) + B(p)\sqrt{(t-t_0)} \qquad (1)$$

Where H is the pressure dependent chloride thickness at time t in a diffusion limited regime following an initial linear growth to thickness H_0 in time t_0.

We define the quasi equilibrium thickness, H_2, as that addressed by successive laser pulses which remove an amount, ΔH, to leave thickness H_1. The two thicknesses H_2 & H_1 may be identified on the growth curve as occuring in 'growth-time' at t_2 & t_1 respectively. Thus the etch-rate, z, and laser prf, f, are related to these by:

$$z = \Delta H = H_2 - H_1 \qquad (2)$$

$$1/f = \Delta t = t_2 - t_1 \qquad (3)$$

from (1):

$$t_2 = t_0 + (H_2 - H_0)^2 / B^2 \qquad (4)$$

and subtracting a similar expression for t_1, the pressure dependence of B and H being implicit, gives:

$$1/f = H_2^2 - H_1^2 - 2H_0(H_2 - H_1) / B^2 \qquad (5)$$

and from (2), substituting for H_1:

$$1/f = 2H_2 z - z^2 - 2H_0 z / B^2 \qquad (6)$$

hence:

$$H_2 = (B(p)^2 / 2fz) + (z/2) + H_0 \qquad (7)$$

This function is shown for two values of prf (2.5 & 10 Hz) and in the range 0.1-5.0 torr in Fig.4.6.1.

From (7) it can be seen that the model predicts a characteristic quasi-equilibrium thickness, regulated by the pressure and prf, for each removal rate per pulse. This is also necessarily true when the etch rate is not constant but rather some function of chloride thickness. It should be remembered that in the experimental situation we do not have a stoichiometric CuCl layer but one in which the copper

concentration gradient is a function of thickness and which, in thin films, may limit the ability of a given fluence to remove material. A model, therefore, in which the etch-rate per pulse increases with increasing thickness, up to a maximum representing the stoichiometric case, is intuitively realistic.

Fig.4.6.2 shows the results of computer modelling of the etching process with different etch rate dependencies, viz;

(a) Constant etch-rate, $z = Const.$

(b) Linear dependence on thickness, $z = A \times H$.

(c) Quadratic dependence, $z = (A \times H) + (B \times H^2)$

(d) Exponential dependence, $z = A \exp[B \times H]$

It can be seen, using a suitable choice of parameters A and B, that the same steady state etch-rate and, hence, quasi-equilibrium thickness may be achieved via a number of different routes. It should be noted that the number of laser pulses to achieve equilibrium varies with the functional dependence of etch-rate on chloride thickness.

Since we only have access to the steady state etch-rate data and at a limited number of fluences, pressure and prf combinations it is not possible to deduce the functional form of the etch-rate dependence on these parameters. The model does illustrate, however, that the supposition of etch-rate dependence on chloride thickness goes some way towards a qualitative explanation of the observed behaviour. This is illustrated in Figs.4.6.3 & 4: Here the etch process is modelled using a linear dependence of etch rate on chloride thickness, with prf and pressure as variable parameters respectively.

The model may be used to predict the signal expected from monitoring the reflected HeNe laser probe beam during the ablation process. In this case the reflectivity is calculated from the model growth and ablation curves and a reflectivity vs time curve synthesised.

Fig.4.6.5 compares the reflectivity calculated from a growth curve with that of the growth plus ablation case. It can be seen that at each ablation step the reflectivity is instantaneously reset to the appropriate point on the growth signal curve. Fig.4.6.6 indicates that the shape of reflectivity trace is dependent upon the etching parameters and the steady state etching regime is readily identified by the repetitive nature of the signal.

Experimentally obtained traces of the reflected probe beam signal as a function of time are shown in Fig.4.6.7. Quantitative analysis of such data is clearly difficult but it may be seen that laser mis-fires, whilst causing discontinuities in the curve, do not radically change the overall shape which is consistent with that expected from the model.

The signal trace shown in Fig.4.6.8, whilst rather more complex, does show some of the features of the etching process. The removal of the oxide is characterised by an increase in the reflected amplitude at B followed by a rapid fall as the chloride layer starts to grow. The progression along the growth curve, but now modified by the ablation steps, is represented by the broad band of the trace ,C. Almost at the centre of the trace at D the ablation was stopped to illustrate the chloride growth. The increasing

separation of the maxima with time indicates the diffusion limited growth regime. Upon restarting the ablation at E the, now substantially thicker, chloride layer is soon reduced to the near equilibrium thickness. Finally, on removing the chlorine from the cell at point F the recovery of the reflected beam amplitude at G to a value consistent with that for the metal surface is observed.

Finally, in order to check the possibility of a pyrolytic ablation mechanism, an estimate of the surface temperature of the irradiated chloride is made from simple energy balance considerations. If the absorbed fluence, F(1-R), is assumed to be distributed to a depth, h, then the temperature, T, is given by;

$$T = F(1-R) / hCx10^{4}$$

Where C is the heat capacity (specific heat x density) and the factor 10^{4} is included because we use fluence rather than energy input. Taking values of 4140 kg m^{-3} for the density of CuCl and 629 K J^{-1} kg^{-1} for its specific heat [16], the temperature rise at the threshold fluence is found to be $\approx$ 1630 K for h = 0.1 μm, this being the sum of optical absorption length and thermal diffusion depth discussed in section 4.3. A temperature rise of this magnitude is not inconsistent with a thermal removal mechanism [17] and would produce a vapour pressure close to that of the ambient chlorine pressure [18].

Fig.4.6.1.

STEADY-STATE ETCHING OF COPPER IN CHLORINE

Quasi-equilibrium chloride thickness, H , as a function of etch-rate, z, for chlorine pressures 0.1-5.0 torr. 2.5 α 10 Hz prf.

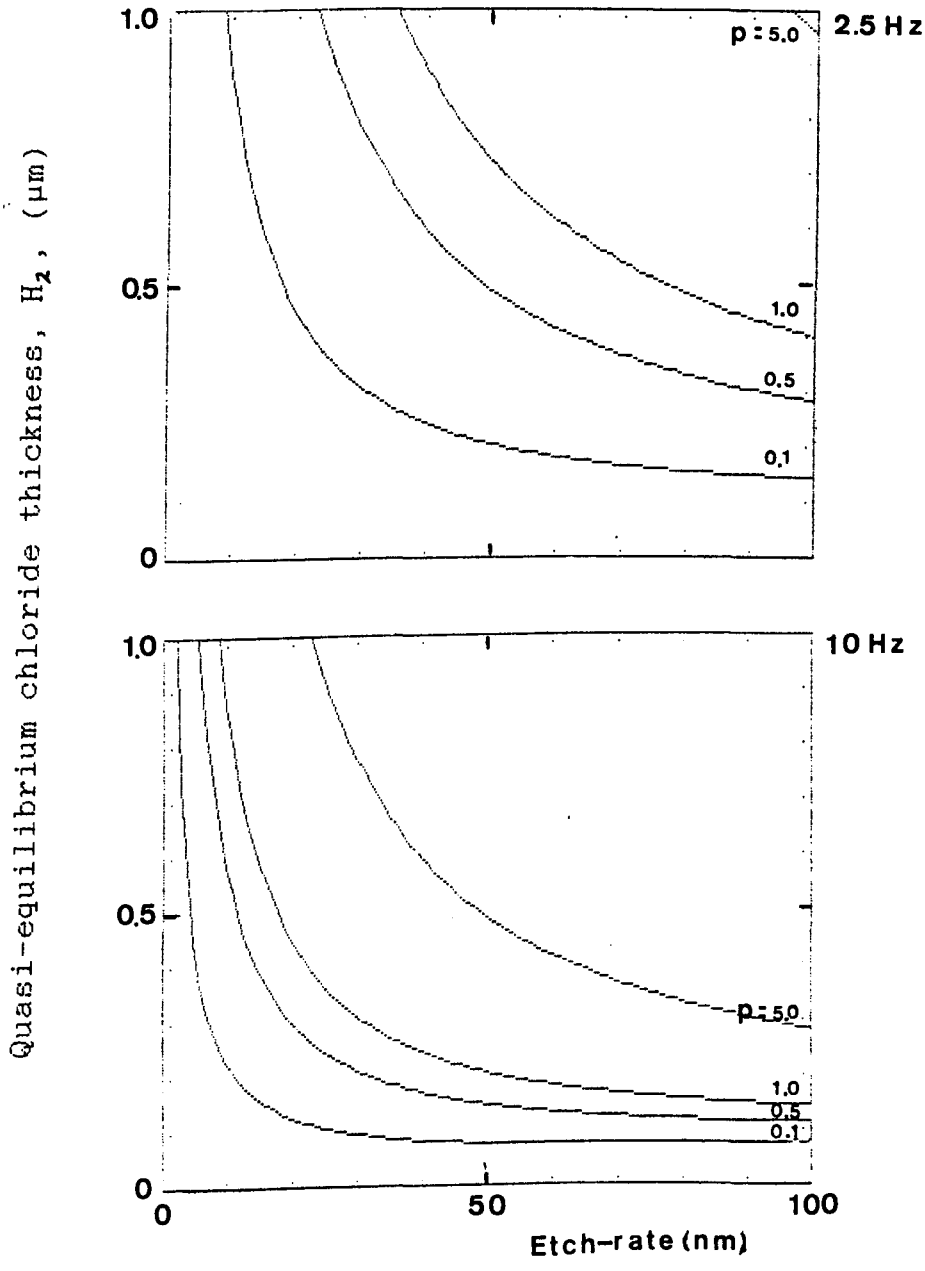

Fig.4.6.2.

GROWTH-ABLATION MODEL: COPPER-CHLORINE

Etch-rate, z, dependence on thickness, H.

a: $z = A$, b: $z = AxH$.

c: $z = (AxH) + (BxH^2)$, c: $z = A \exp(BxH)$.

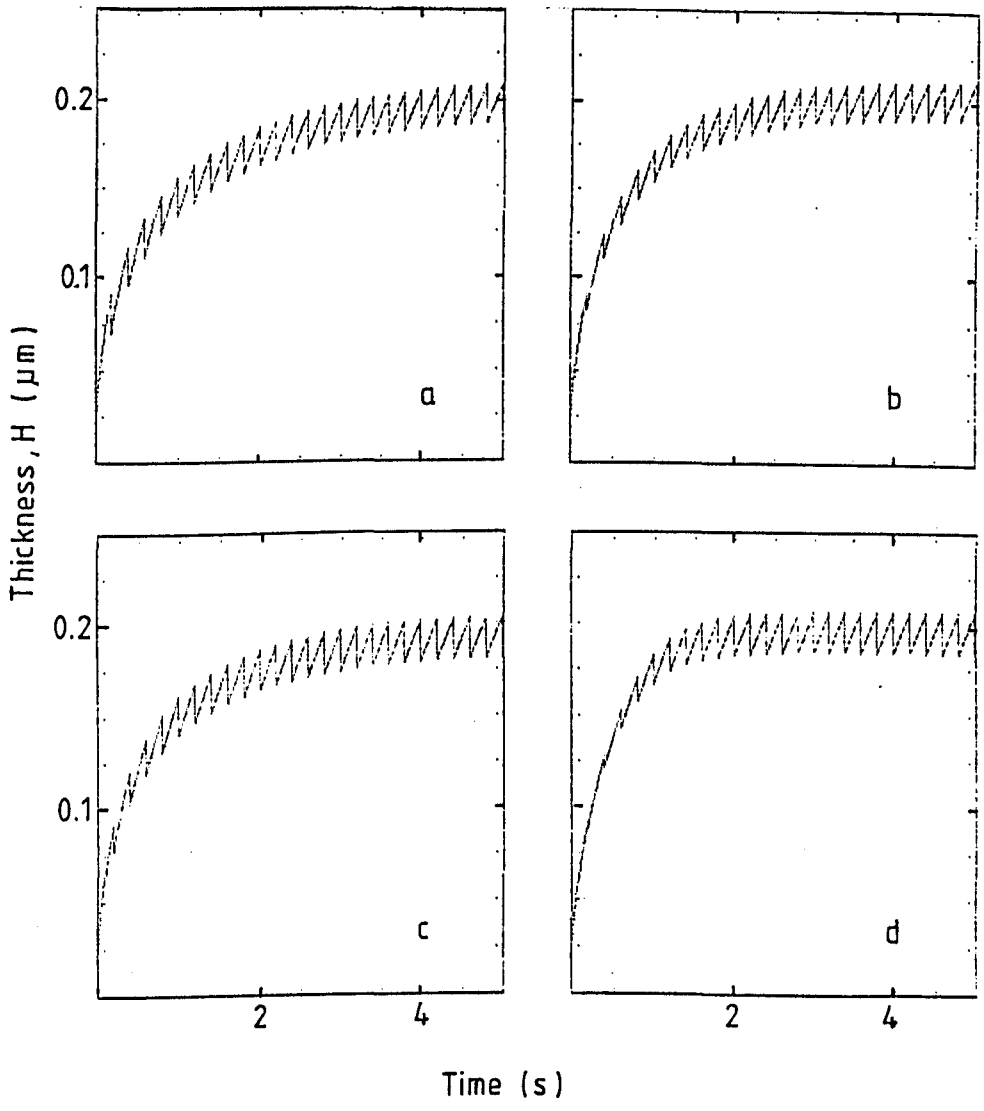

Fig.4.6.3.

GROWTH-ABLATION MODEL: COPPER-CHLORINE

Development of quasi-equilibrium thickness.

Etch-rate: z = AxH.

a: 1 Hz. b: 2.5 Hz.

c: 5 Hz. d: 10 Hz.

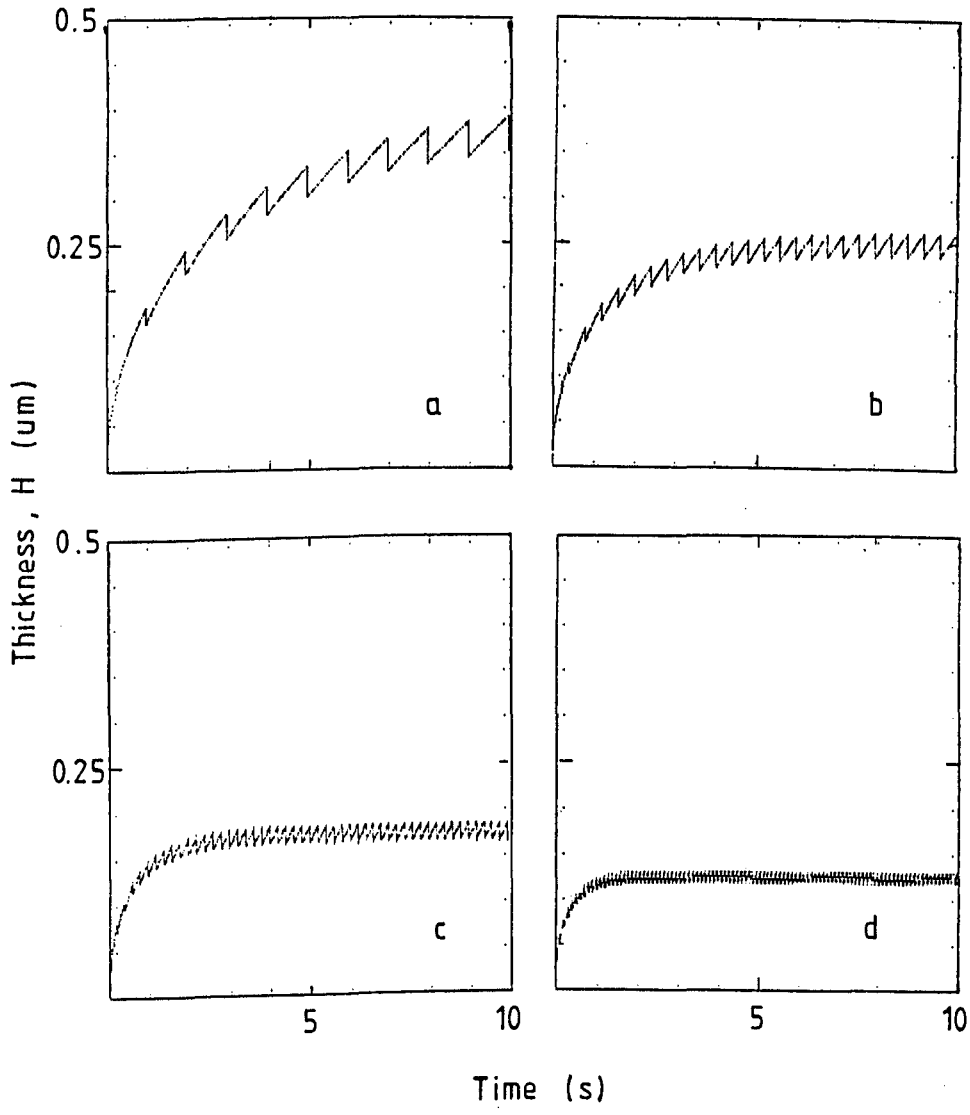

Fig.4.6.4.

GROWTH-ABLATION MODEL: COPPER-CHLORINE

Development of quasi-equilibrium thickness.

Etch-rate: z = AxH. prf = 5 Hz.

a: 1 torr b: 0.5 torr.

c: 0.25 torr d: 0.1 torr.

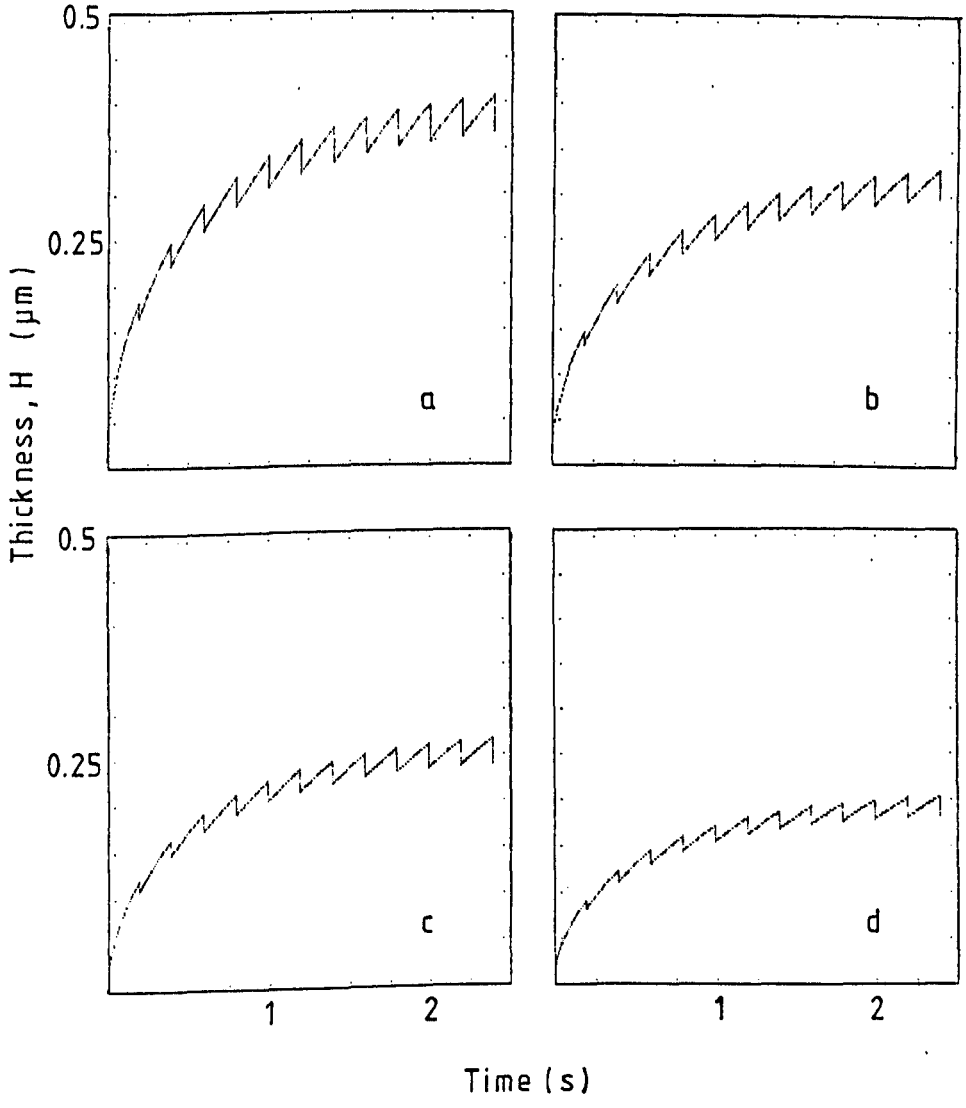

Fig.4.6.5.

GROWTH-ABLATION MODEL : REFLECTIVITY

a: growth only

b: growth and ablation

← 'reset' position.

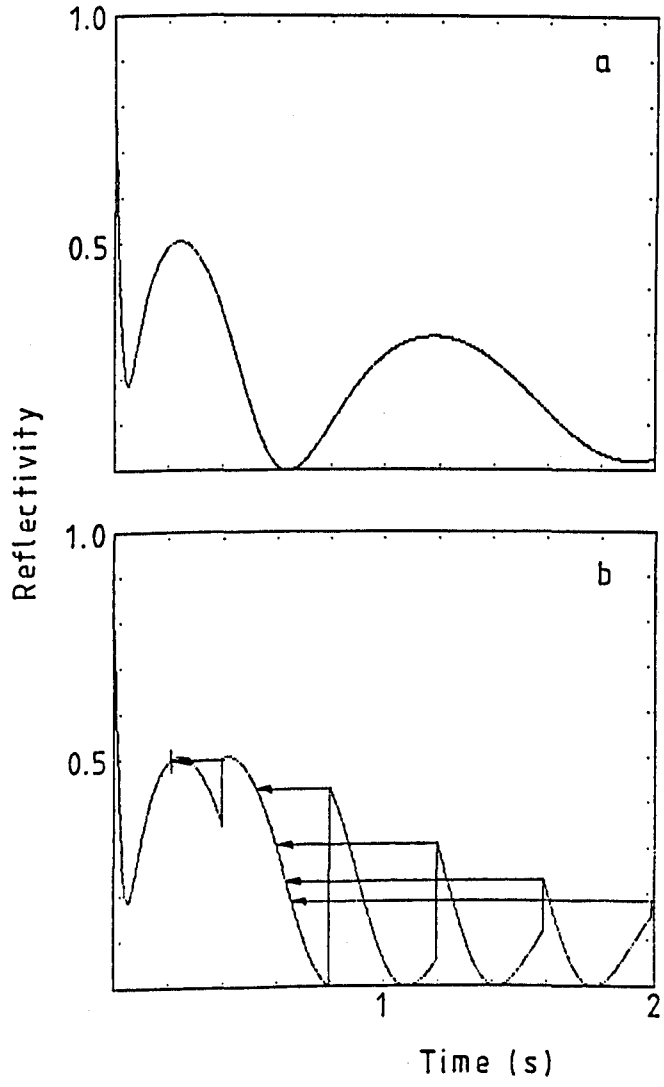

GROWTH-ABLATION MODEL : REFLECTIVITY

Pressure = 0.5 torr.

a: z = 0.05xH, 2.5 Hz.

b: z = 0.1xH, 5 Hz.

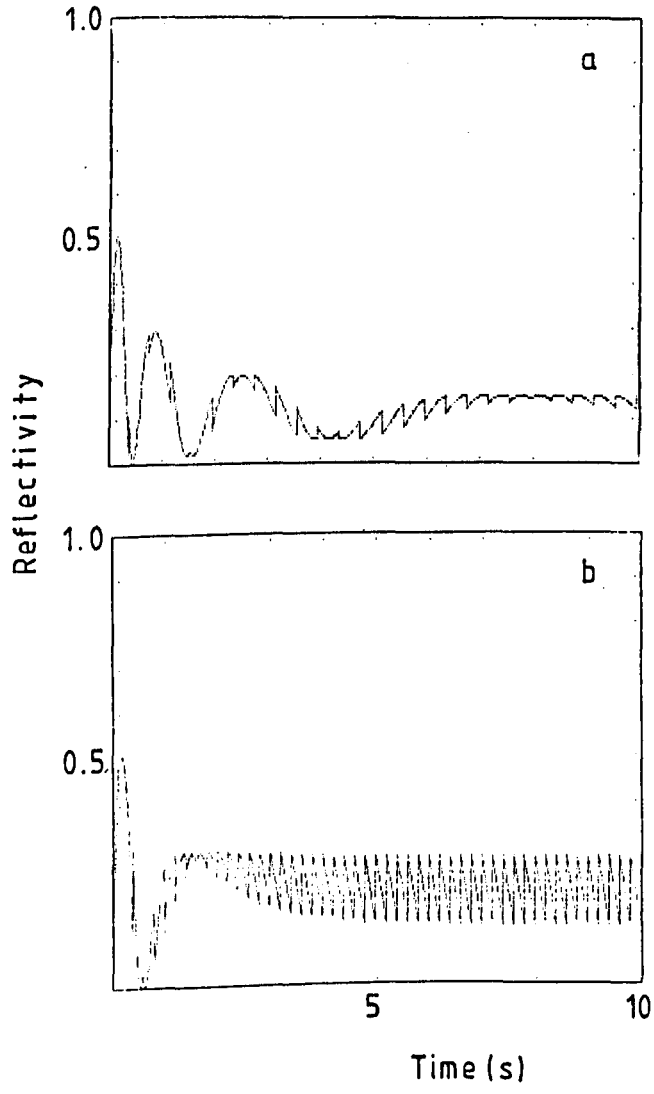

REFLECTIVITY: COPPER ABLATION IN CHLORINE

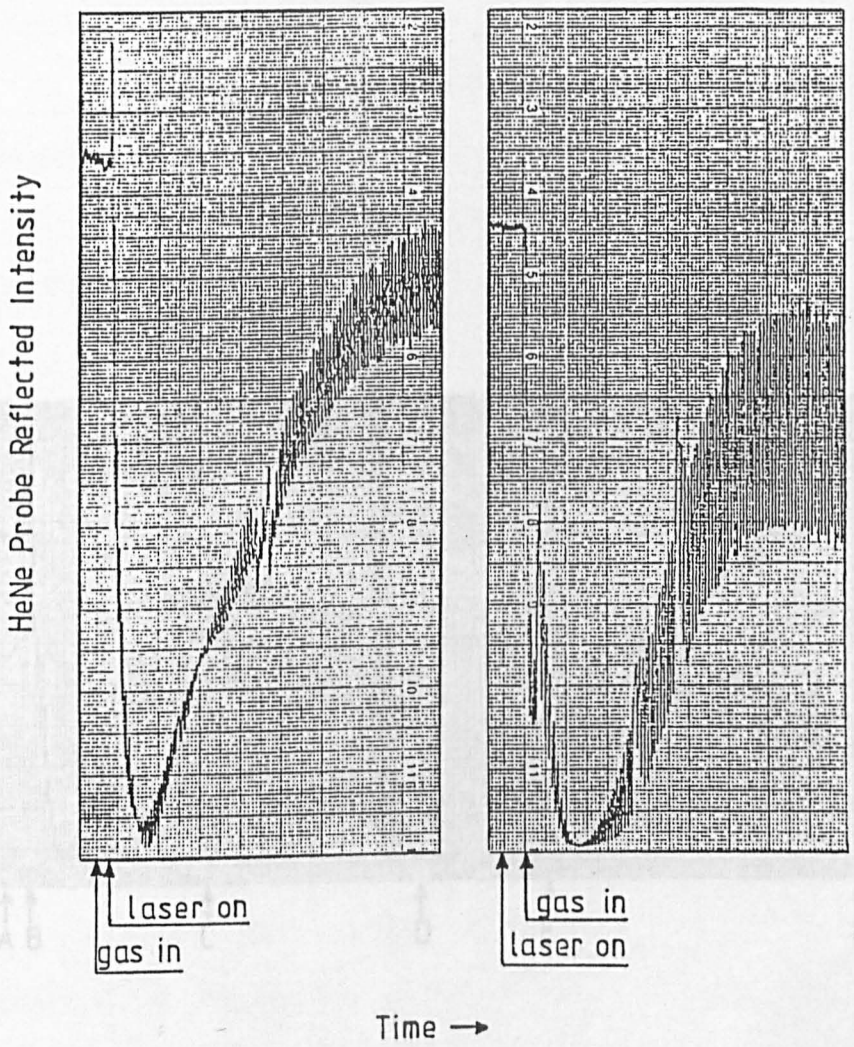

Fig.4.6.8.

REFLECTIVITY: COPPER ABLATION IN CHLORINE

A: Chlorine in cell.

B: UV-laser on, oxide removed.

C: Growth-etch cycle proceeding.

D: UV-laser off, growth continues.

E: UV-laser on, steady-state re-established.

F: Chlorine removed from cell.

G: All chloride removed, bare copper.

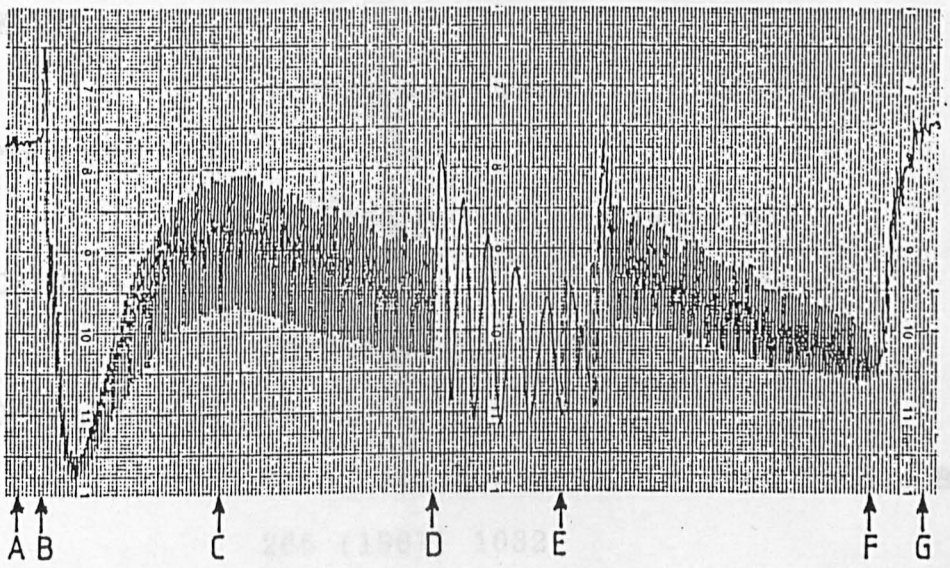

4.7

REFERENCES

[1] Milek,J.T. & Neuberger,M.
'Linear Electrooptic Materials'
Handbook of Electronic materials Vol 8
IFI / Plenum, New York, 1972

[2] Alonas,P. et al.
Applied Optics, 8 (1969) 2557.

[3] Chemla,D. et al.
IEEE J.Quantum Electron. QE7 (1971) 126.

[4] Feldman,A & Horowitz,D
J.Opt.Soc.Am. 59 (1969) 1406.

[5] Kaifu,Y. et al.
J.Phys.Soc.Japan. 22 (1967) 517.

[6] Kaifu,Y. et al.
J.Phys.Soc.Japan. 25 (1968) 644.

[7] McCarthy,D.E.
Applied Optics, 4 (1965) 317.

[8] Cardona,M.
Phys.Rev. 129 (1963) 69.

[9] Jerphagnon,J. et al.
Acad. des Sciences, Comptes Rendus B
265 (1967) 1032.

[10] Koren,G. & Oppenheim,U.P.
Appl. Phys. B 42, (1987), 41.

[11] Zaidel,A.N. et al.
'Tables of Spectral Lines'
Pergamon, Berlin, 1961

[12] Rosen,B. et al.

'Constantes Selectionees -
Donnees Spectroscopiques concernment
les Molecules Diatomiques'
Hermann & Cie. Paris, 1951

[13] Pearse,R.W.B & Gaydon,A.G.

'The Identification of
Molecular Spectra'
Chapman & Hall, London, 1963

[14] Rothenberg,J.E.,Koren,G & Ritsko,J.J.

J. Appl. Phys. 57 (1985) 5072.

[15] Key,P.H.

"The Interaction of Excimer Laser
Radiation with Metal Surfaces"
M.Sc.Thesis, University of Hull,1985.

[16] Kubeschewski,O.,Evans,E.LL. & Alcock,C.B.

'Metallurgical Thermochemistry'
Pergamon, Oxford, (1967).

[17] Winters,H.F.

J. Vac. Sci. Technol. A 3, (1985), 786.

[18] Shelton,R.A.J.

Trans. Faraday Soc. 57, (1961), 2113.

CHAPTER FIVE

EXCIMER LASER ETCHING OF ALLOYS & CERAMICS

5.0

INTRODUCTION

The etching of thermally-thick (≥ 3 μm) polycrystalline copper samples with multiple pulses of low fluence (≤ 1 J cm^{-2}) UV-excimer laser radiation was shown to occur only in ambient conditions which allow the copper surface to be converted to a lower removal threshold material. Chemical assisted laser ablation schemes have also been devised, using both liquid and gaseous environments, for a number of materials [1-5].

In this chapter some results of excimer laser etching of a variety of materials are presented. These studies are intended as an indication of the versatility of laser ablation and, as such, are rather more qualitative than those of the preceding chapter. A good deal of work has been done on the laser assisted processing of semi-conductor materials such as Si, Ge, InP and GaAs [6-9] and these are not covered here.

Spec-pure nickel foils and bulk samples of copper-nickel alloys were ablated in a chlorine environment and the results are presented in the next section. Here it will be seen that the variation of etch-rate, from low with pure nickel to high with pure copper, depends upon the copper concentration. The etch-rate is seen to be a non-linear function of composition.

Two materials of interest as microelectronic substrates; ceramic alumina (Al_2O_3), and polycrystalline strontium titanate ($SrTiO_3$) were ablated. For the former the results

of ablation in air using two UV wavelengths are compared. Strontium titanate samples were ablated using a single wavelength in vacuum and, in order to induce reduction of the oxide as one of the processing steps, in a hydrogen ambient.

A third class of materials represented by glass and fused quartz are shown to be capable of excimer laser machining and, again, the results obtained are found to be dependent upon the environmental conditions.

5.1.

NICKEL AND CUPRO-NICKEL ALLOYS

Whereas a clean copper surface was seen in chapter 3 to react immediately with a chlorine gas ambient to form substantial chloride layers which are readily ablated using a UV-excimer laser, this was not found to be the case for nickel. Often chosen as a plating material for use in corrosive environments, nickel was not readily observed to react with chlorine at room temperature. Extended exposure of a few hours does, however, result in a loss of lustre of a polished nickel surface but He-Ne laser probe beam reflectivity measurements were unable to yield any indication of the growth of a surface compound.

The formation of NiCl is an endothermic reaction ($-\Delta H \approx -14$ kJ mol^{-1}) and the close-packed structure of the thin layer (≤ 1 nm) of chloride formed prevents diffusion of the metallic cation through the layer. Hence the thickness of the 'passivation' layer represents the maximum thickness of chloride availiable for laser ablation.

A constant etch-rate of 1.0±0.25 nm per pulse was found at fluences of 0.5, 1.0 and 2.0 J cm^{-2} using the XeCl laser. No change in etch-rate was observed with changing chlorine pressure or when the prf was increased from 1 to 5 Hz.

Copper and nickel atoms have common valence (Cu:1,2. Ni:0,1,2,3), similar electronegativity (Cu:1.9, Ni:1.8), are similar in atomic diameter (Cu:128 pm, Ni:124 pm) and form the same crystal structure (fcc). These criteria (Hume-Rothery rules) being satisfied allows substitutional

solid solubility in all proportions of both components. Thus, under equilibrium cooling conditions from the melt, Cu-Ni alloys form a single homogeneous phase. Since the slow cooling rates required to produce the necessary equilibrium conditions are seldom achieved in practice it is usually necessary to anneal the alloy and rely on diffusion to obtain the desired homogeneity.

This is particularly important for the 50%-50% alloy, 'Constantan', used in strain gauges since the electrical properties such as the extremely low temperature coefficient of resistance must be accurately controlled. Constantan foil for strain gauges is usually rolled to thicknesses of a few microns after heat treatment and the resultant polycrystalline, highly strained structure gives good elastic properties.

As previously stated in chapter 1, such foils of 5 μm thickness and backed with a 100 μm polyimide support were found to be out of the thickness regime for the single UV-excimer laser pulse patterning technique. These foils together with spec-pure nickel foils and bulk samples of 30%Cu-70%Ni and 60%Cu-40%ni alloys were ablated in a chlorine environment using a UV-excimer laser in order to assess the effect of copper concentration on the etch-rate. The etch-rates of these metals in 2.5 torr chlorine with 1 J cm^{-2}, XeCl laser pulses at 1 Hz are shown in Fig.5.1.1. Here it can be seen that the etch-rate increases with copper concentration but the increase is not a linear function of the proportion of copper. The same data are plotted for ln(etch-rate) as a function of copper concentration in

Fig.5.1.2 and the data are a good fit to a straight line described by:

$$\text{etch-rate} = 0.645 \exp(0.042x\langle Cu\rangle)$$

where <Cu> is the atomic percentage of copper in the alloy. An increase in etch-rate with increasing iron concentration found in Fe-Ni alloys in chlorine gas using a N_2 laser (337 nm) has been reported in the literature [10]. Here too, the etch-rate was found to vary non-linearly with Fe concentration. The reasons for this behaviour are not, however, understood.

Finally, it was shown in section 2.3 that high fluence ($\approx$5 J cm^{-2}) irradiation of bulk constantan samples in air resulted in the formation of a thick layer, thought to be either an oxide or nitride, as a result of the transient heating of the surface. In these thinner foils it was found that ablation in air was possible at $\approx$2.0 J cm^{-2} but that this produced rather poor quality patterns. This may be due to the slow diffusion of heat away from the irradiation site resulting in extended oxide formation at different rates on different crystallite sites.

The etch rate in this case was $\approx$1.0 nm per pulse using the KrF laser at 5 Hz and an example of the etched foil is shown in Fig.5.1.3 which may be compared with the results of etching in 2.5 torr chlorine using 1 J cm^{-2}, 5 Hz XeCl laser pulses shown in Fig.5.1.4.

Fig.5.1.1.

EXCIMER LASER ETCHING OF Cu-Ni ALLOYS IN Cl

Etch-rate as a function of composition of Cu, Ni and Cu-Ni alloys.
1 J cm ^{2} XeCl laser at 1 Hz in 2.5 torr Cl

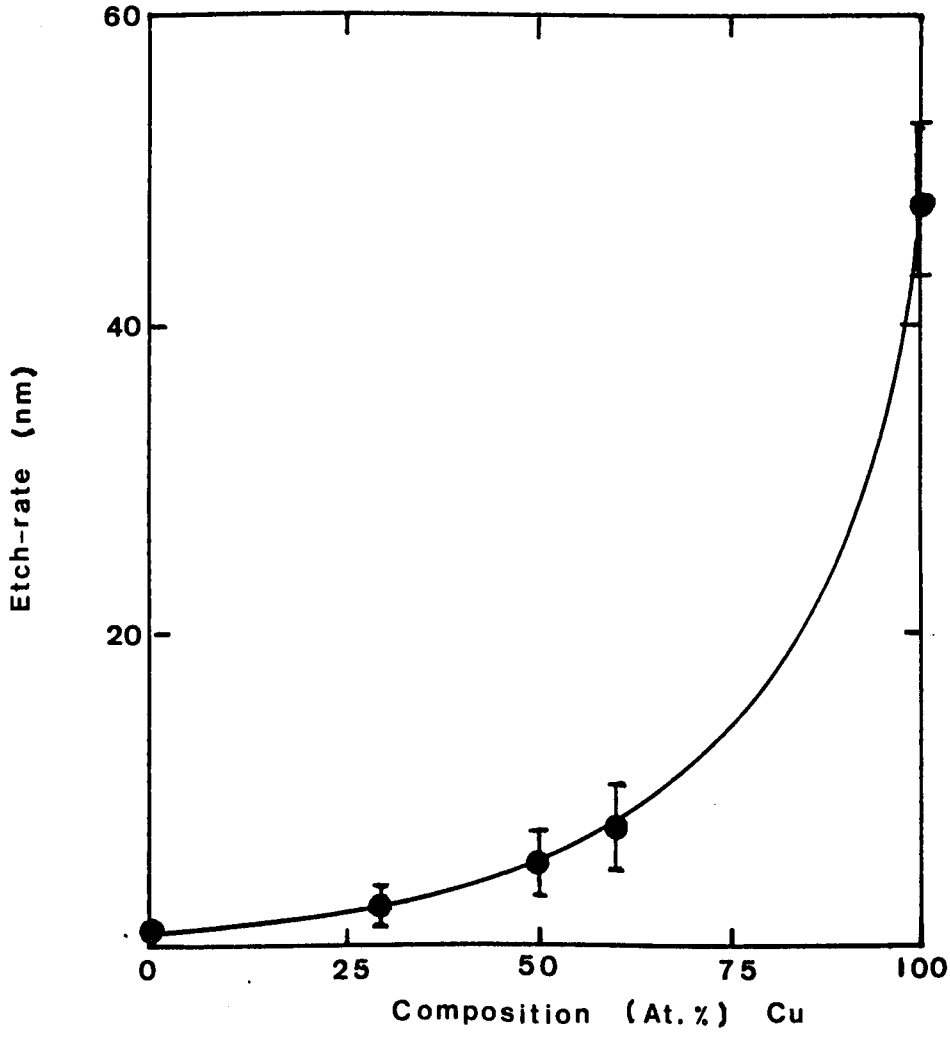

Fig.5.1.2.

EXCIMER LASER ETCHING OF Cu-Ni ALLOYS IN Cl

ln(Etch-rate) as a function of composition of Cu, Ni and Cu-Ni alloys.
1 J cm $^{-2}$ XeCl laser at 1 Hz in 2.5 torr Cl

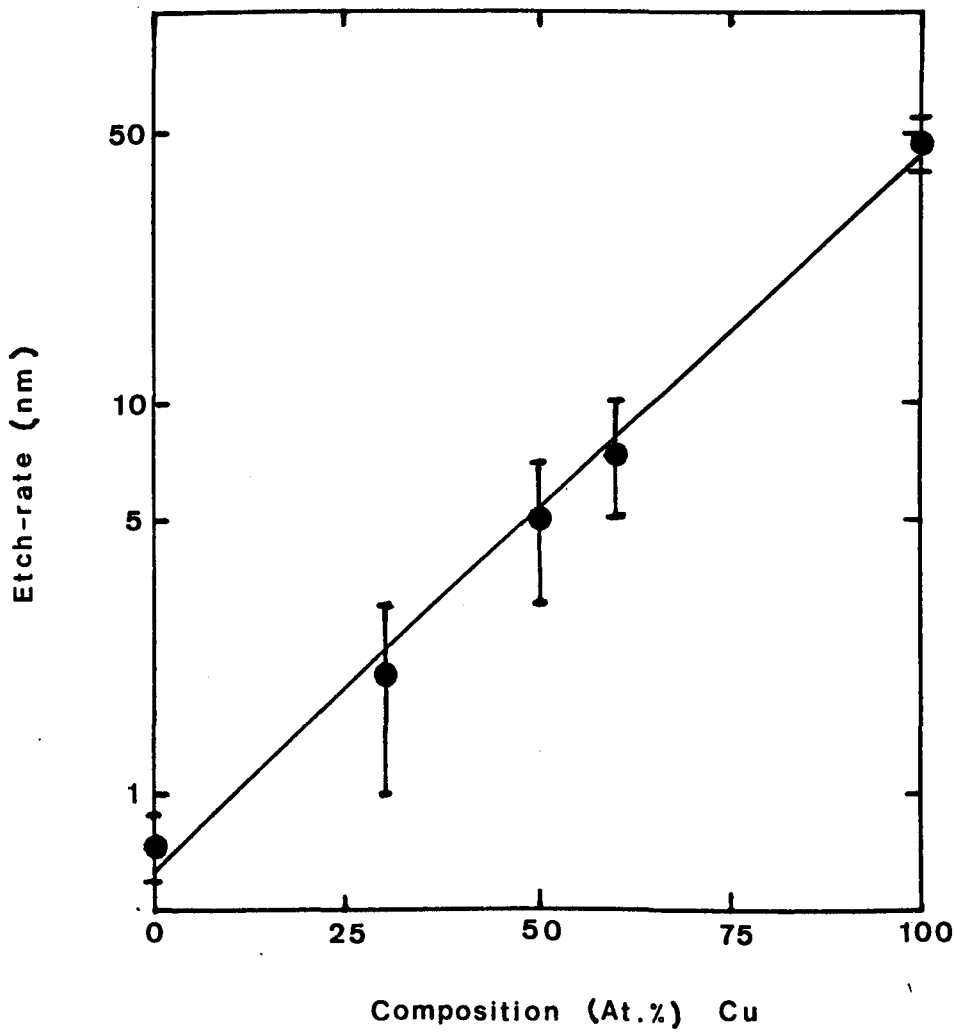

Fig.5.1.3.

UV-EXCIMER LASER ETCHED CONSTANTAN

50%Ni-50%Cu alloy etched in air.

KrF laser, 2 J cm $^{-2}$. 5 Hz.

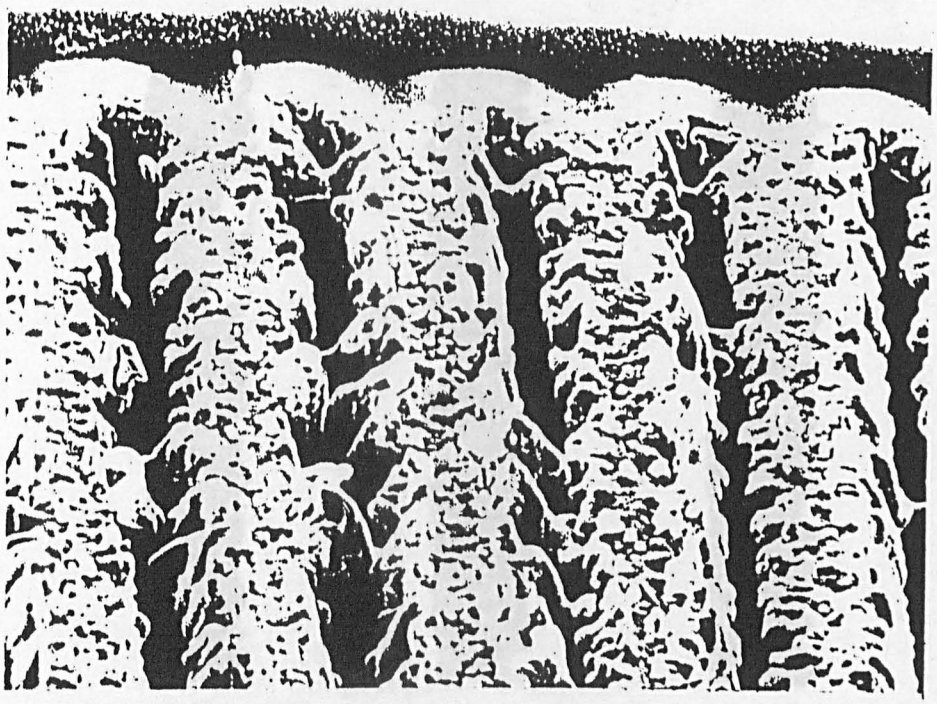

20 μm

Fig.5.1.4.

UV-EXCIMER LASER ETCHED CONSTANTAN

50%Ni-50%Cu alloy etched in chlorine.

XeCl laser, 1 J cm ^{2}. 5 Hz.

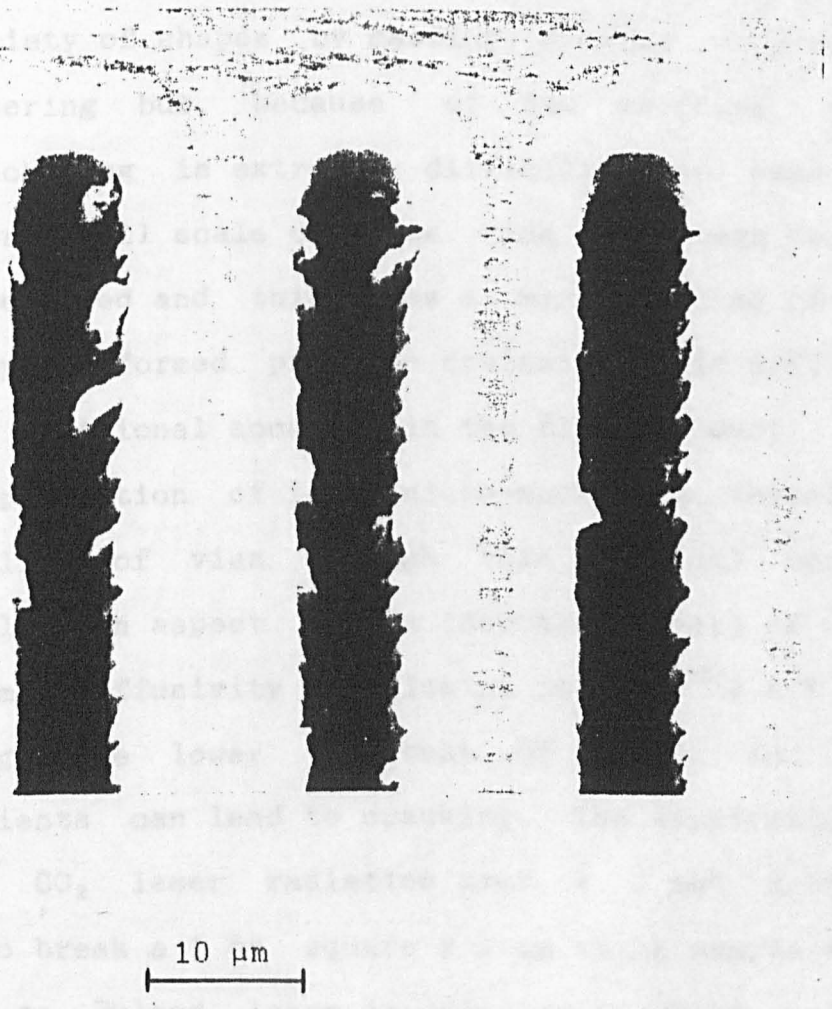

5.2.

CERAMIC ALUMINA

Ceramic Alumina (Al_2O_3) is a sintered material having low chemical reactivity, good thermal stability and a high melting temperature (2300 K). It is a hard, strong material and an excellent electrical insulator and is, therefore, finding increasing application, along with Zirconia and Boron nitride which have similar properties, as a substrate material for hybrid circuits in harsh environments.

Like any other ceramic material, alumina may be formed into a large variety of shapes by casting, drawing or pressing before sintering but, because of its hardness, post-sintering machining is extremely difficult. When used as a substrate for small scale circuits, vias (through holes) are often required and this poses a manufacturing problem since if they are formed prior to sintering it is difficult to guarantee positional accuracy in the final product.

A possible application of laser micro-machining, therefore, is the drilling of vias through thin (≈0.5 mm) ceramic sheets usually with aspect ratios (depth/diameter) of up to 10. The thermal diffusivity of alumina is ≈1 10^{-5} W m^{-2} , an order of magnitude lower than that of metals, and high thermal gradients can lead to cracking. The application of 25 W of CW CO_2 laser radiation over a 1 mm^2 spot is sufficient to break a 1 cm square x 1 mm thick sample after a minute or so. Pulsed laser irradiation in which most of the absorbed energy is removed with the ablated material, may provide a technique of deep hole drilling without risk

of destroying the work piece.

The laser sputtering of single crystal Al_2O_3 (sapphire) has been studied by Kelly and co-workers [11,12] at a variety of wavelengths. These studies, using 523 nm and 266 nm Nd:YAG and 248 nm and 193 nm UV-excimer lasers at $\leq$ 10 Hz, were based on laser induced fluorescence, SEM examination of the irradiated surfaces and electron density measurements in the ablation plume with a Michelson interferometer. At the longer wavelengths exfoliation resulting from thermal stress induced microfractures was deduced to be the primary removal mechanism. At shorter wavelengths F and F^+ centres were observed but a defect enhanced removal mechanism was not thought to apply. Rather, the ablation was suggested to be due to electronic mechanisms such as the 'cold plasma' described by Itoh and co-workers [13,14].

One of the problems faced in laser ablation of ceramic materials is the inhomogeneity of structure encountered by the incident radiation. There is not a continuum of solid surface but rather a collection of small particles with voids the size of which are a function of the particle size and degree of sintering. Where particle sizes are of the same order of magnitude as the laser wavelength, large angle scattering of the incident radiation can occur and hence distribute the beam energy over a larger area than the original spot size. Once a crater is formed the scattered reflections from the side walls can lead to expansion of the ablated hole, deflection from the required direction of etching or cessation of etching due to a reduction of effective fluence.

Ceramic alumina samples 0.5 mm and 1 mm thick were ablated in air using the XeCl (308 nm) and ArF (193 nm) lasers. Irradiation with the 308 nm laser at ≤ 2 J cm^{-2} did not yield any evidence of ablation at ≤ 10 Hz but at 200 Hz a measurable etch-rate was obtained and this is shown in Fig.5.2.1. Here the large error bars indicate the variations found in etch-rates between different samples and at different points on the same sample, illustrating the degree of inhomogeneity found with this material. The data can be fitted to both a linear dependence of etch-rate on fluence and on ln(fluence) to approximately the same correlation coefficient (0.98). Studies at higher fluences than available from the laser used would be needed to clarify the form of the dependency. The requirement for a high laser prf for ablation may indicate that either a thermal or defect induced mechanism is operative in this case.

At 193 nm a prf of 2 Hz was adequate to produce a similar etch-rate, Fig.5.2.2, and this may be due to the increased photon energy or to better optical coupling to the target together with a decrease in scattering angle because of the shorter wavelength. Single crystal alumina (sapphire) has high internal transmission down to ≤193 nm and it must be assumed, therefore, that surface effects such as defects are an important factor in UV-laser ablation of the polycrystalline material.

Using the ArF laser 50 μm diameter vias with good side-wall parallelism were made in 1 mm thick ceramic alumina sheets.

Fig.5.2.1.

EXCIMER LASER ETCHING OF CERAMIC ALUMINA

Etch-rate as a function of laser fluence.

XeCl laser at 200 Hz.

---- Etch-rate ≈ 13xF - 9.5 nm.

——— Etch-rate ≈ 15.4x ln(F/0.78) nm.

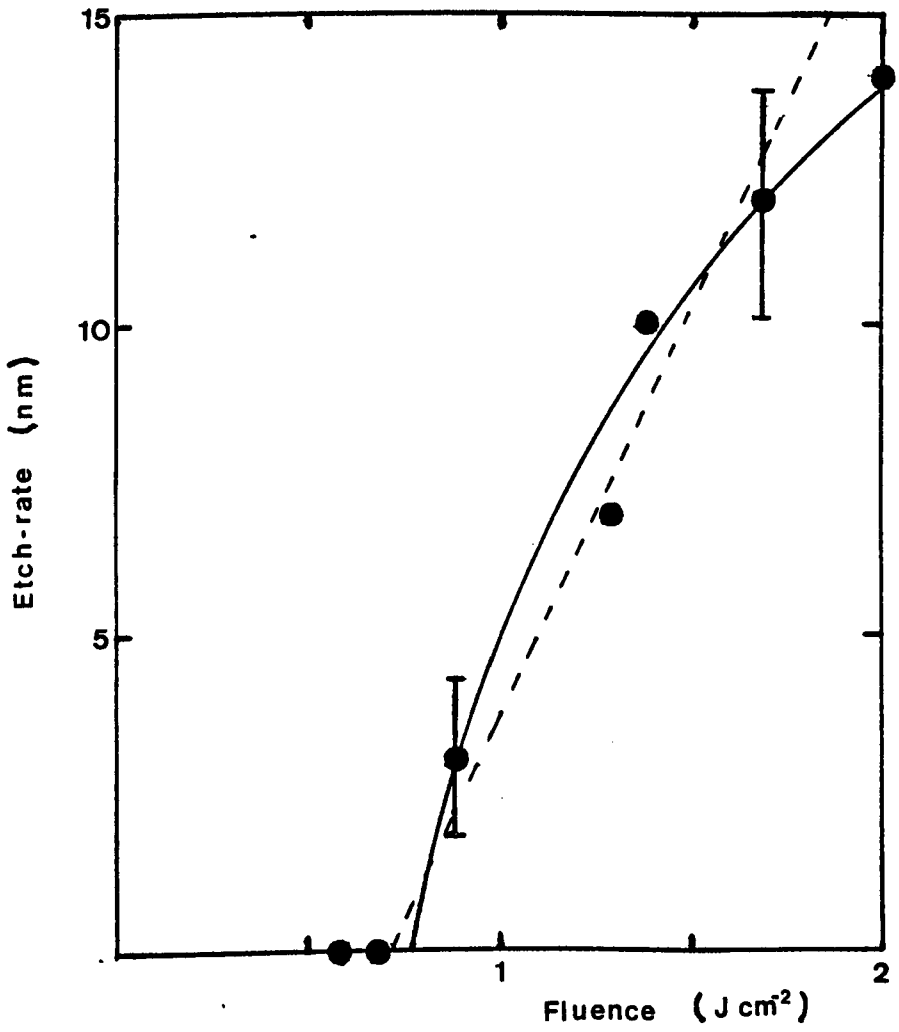

Fig.5.2.2.

EXCIMER LASER ETCHING OF CERAMIC ALUMINA

Etch-rate as a function of laser fluence.

ArF laser at 2 Hz.

---- Etch-rate ≈ 5.9xF - 2.7 nm.

——— Etch-rate ≈ 12.5x ln(F/0.75) nm.

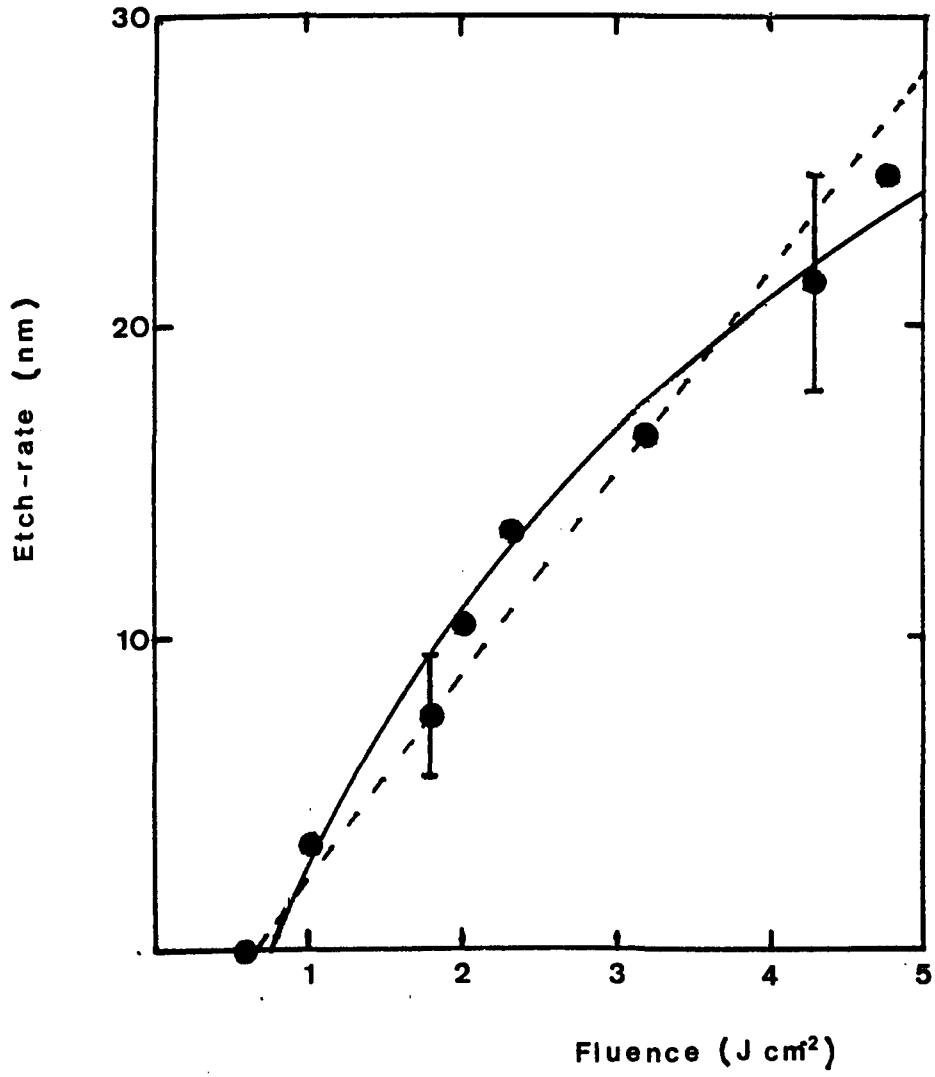

5.3.

STRONTIUM TITANATE

Like Al_2O_3, strontium titanate ($SrTiO_3$) exhibits good dielectric properties and whilst not having the intrinsic strength of ceramic alumina is a suitable material for microelectronic substrates. Strontium titanate is availiable as single crystals or in ceramic form, often with the addition of barium, and is used extensively as the dielectric medium in rapid discharge, high voltage capacitors.

Laser processing of single crystal $SrTiO_3$ and $BaTiO_3$ together with ceramic $PbTi_{1-x}Zr_xO_3$ (PZT) has been studied by Bauerle and co-workers [15,16] using CW laser irradiation from Ar^+ and Kr^+ lasers. Their results show that the production of oxygen vacancies by irradiation in a H_2 atmosphere results in the reduction of the oxide at the surface. This re-metallisation is characterised by an increase in electrical conductivity which is proportional to the logarithm of laser power density and a black coloration of the conducting track. Scanning speeds of $\approx$40 $\mu m\ s^{-1}$ with incident powers $0.9 \leq P \leq 1.3$ W over a $\approx$40 μm spot resulted in a decrease of linear suface resistance from 10^4 Ω/mm to 50 Ω/mm in PZT and from 12 kΩ/mm to 2 kΩ/mm in the single crystals. Increases in laser power lead to the etching of grooves up to 400 μm deep.

Ceramic strontium titanate was ablated in hydrogen (50 torr) and vacuum (10^{-4} torr) using KrF (248 nm) laser radiation at 5 Hz. The etch-rates for the two cases are shown in

Fig.5.3.1 from which it can be seen that the presence of hydrogen in the fluence range used has little effect on the etch-rate. This may, in part, be due to a flux limited removal regime as discussed earlier. Studies of etch-rate as a function of ambient hydrogen gas pressure would help to clarify this.

Scanning Electron Micrographs of the irradiated areas at high ($\approx$ 3 J cm^{-2}) and low ($\approx$ 0.5 J cm^{-2}) fluences are shown in Figs.5.3.2 & 3. There are only small differences in morphology between the results from the two sets of environmental conditions. The SEMs of the ablated zone in the hydrogen environment show a greater amount of re-deposited material as might be expected from collisions between the ablated material and the comparatively high pressure ambient gas. The granular appearance of the edges of the etched grooves may be due to preferential removal of one of the constituents.

Deep groove etching of the material in vacuum is shown in Fig.5.3.4. Here, reasonably parallel side walls and aspect ratios (depth/width) of up to 20 are seen to be readily achieved.

Fig.5.3.1.

EXCIMER LASER ETCHING OF STRONTIUM TITANATE

Etch-rate as a function of laser fluence.

KrF laser at 5 Hz.

□ Hydrogen.

● Vacuum.

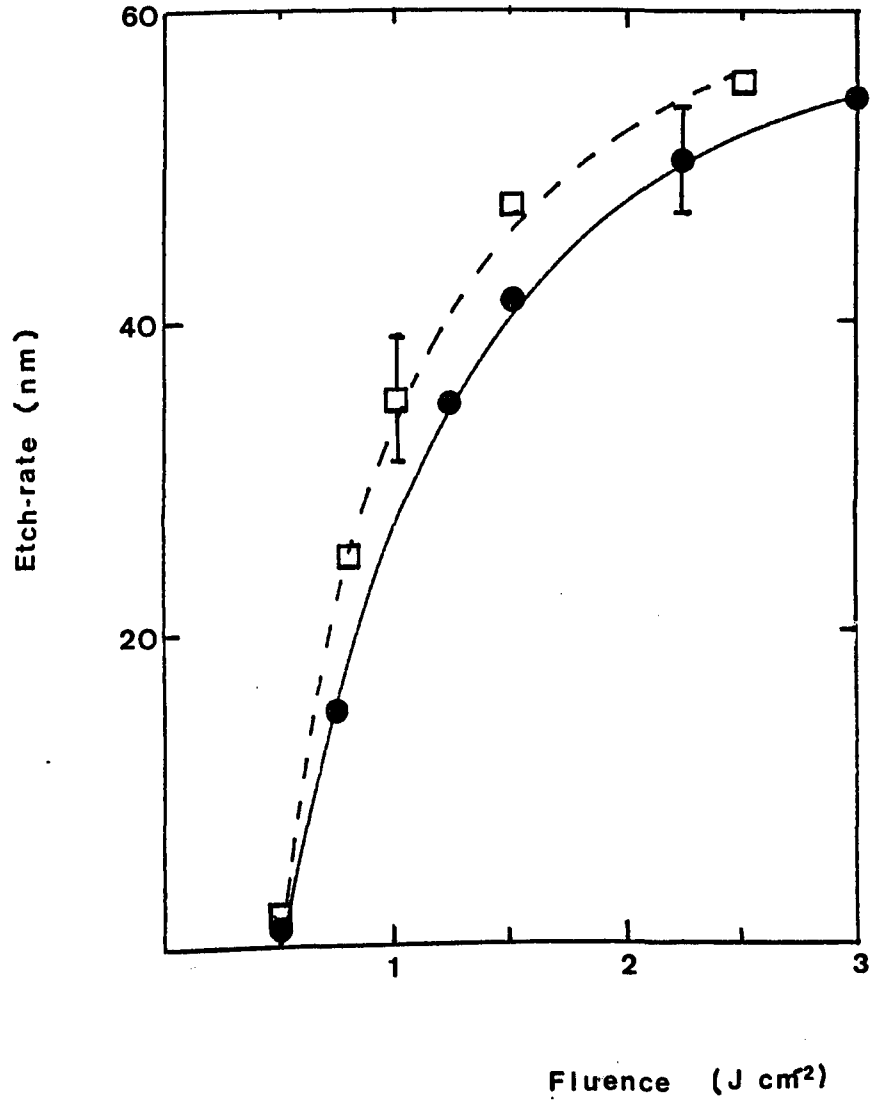

Fig.5.3.2.

EXCIMER LASER ETCHED STRONTIUM TITANATE

XeCl laser at 3 J cm $^{-2}$.

(a) Vacuum

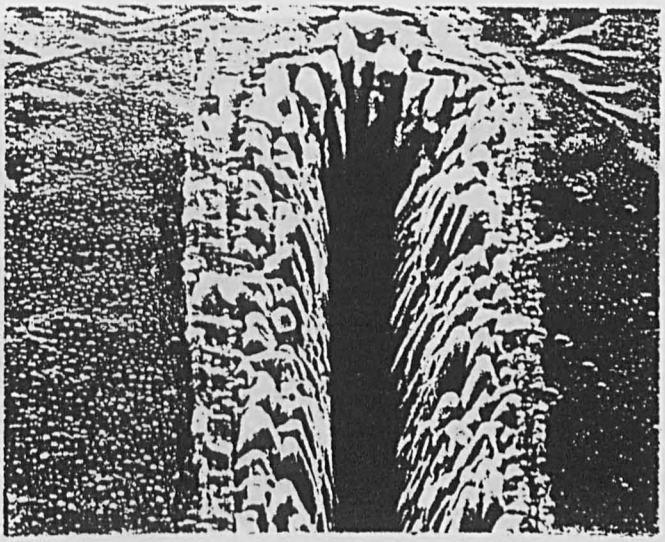

10 μm

(b) Hydrogen

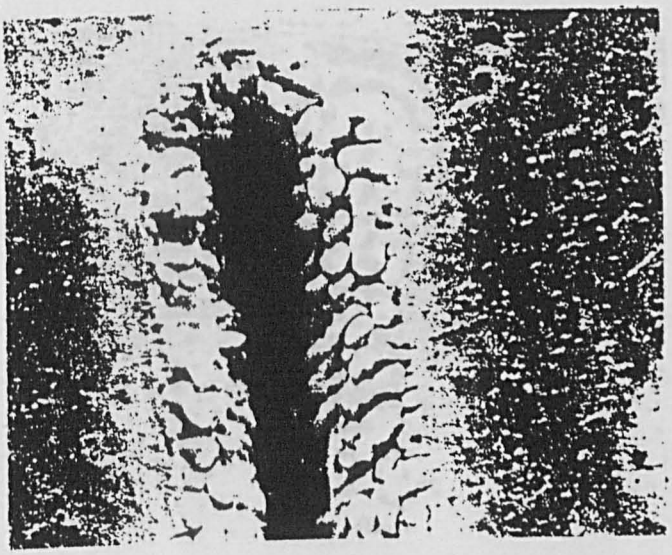

10 μm

Fig.5.3.3.

EXCIMER LASER ETCHED STRONTIUM TITANATE

XeCl laser at 0.5 J cm $^{-2}$.

(a) Vacuum

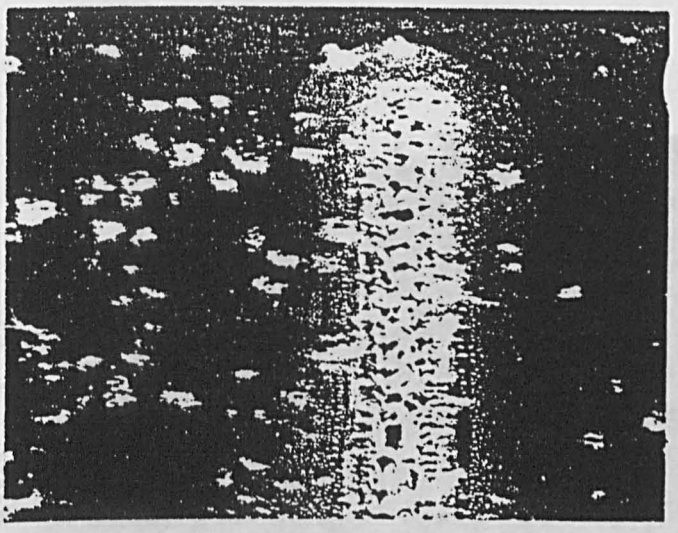

10 μm

(b) Hydrogen

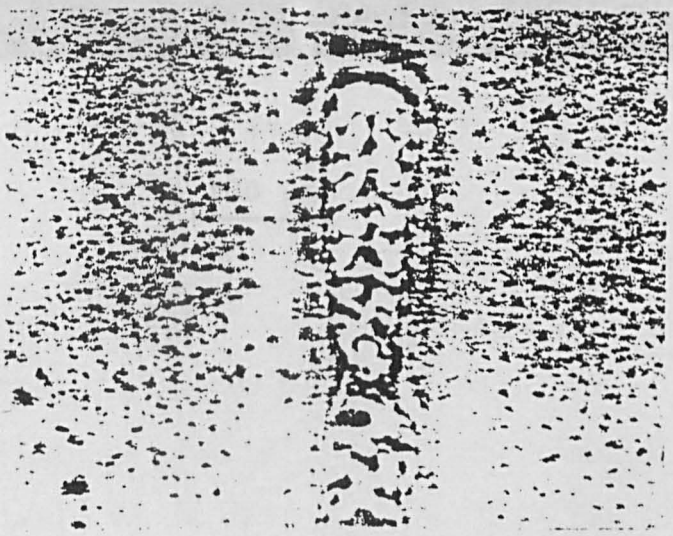

10 μm

Fig.5.3.4.

EXCIMER LASER ETCHED STRONTIUM TITANATE

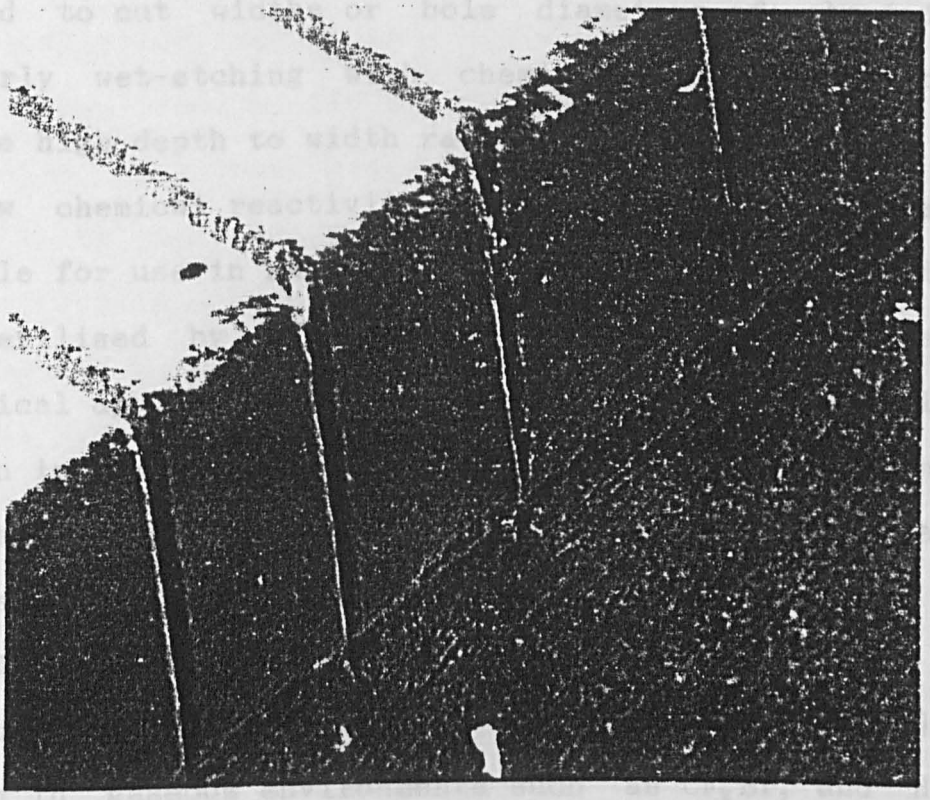

100 μm

5.4.

FUSED QUARTZ AND GLASS

Fused quartz and optical grade glasses are hard, brittle, materials and difficult to machine. Small holes may be made in the near-molten state using a fine wire but a lip around the hole usually results. Abrasive methods of machining are limited to cut widths or hole diameters of about 1 mm. Similarly wet-etching with chemicals such as HF cannot produce high depth to width ratios.

The low chemical reactivity of these materials makes them suitable for use in harsh environments and their ability to be sterilised by autoclave allows them to be used in biological applications such as re-usable filters. SiO_2 is also an important microelectronics material since it may be used as dielectric layers in Si based semiconductor devices and its patterning is therefore a desirable goal.

Optical glass has been sucessfully etched in HF using a CO_2 laser at rates higher than with the chemical alone [17]. Dry etching in gaseous environments such as CF_2Br_2 and H_2 has also been achieved using UV-excimer lasers [18,19].

IR and visible lasers have been used to etch SiO_2 in environments of CF_3Br and Cl_2 and in H_2SO_4 solutions [20-22]. UV-excimer laser induced etching of SiO_2 has been carried out in CF_2Cl_2, NF_3 and H_2 [23,9,19].

The absorption in fused quartz is very low down to ≈180 nm and it is thus used as an optical material for UV-excimer lasers. The absorption in Pyrex glass is considerably higher and although thin samples will transmit at 308 nm

relatively high fluences are required to damage and remove the surface. ArF laser radiation is not transmitted at all by Pyrex and although the internal transmittance of UV-grade fused quartz is high surface effects may result in significant absorption. The optical properties of glasses and fused quartz, and especially the absorption index which is strongly influenced by impurities, vary both with grade and from batch to batch.

UV optical grade fused quartz and glass samples were ablated in air and vacuum (10^{-2} torr) using ArF laser pulses. Etch-rates were only measured for glass, in the form of 150 μm thick microscope slide cover slips, in ambient air and the results are shown in Fig.5.4.1. It can be seen that the theshold is approximately 1 J cm^{-2} and that significant material removal occurs (250 nm / pulse) at 6 J cm^{-2}. In Fig.5.4.2 the data are plotted as a function of ln(fluence) and it can be seen that a good straight line fit is obtained.

Examples of patterns in glass etched in air using the ArF laser are shown in Figs.5.4.3. The results obtained in vacuum, examples of which are shown in Fig.5.4.4, show much cleaner surfaces than the samples etched in air. Whilst redeposition of ablated material is a contributing factor to the poor quality in an air ambient, surface chemical reactions during the irradiation may also be involved.

Fig.5.4.1.

EXCIMER LASER ETCHING OF GLASS IN AIR

Etch-rate as a function of laser fluence.

ArF laser at 10 Hz.

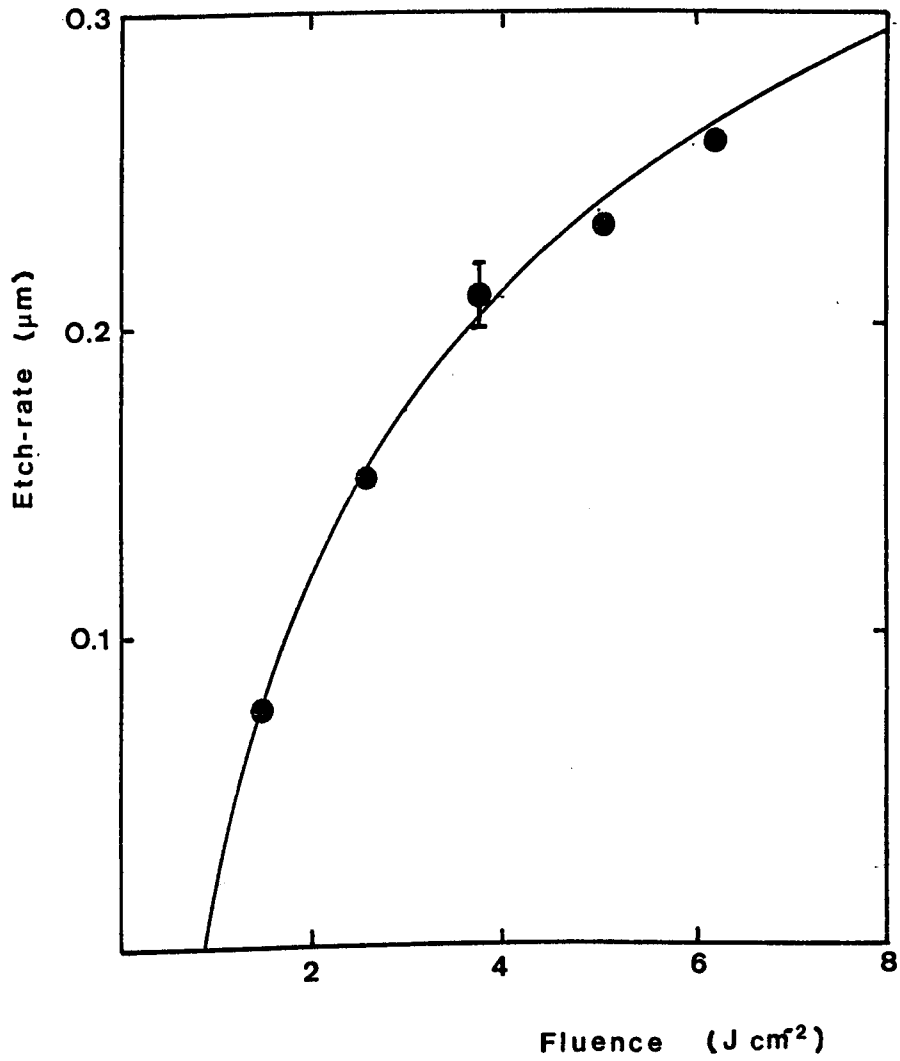

Fig.5.4.2.

EXCIMER LASER ETCHING OF GLASS IN AIR

Etch-rate as a function of ln(fluence).

ArF laser at 10 Hz.

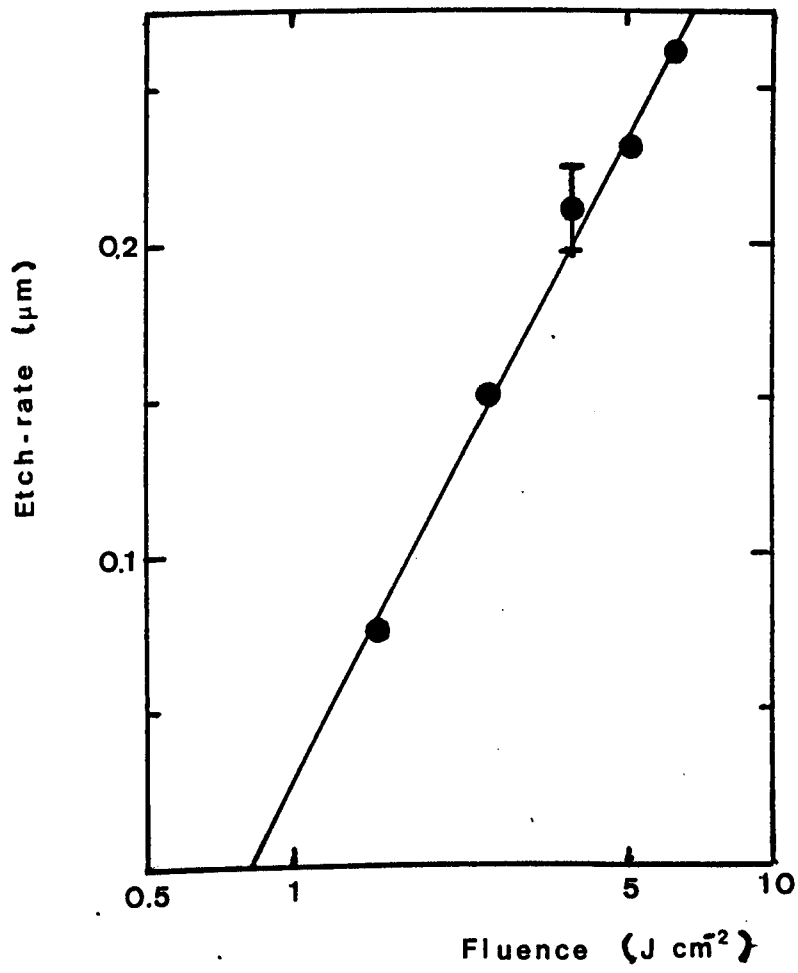

Fig.5.4.3.

UV-EXCIMER LASER ETCHED GLASS

ArF laser etched in air.

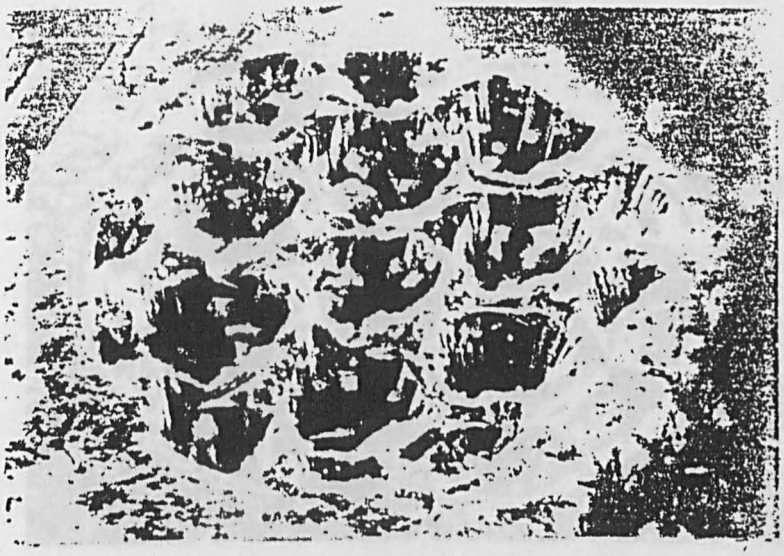

40 µm

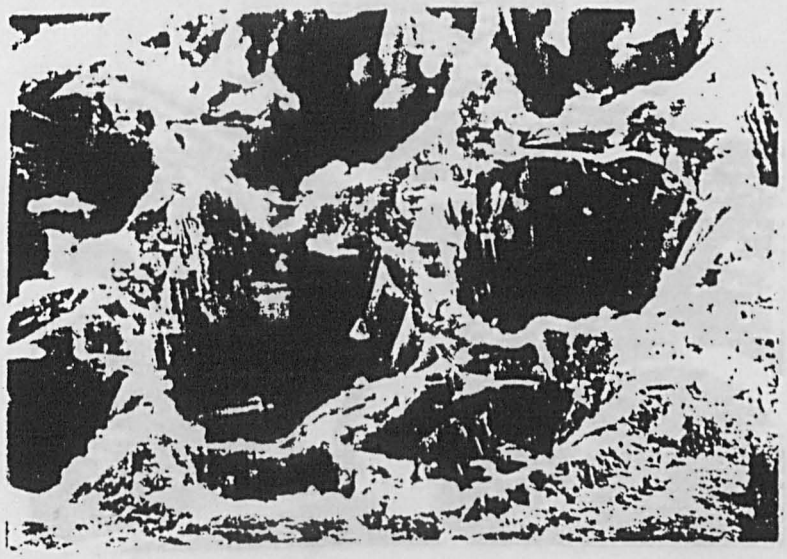

20 µm

Fig.5.4.4.

UV-EXCIMER LASER ETCHED GLASS

ArF laser etched in vacuum.

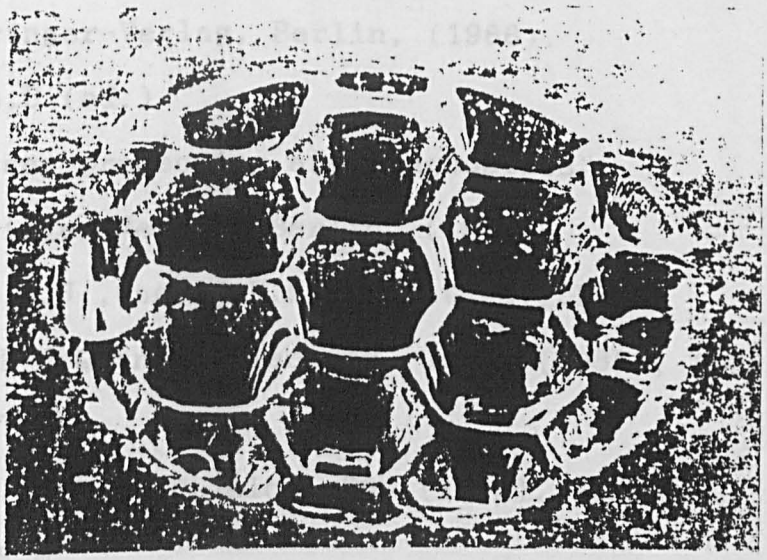

40 μm

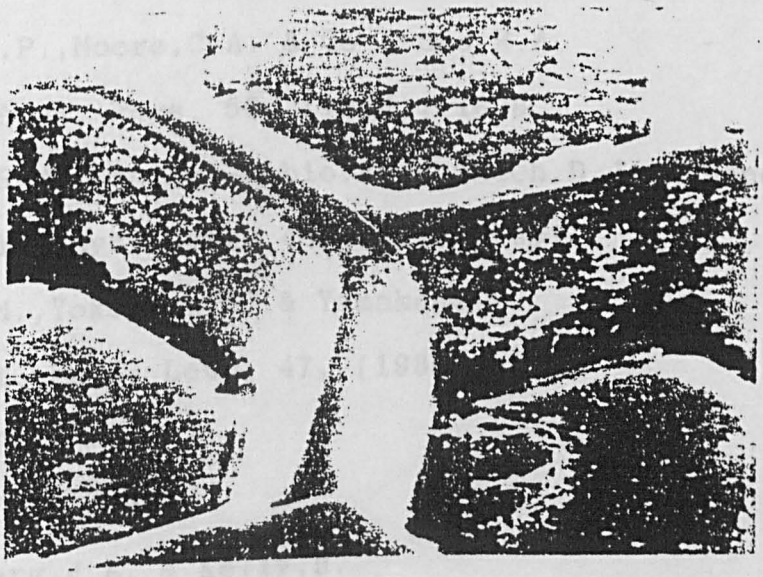

10 μm

5.5

REFERENCES

[1] Bäuerle,D.

'Chemical Processing with Lasers'

Springer-Verlag, Berlin, (1986).

[2] Bäuerle,D (ed.)

'Laser processing and Diagnostics"

Springer-Verlag, Berlin, (1984).

[3] Ehrlich,D.J.,Osgood,R.M. & Deutsch,T.F.

IEEE J.Quantum Electron. QE16, (1980), 1233.

[4] Chuang,T.J.

IBM J. Res. Develop. 26, (1982), 145

[5] Osgood,R.M.

J. de Physique. Coll. C5, 44, (1983), 133.

[6] Okano,H.,Horiike,Y. & Sekine,M.

Jap. J. Appl. Phys. 24, (1985), 68.

[7] Davis,G.P.,Moore,C.A. & Gottscho,R.A.

J. Appl. Phys. 56, (1984), 1808.

[8] Osgood,R.M.,Sanchez-Rubio,A.,Ehrlich,D.J. & Daneu,V.

Appl. Phys. Lett. 40, (1983), 391.

[9] Hirose,M.,Yokoyama,S. & Yamakage,Y.

Appl. Phys. Lett. 47, (1985), 389.

[10] Chuang.T.J.

in [2]. p.309.

[11] Rothenberg,J.E. & Kelly,R.

Nucl. Instr. & Meth.B., 1, (1984),291.

[12] Dreyfus,R.W.,Walkup,R.E. & Kelly,R.
'Radiation Effects in Insulators -3' Proc.
University of Surrey, Guilford, (1985), 683.

[13] Itoh,N. & Nakayama,T.
Phys. Lett. 92A, (1982), 471.

[14] Nakayama,T.,Okigawa,M. & Itoh,N.
Nucl. Instr. & Meth.B., 1, (1984), 301.

[15] Otto,J.,Stumpe,R. & Bäuerle,D.
in [2], p.320.

[16] Kapenieks,A.,Eyett,M. & Bäuerle,D.
Appl. Phys. A., 41, (1986), 331.

[17] Daree,K. & Kaiser,W.
Glass Technol. 18, (1977), 19.

[18] Brannon,J.H.
in 'Laser Chemical Processing of Semiconductor
Devices', eds Houle,F.A.,Deutsch,T.F.& Osgood,R.M.
Mat. Res. Soc. Symp., Boston, (1984), 112.

[19] Ehrlich,D.J.,Tsao,J.Y. & Bozler,C.O.
J. Vac. Sci. Technol. B3, (1985), 1.

[20] Steinfeld,J.I. et al.
J. Electrochem. Soc. 127, (1980), 515.

[21] Ehrlich,D.J.,Osgood,R.M. & Deutsch,T.F.
Appl. Phys. Lett. 38, (1981), 1018.

[22] Donohue,T.
in [2], p.332.

[23] Loper,G.L. & Tabat,M.D.
Appl. Phys. Lett. 46, (1985), 654.

CHAPTER SIX

PATTERN GENERATION AND RESOLUTION

6.0
INTRODUCTION

The ability to remove material from a surface by laser ablation, with or without the assistance of gas-surface interface chemistry, is of practical value in itself as a source of material for re-deposition on a substrate or for fundamental studies of ablation processes.

Where large surface areas can be etched in a controlled manner the process may find use for morphological modification such as planarisation. However, the selective laser ablation to form patterns is of particular interest. The creation of conductor networks in metals is an obvious application as is the patterning of semi-conductors for electronic device microfabrication. In the case of insulators the ability to form vias in substrate materials or the formation of 'islands' for detector arrays are also possible applications.

Patterns are, in general, generated in one of three ways;

(a) Contact or Proximity Printing in which the material is exposed to the radiation through a mask placed in contact with or in close proximity to the surface respectively.

(b) Direct Write techniques involving the relative movement of a small spot of laser radiation and the target.

(c) Projection Etching in which a remote mask containing the desired information is imaged onto the target surface.

These techniques are described, together with their relative merits, in the next section.

In projection etching the ultimate smallest feature size

is limited by the resolution of the optical system used to project the mask. In section 6.2 the contrast, ie. the energy distribution, of the image is discussed. Aberrations and diffraction effects are considered in determining the theoretical minimum feature size that can be reproduced together with the depth of focus which will determine the aspect ratio (etch depth to feature size) that can be achieved.

In section 6.3 the response of the target material to a finite fluence gradient at the edge of a feature (rather than a step fall-off) is considered. It is shown that with the non-linear etching response exhibited by some materials it is possible to achieve edge resolution and feature sizes that are better than expected on the basis of optical resolution alone. Examples of patterns produced by the projection etching technique are presented.

Concluding remarks are made in section 6.4.

6.1.
PATTERN GENERATION TECHNIQUES

Contact or Proximity Printing is a widely used technique in conventional lithographic processing of materials in which a photo-sensitive resist coating is exposed through a high quality mask, usually chromium on quartz, which carries the pattern information. Subsequent development of the resist material leaves a contacted 'mask' through the clear portions of which etching of the target suface by chemical action, ion or electron beams can occur. The initial exposure is often referred to as 'contact printing', however, atomic scale contact between mask and surface may not be achieved over large areas and in this case 'proximity' more correctly describes the arrangement.

Large area exposure can be achieved by this technique and, provided the illumination is uniform over the mask area, only positional accuracy of mask-substrate registration is needed. When mask and substrate are firmly held in the correct relative positions vibrational isolation with other parts of the illumination system are unnecessary.

Whilst these factors provide for an almost ideal technique for photo-resist exposure there are a number of disadvantages found in its application to direct laser ablative etching. Since material must be allowed to escape from the ablation zone the clear sections of the mask must be both optically transparent and kept physically clear in the face of material redeposition. Furthermore, since the mask is close to the target plane it is exposed to the

relatively high fluences necessary for material removal and may thus be itself subjected to etching. This places demands on the mask robustness not normally associated with lithographic techniques.

Direct write techniques require the relative motion of laser beam and target which may be achieved by beam deflection or by moving the workpiece. The availiability of computer controlled sub-micron positional accuracy X-Y translation stages makes the latter method the more attractive given the difficulties involved in achieving beam deflection with the same precision.

Patterns may be generated by raster scanning, in which the beam traces a series of parallel paths across the surface and is switched on and off as required, or by vector plot in which the pattern is defined by a point to point progression over the surface.

The major disadvantage with direct write for pattern etching is the low speed of processing since the area defined by the laser spot is small in comparison to the overall pattern field and must usually receive several laser pulses to achieve the required etch depth.

A laser spot moving relative to the target in the X direction in order to etch a continuous line must have dimensions greater than the step accuracy of the translation system. Thus a square spot of,say, 5 μm edge length used with a 1 μm resolution stepper system can describe a feature edge in either the X or Y direction to the limits of the optical resolution of the spot. For a diagonal line, however, the edge resolution will be equal to half the

diagonal of the X-Y step ie 0.707 μm. For sub-micron steppers, however, the optical resolution, which is of the same order as the wavelength of the laser, may be the limiting factor in edge resolution.

The minimum width of a line-pair, ie a line and space, etched in this way is the sum of the laser spot dimension, the stepper resolution and the optical resolution. Thus high processing rates and high densities of line pairs are incompatible.

For laser beams with circular symmetry, ie TEM_{oo} Gaussian beam, a circular laser spot is often most convenient. In this case the X or Y direction scan will produce a feature edge resolution that is inversely proportional to the spot diameter. A spot of diameter, 2r, moved in discrete steps by a distance, x, will result in a small area between overlapping circles and this projection from the line defining the edge of the spots may be considered as the edge resolution, a, which from the geometry is described by;

$$a = r - \sqrt{(r^2 - x^2/4)}$$

The edge resolution is a simple function of spot radius and stepper resolution. The ratio of edge resolution to step resolution, a/x, as a function of the ratio of spot radius to step resolution, r/x, is shown in Fig.6.1.1. Clearly a high resolution for feature edges is incompatible with small line-pair dimensions.

The projection etch technique, in which the image of a mask is projected onto the target, often employs de-magnification optics. In this case the limits to pattern density and edge

resolution are those imposed by the optical system. Significant de-magnification places much less of a demand on mask making, since errors in the mask are also demagnified, and hence can dramatically reduce mask costs over those of proximity printing.

For high feature density applications, in which high resolution of feature edges is implicit, an optical system with large Numerical Aperture (NA = Sin U, where U is the angle subtended at the target) is required which places practical limits on the field. For repetitive patterns over large fields the projection system may be combined with a stepper and a step-expose-repeat sequence adopted. For large non-repetitive fields, systems have been developed in which the mask and target are scanned through the optical axis. Both of these technologies are, however, more suited to resist development applications rather than direct etching.

In the present studies some projection etch patterning was used to assess the patterning capabilities of a simple optical system with excimer laser illumination bearing in mind the need to compromise between feature edge resolution, feature density, field size and depth of etching together with the constrains placed by the target materials.

Fig.6.1.1.

DIRECT WRITE: EDGE RESOLUTION

Edge resolution, a, as function of scan spot radius, r, normalised to scan step, x.

$$a = r - \sqrt{(r^2 - x^2/4)}$$

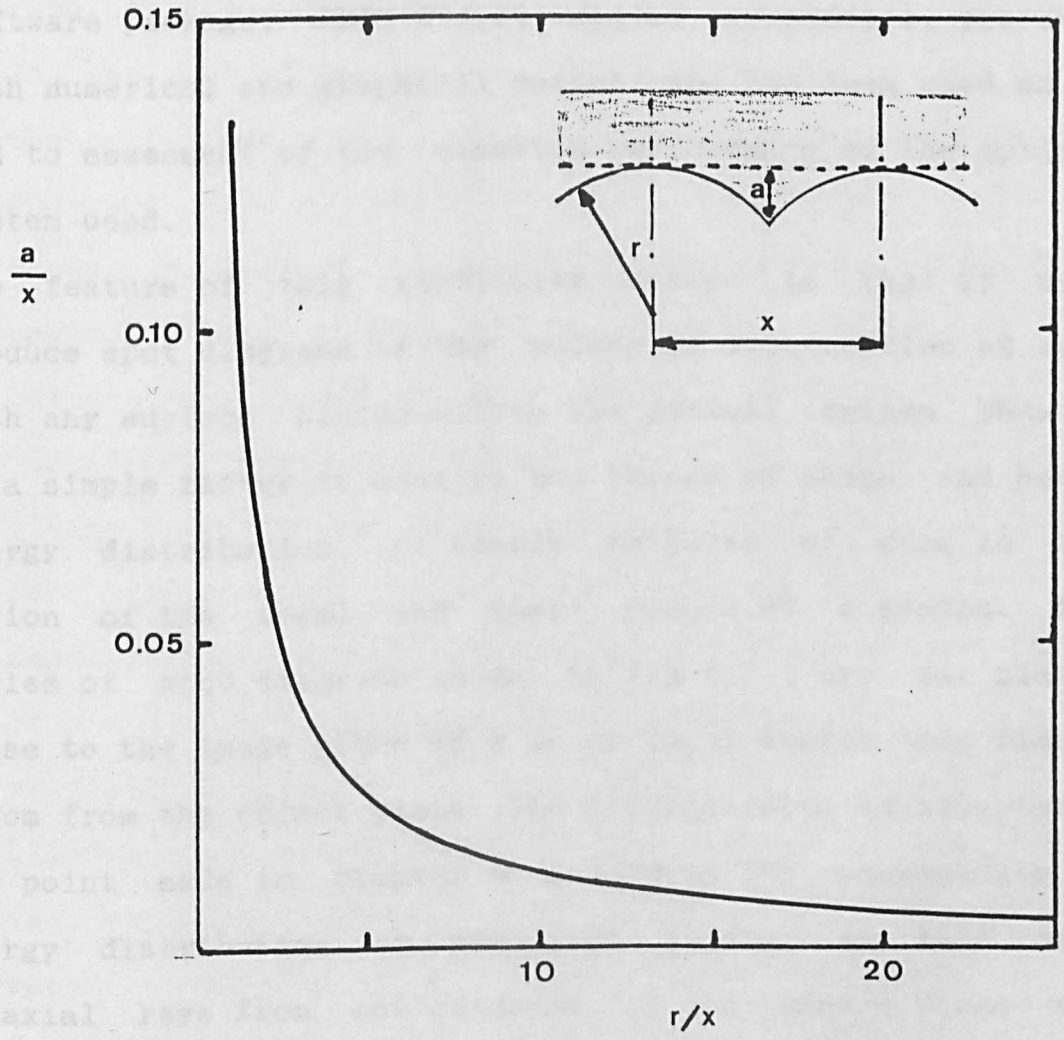

6.2.
OPTICAL CONSIDERATIONS

Optical system design is an iterative process in which the parameters of refractive index, surface curvature and element position are adjusted to minimise aberrations, given some goal with respect to resolution and field size. The calculations can become extremely time consuming and geometrical ray tracing may best be perfomed by computer. A number of software packages for optical design have been developed and are commercially available, the level of sophistication being reflected in the price. One such software package, "BEAM 2" [1], whilst inexpensive, provides both numerical and graphical output and has been used as an aid to assesment of the expected performance of the optical system used.

One feature of this particular package is that it will produce spot diagrams of the points of intersection of rays with any surface placed within the optical system. Thus it is a simple matter to observe the change of shape, and hence energy distribution, of simple patterns of rays in the region of the focal and image planes of a system. The series of spot diagrams shown in Fig.6.2.1 are for planes close to the image plane of a 10 cm focal length lens placed 60 cm from the object plane. The figures serve to illustrate the point made in chapter 4 regarding the uncertainty in energy distribution at non-image planes. In this case paraxial rays from one quadrant of the source plane are considered and their relative separation can be taken as a

measure of intensity distribution. It can be seen that only in the region of the image plane can the energy distribution be considered to be uniform within the limits of aberrations introduced by the optical system. Beyond the image plane the rays diverge and the fluence falls off rapidly.

Since it was not one of the objectives of this work to design an optimal projection etching optical system the remainder of this section is concerned with the description of design criteria for a simple single element lens system. Third order aberrations and the effects of diffraction are enumerated in order to assess the capability of the lens for etching patterns with aspect ratios (depth to feature edge resolution) greater than unity.

The optical system was, to a large extent, constrained by the availiable zone of uniform fluence produced by the laser and the fluence requirements at the target since these factors determined the magnification of the system and the maximum field dimensions at the image plane. The laser output was spatially filtered using a 10x5 mm^2 rectangular aperture to select a region of uniform fluence, giving 6 mJ transmitted energy and a fluence of 12 mJ cm^{-2}. For fluences at the target of 1 J cm^{-2} an areal magnification of 0.012, equivalent to a linear magnification of m = 0.11, was required. A linear magnification of m = 0.1 provided a maximum field of 1x0.5 mm at the target and allowed for energy losses at the lens and cell window.

The magnification of the system determines the conjugate ratio (object distance/image distance) and, for a given focal length, the overall system length. It was necessary to

choose a lens with a focal length to allow a lens-target working distance sufficiently large to allow space for diagnostics, ie. He-Ne laser probe beam and optical stereo-microscope, via the front window. If the focal length was too large, however, then the angle subtended by the lens at the target would be small and the fluence at the cell window could be high enough to cause damage. Using a ratio of fluence at the window to that at the target of about 0.1, in order to provide an adequate margin of safety, resulted in the choice of a 15 cm focal length lens since the target to window distance was approximately 5 cm.

The shape and orientation of lenses can conveniently be described by the Coddington shape factor, Q, defined as

$$Q = (r_2 + r_1) / (r_2 - r_1)$$

where r_1 & r_2 are the radii of curvature of the lens surfaces. Fig.6.2.2 shows the longitudinal and transverse spherical aberrations, obtained from ray-tracing, as a function of Q for a 10 cm focal length lens [2]. It can be seen that these aberrations are minimised for $Q \approx 0.75$, however, asymmetric lenses carry a significant cost penalty over plano-convex forms. Since the difference in aberrations between the Q = 0.75 and Q = 1.0 forms are small the latter, in UV transmitting fused quartz (Suprasil), was used in this work.

Manufacturers specify the focal lengths of lenses at a given wavelength and in this case the specification was 15 cm ±5% at 546.1 nm. The dependence of focal length on wavelenth for fused quartz in the 150 to 400 nm region is shown in

Fig.6.2.3 [3]. The resulting deviation from the design focal length has been calculated and is shown in Fig.6.2.4.

The Modulation Transfer Function (MTF) is used to describe the ability of an optical imaging system to reproduce the contrast present in the obect plane at the image plane [4]. The MTF may be found from measurements of the spatially varying image contrast ratio for an object with a sinusoidal transmission. The contrast or modulation, C, is given by the ratio of the difference and sum of intensity maxima and minima, ie;

$$C = (I_{max}-I_{min})/(I_{max}+I_{min})$$

and the MTF is the ratio of contrasts in the image and object planes;

$$MTF = C_{im}/C_{obj}$$

When the spatial frequency, v, of the object sinusoid is zero, ie. uniform field illumination, the MTF is equal to unity. As the spatial frequency is increased, the MTF is reduced until no modulation of contrast in the image plane is observed; this is the 'cut off' frequency, v_o. The physical measurement of MTF, necessarily, includes all abberations and is thus a useful figure of merit for comparing the performance of optical systems.

Analytic expressions for the MTF which include all possible abberations are difficult to derive, but expressions for the MTF of simple abberation free systems are useful for describing 'perfect' systems with which to compare practical arrangements. Analytic curves of MTF are usually expressed in terms of the relative spatial frequency, v/v_o. Where aberrations are of similar magnitude to diffraction

effects at the system aperture, the interaction between these becomes very complicated. In an aberration free system the MTF is related to the size of the diffraction pattern and is a function of the N.A. and wavelength, viz [4]:

$$MTF(v/v_o) = 2/\pi\ (\phi - Cos\phi Sin\phi)(Cos\theta)^j$$

where $\phi = Cos^{-1}(\lambda vf/d)$, θ is the half field angle and $j = 1$ for radial lines and 3 for tangential lines. The MTF curve shown in Fig.6.2.5. represents the performance of a circularly symmetric single lens which cannot be exceeded. The physical significance of these curves is simply that the image becomes more difficult to resolve as the spatial frequency of features is increased.

Since a step fall-off in illumination at the sharp edge of a real object can be represented by a sum of sinusoids with appropriate choice of frequency, amplitude and phase relationship, it is clear from the MTF curve shown that the contribution to the image from higher spatial frequencies will be less than ideal. The resulting image feature edge no longer appears as a step but rather exhibits as a finite distance, w, over which the illumination increases from zero to its maximum value.

The characteristic distance, w, may be taken as representing the resolution of edge features that might be expected from the system. The response of the irradiated medium to variations in intensity will determine the edge resolution obtained in practice as will be seen in the next section. However we may estimate the best possible edge resolution to be close to the reciprocal of the 'cut-off' spatial frequency.

It is clear from the expression given previously that the MTF will be zero when ϕ is zero, therefore;

$$v_o = d/f\lambda$$

where f/d = 1/2N.A. is the ratio of focal length to effective aperture of the lens. Thus the edge resolution, $w = 1/v_o$, is approximately equal to Rayleigh's criterion for resolution(1.22 λf/d), ie. lies at the diffraction limit. Chromatic aberrations are, of course, absent for a monochromatic source and for an excimer laser with spectral line-width of less than 1 nm and a Suprasil lens will make only a small contribution to the reduction of edge resolution. Similarly, coma may be reduced to negligable proportions by appropriate positioning of the lens aperture stop.

Spherical aberration, on the other hand, is likely to make a significant contribution to the loss of edge resolution. The Transverse Spherical Aberration (TSA) is a function of focal length, aperture, lens shape and refractive index. The extent to which TSA limits the edge resolution may be estimated by considering the minimum spot size that can be formed for a distant object as this is an indication of the finest detail that can be resolved. The TSA limited spot size, x_{SA}, can be expressed as [2]:

$$x_{SA} = K(N)\ d^3/f^2$$

where K(N) is a specific function of refractive index, N, and lens shape and for Q = 1 is given by [2]:

$$K(N) = 1/(32(N-1)^2)\ (N^2-2N+2/N)$$

This function is shown in the range of refractive index of interest in Fig.6.2.6.

For the chosen 15 cm focal length lens, the minimum spot sizes at 308 nm due to TSA and diffraction are shown as a function of f/d in Fig.4.2.7. If the maximum edge resolution is dominated by the greater of the two effects at any given value of f/d then the optimum value occurs when the two effects are equal, ie. f/d≈15, yielding a spot size of ≈4.5 μm. On the other hand if the effects of TSA and diffraction are additive the optimum occurs at f/d≈20 as seen in Fig.6.2.8. Taking an optimistic point of view and avoiding vignetting for a 1 cm field, a value of f/d=15 was chosen for the experiments. From the above, therefore, the intensity at the edge of a feature is estimated to fall to zero over a distance of at least 4.5 μm so that the minimum width of etched line is expected to be twice this value.

The range of material thickness over which this resolution can be maintained may be estimated from the depth of focus, Δf. This may be considered as being twice the change in distance from the lens to image due to a shift of one Raleigh limit ($\lambda/4$) at the lens and is given by [2]:

$$\Delta f = \lambda f^2/d^2$$

Thus we expect the edge resolution to be maintained for etch depths corresponding to an aspect ratio of depth to edge resolution of 15.

It is shown in the next section that the resolution of etched patterns depends not only on the intensity gradient at the edge of patterns but also upon the material response which can lead to resolution better than expected from optical considerations alone.

Fig.6.2.1.

ENERGY DISTRIBUTION: SPOT DIAGRAMS

Planes near focal plane of lens with conjugate ratio of 5. Image at z=120 mm.

A: z-3 mm, B: z-2.25 mm, C: z-2 mm,
D: z-1.95 mm, E: z-1.75 mm, F: z-1 mm.

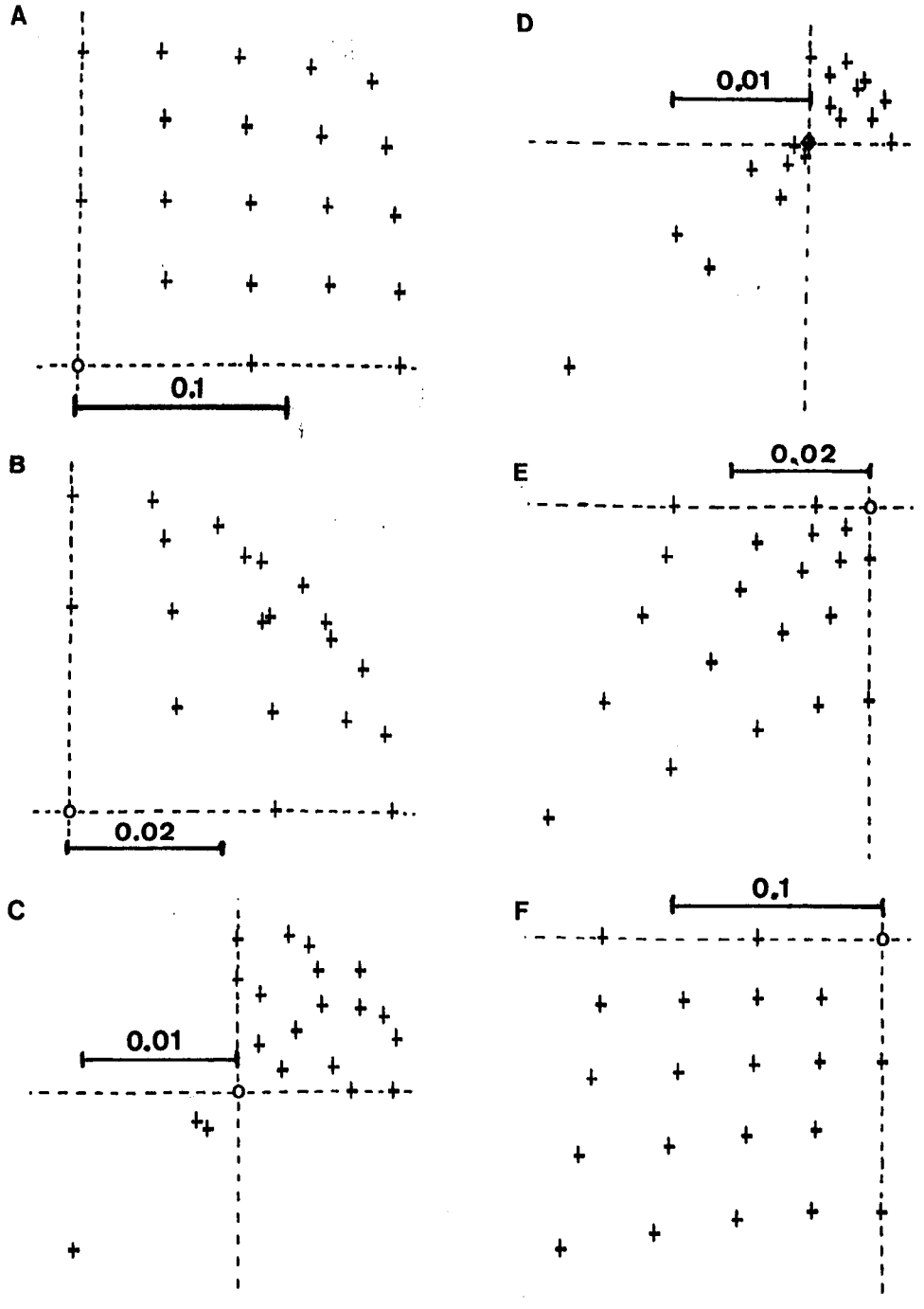

Fig.6.2.2.

ABERRATION DEPENDENCE ON LENS SHAPE

Longitudinal Spherical aberration, LSA,
and Transverse Spherical aberration, TSA,
as a function of Coddington shape factor, Q.
focal length = 100 mm, aperture = 20 mm.

LENS SHAPE

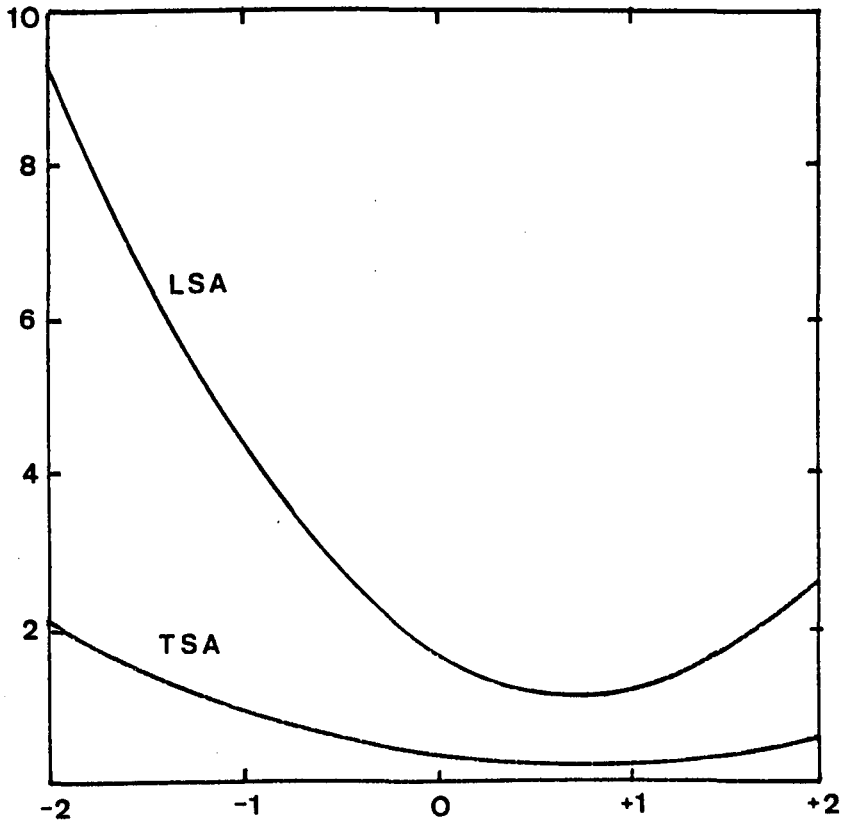

Shape factor, Q

Fig.6.2.3.

UV GRADE FUSED QUARTZ

Refractive index, n, of fused quartz as a function of wavelength in the excimer laser region.

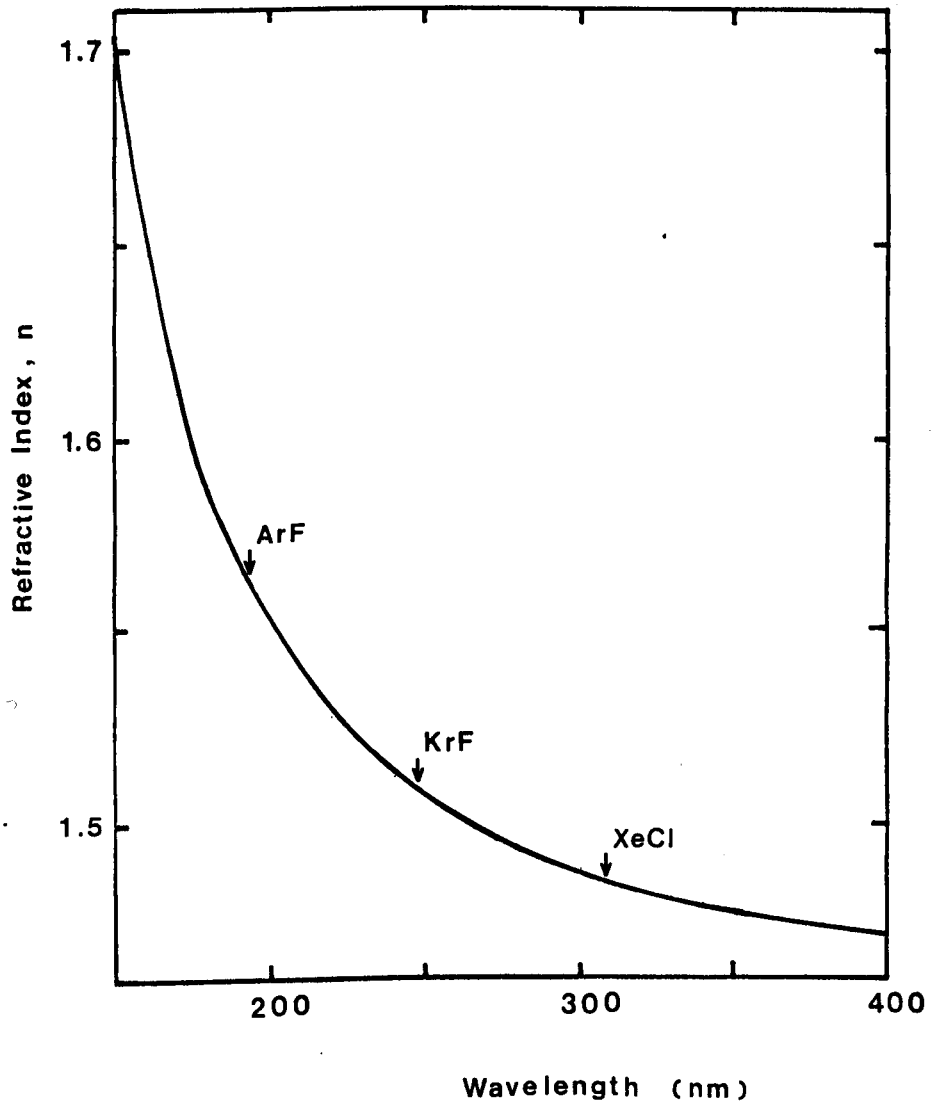

Fig.6.2.4.

UV GRADE FUSED QUARTZ LENS

Variation in focal length of fused quartz lens from design focal length as a function of wavelength.
Design focal length = 150 mm at 546 nm.

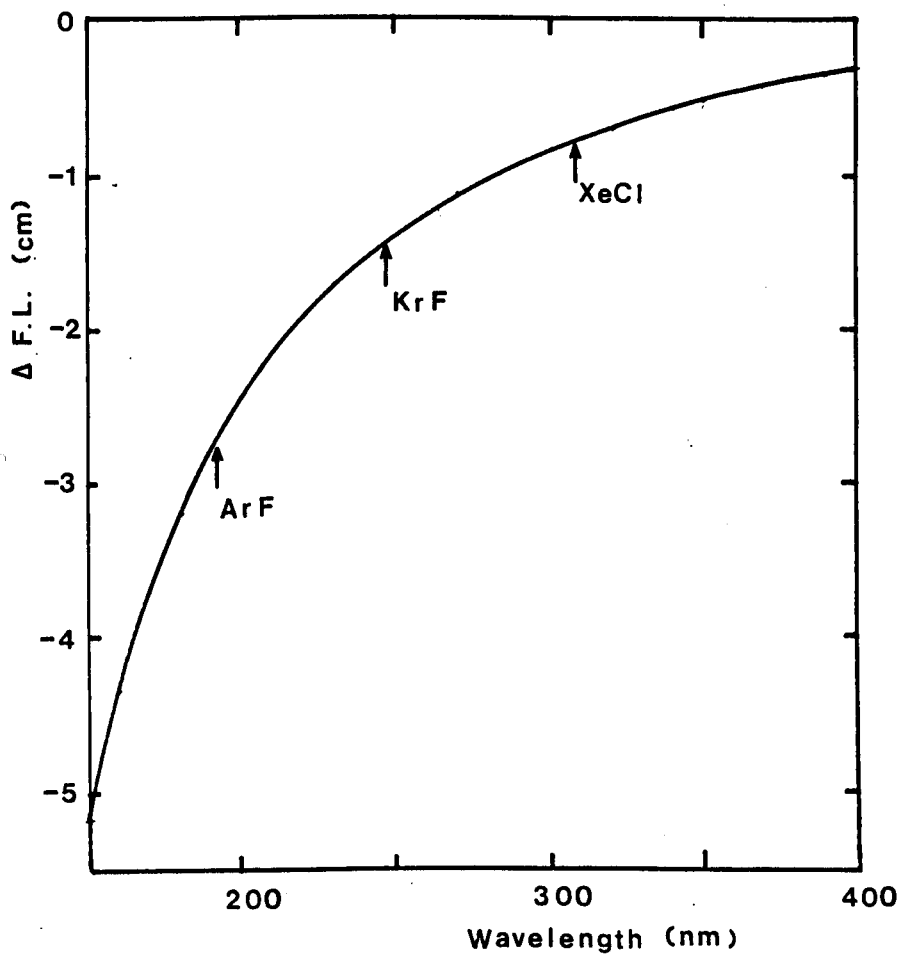

Fig.6.2.5.

MODULATED TRANSFER FUNCTION (MTF)

MTF of aberration free system as a function of normalised spatial frequency, v/v_0 . Circular symmetry single lens.

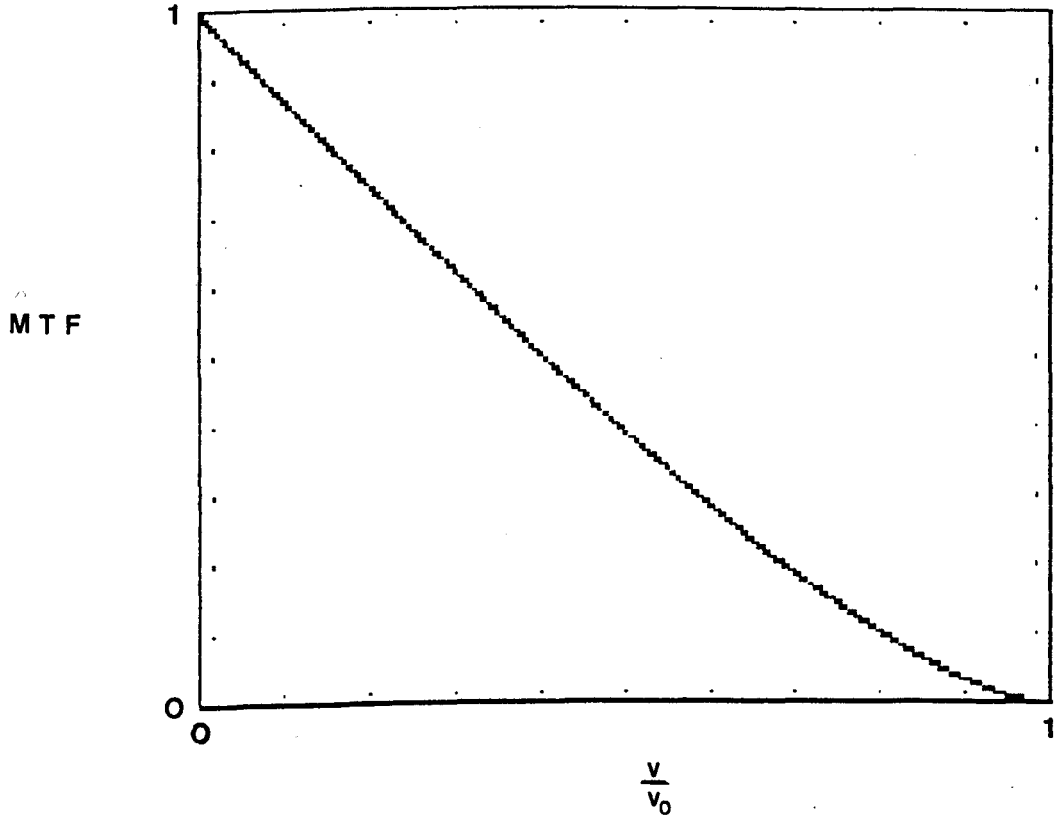

Fig.6.2.6.

FUSED QUARTZ LENS : Q = 1.

Factor K to determine the TSA limited minimum spot size as a function of refractive index, N. From [2].

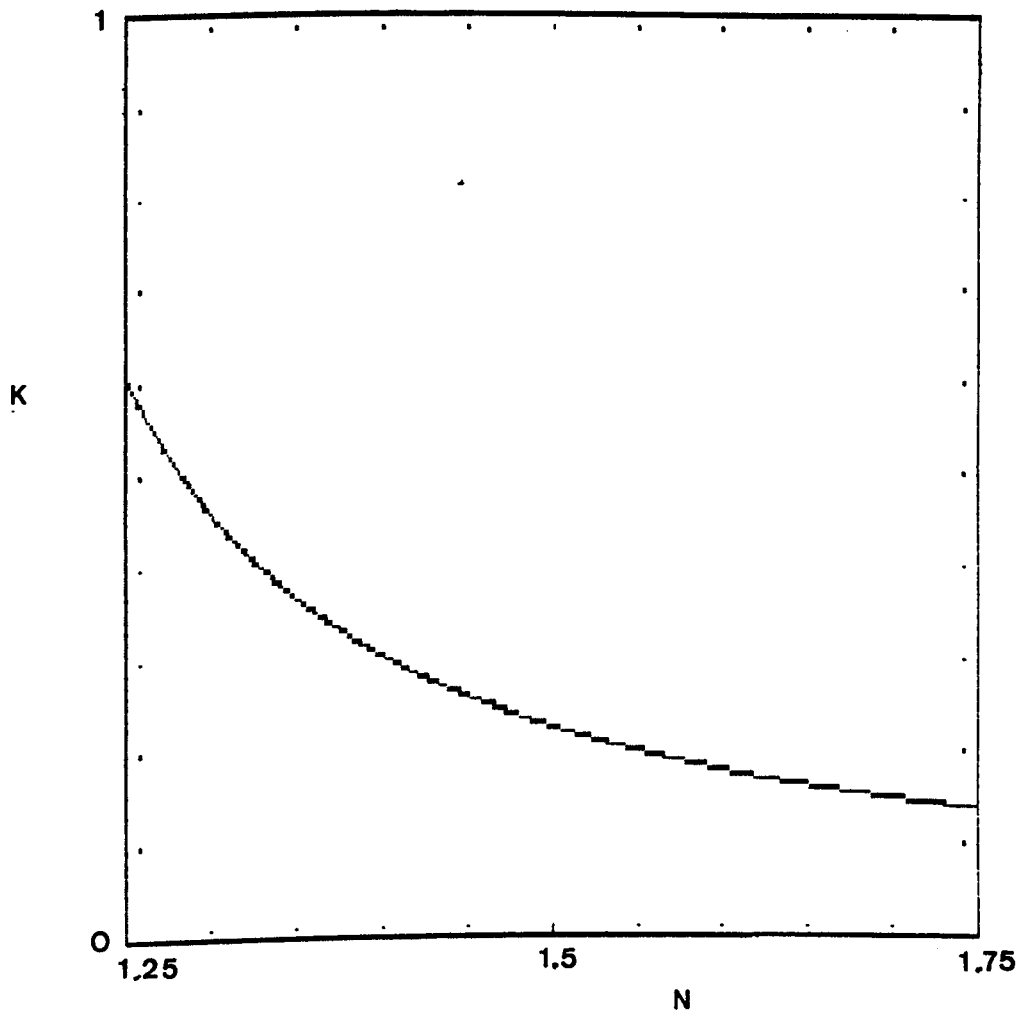

Fig.6.2.7

FUSED QUARTZ LENS: f = 150 mm at 308 nm

Minimum spot image size due to TSA and diffraction as a function of f/d

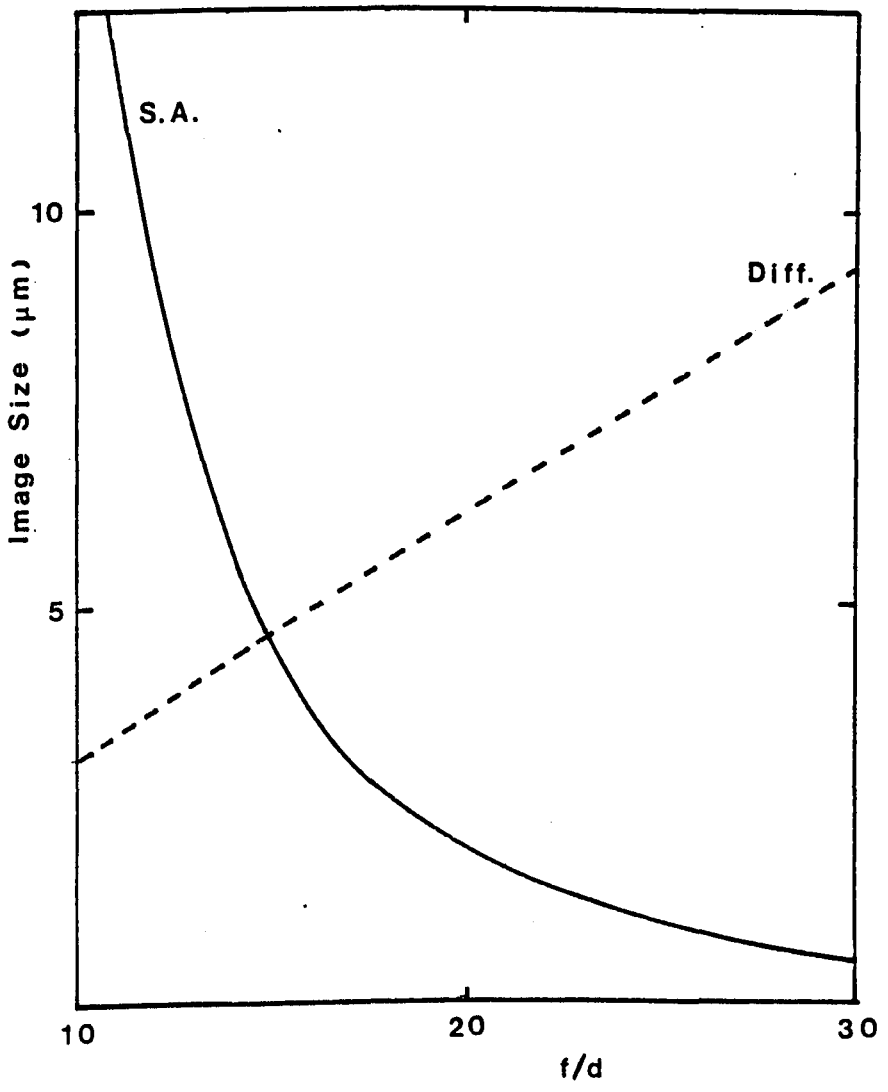

Fig.6.2.8

FUSED QUARTZ LENS: f = 150 mm at 308 nm

Minimum spot image size due to the SUM of effects of TSA and diffraction as a function of f/d

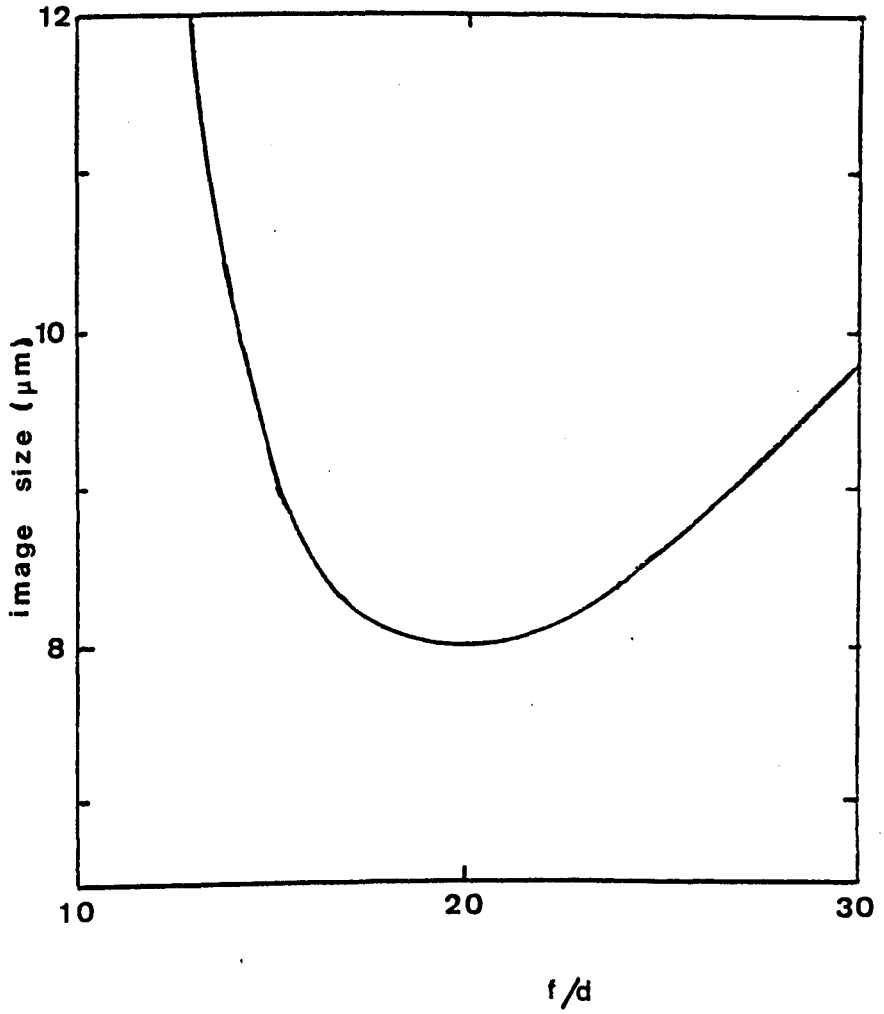

6.3. MATERIAL RESPONSE AND EXAMPLES

The limits of resolution to which a material may be patterned depends not only on the optical resolution but also upon the material response to the variation in fluence found at a feature edge. The fluence fall-off at an edge will follow the near-field Fresnel form for a proximity mask whereas in projection patterning the far-field Fraunhoffer diffraction is modified by lens aberrations and is more difficult to predict. The energy distributions resulting from the partial overlapping of two feature edges in close proximity adds further complexity. The edge resolution achieved will be a function of the energy distribution, the threshold fluence for material removal and the non-linear dependence of etch-rate on fluence.

Using some model fluence distributions and fluence dependent material removal rates, examples of the way in which etched patterns with resolution better than the optical resolution can be achieved are given in this section. Examples of projection etched patterns are shown to have edge resolution better than the minimum of 4.5 μm predicted for the optical system used.

We consider first the case in which the minimum fluence for material removal is also the maximum necessary for complete removal, i.e. the single excimer laser pulse removal of thin metal films described in chapter 1. Assuming a mask consisting of parallel, equi-distant bars and spaces illuminated uniformly and projected to form an image at the

target surface. Consider the case in which the light transmitted through the system forms a pattern in which all of the spatial frequencies other than the fundamental have been lost and this sinusoidally varying fluence falls upon the target with a spatial frequency corresponding to that of the mask and de-magnification of the projection system. We will also assume that the intensity falls to zero at the minima of the pattern. Fig.6.3.1 illustrates the resulting single pulse etched patterns for three removal fluence thesholds. If the threshold fluence occurs at half the maximum intensity, Fig.6.3.1(ii), then the pattern fidelity and edge resolution will be such that the mask pattern is exactly reproduced, despite the failure of the optical system to provide a step fall-off in fluence at the feature edge.

If the threshold fluence occurs at other values of intensity then, although the sharpness of the pattern edge may be maintained, the fidelity of reproduction in terms of the mark-space ratio of the pattern is lost, Fig.6.3.1(i&iii).

The single UV-excimer laser pulse patterning of a gold film on a Kapton substrate is shown in Fig.6.3.2. Here the image of a mask of ≈40 μm bars and spaces was reproduced using the optical system with M = 0.25. The edge detail shown in Fig.6.3.2.(b) indicates that, although there is a minimum fluence for removal, there may be some loosening of the film due to the thermal gradient at the feature edge compounded by sub-threshold illumination. If this band of disturbed material is defined as the edge resolution, w, it can be seen w ≈ 2 μm and is equal to the thermal diffusion length

during the laser pulse.

In the cumulative pulse etching regimes, differential etch-rates, concomitant with variations in fluence at feature edges, can lead to edge profiles with quite different forms to the fluence gradients from which they arise. Here, we consider a simplified case in which the fluence falls off linearly over a distance, r, representing the optical edge resolution.

For a linear dependence of etch-rate on fluence with no threshold requirement, the etch depth at each point along the edge profile, after a number of laser pulses, will clearly follow a linear form Fig.6.3.3(a). If there is a threshold fluence for removal, the actual edge resolution, r•, will be smaller than r to a degree depending on the magnitude of the threshold, Fig.6.3.3(b). Thus, for a given incident fluence, a high threshold material will give a small value of r•.

The additional edge profiles shown in Fig.6.3.3(c&d), represent cases calculated for an etch-rate that is proportional to the logarithm of fluence both with and without a threshold requirement.

More realistically we might expect the fluence profile to follow some functional form such as that for Fraunhoffer diffraction, viz;

$$F(r) = F_o (\mathrm{Sin}\phi/\phi)^2$$

where ϕ is expressed in radians and is related to the spatial dimension, r, at the target by the lens-target distance and F_o is the maximum fluence. Substituting this into the usual Beers Law expression for etch rate gives

the etch depth per pulse as;

$$H(r^{\bullet}) = \delta \ln(F(r)/Ft)$$

$$= \delta \ln[F_o/Ft\ (Sin\phi/\phi)^2]$$

where δ is the optical absorption depth, and the superscript, $\bullet$, is now used to denote "etch-space" rather than "fluence-space".

Similarly, for a TEM_{oo} Gaussian beam we have;

$$F(r) = F_o exp[-r^2/w^2]$$

where w is the width (1/e fluence point) of the half beam. Hence the etch depth per pulse is given by;

$$H(r^{\bullet}) = \delta\ [\ln(F_o/Ft) - r^2/w^2]$$

It is clear from the above that in order to minimise the effect of fluence fall-off at feature edges, i.e. to "sharpen" the etched feature, a high ratio of incident to threshold fluence is required. However, as the Rayleigh limit is approached and the fluence profiles from two adjacent features start to overlap, unwanted etching in the nominally "dark" regions will occur and this mitigates against high fluences.

Examples of computed etch depth profiles and their associated fluence distributions are shown in Figs.6.3.4-7. As etching proceeds and an etched gradient at the edge of features develops, then both the angle of incidence of the laser radiation and the area addressed over this zone will increase. This increase results in an effective local reduction in fluence and hence a concomitant reduction in etch-rate. This phenomenon, in which etching proceeds until some critical gradient of feature edge is reached when the effective fluence falls to the threshold value, has been

investigated by Jenkins [5].

Figs.6.3.8-10 show some examples of 308 nm excimer laser etched patterns in free-standing, 25μm thick copper foils in a chlorine environment. In these cases a single 150 mm focal length lens with f/d = 15 was used. It can be seen that sloping walls of etched edges are a common feature. However, in each case the edge resolution of the pattern and the fidelity, in terms of the relative positions of features, are found to be better than predicted by simple optical resolution considerations. This is particularly well illustrated in Fig.6.3.9 where the optical resolution of ≈5 μm would predict no through etching of the 10 μm bars and spaces pattern. Thus the non-linear dependence of etch-rate on fluence and the existence of a threshold fluence for ablation allow improvements on the optical resolution to be achieved.

Fig.6.3.1.

SINGLE PULSE PATTERNING

Schematic representation of effect of single value removal fluence or threshold on pattern fidelity.

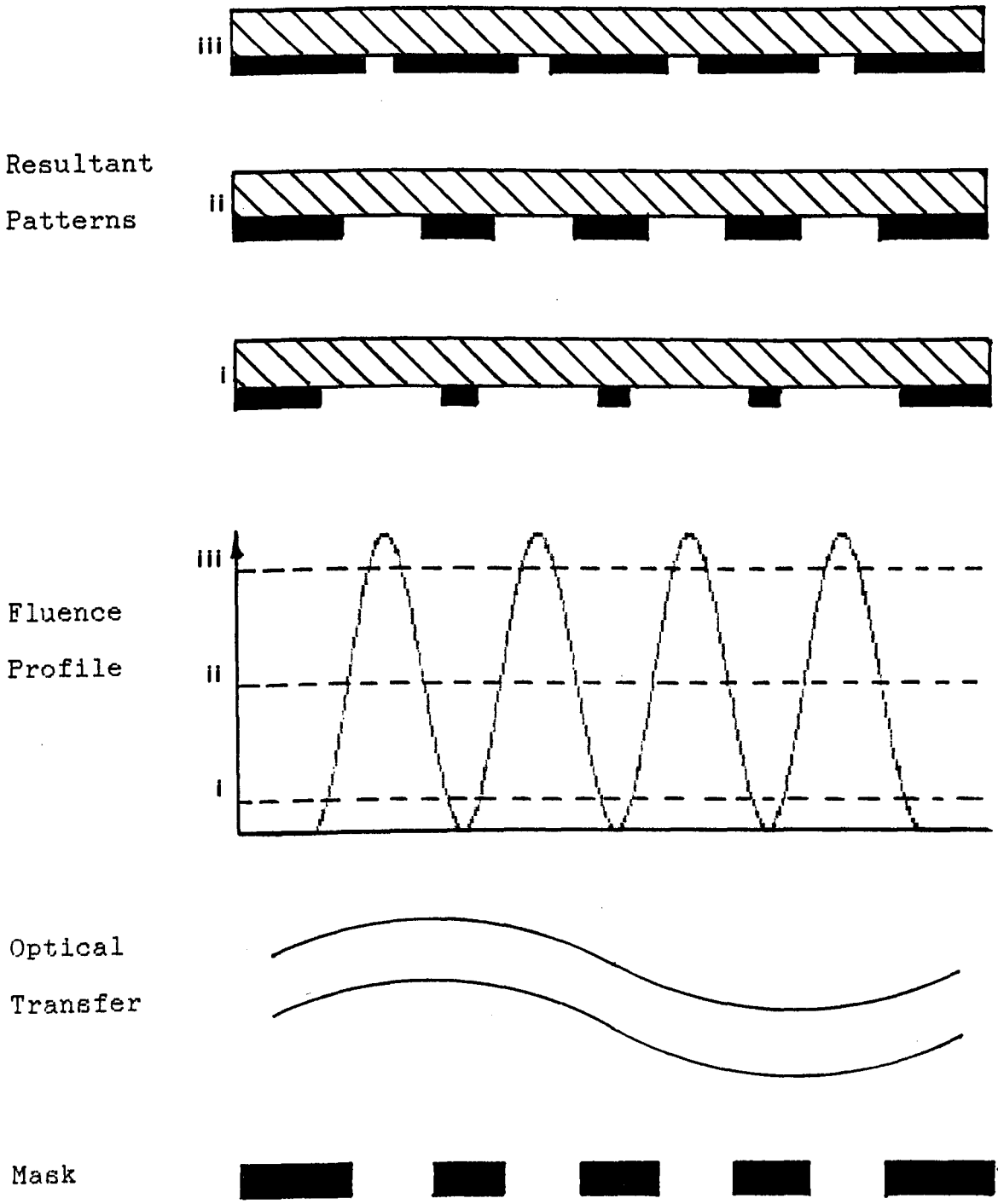

Fig.6.3.2.

SINGLE PULSE PATTERNING of Au film on Kapton

(a)

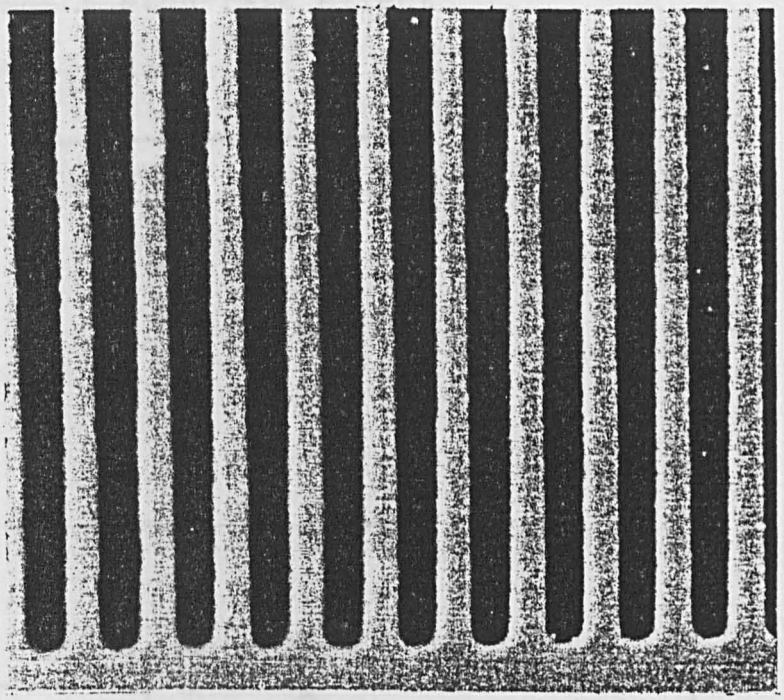

40 μm

(b)

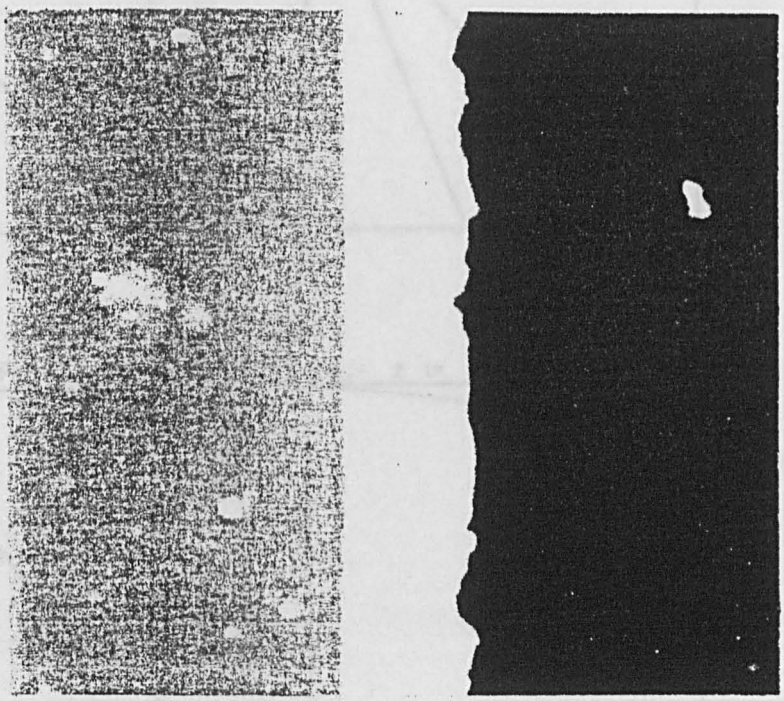

2 μm

PATTERN EDGE RESOLUTION

Fluence dependent etch-rate effect

on optical resolution.

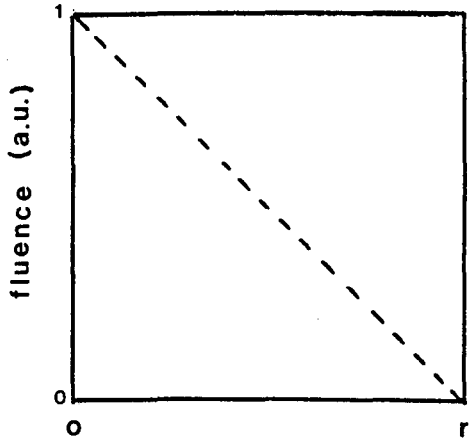

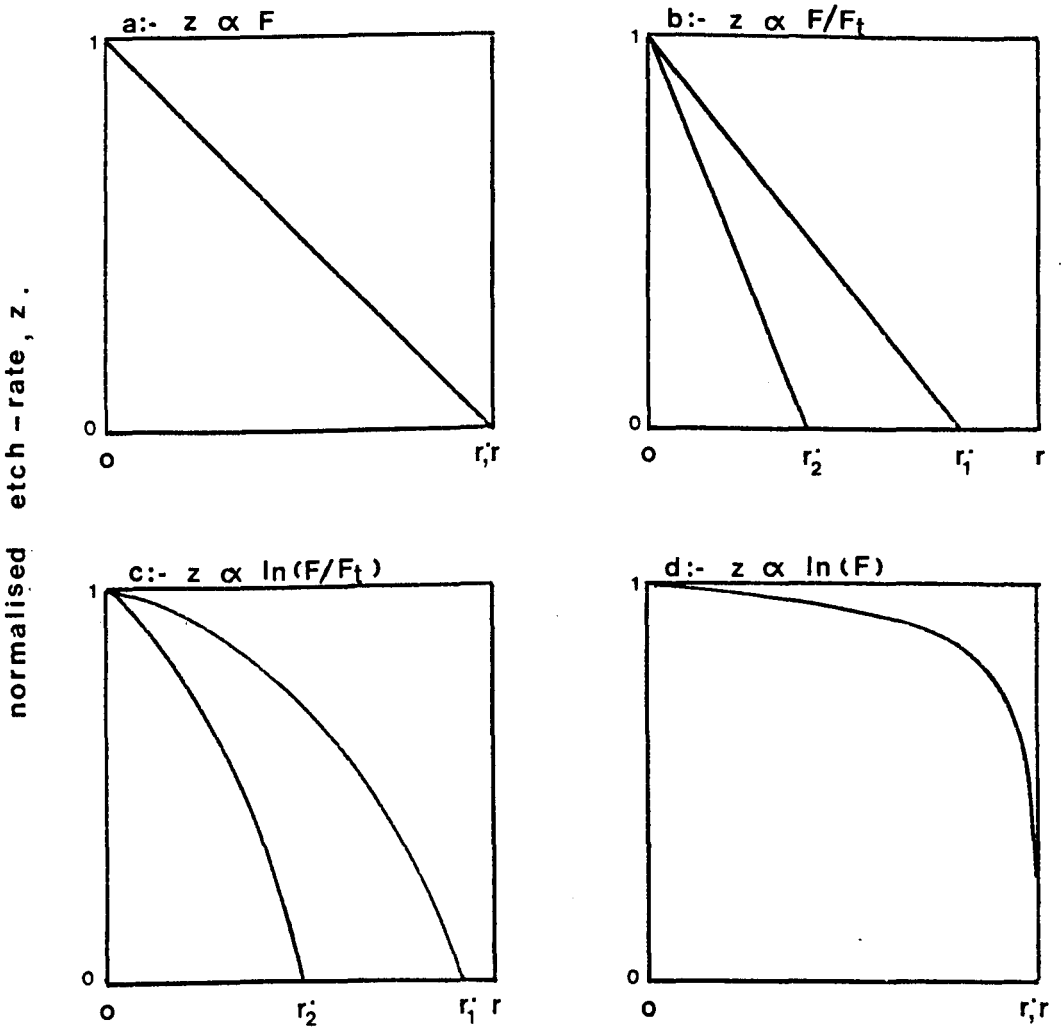

Fig.6.3.4

ETCH-RATE 'ENHANCED' OPTICAL RESOLUTION

Fraunhoffer Diffraction edge profile.
Normalised fluence and normalised
etch-rate profiles.
Threshold at 0.1 max etch-rate fluence.

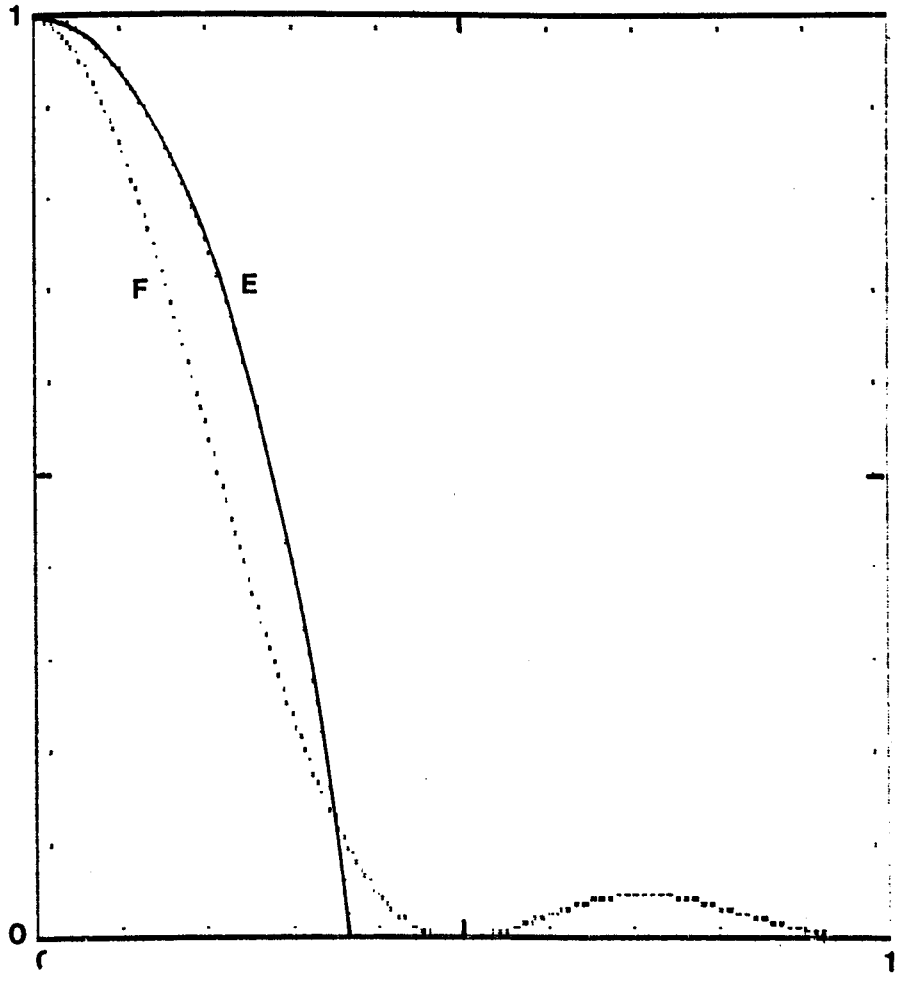

Fluence, F.
and
Etch-rate, E.

Distance, r (arb. units)

Fig.6.3.5.

ETCH-RATE 'ENHANCED' OPTICAL RESOLUTION

Fraunhoffer Diffraction edge profile.

Normalised fluence and normalised

etch-rate profiles.

Threshold at 0.025 max etch-rate fluence.

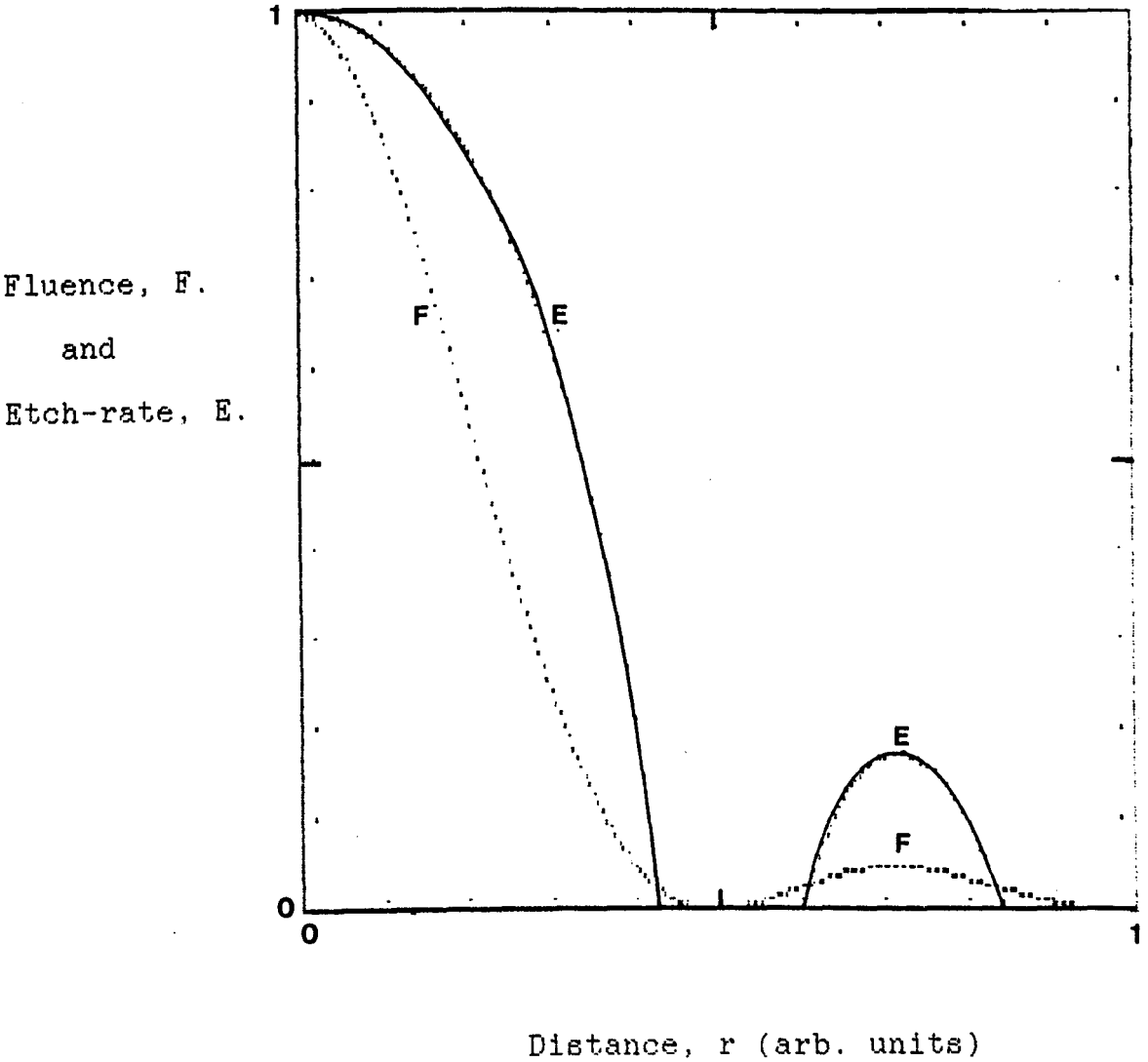

Fig.6.3.6.

ETCH-RATE 'ENHANCED' OPTICAL RESOLUTION

Gaussian edge profile.

Normalised fluence and normalised etch-rate profiles.

Threshold at 0.1 max etch-rate fluence.

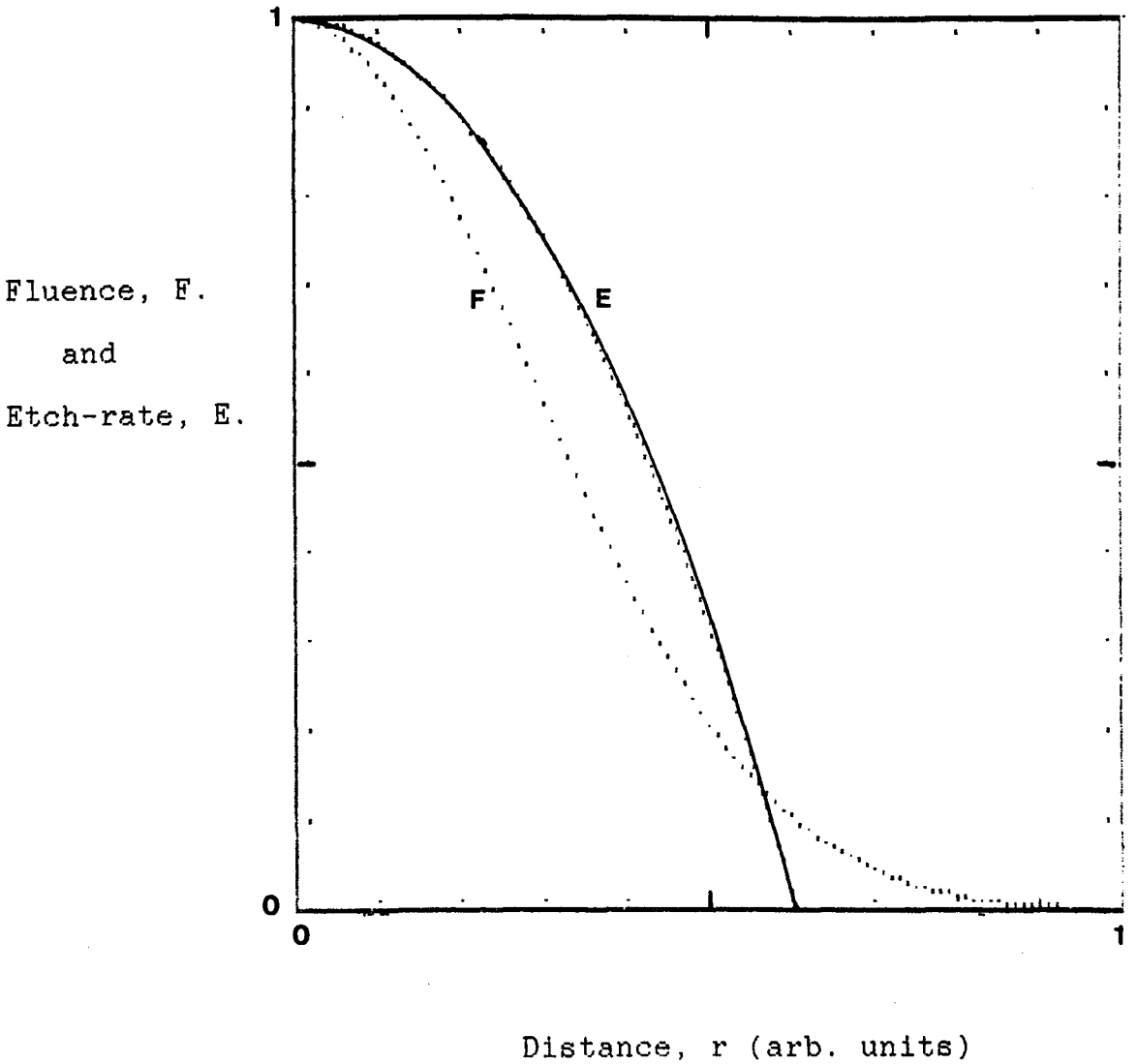

Fig.6.3.7.

ETCH-RATE ENHANCED OPTICAL RESOLUTION

Gaussian edge profile.

Normalised fluence and normalised

etch-rate profiles.

Threshold at 0.025 max etch-rate fluence.

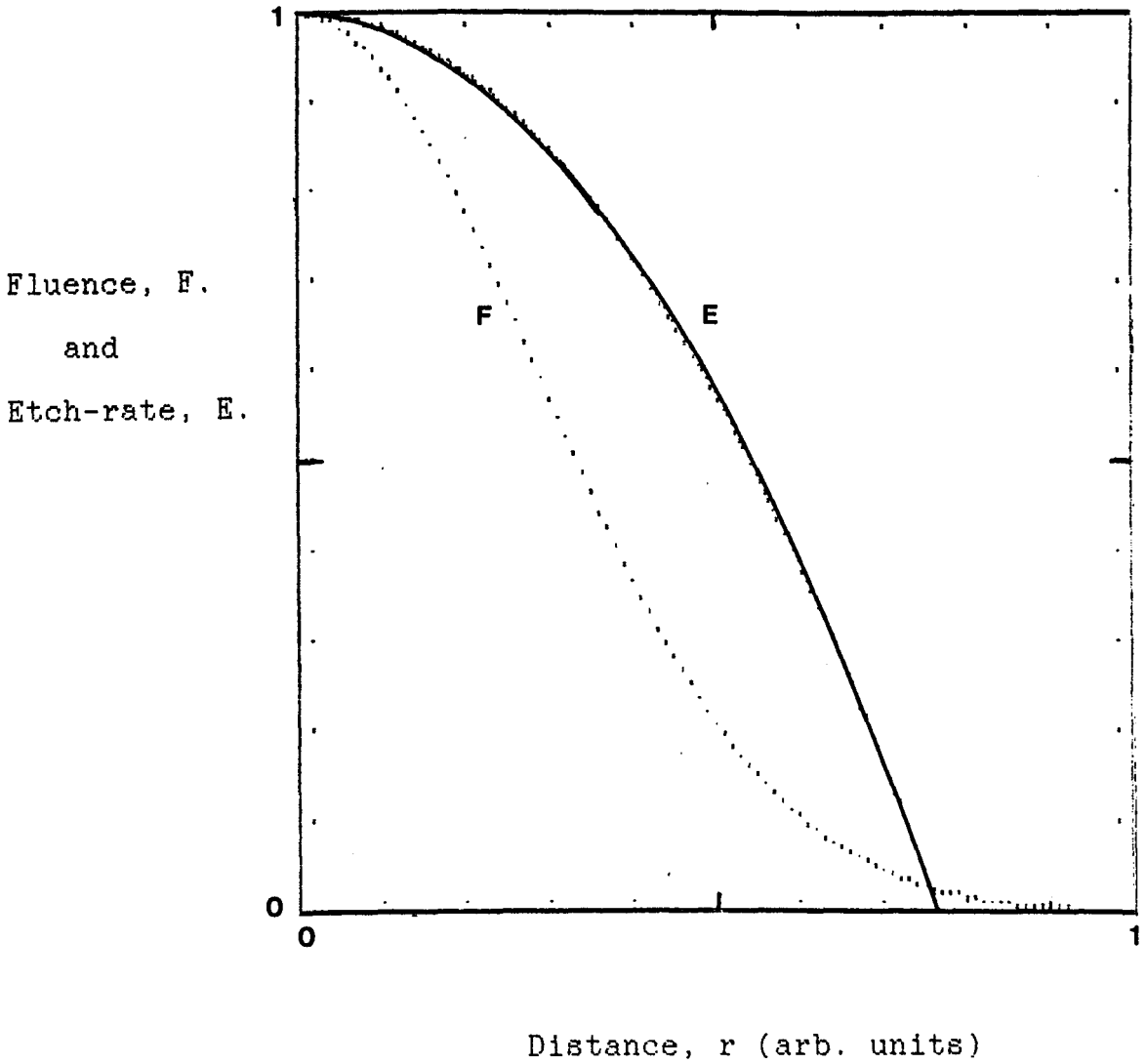

Fig.6.3.3.

XeCl LASER PATTERNING OF COPPER IN CHLORINE

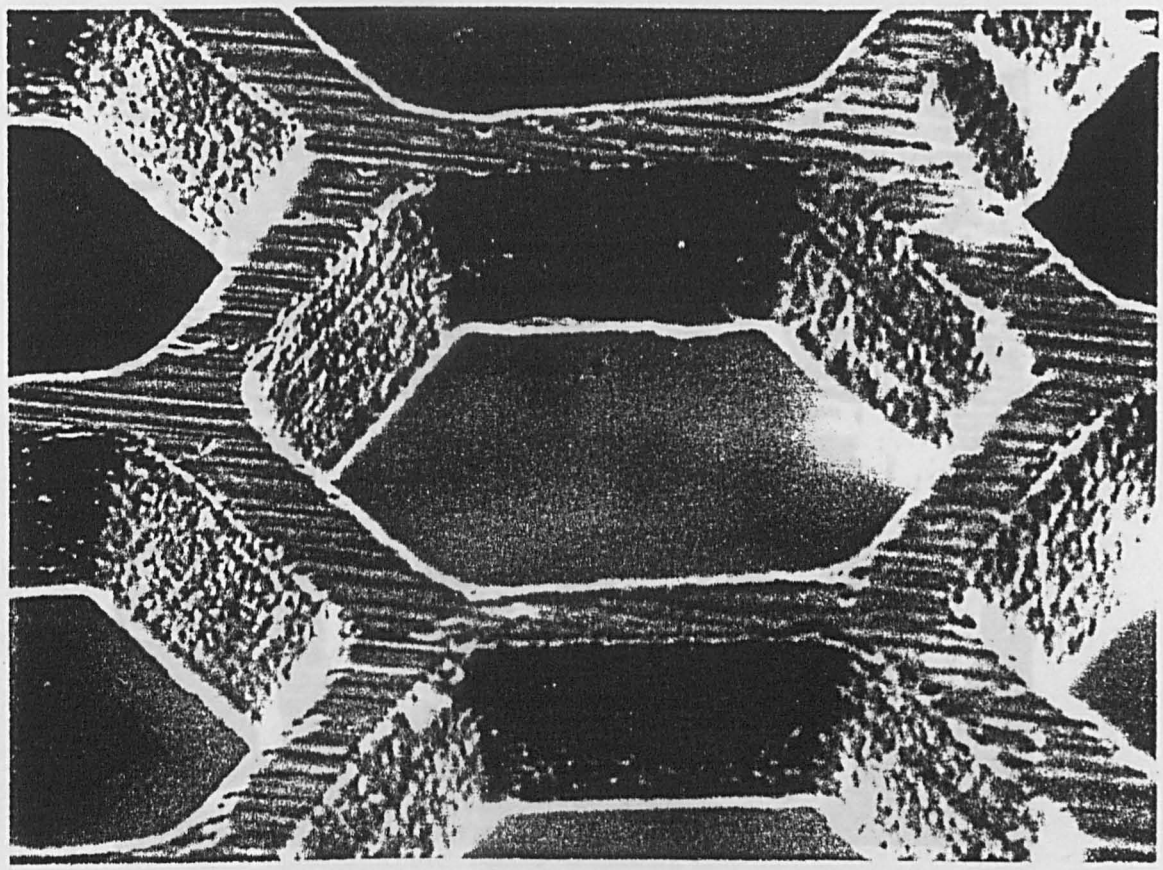

20 μm

Fig.6.3.9

XeCl LASER PATTERNING OF COPPER IN CHLORINE

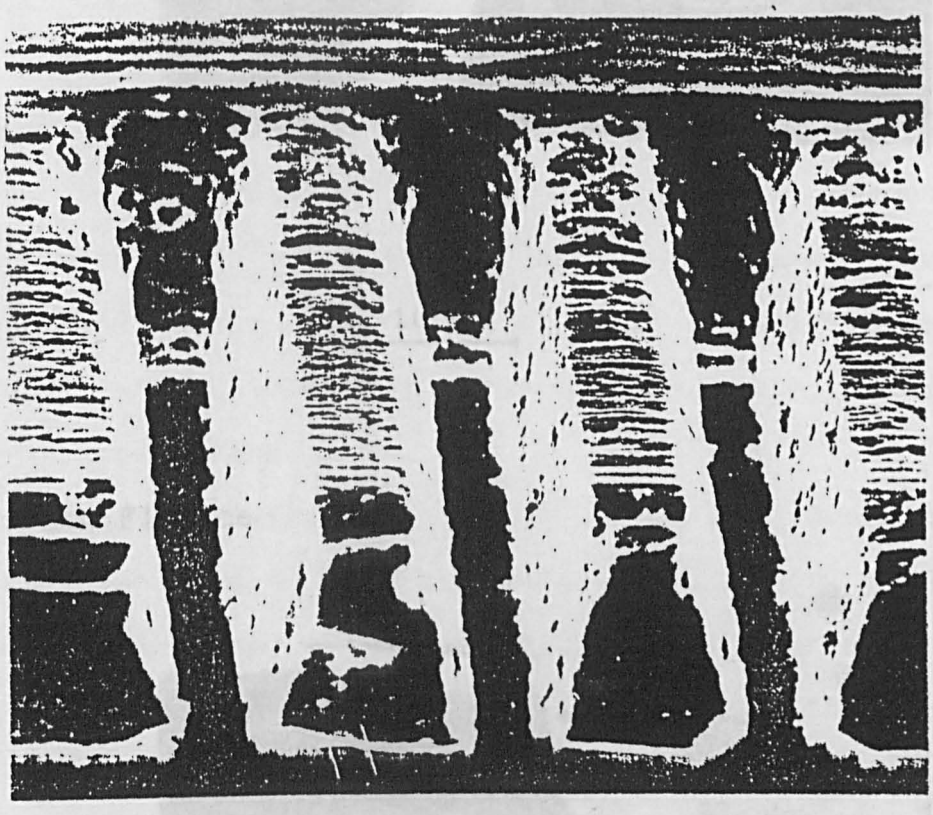

10 μm

Fig.6.3.10.

XeCl LASER PATTERNING OF COPPER IN CHLORINE

(a) High Fluence

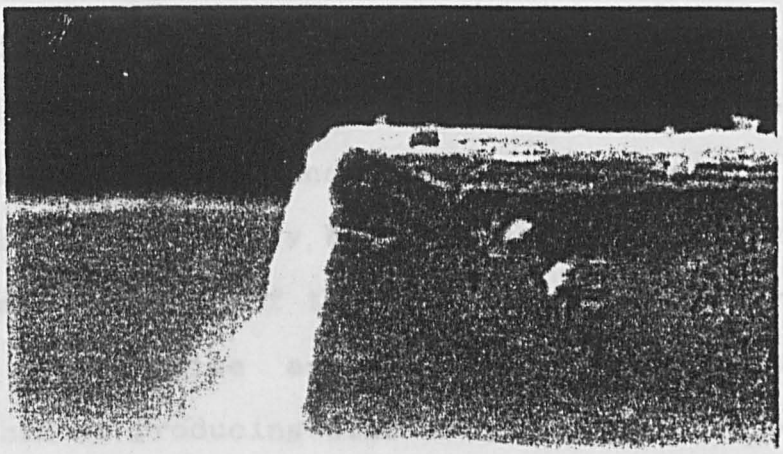

10 μm

(b) Low Fluence

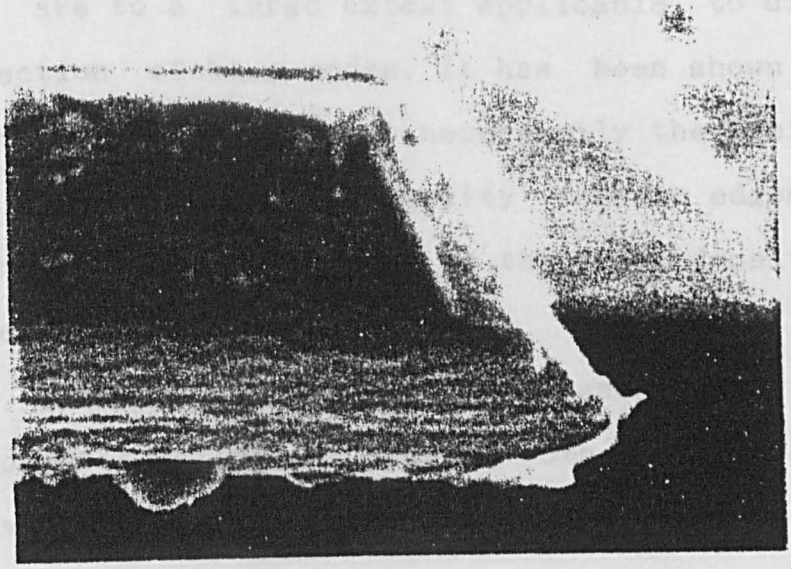

10 μm

6.4. CONCLUSIONS

The patterning of materials by laser ablation may be achieved by any of the three basic techniques outlined in the first section of this chapter. The proximity mask method is, however, best suited to relatively coarse patterning applications where simple, inexpensive, sacrificial masks may be used. Large areas may be processed in this way by step and repeat exposure of the mask-target assembly. The choice between direct write and projection etching methods, which are capable of producing similar results, is dependent upon the application. The former, a relatively slow method, is most suitable for prototype and low volume production such as mask making. Projection etching techniques, on the other hand, are suitable for large area, repetitive and high throughput processing.

The constraints placed on resolution by the demagnifying optical system are to a large extent applicable to direct write and projection etching modes. It has been shown here that the optical resolution is not necessarily the limiting factor in the production of high quality feature edges but it does take on greater significance as the areal density of features is increased.

Sophisticated systems specifically designed for high resolution projection patterning, using both reflective [6] and transmissive [7] optics, have been used with UV-excimer lasers to produce feature sizes of the order of the wavelength of light used.

It has been demonstrated, in this chapter, that features with dimensions of only a few wavelengths can be patterned using a simple, uncorrected, single spherical lens system at a suitable numerical aperture. The results indicate that a non-linear dependence of etch-rate on fluence, together with a threshold for ablation, leads to a significant enhancement of the attainable resolution.

It should be noted that a rigorous analysis of the optical imaging system performance should include consideration of the degree of spatial coherence of the illuminating source. In this present work the highly multi-mode output of the UV-excimer laser and low numerical aperture of the obective lens provides for a low degree of spatial coherence [8] and approximations based on an incoherent source were used in assessing the system performance.

6.5.

REFERENCES

[1] (C)1986, Stellar Software
P.O.Box 10183, Berkeley Ca. 94709.

[2] Melles Griot
Optics Guide 3
Irvine, Ca. (1987)

[3] Malitson,I.H.
J. Opt. Soc. Amer. 55, (1965), 1205.

[4] Smith, W.J.
'Modern Optical Engineering'
McGraw-Hill, New York, 1966

[5] Dyer,P.E.,Jenkins,S.D. & Sidhu,J.
Appl. Phys. Lett. 49, (1986), 453.

[6] Rothschild,M. & Ehrlich,D.J.
J. Vac. Sci. Technol. B5, (1987), 389.

[7] Goodall,F.N.,Moody,R.A. & Welford,W.T.
Optics Comm. 57, (1986), 227.

[8] Rothschild,M. & Ehrlich,D.J.
in 'Emerging Technologies for In-Situ Processing'
Martinus Nijhoff, Dordrecht, (1988).

CHAPTER SEVEN

7.0 Summary

7.1 Discussion

7.2 Applications

7.3 Presentations and Publications

7.0.

SUMMARY

Laser assisted or initiated chemical etching represents a small proportion of the current interest in the rapidly expanding subject area of laser processing of materials. One particular system, the UV-excimer laser etching of copper foils in chlorine gas, has been described in detail in this thesis. Preliminary investigations of excimer laser etching of some other inorganic materials have also been described. The review in chapter 1 of earlier work on the single excimer laser pulse ablative patterning of thin metal films, together with the limited review of laser interaction studies reported in the literature, was intended to set the work descibed in this thesis in context.

It was seen that a number of thin metal films, deposited on a variety of substrate materials, can be patterned using a single UV-excimer laser pulse. For this regime of processing a threshold fluence for patterning was found to exist below which there was little or no material removal and above which pattern reproduction was severely disrupted and substrate damage could occur.

In the case of copper, the removal threshold was found to be independent of the excimer laser wavelength used provided the UV reflectivity and pulse lengths were similar. It was futher shown that the maximum film thickness that could be removed in this regime was limited to thicknesses approximately equal to the thermal diffusion length in the time of the laser pulse. The energy deposited into the film

was found to be close to that required to achieve melting of the film.

These observations formed the basis for suggesting that the removal mechanism was primarily a thermal one. It essentially involves a rapid temperature rise ($\approx 10^{10}$ °C s^{-1}) at the film-substrate interface due to the high thermal diffusivity of the metal, leading to an explosive removal by degassing or surface decomposition of the substrate.

The removal mechanism is thought to be generally applicable to combinations of high thermal conductivity films on low thermal conductivity substrates and no variations in results were found between in-house deposited films from thermal evaporation sources and commercial films formed by sputter coating.

It was shown that etch-rate measurements alone rarely give conclusive evidence of the mechanisms involved in laser ablation and this is particularly true in the fluence regime up to a few times the threshold fluence. Where the etch-rate is largely independent of wavelength, the assumption of a purely thermal removal mechanism may be erroneous due to a lack of consideration of the time over which the irradiation takes place. Thus care must be exercised in making comparisons of yields using different lasers since temporal variations in the pulse shapes result in different absorbed power densities.

The examples of laser-material processing cited in the latter part of the first chapter are intended to indicate the variety of materials that have been studied and the strategies that have been employed, together with the

complexity of the mechanisms involved.

In the first section of chapter 2, the optical properties of materials were outlined and typical values for the reflectivity of metals in the infrared to ultraviolet region of the spectrum given. It was shown that the wavelength dependence of optical properties is more marked at shorter wavelengths.

The thermalisation of absorbed photon energy and its redistribution as sensible heat in the solid was discussed in the second section. The transient heating of free-standing metal foils was shown to be described by a particular solution to the heat conduction equation. Measurements of the rear face temperature rise of laser irradiated metal foils were shown to be consistent with the transient heating model. The development of a quasi-steady state temperature was seen to occur at laser prf's as low as 1 Hz, whilst at higher prf (≈500 Hz) temperatures approaching those required for melting of the film were achieved.

Surface contamination was shown to play an effective role in the etching of bulk metal samples by lowering the threshold fluence for removal. The etch-rate of copper was seen to be dramatically enhanced by the simple expedient of irradiating in a gaseous environment capable of forming surface layers of metal-gas compound in the period between laser pulses. These preliminary results formed an introduction to the detailed studies of UV-excimer laser ablation of copper in chlorine gas.

The chemisorption of gaseous species on clean metal surfaces

was discussed in the opening section of chapter 3. Particular attention was paid to the 'dark reactions' of oxidation and halogenation of copper.

The modulation of reflectivity of a film-substrate combination due to variations in film thickness was outlined and the technique of film thickness measurement by real-time recording of interference maxima during film growth was described. The use of this technique for studying the growth of chloride layers on copper substrates was presented in the third section of chapter 3.

It was seen that the rate of appearance of reflectivity maxima for copper chloride layers using a He-Ne laser probe beam decreased with time. The resultant growth curves revealed that the thickness of chloride layers, following the exposure of copper to chlorine gas in the pressure range 0.1 - 5.0 torr, followed a $\sqrt{t}$ dependence and it was deduced that a diffusion-limited growth regime obtained. It was further found that the growth-rate increased with increasing temperature.

The fourth chapter was devoted to studies of the UV-excimer laser etching of copper in a chlorine environment. The experimental procedure was described and the spatial energy distribution of the laser output beam evaluated. The optical absorption by the chlorine at the laser wavelength was found from both low intensity UV lamp and laser transmission measurements. No significant differences between the two were found.

Etch-rates of copper in chlorine gas were measured as a

function of laser wavelength, prf and gas pressure in order to establish their relative importance.

The measured etch-rates of copper in 2.5 torr chlorine using 1 Hz UV-excimer laser pulses at upto 1 J cm^{-2} did not exhibit any significant wavelength dependence for 193, 248 or 308 nm irradiation.A comparison of the etch-rate (≈50 nm / pulse at the maximum fluence used) and the thickness of chloride addressed by the first laser pulse (≈500 nm) revealed that the etch-rate was not simply chloride growth-rate limited. The remainder of the etch-rate measurements were made using the XeCl laser because of its reliability and long gas lifetime.

It was argued that, since the chloride growth-rate curve at 2.5 torr chlorine indicated a thickness of ≈100 nm after 0.1 s exposure, the etch-rate up to 1 J cm^{-2} was not expected to be growth-rate limited at 10 Hz and the temporal etch-rates up to this prf should be simple multiples of the 1 Hz data. This was found, however, not to be the case. At low fluences (≈0.1 J cm^{-2}) the temporal etch rate at 10 Hz was found to be 10 times that at 1 Hz whereas at higher fluences (≈1 J cm^{-2}) there was only a factor of three difference between the two prfs. This behaviour was attributed to an increase in absorption in the thinner films addressed by the laser at the higher pulse repetition frequency.

At a fixed prf, different thicknesses of film could be addressed by varying the chlorine pressure and hence controlling the interpulse growth of the chloride layer. Etch-rate measurements under varying chlorine pressures

were made and the etch-rates found to decrease with decreasing chlorine pressure.

The etch-rates at fluences in excess of four times the threshold were found to give a good fit to a linear dependence of etch-rate on the logarithm of fluence. The gradients of these curves were used to evaluate the CuCl equivalent optical absorption lengths as a function of chlorine pressure.

The etch-rate was found to increase with increasing pressure up to approximately 2.5 torr chlorine. As the pressure was further increased, however, a decline in etch-rate was observed. The maximising of the etch-rate at about 2.5 torr chlorine was found to occur in the fluence range 0.1 to 1.0 J cm^{-2}.

In order to assess the influence of energy absorption by the ambient chlorine, measurements of etch-rate were made with upto 50 torr chlorine in the cell.

It was found that the decline in etch-rate was consistent with loss of incident energy at the target due to chlorine absorption. This deduction was confirmed by repeating the experiments with the incident energy on the cell adjusted to maintain constant fluence at the target. The etch-rate was then shown to be independent of the ambient chlorine pressure in the range 2.5 to 25 torr.

The introduction of an inert buffer gas, argon, at pressures up to 1.6 atmospheres in addition to a fixed chlorine pressure, also resulted in a decrease in etch-rate. This was attributed to the combined effects of a shift in the desorption-readsorption equilibrium to higher temperatures

and to re-deposition of ablated fragments.

UV-visible spectroscopy of the light emitted by the plume of ablated material revealed that the main emitting species were copper, chlorine and CuCl neutrals. Similar integrated spectra were obtained with a variety of fluence, prf and pressure conditions, the only significant changes being in the emission intensity due to changes in etch rates.

Examination of time resolved signals from selected spectral features at varying distances along the target normal allowed the velocity of the species to be calculated. The velocity of the fastest species was estimated to be approximately 6.6×10^5 cm s^{-1} and the velocity of the most abundant species, derived from the peak of the signal, estimated to be about 4×10^5 cm s^{-1}. The most abundant velocity was observed to decrease with distance from the target to about half of its original value over a distance of 2 mm and this deceleration was thought to be due to the products having to push the ambient gas ahead of the plume.

In the final section of chapter 4, a model was developed in support of the argument that the etch-rate, at a given fluence, was dependent upon the thickness of chloride addressed by the laser pulse. This model was used to predict the form of the reflectivity signal during the ablation process. Reflectivity measurements were found to be in qualitative agreement with this model.

The fifth chapter of this thesis was devoted to the investigations of ablation of a number of different inorganic materials. Studies of the ablation of copper-nickel alloys in chlorine atmospheres showed that the

etch-rates were highly dependent upon the composition and increased with increasing copper concentration. The quality of etched patterns using a chlorine ambient were seen to be far better than those etched in air and were achieved at lower fluence.

The etch-rate dependence on fluence for the ablation of ceramic alumina was not fitted by a simple model for fluences upto a few times the threshold value . The etch-rates up to 2 J cm^{-2} were found to be similar for both the XeCl and ArF lasers.

Ceramic strontium titanate was ablated using the KrF laser. A comparison of the results obtained for ablation in vacuum and a hydrogen atmosphere showed that there was a small advantage gained by employing H_2. The presence of the ambient gas, however, resulted in an increase in redeposited material around the ablation site. Etching of deep grooves with high aspect ratios (depth/width) were readily achieved with this material.

High etch-rates at fluences above the threshold of about 1 J cm^{-2} were found for glass in air using the ArF laser at 10 Hz. Samples ablated in air showed evidence of the formation of surface compounds whereas ablation in vacuum produced very smooth, clean patterns.

The generation of patterns by laser ablation was discussed in chapter 6. Here a number of relevant techniques for patterning by laser ablation in a dry environment were described and particular attention was paid to projection patterning techniques. The factors taken into consideration for the design of the simple optical system used were

described. The considerations of aberrations and diffraction were used to asses the pattern resolution that might be achieved.

The non-linear dependence of etch-rate on fluence and the existence of a threshold fluence requirement were discussed. Consideration of these factors revealed that edge resolution better than that estimated from optical considerations alone could be achieved. This was illustrated with examples of patterns produced in free-standing copper foils by ablation in chlorine using the projection etch technique.

7.1. DISCUSSION

The nomenclature for the processing described in the central portion of this thesis, in terms of the choice between Laser Assisted Chemical Etching (LACE) and Laser Induced Chemical Etching (LICE), is to some extent arbitrary, although the mnemonic for the former has greater aesthetic appeal. In view of the fact that the laser radiation was necessary to remove the products of the chemical reaction as well as defining the reaction area, LACE is probably the most appropriate choice.

The conversion of a copper surface to its chloride in the presence of dry chlorine gas is a spontaneous process, being energetically favourable in the absence of external activation energy at temperatures down to, at least, 5 °C. The growth-rate of the chloride layer is diffusion limited and the thickness of chloride layer that can develop in a given time is dependent upon the chlorine gas pressure and the copper substrate temperature. Since diffusion mechanisms require a concentration gradient, the chloride layer is thought to be copper rich in the region of the interface.

The chloride may be ablated from the surface using UV-excimer laser pulses with fluences in excess of some threshold value, this being ≈ 0.05 Jcm^{-2} for the XeCl laser at 308 nm (≈5 ns fwhm). At 1 Hz pulse repetition frequency and with an ambient of 2.5 torr chlorine the etch-rate, in terms of the thickness removed per laser pulse, is approximately proportional to the logarithm of the ratio of

incident to threshold fluences.

At higher pressures, for the in-cell optical path length used, significant absorption by the chlorine at 308 nm occured and was accompanied by a proportionate decline in etch-rate.

At lower pressures, or with higher prf, a regime of processing is encountered in which the etch-rate, at fluences up to 1 J cm^{-2}, is controlled by the thickness addressed by each laser pulse. In this regime the optical properties of the chloride layer assume increasing importance.

Thin chloride layers, in which the copper concentration gradient is steep, present an effective absorption coefficient which increases, in some manner, with increasing gradient. The largest copper concentration gradients occur with the thinnest layers and hence lead to a reduction in etch rate. Thus the etch-rate is proportional to the chloride layer thickness, the growth of which is a function of chlorine gas pressure and the time between laser pulses.

Even with very low gas pressures a sharp plateau in etch-rate may not be achieved since energy in excess of that removed with the ablation products will be deposited into the substrate and the resultant temperature rise will increase the rate of chloride growth. A quasi-steady state is reached when the temporal etch-rate is equal to the chloride growth-rate in the interpulse period.

Thus the etching of copper in a chlorine environment is a complex system in which the etch-rate cannot readily be described by a simple functional relationship between the

processing variables.

The details of the ablation mechanism have not been resolved although the lack of dependence of etch-rate on wavelength would tend to suggest that the removal is primarily thermal. Whilst some information on the ablated species and their velocities was obtained from the time integrated and time resolved emission spectra, ion probe and mass spectra data would help to give greater insight.

Anisotropy of etching on different crystal planes could be investigated by using single crystal substrates. This would also be useful in helping to assess the influence of diffusion at grain boundaries.

The rather long exposure of copper to the chlorine gas in regions where the protective oxide layer has been removed (eg. at the side walls of etched features) may lead to extensive diffusion of the gas into the metal. This would make the dark reaction chlorination process unsuitable for micro-electronics applications. However, this contamination may be reduced by using a photo-activated chlorination mechanism. Such a process would involve the localised release of chlorine by laser photo-dissociation of a non-reactive donor molecule such as CCl_4. The chlorination in this case would, therefore, be also controlled by the laser and introduce an additional variable processing parameter. Since the growth of chloride would only proceed for periods of time of the same order as the laser pulse length the etch-rates achievable are likely to be much lower than in the regime reported in this work.

Further work is necessary to determine the role of nickel in

inhibiting the etch-rate of copper-nickel alloys. It would be of use to examine the composition of Cu-Ni alloy surfaces that have been exposed to chlorine as well as etched samples in order to determine if a non-congruent removal mechanism is operative. If this were the case then it is likely that the nickel atoms are removed as a result of having the copper atoms removed from around them.

The studies of patterning thin films, free-standing metal foils and other bulk materials has demonstrated that good edge resolution and fidelity of pattern reproduction may be achieved using the projection etching technique.

The material response to variations in fluence across feature edges may compensate to a limited extent for the failings of the optical system. The functional form of the etch-rate dependence on fluence is largely influential in determining the gradient of feature edges and the existence of a threshold for removal is an important factor in producing small scale pattern features.

7.2
APPLICATIONS

Some aspects of micromachining of inorganic materials by UV-excimer laser ablation patterning in a controlled gaseous environment have been described in this thesis. This type of laser assisted chemical etching represents a regime of material processing intermediate between those of large scale, mainly thermal, cutting or shaping and sub-micron lithographic techniques suitable for micro-electronics technologies.

Because of the feature size and thickness of copper foils described in this work, a possible application of the technique is for electronic conductor tracks as found in printed circuit boards. It is useful to make some comparisons between the laser assisted chemical etching technique and conventional wet etching technology.

Wet chemical etching through exposed and developed etch resists is, in general, isotropic and results in feature edge resolution limited by the degree to which the defined pattern on the etch resist is undercut. This undercutting is dependent upon the exposure time and is thus a function of the thickness of metal layer to be removed. In a well controlled wet chemical etching process the edge resolution of features is approximately 30% of the metal thickness and thus gives an aspect ratio (thickness / edge resolution) of ≈3. This is independent of the resolution of the etch resist mask and thus represents the physical limit of aspect ratio that can be achieved using conventional wet

etch techniques.

In contrast, it was seen that the laser assisted etching of 25 μm thick copper foils resulted in feature edge widths smaller than the 5 μm predicted optical resolution limit for the simple lens system used. Thus the worst case aspect ratio of patterns described in this thesis is ≈5, a significant improvement on the wet etch technique. Furthermore the laser assisted chemical etching was achieved without the use of an applied etch resist layer to the metal surface.

The main disadvantage with the laser based technique lies in the current state of excimer laser development which does not currently allow large area processing. Conversely, the move towards higher densities of integrated circuit packages on boards requires smaller dimension interconnect tracks and is leading to smaller overall dimensions of circuits.

For prototype and customised applications of printed circuit board manufacture, the raster or vector scan technique of laser processing may hold some distinct advantages. The capability of computer controlled pattern generation with resistless processing eliminates the steps of mask art-work preparation, etch resist exposure and development, and subsequent stripping of the etch resist layer.

The versatility of laser machining, as far as the variety of materials that may be patterned by laser ablation is concerned, allows the drilling of vias in the substrate material with the same laser. This is of particular importance for high performance substrate materials such as

ceramic alumina and strontium titanate.

The controllability of the etch depth with the laser technique shows promise for the thinning of conductor layers and the integration of resistive elements and fusable links as part of the board rather than as added components.

Thin film deposition is of growing interest and their patterning may be achieved by whole area coverage and subsequent etching or by deposition through contact masks. In the latter case, the technique of laser assisted chemical etching of thin metal foils would allow disposable masks to be made at relatively low cost. Similarly masks for ion and electron beam etching could be made using this technique.

Finally there are a number of possible applications of the technique to small mechanical component manufacture. Typical examples include jets and nozzles, oil ways, hole drilling and the machining of parts such as springs without disruption of their mechanical properties. The advantage here is in the variety of shapes which can be etched and which are difficult to achieve with rotary cutting tools, such as square internal corners. Intricate and delicate structures can be laser etched at high densities since there is no mechanical stress imposed upon the surrounding region during the machining.

It is concluded, therefore, that the laser assisted chemical micro-machining of materials may find a number of applications in the manufacture of electical, optical and mechanical components with feature sizes and aspect ratios that are difficult or impossible to achieve using other existing technologies.

7.3

PUBLICATIONS AND PRESENTATIONS

"Metal film removal and patterning using a XeCl laser"
J.E.Andrew, P.E.Dyer, R.D.Greenough & P.H.Key.
Applied Physics Letters, 43(11), p1076, (1983).

"Metal film removal and patterning using a XeCl laser"
J.E.Andrew, P.E.Dyer, R.D.Greenough & P.H.Key.
Conference on Lasers & Electro Optics (CLEO),
Baltimore, USA, May 1983.

"Excimer laser micromachining of metal and polymer films"
J.E.Andrew, P.E.Dyer, R.D.Greenough & P.H.Key.
VI National Quantum Electronics Conference,
University of Sussex, UK, 1983.

"Interaction of UV excimer laser radiation with metallic surfaces"
P.E.Dyer, G.Bishop, R.D.Greenough, P.H.Key & S.A.Ramsden
Symposium on LSDW, Whitehall, London, 1985.

"Excimer laser assisted gas-phase etching of copper"
P.E.Dyer, J.Grantham, R.D.Greenough & P.H.Key.
IEE Colloquium 'Laser Processing of Materials', Savoy Place,
London, December 1986 and in IEE Digest No.1986/129.

"Excimer laser patterning and etching of metals"

P.H.Key, P.E.Dyer & R.D.Greenough.

NATO Advanced Study Institute, Cargese, Corsica, May 1987 and in 'Emerging Technologies for In-Situ Processing', Ed. D.J.Ehrlich and V.T.Nguyen (Pub. Martinus Nijhoff, Dordrecht, 1988).

"An etch in time saves ...."

Philip H. Key.

Materials Research Society Bulletin, 13, p56, 1988.